UNIVERSITY OF CAPE COAST

SUPRAMOLECULAR STUDIES INTO THE CO-CRYSTALLIZATION OF FERRON WITH SULPHAMETHOXAZOLE AND CARBAZOLE

BY

ANDREWS SELOM QUASHIE

Thesis submitted to the Department of Chemistry of the School of Physical Sciences, College of Agriculture and Natural Sciences, University of Cape Coast, in partial fulfilment of the requirements for the award of Doctor of Philosophy degree in Chemistry

FEBRUARY 2017

DECLARATION

Candidate's Declaration

I hereby declare that this thesis is the result of my own original research and that no part of it has been presented for another degree in this university or elsewhere.

Candidate's Signature ..... Date 16/02/17

Name: Andrews Selom Quashie

Supervisors' Declaration

We hereby declare that the preparation and presentation of the thesis were supervised in accordance with the guidelines on supervision of thesis laid down by the University of Cape Coast.

Principal Supervisor's Signature ..... Date 24/02/2017

Name: Professor Victor Patrick Yao Gadzekpo

Co-Supervisor's Signature ..... Date 20/02/2017

Name: Professor Robert Kingsford-Adaboh

ABSTRACT

The mechano-synthesis methods of mixing, grinding and kneading were used to co-crystallize Ferron with Sulphamethoxazole and Ferron with Carbazole. Samples are prepared by mixing with a spatula, grinding for 10, 20 and 30 minutes and kneading for 10, 20 and 30 minutes. The starting compounds and the resulting products are characterised using UV/Vis Spectroscopy (UV), Infra-Red Spectroscopy (IR), Powder X-Ray Diffractometry (PXRD), Thermogravimetric Analysis (TGA), Differential Scanning Calorimetry (DSC) and Scanning Electron Microscopy (SEM). Kneading of Ferron with Sulphamethoxazole for 30 minutes yielded a co-crystal with cell parameters: a = 21.00356 Å; b = 10.43984 Å; c = 28.16611 Å; β = 133.584°; cell volume is 4,473.721 $Å^3$ and space group C2/m. Combining Ferron with Carbazole did not yield a co-crystal. The melting point of the combination products of Ferron and Carbazole varies between 208°C and 219°C. When Ferron is mixed or ground with Sulphamethoxazole, the particles of Sulphamethoxazole are found on the surface of the Ferron particles. The same effect is obtained when Ferron is kneaded with Sulphamethoxazole for less than 30 minutes. On the other hand, the particles of Carbazole remain on the surface of the Ferron particles no matter the process applied or its duration.

KEY WORDS

Carbazole

Ferron

Mechano-synthesis

Pharmaceutical Co-crystals

Powder Structure Solution Program

Sulphamethoxazole

ACKNOWLEDGEMENTS

My first and greatest acknowledgement is to the Holy Trinity, Father, Son and Holy Spirit, for being with me all these years and especially during the trying moments of this project.

I would like to thank both Professor Victor P. Y. Gadzekpo of the University of Cape Coast and Professor Robert Kingsford-Adaboh of the University of Ghana for giving me the opportunity to work with them to accomplish this feat and also for all the help and guidance they provided me during the course of my research.

Much thanks go to Dr. Charmaine Arderne of the University of Johannesburg, South Africa, for her support in getting the thermal analysis of the samples done within a short time and also for helping with the analysis of the results.

My appreciation also goes to Mr. Mawuena Aggey and Mr. Joseph Amoah for their timely advice and support for this work when it was very much needed. I would also like to acknowledge all the supporting staff, especially Beatrice, Esther, Julie and Elena, who showed deep interest in my work.

Special thanks go to the School of Graduate Studies, University of Cape Coast, for their financial support through the School of Graduate Studies Research Grant that came in just at the right time.

Last but not the least, I wish to acknowledge my wife, Doris, and kids, Denis, Louis and Terence for putting up with my long absence from home and from their lives while I undertook this project.

DEDICATION

To my wife and children,

Doris, Denis, Louis and Terence Quashie

TABLE OF CONTENTS

CHAPTER TWO: LITERATURE REVIEW

LIST OF TABLES

LIST OF FIGURES

LIST OF PLATES

LIST OF ACRONYMS

API – Active Pharmaceutical Ingredient

BZA - Benzimidazoles

CA - Co-crystallizing Agent

CBAS – College of Basic and Applied Science

DSC – Differential Scanning Calorimetry

DTG – Derivative Thermogravimetry

GI – Gastro-Intestinal

GRAS - Generally Recognised as Safe

IR – Infra-Red

NTD - Neglected Tropical Diseases

SEM – Scanning Electron Microscopy

TGA – Thermal Gravimetric Analysis

UV-Vis – Ultraviolet Visible

CHAPTER ONE

INTRODUCTION

Multiple diseases are a frequent occurrence in many patients. Fortunately, these diseases are usually known and have known drugs for their treatment. Many patients however face the complex problem of taking different pills at different times and dosages in order to be cured. One way to get around this complexity issue is to combine as many of these different drug pills into one pill.

Co-crystallization has been determined to be one of the most effective ways of combining two or more drugs into one dosage form without compromising the efficacy of either of them. An added advantage is these drugs are produced in an environmental friendly way. Unfortunately, combined pills to cure common co-infections of venerable groups as children and the elderly, especially in less developed areas in the world, are not easily available.

This study therefore is aimed at contributing to filling this gap by developing knowledge on combining known active pharmaceutical ingredients in an environmentally friendly way into one single product without compromising on the efficacy of any of them. This chapter introduces the idea of co-crystallization and one of the most effective methods for co-crystallization, the mechanochemical method. The software used in this study are also introduced in this chapter.

Background to the Study

Co-crystallization is a deliberate attempt at bringing together different molecular species within one periodic crystalline lattice without making or

breaking covalent bonds. Co-crystallization is a form of supramolecular chemistry since it focuses on assembling molecular components, in this case, crystals. Aakeröy and Salmon (2005) postulate that recrystallization and co-crystallization processes are, in essence, only distinguishable by their intents. The goal of the former is a homomeric product, whereas the latter procedure strives for a heteromeric product. However, being successful in recrystallization does not necessarily mean a failure in co-crystallization especially if the purpose is to refine the co-crystal.

Co-crystallization can improve physicochemical properties like solubility, dissolution rate, absorptivity, bioavailability, chemical stability and melting point as shown by work done by Kotak et al (2015) especially on pharmaceutical products. This is important because an effective drug must be absorbed quickly in the stomach and gastro-intestinal, GI, tract (especially any oral drug, in tablet form) (Halden, 2014). Interactions which are responsible for the formation of co-crystals include hydrogen bonding, pi (π)-stacking, and van der Waals forces. Knowledge of the stability of molecule also helps in selecting proper formulation and package as well as providing proper storage conditions and shelf life, which is essential for regulatory documentation (Blessy, Patel, Prajapati, & Agrawal, 2014).

The use of some drugs have been discontinued because of shortcomings usually related to their physical properties. At the same time, there is the re-emergence of certain disease-causing agents which had responded to some of these drugs in the past but which have developed resistance to drugs being used currently. There is a trend now to re-examine these 'old' drugs, improve on their

shortcomings and use them to manage these drug –resistant strains of disease-causing agents (Falagas & Kasiakou, 2005, Giamarellou & Poulakou, 2009; .Falagas, Grammatikos, & Michalopoulos, 2008). One of the methods which can be used to improve on the physical properties of these drugs is co-crystallisation.

In the pharmaceutical industry safe co-crystals must be formed from compounds selected from a benign group of chemicals that are considered safe by the U.S. Food and Drug Authority (FDA) or Generally Recognised as Safe (GRAS) to ensure that the final product will also be safe. One group of such benign chemicals are drugs which have already been developed and used. In this study, the compounds used, Ferron, Sulphamethoxazole and Carbazole are known to have some pharmaceutical properties and have already been developed as drugs.

One of the methods for the production or formation of co-crystals is the mechanochemical method (Braga, Giaffreda, Grepioni, & Polito, 2004). Mechanochemistry or mechanical chemistry, which is the coupling of mechanical and chemical phenomena on a molecular scale (Munnings, Badwal, & Fini, 2014) is being applied in pharmacy, synthesis and preparation of catalysts, and manufacture of pigments.

Mechanochemical procedures have been determined to be environmentally friendly. The main advantages in comparison with the traditional technological procedures are:

1. Decrease in the number of technological stages. This simplifies the process,

2. Ecological safety of the method, resulting from excluding the operations that involve the use of solvents, intermediate fusion, etc.,
3. The possibility of obtaining a product in the metastable state, which is difficult (or impossible) to obtain using traditional technological methods (Boldyrev & Tkáčová, 2000).

Thus mechanochemistry promotes the use of green chemistry principles in the production of pharmaceutical drugs. Green chemistry principles are a set of twelve principles which can be adopted to eliminate the hazard intrinsic in the design and production of materials or chemicals as compared to attempting to reduce the risk of exposure to the toxic by-products which may simultaneously be produced (Warner, Cannon, & Dye, 2004). In this study, the mechanochemical methods of mixing, grinding and kneading are used because they are environmentally friendly.

Two or more active pharmaceutical ingredients (APIs) can be combined in a single dosage form by manufacturers, known as a fixed-dose combination (FDC), or by pharmacists to produce a combination drug (Collier, 2012). The purpose of combining two or more APIs is usually to manage multiple diseases in a patient. In certain cases however, it has been observed that compounding has improved the physical properties of one or the other of the initial APIs, albeit not an intended effect. This improvement in the properties of drugs is believed to be sometimes due to the possible formation of co-crystals of the APIs (Lu, 2012; Vishweshwar, McMahon, & Zaworotko, 2006; Braga et al., 2012; Nishioka, Nakanishi, Fujiwara, & Tomita, 1984).

Diseases caused by bacteria and protozoa are quite common in Africa. Some of them are designated as Neglected Tropical Diseases (NTD) by the World Health Organisation. Examples of such diseases are Trachoma, Buruli Ulcer (both caused by bacteria), and Chagas disease (caused by protozoa). These diseases can co-infect a single patient simultaneously especially in environments in which the conditions for both infections exist (Farrar et al., 2013; Brooker et al., 2007).

There are conflicting results from studies conducted into the effect of multiple parasites on the hosts' response to a single infection (Strachan, 1989; Cooper, 2004). Some studies show that it is beneficial while others show it effect to be detrimental. This notwithstanding, co-infection of tropical diseases can still be managed by treating each infection in a patient independently preferably with a 'single' combination drug or 'polypill' (Collier, 2012) in which the various APIs needed to manage the infections are combined. Forming a co-crystal of the combined drug improves the physical properties of the drug making it more effective (Sekhon, 2009).

Statement of the Problem

Ghanaian pharmaceutical manufacturing companies mainly focus on the final formulation and packaging stage of drugs with the vast majority of its raw materials (in the form of chemicals, both synthetic and natural) being sourced from international suppliers (Agyemang-Mensah, 2014). This is because there is no well-developed chemical industry locally to support these companies. The industry also faces challenges in the disposal of waste from their production processes.

To compound these issues is the emergence of drug-resistant strains of disease-causing agents that cannot be managed by new drugs being designed and produced in the developed economies. Unfortunately, these drug-resistant strains include some of the neglected diseases which plague the country.

A study by Brooker et al (2006) reported that about 45% of school-aged children in Africa are estimated to be at risk of coincident infection of malaria and hookworm. Ralf Krumkamp et al (2015), in a similar study on Ghanaian school children also concluded that though co-infections occurred frequently, most infections presented themselves independently of other infections.

There is the need, therefore, to develop a system which uses the green chemistry approach to design and produce drugs which will be effective against these drug-resistant strains. One way to quicken the output of results will be to examine the 'old' shelved/forgotten drugs and improve on their properties using technologies and or processes which are sustainable in the local economy.

Objectives

The project will characterise and investigate the properties of co-crystals of Ferron, a known anti-protozoal and anti-mycotic agent, Sulphamethoxazole, a known antibiotic agent and Carbazole, an anti-inflammatory and anti-bacterial agent.

The specific objectives of this study are to

1. use Supramolecular Chemistry principles and methods to design and produce the co-crystals of Ferron with azoles (Sulphamethoxazole and Carbazole),
2. characterise both starting materials and the products formed,

3. use computational modelling techniques to predict properties of both the starting materials and the co-crystals formed.

Research Questions and Hypotheses

In addition to the above objectives, the following research questions will be explored:

1. Does the co-crystallization of the candidate compounds improve their individual physico-chemical properties?
2. Does the mode of preparation of the co-crystals have any effect on their properties?
3. Does the calculated physicochemical properties of the starting materials remain unchanged when the co-crystallization is effected?

Significance of the Study

This study will contribute significantly to the design and establishment of production methods of co-crystals of active pharmaceutical ingredients (APIs) for the preparation of drugs for the treatment of common tropical diseases.

The study will also help in streamlining the ability to combine known APIs using green chemistry principles to reduce the quantity of different drugs which need to be taken ('pill burden') by patients, especially African children, of co-infections of neglected tropical diseases.

Delimitations

To facilitate the design of the co-crystals using basic principles of supramolecular chemistry, the starting compounds are selected so that the resulting structures or networks will be sustained by non-covalent bonds (Lehn, 1995; Moulton & Zaworotko, 2001; Braga, Grepioni, & Desiraju, 1998; Hosseini, 2003).

The starting materials are heterocyclic since many pharmaceuticals and agrochemicals contain at least one heterocyclic unit and heterocyclic systems are important building-blocks for new materials possessing interesting electronic, mechanical or biological properties (Eicher & Hauptmann, 2003).

The compounds selected are active pharmaceutical ingredients, APIs, which are solids under ambient conditions (Almarsson & Zaworotko, 2004), and their molecules contain exterior hydrogen-bonding moieties.

The synthesis of these co-crystals should modify these properties without making or breaking covalent bonds (*non-covalent derivatization*) (Cannon & Warner, 2002; Foxman, Guarrera, Taylor, VanEngen, & Warner, 1998).

Mechano-synthesis of co-crystals are by simple mixing, grinding or kneading (solvent-drop grinding) of the solid starting materials (Trask, Motherwell, & Jones, 2004; Shan, Toda, & Jones, 2002).

***In Silico* Analysis**

This section introduces the computer software used to analyse the data, computational chemistry, to enable inferences to be made and software used to interpret the data, instrumental data analysis, from the analytical equipment.

Computational Chemistry

Gaussian 09 software package (M. J. Frisch, Trucks, Schlegel, et al., 2009) and GaussView 05 software (Æ. Frisch et al., 2009) are used for the analysis of the starting materials and the products formed from the synthesis.

VEDA 4 (Jamróz, 2013) is used for the theoretical interpretation of the infra-red spectra as it enabled Potential Energy Distribution (PED) analysis of theoretical vibrational spectra .

Powder Structure Solution Program (PSSP) (Stephens & Huq, 2002). This program is used to solve molecular crystal structures from X-ray powder diffraction data using the simulated annealing algorithm, The molecules can be rigid or flexible and the asymmetric unit can contain one or more molecules.

Instrumental Data Analysis

General Structure Analysis System (GSAS) (Larson & Von Dreele, 2004) is used for the processing and analysis of the powder diffraction data obtained. It is capable of handling all of these types of data of a given structural problem. In addition, it can handle powder diffraction data from a mixture of phases refining structural parameters for each phase.

Materials Analysis Using Diffraction (MAUD) 2.70 (Ferrari, Lutterotti, Matthies, Polonioli, & Wenk, 1996; Matthies, Lutterotti, & Wenk, 1997; Lutterotti, Bortolotti, Ischia, Lonardelli, & Wenk, 2007) is a Rietveld extended program used to perform combined analysis. It is used to fit diffraction, fluorescence and reflectivity data using X-ray, neutron, TOF or electrons.

CMPR (Toby, 2006) is a multipurpose program for powder diffraction data that uses any type of diffraction data and provides read support for many ASCII data formats and multiple datasets may be plotted at one time.

Argus-Lab 4.0.1 (Thompson, 2005) is a molecular modelling, graphics, and drug design program for Windows operating systems.

Mercury 3.9 (Macrae et al., 2008) is designed primarily as a crystal structure visualization tool. Mercury offers a comprehensive range of tools for 3D structure visualization and the exploration of crystal packing. Mercury is able to load structural data from a variety of formats and provides an extensive array of options to aid the investigation and analysis of crystal structures. Generate packing diagrams of any number of unit cells in any direction, define and visualise least-squares and Miller planes, and take a slice through a crystal in any direction. Simulated diffraction patterns can be calculated for any displayed crystal structure.

publCIF (Westrip, 2010) is an application designed for creating, editing and validating crystallographic information files (CIFs) that are used in journal publication. It offers the user a more familiar interface to the CIF through an HTML representation of the required publication data, although the raw CIF can still be viewed.

Ortep-3 (Farrugia, 2012) can directly read most crystallographic ASCII file formats that contain information on the positional and anisotropic displacement parameters. The graphical representations of thermal ellipsoids for any element or selected sets of atoms can be individually set.

Spekwin 32 software (Menges, 2015) is used to display spectra such as Ultra-violet and Infra-red spectra since it gives fast displays , it is easy to manipulate and can handle data from different equipment/sources.

Limitations

In a study of this magnitude, some conditions and influences could not be controlled and thus placed restrictions on the methodology and therefore the conclusions. This sections enumerates some of them.

Crystallization of products

Production of crystals suitable for single-crystal X-ray diffraction was not possible because mechno-synthetic methods were used for co-crystal preparations (Fujii, Young, & Harris, 2011; Braga, Giaffreda, Grepioni, & Polito, 2004; Muller, 2009; Desiraju, 1995).

Apparatus and equipment

Apparatus and analytical equipment used in project were scattered in different laboratories making the smooth and efficient performance of experiments difficult.

Organisation of the Study

The study was organised into various parts comprising literature review of crystallization methods which could be used to produce co-crystals and a literature search for suitable compounds which are known active pharmaceutical ingredients.

The study involved *in-vitro* research to produce the required co-crystals and find out their physical properties. Laboratory characterisation of the starting materials and the co-crystals formed using analytical equipment was also done.

Finally, a thesis which reports and discusses the results, draws conclusions and makes some recommendations was produced.

Chapter Summary

Co-crystallization of active pharmaceutical ingredients is suggested as the viable and ecologically friendly method for the design and production of combined drugs with the necessary bioavailability using known and proven compounds. One of the most effective methods for co-crystallization, the mechanochemical method has been introduced. This chapter covers the statement of the problem and introduces the objectives of the study. Research questions and hypotheses have also been raised. The delimitations and limitations of the study are given.

This study is expected to significantly introduce methods and technology to produce drugs to help solve the issue of neglected tropical diseases such as Buruli ulcer, Human African trypanosomiasis and Flavivirus infections that are still plaguing African children.

The softwares used in this study are also introduced in this chapter. The chapter ends with a description of how the study is organised.

CHAPTER TWO

LITERATURE REVIEW

This chapter reviews the theory of crystallization and distinguishes it from molecular synthesis. The nature of interactions found in crystals between the component entities such as hydrogen bonding, and looks at crystal synthesis. Crystal engineering is introduced here as the design and understanding of the way in which molecules crystallise to produce new materials with controlled and understood structure. Co-crystals are defined and explained in this chapter as a crystalline solid containing more than one kind of molecule.

The chapter looks at how co-crystals are formed, how candidates are selected to be used in co-crystallization, the techniques used in forming co-crystals, how co-crystals are characterised and examples of co-crystals. The review highlights pharmaceutical co-crystals, their properties and examples of drugs whose properties have been improved by co-crystallization. Mechanochemistry and how it is used in co-crystallization has been discussed in detail in this chapter.

The chapter ends with a discussion on neglected tropical diseases, NTDs, and an introduction of the compounds used in this study, Ferron, Sulphamethoxazole and Carbazole.

Supramolecular Chemistry and Crystal Self Assembly

The crystallisation process is a self-assembly process in which the component molecules or ions encounter and recognise one another, usually in solution. They then pack together as close as possible to their optimum orientation in the time available, according to their intrinsic steric and electronic

properties. The resulting aggregate, as an assembly, then goes on to accumulate further molecules or ions faster than the dissociation of those already comprising the aggregate, ultimately resulting in an ordered nucleus of more than transient stability. This nucleus continues to grow by adding molecules from solution to produce the whole crystal (Steed & Atwood, 2009a; Braga, Brammer, & Champness, 2005).

Molecular and crystal synthesis are distinguished from one another by both scale and diversity. In terms of scale, atoms and molecules are microscopic entities possessing quantum mechanical properties. Crystals are macroscopic objects exhibiting long-range order and bulk properties (melting point, dissolution rate, heat capacity *etc.*) (Steed & Atwood, 2009a; Braga et al., 2005).

In terms of diversity, the covalent bond is a complicated, yet well-studied interaction, with high strength over a short range, directionality and synthetic malleability. The synthesis of crystals on the other hand involves the manipulation of a synergistic whole of long- and short-range interactions. Some interactions fall off rapidly with distance (induction and dispersion depend on the sixth power of distance between the interacting partners), while others such as hydrogen bonds and dipolar interactions may be effective at very long range (Steed & Atwood, 2009a; Braga et al., 2005).

In molecular chemistry, the fundamental building block or synthon is the atom. Atoms interact with other atoms *via* the formation of covalent bonds to give molecules. Small molecules, in turn, undergo reactions to form larger molecules. Often these reactions involve particular chemical groups (Desiraju, 1995).

Crystal self-assembly represents the supramolecular equivalent of this view of molecular chemistry. The building blocks are now molecules instead of atoms, and are termed *tectons*[a]. The molecules interact with one another *via* the formation of non-covalent bonds to give crystalline solids, solution and gas phase aggregates. The non-covalent bond linking these tectons can be thought of as a *supramolecular synthon* if it reliably and reproducibly forms the same kind of supramolecular interaction between tectons with particular kinds of functional groups (Desiraju, 1995). Supramolecular synthons are further divided into two kinds (Figure 1):

a) Supramolecular Homosynthon: Made up of identical self-complementary groups
b) Supramolecular Heterosynthon: Made up of different but complementary groups.

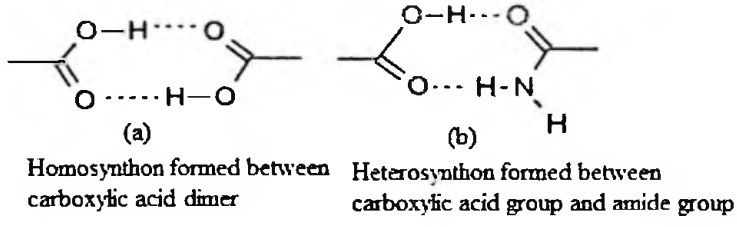

Figure 1: Types of supramolecular synthons.
Source: Kotak et al., 2015

[a] *Tectons* are defined as molecules whose interactions are dominated by specific attractive forces that induce the assembly of aggregates with controlled geometries(Su, Wang, Simard, & Wuest, 1995)

The various bonds between the synthons are usually halogen bonds (Figure 2).

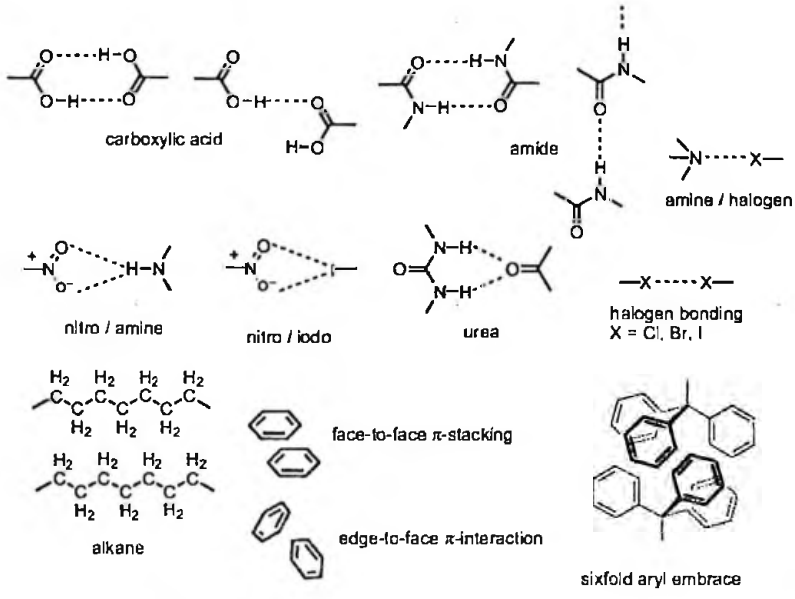

Figure 2: Common supramolecular synthons.

Source: Kotak et al., 2015

Crystal self-assembly is fundamentally a non-equilibrium phenomenon in which both kinetic and thermodynamic aspects contribute to the eventual structure. Solution self-assembly, on the other hand, is a thermodynamically controlled equilibrium reaction in which components are able to sift through a variety of possible structures until they find one of the maximum stability.

In crystal self-assembly, structures that form faster may well predominate over structures that are most stable. The synthesis method used in this study is a crystal self-assembly since the starting materials are in crystal form. The structures are expected to form fast but may not be the most stable. This is based on the background that the synthesis of crystals is a difficult

process to control since it involves manipulation of a synergistic whole of long- and short-range interactions.

Nature of Supramolecular Interactions

In general, supramolecular chemistry concerns noncovalent bonding interactions, the most well-known being hydrogen bonding. There are other interactions (Steed & Atwood, 2009b), the most important, along with an indication of their approximate energies, are given subsequently.

Ion-Ion interactions

Ionic bonding is comparable in strength to covalent bonding. Bond energy is typically between 100 $kJmol^{-1}$ and 350 $kJmol^{-1}$. A typical ionic solid is sodium chloride, which has a cubic lattice in which each Na^+ cation is surrounded by six Cl^- anions. This simple ionic lattice does illustrate the way in which a Na^+ cation is able to organize six complementary donor atoms about itself in order to maximise non-covalent ion–ion interactions. This kind of lattice structure breaks down in solution because of solvation effects to give species such as the labile, octahedral $Na(H_2O)_6^+$ (Anslyn & Dougherty, 2006).

Ion-dipole interactions

The bonding of an ion, such as Na^+, with a polar molecule, such as water, is an example of an ion-dipole interaction. Bond energy varies from 50 $kJmol^{-1}$ to 200 $kJmol^{-1}$. This kind of bonding is seen both in the solid state and in solution. Ion–dipole interactions also include coordinative bonds, which are mostly electrostatic in nature in the case of the interactions of non-polarisable metal cations and hard bases (Anslyn & Dougherty, 2006).

Dipole-dipole interactions

Alignment of one dipole with another (Figure 3) can result in significant attractive interactions from matching of either a single pair of poles on adjacent molecules or opposing alignment of one dipole with the other, with bond energy between 5 $kJmol^{-1}$ and 50 $kJmol^{-1}$.

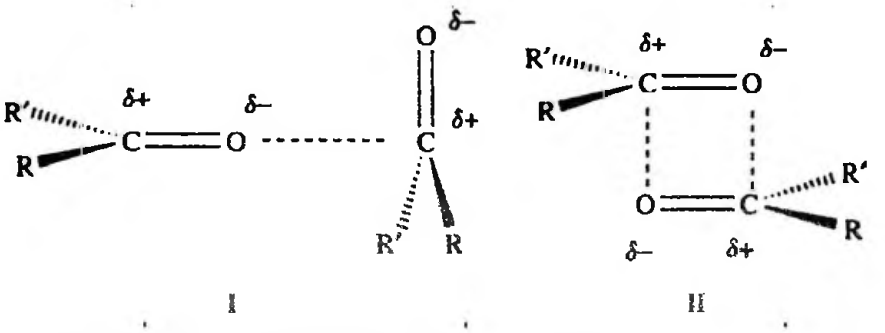

Figure 3: Dipole–dipole interactions in carbonyls.

Source: Kotak et al., 2015

Hydrogen bonding

A hydrogen bond may be regarded as a particular kind of dipole-dipole interaction in which a hydrogen atom attached to an electronegative atom (or electron withdrawing group) is attracted to a neighbouring dipole on an adjacent molecule or functional group. Because of its relatively strong and highly directional nature, hydrogen bonding has been described as the 'masterkey interaction in supramolecular chemistry'. The bond energies vary from about 4 $kJmol^{-1}$ to 120 $kJmol^{-1}$ (Jeffrey, 1997).

Hydrogen bonds are ubiquitous in supramolecular chemistry. In particular, hydrogen bonds are responsible for the overall shape of many proteins, recognition of substrates by numerous enzymes and for the double helix structure of DNA (Jeffrey, 1997).

Though there is a direct correlation between hydrogen bond strength (in terms of formation energy) and the crystallographically determined distance between hydrogen bond donor and acceptor in hydrogen bonds between neutral species (Anslyn & Dougherty, 2009), Braga et al have shown that this is not necessarily true in the case of ionic compounds (Jeffrey, 1997).

Recent interest has also focused on apparent hydrogen bonding interactions involving hydrogen atoms attached to carbon, rather than electronegative atoms such as N and O (electronegativities: C: 2.55, H: 2.20, N: 3.04, O: 3.44). While these interactions are at the weaker end of the energy scale of hydrogen bonds, the presence of electronegative atoms near the carbon can enhance significantly the acidity of the C-H proton, resulting in a significant dipole.

Jeffrey (1997) classifies hydrogen bonds into three general categories: strong, medium and weak, according to the energy of the interaction (Table 1).

Table 1: Properties of hydrogen bonded interactions

Property	Strong	Moderate	Weak
A-H...B Interaction	Mainly covalent	Mainly electrostatic	Electrostatic
Bond energy ($kJmol^{-1}$)	60-120	16-60	<12
Bond Lengths (Å)			
H...B	1.2-1.5	1.5-2.2	2.2-3.2
A...B	2.2-2.5	2.5-3.2	3.2-4.0
Bond angles (°)	175-180	130-180	90-150
Relative IR vibration shift (stretching symmetrical mode, cm^{-1})	25%	10-25%	<10%
^{1}HNMR chemical shift downfield (ppm)	14-22	<14	?
Examples	Gas phase dimers with strong acids/bases; Proton sponge; HF complexes	Acids Alcohols Biological molecules	Minor components of bifurcated bonds C-H hydrogen bonds O-H...π hydrogen bonds

Source: Anslyn & Dougherty, 2009

The co-crystals in this study are expected to exhibit moderate hydrogen bonding of the N-H...O and O-H...C type and C-H...N and N-H...C weak hydrogen bonds.

Cation-π interactions

The interaction of alkaline and alkaline-earth metal cations with C=C double bonds is a noncovalent interaction and plays a very important role in biological systems. The bond energies are typically between 5 $kJmol^{-1}$ and 80 $kJmol^{-1}$ (Ma & Dougherty, 1997).

Anion-π interactions

There is a charge difference between an overall neutral aromatic ring and an anion and therefore in principle the possibility exists for an electrostatic attraction. The charge transfer also results in strong red or yellow colourations for the complexes and a number have been characterised by X-ray crystallography. The crystal structures reveal that the anion sits in a offset fashion at the edge of the aromatic rings rather than above the centroid with anion–carbon distances as short as 2.93 Å for tetrachloro *o*-quinone and Br^-, shorter than the sum of the van der Waals radii (3.55 Å) (Berryman, Bryantsev, Stay, Johnson, & Hay, 2007).

pi-pi (π-π) stacking

This weak electrostatic interaction occurs between aromatic rings, often in situations where one is relatively electron rich and the one is electron poor. The bond energies vary from 0 $kJmol^{-1}$ to 50 $kJmol^{-1}$. There are two general types of π-stacking: face-to-face and edge-to-face, although a wide variety of intermediate geometries are known (Hunter, Lawson, Perkins, & Urch, 2001). The compounds in this study are aromatic. The interaction within the co-crystals are expected to be π-π stacking.

Van der Waals forces and close packing in the solid state

Van der Waals interactions arise from the polarization of an electron cloud by the proximity of an adjacent nucleus, resulting in a weak electrostatic attraction. They are non-directional and hence possess only limited scope in the design of specific hosts for selective complexation of particular guests. In general, van der Waals interactions provide a general attractive interaction for

most 'soft' (polarisable) species with an interaction energy proportional to the surface area of contact (Kitaigorodskii, 1961).

In examination of solid state (i.e., crystal) structures, the need to achieve a close packed arrangement is also a significant driving force. This has been summed up in the truism 'Nature abhors a vacuum', but according to the close packing theory of Kitaigorodsky (1973), it is simply a manifestation of the maximization of favourable isotropic van der Waals interactions. Kitaigorodsky's theory tells us that molecules undergo a shape simplification as they progress towards dimers, trimers, higher oligomers, and ultimately crystals.

Closed shell interactions

In some cases, closed shell atoms of neutral or like charges do form significant interactions. These interactions are termed closed shell interactions. They include secondary bonding interactions, metalophilic interactions and halogen bonding. Closed shell interactions are broadly comparable in strength with moderate strength hydrogen bonds and are thought to arise from electron correlation effects, significantly strengthened by relativistic effects in heavy elements, particularly gold (where they are termed *aurophilic interactions*) (Pyykkö, 1997).

Hydrophobic effects

Although occasionally mistaken for a force, hydrophobic effects generally relate to the exclusion from polar solvents, particularly water, of large particles or those that are weakly solvated (e.g., via hydrogen bonds or dipolar interactions). The effect is obvious in the immiscibility of mineral oil and water.

Essentially, the water molecules are attracted strongly to one another resulting in a natural agglomeration of other species (such as non-polar organic molecules) as they are squeezed out of the way of the strong inter-solvent interactions. This can produce effects resembling attraction between one organic molecule and another, although there are in addition van der Waals and π–π stacking attractions between the organic molecules themselves (Southall, Dill, & Haymet, 2002).

Solvation

In the solid state, solvent is often included as a guest in the crystal lattice and usually mediates the nucleation and deposition of a crystalline (or otherwise) compound from solution. In solution all complexation phenomena are in competition with solvation interactions and the solvent is almost invariably in a huge molar excess. Polar solvents, particularly water, compete very effectively for binding sites, particularly hydrogen bonding functionality, making hydrophobic (or solvophobic) effects of paramount importance. In non-polar solvents and in the gas phase specific host-guest dipolar and hydrogen bonding interactions are much more significant (Smithrud, Sanford, Chao, & Al, 1990). In this study, this effect may not be seen because little or no solvent will be used in synthesising the co-crystals.

Supramolecular Synthesis

In supramolecular synthesis, the term 'supramolecular synthon' has been defined by Desiraju (1995) as 'a robust, transferable connector that can be used for linking molecules together using noncovalent interactions'.

Synthons describe recognition events that take place when molecules assemble into supermolecules and offer an important illustration of the conceptual similarities between retrosynthetic organic synthesis and supramolecular assembly (Nangia & Desiraju, 1998).

Covalent and non-covalent synthesis

Covalent synthesis has become an powerful discipline (Corey, 1988; Nicolaou & Sorensen, 1996) because organic chemists have been able to establish reproducible links between molecular structure, reactivity, and reaction pathways through systematic studies of innumerable organic reactions. The explicit correspondence between chemical functional groups and their reactivity has provided a foundation for highly efficient construction of new molecules of enormous variety and complexity.

In contrast, supramolecular synthesis (Lehn, 1995) has not reached anywhere near the same level of sophistication. Currently, there is no 'dictionary' that allows or makes it possible to translate from molecular structure to supramolecular assembly (Aakeröy & Salmon, 2005).

So far only a fraction of the considerable understanding of solution-based molecular recognition phenomena has been converted into practical solid-state targeted crystal engineering.

There is still much to be done when it comes to the preparation of molecular co-crystals, a synthesis that requires the assembly and spatial organization of different molecular building blocks within the same periodic crystalline lattice.

Beyond the design of building blocks and the consideration of intermolecular forces and supramolecular synthons, making new materials through crystal engineering necessarily requires a choice of method for crystal synthesis itself.

Brag et al report that simple solution phase methods such as solvent evaporation or diffusion and slow cooling are widely used and can include a variety of sophisticated variations in such methods (Braga et al., 2005). On the other hand, lesser known methods of crystal synthesis such as solvothermal synthesis, solvent-free grinding of components sometimes known as mechanochemical synthesis, crystal growth at elevated pressures and at very low temperatures have also been used (Braga et al., 2005).

Crystal Synthesis

Crystal synthesis involves the study and understanding of intermolecular interactions and their application in the bottom up construction of sophisticated solid state superstructures starting from suitably chosen ionic and/or molecular building blocks (Braga et al., 2005).

The aim of crystal synthesis is that of controlling collective crystal properties by controlling the way molecular building blocks are assembled in the desired (designed) superstructure (Syssa-Magalé, Boubekeur, Palvadeau, Meerschaut, & Schöllhorn, 2005).

Thus, crystal synthesis is a synthetic endeavour that begins with the synthesis or identification of suitable molecular building blocks which can be combined in a directed manner by self-assembly methods to yield crystalline

products (Braga et al., 2005). The compounds in this study were selected based on their suitability to be building blocks for the co- crystal formation.

A very important difference between molecular and supramolecular synthesis is that covalent bond-forming reactions are carried out in multiple steps whereas self-assembly occurs in a single step from molecular components to the supramolecular crystal (Saha, Nangia, & Jaskólski, 2005).

It is therefore not possible to employ protection–'deprotection' protocols during crystallization, in a way that a synthetic chemist would manipulate covalent reactions of complex molecules. The idea that hydrogen bonding and halogen bonding interactions show selectivity and specificity in supramolecular recognition within each category and, furthermore, have little preference for bonding between the two categories of functional groups means that crystal engineers can exploit the property of structural insulation for the modular build-up of crystal structures (Saha et al., 2005).

Bringing different molecules together into a crystalline solid (without making or breaking covalent bonds) while maintaining control over the primary intermolecular interactions, connectivities, and stoichiometry is not an easy undertaking (Aakeröy et al., 2008).

Although considerable success has been achieved, crystal engineering in general, and co-crystal synthesis, in particular, still face formidable challenges (Aakeröy et al., 2008). To minimize these challenges, in this study compounds were selected based on the presence of synthons which would promote hydrogen-bonding.

Historically, co-crystals have been constructed primarily through heteromeric N–H/O, O–H/O, and N–H/N hydrogen bonds, and there has been number of reports on the successful synthesis of binary (two-component) and ternary (three-component) assemblies with desired connectivities and stoichiometries.

Strong hydrogen bonding involves hard and electronegative donor–acceptor groups (O-H, N-H) whereas the soft and polarizable iodine atom participates in weak halogen bonding interactions with O, N acceptors. Two persistent synthons, namely carboxylic acid-pyridine and iodo-nitro, may be combined to design predictable, multifunctional molecular solids (Saha et al., 2005).

The term halogen bond is used for describing any non-covalent interaction that involves halogen atoms acting as electrophilic species. These interactions are undoubtedly both commonplace and versatile. The strengths of these interactions correlate well with acidity scales and provide additional opportunities for further developing supramolecular synthetic strategies based on a modular view of intermolecular interactions.

Halogen bonds possess all the requirements that one might look for in a suitable supramolecular tool since they are relatively strong, directional, and their strength can be tailored (Bailey et al., 1997). Despite extensive investigation of these systems, however, reliable prediction of the structure of a given complex is still not possible.

Hydrogen bonds and halogen bonds play important roles in the synthesis of co-crystals, and the combination of both in the same synthetic strategy is

particularly attractive as this may allow for the construction of more complex assemblies composed of a larger number of different molecular species.

One major complication in the synthesis of a co-crystal is the appearance of a solvent molecule in the lattice of the desired molecular compound; the unexpected component in the lattice may cause dramatic differences in physical properties such as stability and mechanical strength (Aakeröy et al., 2008; Harrison, Tabuchi, Ishida, & Kingsford-Adaboh, 2009). The absence of solvents in this study precludes this effect.

This could however be advantageous in cases where different physical properties of an active ingredient (such as a pharmaceutically relevant compound) need to be altered (Aakeröy, Forbes, & Desper, 2009).

Several co-crystals of a family of anti-cancer compounds have been synthesized using a precise and well-defined hydrogen-bond based supramolecular approach which has produced structural consistency in the resulting solids. The melting points of the co-crystals correlate very well with the melting points of the individual acids, and the aqueous solubility can be changed in a predictable way compared to that of the individual drug (Aakeröy, 2011).

Although linear relationships between pK_a values and stretching force constants or hypsochromic[b] shifts in the visible band suggests that the pK_a value

---

[b]Hypsochromic shift is a change of spectral band position in the absorption, reflectance, transmittance, or emission spectrum of a molecule to a shorter wavelength (higher frequency). Because the blue color in the visible spectrum has a shorter wavelength than most other colours, this effect is also commonly called a blue shift.

of a given donor is a good indicator of the expected strength of the charge-transfer interaction, other factors such as steric and packing interactions often come into play (Bailey et al., 1997).

Molecular recognition

Molecular recognition refers to the specific interaction between two or more molecules through noncovalent bonding such as hydrogen bonding, metal coordination, hydrophobic forces, van der Waals forces, π-π interactions, halogen bonding, electrostatic and/or electromagnetic effects (Lockett et al., 2013; Breiten et al., 2013; Cosic, 1994).

Molecular recognition can be achieved by balancing a range of weak non-covalent forces. Using a protocol based on three complimentary steps, Aakeröy and his team modified the nature of different building blocks in order to maximize the supramolecular yield and translate molecular function into predictable intermolecular recognition (Aakeröy, Desper, & Smith, 2007).

Aakeroy et al assembled two binary co-crystals with the aid of two different intermolecular interactions, hydrogen bonds and halogen bonds successfully into a supramolecular structure of a desired connectivity. The starting point was iso-nicotinamide, a bifunctional polymorphic compound that has become a near-classic co-crystallizing agent, readily forming co-crystals with a variety of compounds in high supramolecular yield (Aakeröy et al., 2007).

One of the main challenges facing supramolecular synthesis stems from the fact that the reactants need to be held together by reversible intermolecular interactions, which, essentially, limits most supramolecular assembly processes

to one-pot reactions. A possible solution to the problem of making a one-pot synthesis ''sequential'' may be to devise modular assembly processes based on a hierarchy of intermolecular interactions. So far, hydrogen bonds of different strengths have been employed in the deliberate design of binary and ternary co-crystals, but many other synthons, like the ones based on halogen atoms, could, in principle, be brought together simultaneously in a single reaction (Figure 4).

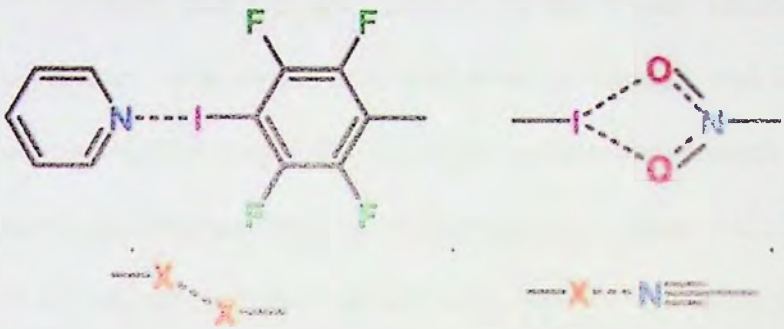

Figure 4: Halogen bonds in a modular assembly.

Source: Aakeröy et al., 2007

A strategy employing a nitrogen-iodine bond for the assembly of a co-crystal, and the amide-amide dimeric synthon for the propagation of the inherent geometry in into infinite 1-D chains was designed by Aakeröy and Co, (Figure 5) (Aakeröy et al., 2008).

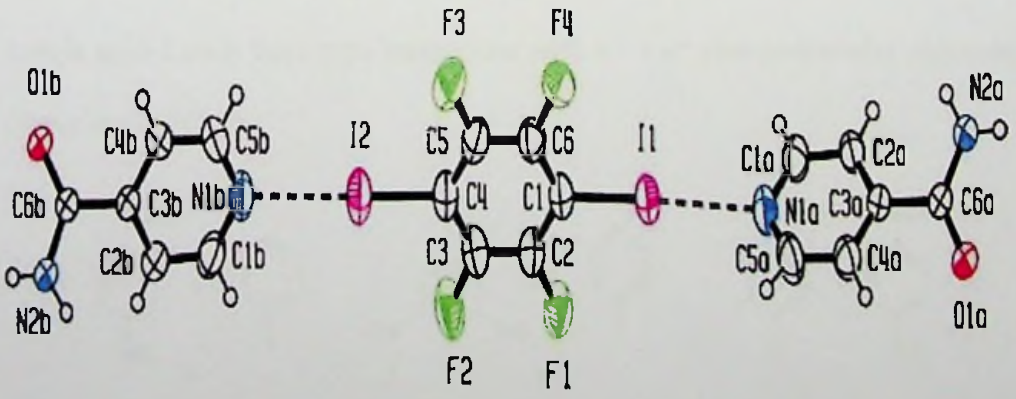

Figure 5: Co-crystal of tetrafluorodiiodobenzene and iso-nicotiamide.

Source: Aakeröy et al., 2007

They concluded that by combining a halogen-bond donor with an appropriate molecule containing

a) an effective halogen-bond acceptor, and

b) a self-complementary hydrogen-bonding moiety (that would act independently of the halogen bond),

the supramolecular target should be readily achieved in each case.

Saha and Co. also worked on the crystal structures of molecular complexes of 4-nitrobenzoic acid.4-iodopyridine[1], and 3,5- dinitrobenzoic acid.4-iodopyridine[2], (Figure 6) to evaluate the strength and selectivity of acid…pyridine and iodo…nitro heterosynthons (Saha et al., 2005) with the aim to utilize complementary functional groups for controlling the organization of molecules in the target architecture because heterosynthons are strong, specific and have a greater probability of occurrence in crystal structures.

The N–H…O amide type and iodo…nitro interactions are present in the complex of 4-nitrobenzamide.4-iodobenzamide[3], (Figure 6). The iodo…nitro interaction is an example of halogen bonding which includes the interaction of soft donor halogens (I, Br) with electronegative heteroatoms (O, N). It is a Lewis acid–Lewis base type interaction with n → σ^* charge-transfer character (Saha et al., 2005).

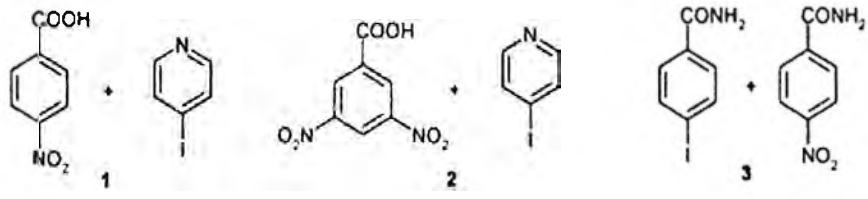

Figure 6: Molecular complexes for co-crystal formation.

Source: Saha et al., 2005

The most commonly used halogen-bond donor is 1,4-diiodotetrafluorobenzene, TFDIB, and this building block offers a deceptively simple linear connector by virtue of having two iodine atoms (activated by the electron withdrawing fluorine atoms on the phenyl ring) in a 1,4 arrangement on the backbone of an aromatic six-membered ring.

Syssa-Magalé and Co used 1,4-diiodotetrafluorobenzene (TFDIB) and hetero-aromatics containing two sp^2 nitrogen atoms with varying steric constraints to discuss and compare the variation of molecular and crystal structures. They used 4,4'- bpy,, 2,3,5,6-tetramethylpyrazine (tmpyr) (**1**), and then 2,2'-bipyridine (2,2'-bpy) (**2**), (Figure 7).

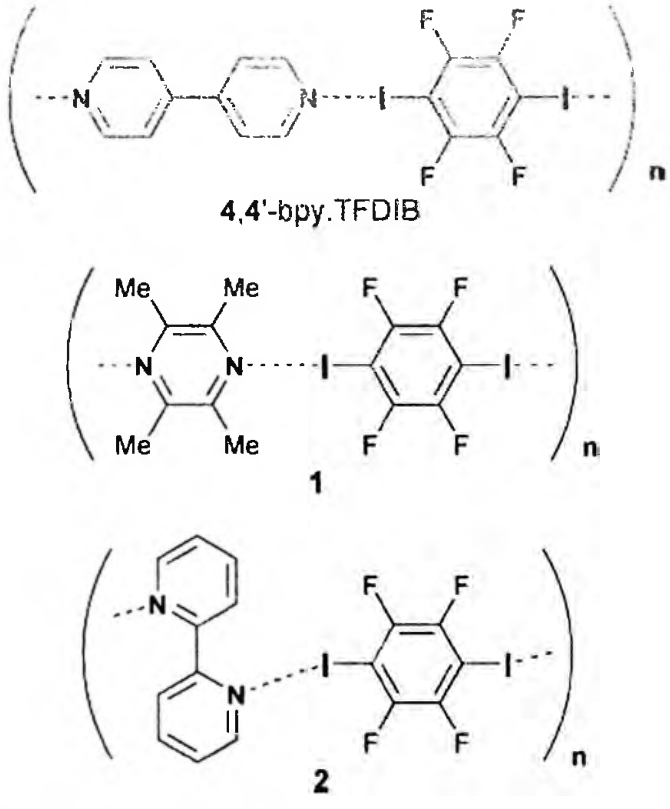

Figure 7: Schematic coordination of TFDIB in cocrystals.

Source: Syssa-Magalé et al., 2005

Their work shows the tailoring of crystal structures via the self-assembly of organic coordination compounds by N...I non-covalent halogen bonds between sterically hindered N-heterocycles and 1,4-diiodo-tetrafluorobenzene.

They concluded that the steric constraints of the aza ligands affect the characteristics of the halogen bonds. As a result both the N...I interatomic distance and the deviation of the corresponding C–I...N angle from linearity increase with respect to unconstrained systems. The reduced strength of the N...I bond is accompanied by a shortening of the covalent C–I bond. Nevertheless, the halogen bonding remains the main directing force in the studied supramolecular coordination networks.

Syssa-Magalé and Co suggests that the rough tuning of the crystal structure can be managed by varying the steric hindrance on the donor sites and thus the transition from infinite $(D...A...)_n$ chains to well-defined termolecular [D...A...D] complexes.

They also showed the interplay of coordinative halogen bonding, CH...F and *pi...pi* interactions in sustaining the self-assembled solid-state architectures. The H...F interactions link the halogen bonded complexes in two-dimensions, and the *pi...pi* stacking determines the packing of the aromatic cycles in the third dimension (Syssa-Magalé et al., 2005).

Crystal Engineering Design

Crystal engineering design is a kind of synthetic chemistry of crystals; i.e.,, the design and understanding of the way in which molecules crystallise to produce new materials with controlled and understood structure.

to one-pot reactions. A possible solution to the problem of making a one-pot synthesis ''sequential'' may be to devise modular assembly processes based on a hierarchy of intermolecular interactions. So far, hydrogen bonds of different strengths have been employed in the deliberate design of binary and ternary co-crystals, but many other synthons, like the ones based on halogen atoms, could, in principle, be brought together simultaneously in a single reaction (Figure 4).

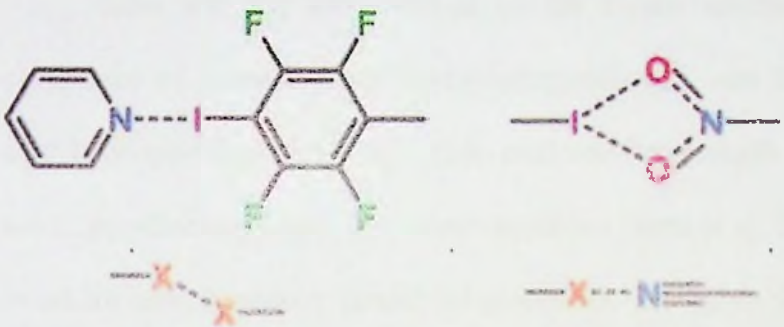

Figure 4: Halogen bonds in a modular assembly.

Source: Aakeröy et al., 2007

A strategy employing a nitrogen-iodine bond for the assembly of a co-crystal, and the amide-amide dimeric synthon for the propagation of the inherent geometry in into infinite 1-D chains was designed by Aakeröy and Co, (Figure 5) (Aakeröy et al., 2008).

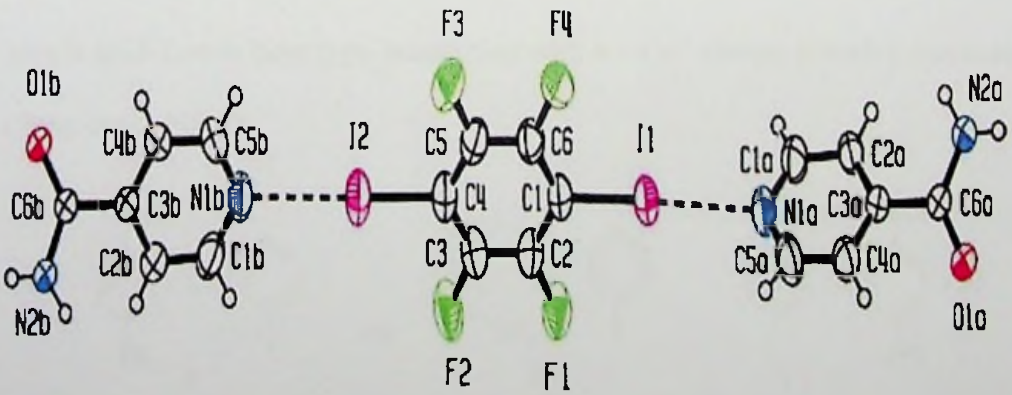

Figure 5: Co-crystal of tetrafluorodiiodobenzene and iso-nicotiamide.

Source: Aakeröy et al., 2007

They concluded that by combining a halogen-bond donor with an appropriate molecule containing

a) an effective halogen-bond acceptor, and

b) a self-complementary hydrogen-bonding moiety (that would act independently of the halogen bond),

the supramolecular target should be readily achieved in each case.

Saha and Co. also worked on the crystal structures of molecular complexes of 4-nitrobenzoic acid.4-iodopyridine[1], and 3,5- dinitrobenzoic acid.4-iodopyridine[2], (Figure 6) to evaluate the strength and selectivity of acid…pyridine and iodo…nitro heterosynthons (Saha et al., 2005) with the aim to utilize complementary functional groups for controlling the organization of molecules in the target architecture because heterosynthons are strong, specific and have a greater probability of occurrence in crystal structures.

The N–H…O amide type and iodo…nitro interactions are present in the complex of 4-nitrobenzamide.4-iodobenzamide[3], (Figure 6). The iodo…nitro interaction is an example of halogen bonding which includes the interaction of soft donor halogens (I, Br) with electronegative heteroatoms (O, N). It is a Lewis acid–Lewis base type interaction with n → σ^* charge-transfer character (Saha et al., 2005).

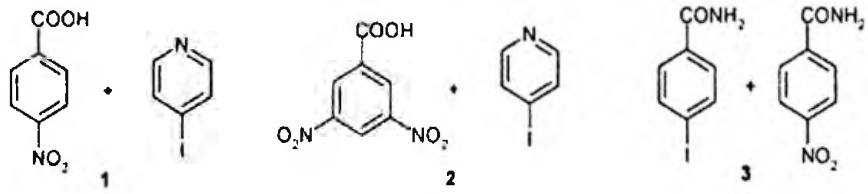

Figure 6: Molecular complexes for co-crystal formation.

Source: Saha et al., 2005

The most commonly used halogen-bond donor is 1,4-diiodotetrafluorobenzene, TFDIB, and this building block offers a deceptively simple linear connector by virtue of having two iodine atoms (activated by the electron withdrawing fluorine atoms on the phenyl ring) in a 1,4 arrangement on the backbone of an aromatic six-membered ring.

Syssa-Magalé and Co used 1,4-diiodotetrafluorobenzene (TFDIB) and hetero-aromatics containing two sp^2 nitrogen atoms with varying steric constraints to discuss and compare the variation of molecular and crystal structures. They used 4,4'- bpy,, 2,3,5,6-tetramethylpyrazine (tmpyr) (**1**), and then 2,2'-bipyridine (2,2'-bpy) (**2**), (Figure 7).

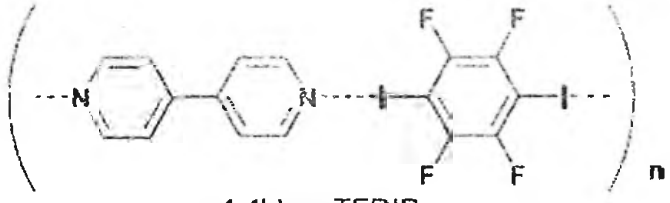

4,4'-bpy.TFDIB

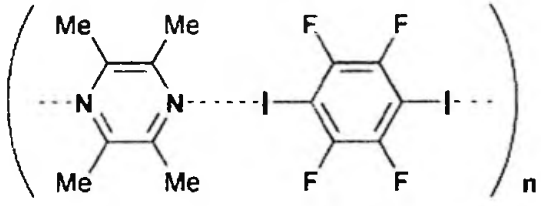

1

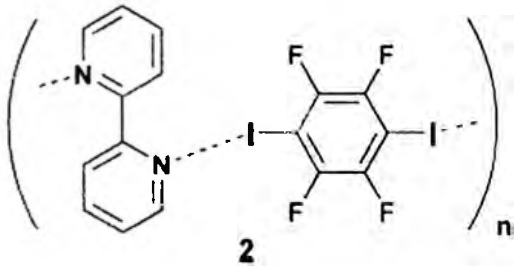

2

Figure 7: Schematic coordination of TFDIB in cocrystals.

Source: Syssa-Magalé et al., 2005

Their work shows the tailoring of crystal structures via the self-assembly of organic coordination compounds by N...I non-covalent halogen bonds between sterically hindered N-heterocycles and 1,4-diiodo-tetrafluorobenzene.

They concluded that the steric constraints of the aza ligands affect the characteristics of the halogen bonds. As a result both the N...I interatomic distance and the deviation of the corresponding C–I...N angle from linearity increase with respect to unconstrained systems. The reduced strength of the N...I bond is accompanied by a shortening of the covalent C–I bond. Nevertheless, the halogen bonding remains the main directing force in the studied supramolecular coordination networks.

Syssa-Magalé and Co suggests that the rough tuning of the crystal structure can be managed by varying the steric hindrance on the donor sites and thus the transition from infinite $(D...A...)_n$ chains to well-defined termolecular [D...A...D] complexes.

They also showed the interplay of coordinative halogen bonding, CH...F and *pi...pi* interactions in sustaining the self-assembled solid-state architectures. The H...F interactions link the halogen bonded complexes in two-dimensions, and the *pi...pi* stacking determines the packing of the aromatic cycles in the third dimension (Syssa-Magalé et al., 2005).

Crystal Engineering Design

Crystal engineering design is a kind of synthetic chemistry of crystals; i.e.,, the design and understanding of the way in which molecules crystallise to produce new materials with controlled and understood structure.

Crystal engineering has been described as a kind of non-covalent synthesis in the solid-state (Desiraju, 1995; Aakeröy, Beatty, & Helfrich, 2002). Crystal engineering design involves the use of knowledge of the optimum intermolecular interactions for the system in question, along with molecular shape, topology and electronic properties in order to select and prepare one or more components that will assemble spontaneously in the solid state into the desired crystal structure. "Modern" crystal engineering is not only making crystals with a purpose but is now also defining new purposes to make crystals (Braga et al., 2005).

In crystal engineering, interactions between molecules are analysed in terms of hydrogen bonds and other directional non-covalent interactions. Crystal structures are viewed in terms of the building blocks (tectons) that are linked via supramolecular synthons. It is often important to be able to evaluate the nature of extended structures and to appreciate structural features such as topology and interpenetration. This is now being achieved using computational approaches (Braga et al., 2005).

Crystal engineering can trace its roots back in the '60s if not earlier. Schmidt's studies of photocyclization reactions in the solid state (Schmidt, 1971) are recognized as the first attempts to rationally design crystals with a purpose, the purpose being that of organizing molecules at a distance and with the appropriate orientation for chemical reaction.

Crystal engineering now spans across all traditional sub-disciplinary barriers of chemistry (organic, inorganic, coordination etc.). Building blocks (molecules, ligands, means and geometry of coordination, ions etc.) from these

sub-areas are used simultaneously and cooperatively to produce new hybrid aggregates with novel structural features (Braga et al., 2005).

New crystalline materials are sometimes prepared using non-solution methods (grinding, milling, etc.). In solution methods on the other hand, the component(s) are ideally mixed in the appropriate ratio in a suitable solvent and allowed to crystallise by a variety of techniques, ranging from slow evaporation and slow cooling, through to more sophisticated methods such as convection, liquid-liquid diffusion or vapour diffusion. The participation of the solution phase is generally necessary because, while solid state mixtures of components may spontaneously form the desired phase on grinding, the kinetics are usually prohibitively slow and the product unsuitable for single crystal diffraction analysis (Desiraju, 1995). Designing crystals using these methods mostly results in failure (generally, most of the presently known host structures were discovered by accident rather than design).

Molecular chemists characterise crystal engineering products with methods such as thermogravimetric analysis, calorimetry, methods for gas absorption and release, solid state NMR spectroscopy, etc. Sometimes it is difficult to grow crystals suitable for single crystal X-ray experiments because of the methods used for crystal synthesis. In such cases, methods for ab-initio structure determination from powder diffraction are used (Erk, Hengelsberg, Haddow, & van Gelder, 2004).

Crystal structure prediction

Much of crystal engineering concerns empirical approaches using chemical concepts such as supramolecular synthons and accumulated

experience concerning intermolecular interactions to predict particular features of crystal structures. This kind of prediction does not give or cannot predict details of the crystal packing, symmetry and space group.

Computational Methods for Crystal structure prediction

In 1988, Maddox described the then inability to predict the structure of molecular solids from a knowledge of their chemical structure as a 'continuing scandal' (Maddox, 1988). Gavezzoti also asked whether crystal structures were predictable (Gavezzotti, 1994), in 1994, [a question repeated by Dunitz in 2003 (Dunitz, 2003a)]. These generated a lot of research into the field of crystal structure prediction. Now, there has been significant progress in more detailed crystal structure prediction, much of it by the use of ever more sophisticated and intensive computational methods (ScienceX, 2007).

One of the most common theoretical approaches, the atom-atom potential method, is based on the initial calculation and minimization of the overall lattice energy, a parameter that may be verified experimentally by measurement of the heat of sublimation of the crystal.

There are several self-evident justifications, on both theoretical and practical grounds, for striving to understand the basic factors that dictate the arrangement of molecules in space when they recognize each other at a short distance and eventually coagulate in a rigid configuration. While present knowledge of intramolecular valence can be considered satisfactory, that of intermolecular 'valence' is rudimentary.

The perspective of being able to design molecular solids with predetermined physical properties, which depend on structure, is appealing to

applied chemists in the fields of pigments, pharmaceuticals, magnets, conductors and photosensitive or optoelectronic materials (Gavezzotti, 1994).

In the early days of X-ray crystallography, guessing at the crystal structure by minimizing intermolecular repulsions was considered a viable method of solving the phase problem, when cell dimensions and diffraction intensities were available. From such a perspective, knowledge of the cell volume implied that intermolecular attractions had been satisfied, and that only mutual avoidance between rigid objects had to be accomplished, either by rough (but surprisingly efficient) mechanical devices or by computer sieving.

These procedures were suddenly made obsolete, and dismissed, by the advent of direct methods. Crystal structure prediction resurfaced only in very recent times, and with a much more ambitious connotation; the new problem is to consider an organic compound for which a structural formula has been written on paper, but whose synthesis (presumably expensive in terms of materials or human resources) has not yet been accomplished (Gavezzotti, 1994).

Thermodynamics holds that any substance must crystallize, provided it is pure and the temperature is low (or pressure is high) enough. But organic chemistry thrives in mild temperature-pressure regimes, prone to the much more elusive dictates of kinetics.

Already known and accepted are the following: Dissolution always works in the proper solvent while crystal growth from solution is problematic; melting nearly always occurs at higher temperatures than freezing; a crystal is more readily destroyed than built.

The organic solid state ranges from waxes or glasses to disordered, strained, or twinned crystals, to powders, and eventually, to well-shaped single crystals. Kinetic control of nucleation mainly has been in the control of solidification, crystal growth, and crystal morphology. For example, sexithienyl, a compound of great importance in nonlinear optics, has a high melting point, yet no single crystals of this substance could be grown, in spite of considerable effort (Gavezzotti, 1994).

A reasonable and stable structure has been predicted by calculations based on empirical potentials (Gavezzotti, 1994) using thermodynamic equations such as the Gibbs Equation. .

$$G = H - TS$$

It expresses the balance between the tendency towards maximal disorder of the molecules in a system and the opposing tendency for attractive intermolecular forces to bring the system into a state where its potential energy is minimized.

As the temperature is lowered, the second tendency gains the upper hand. The attractive forces cause the system to condense into a liquid and on further cooling into the state of maximum order, which is crystalline.

The entropy S of a perfectly ordered crystal is zero; the location of every molecule can in principle be described by an address, a set of numbers specifying its position in the three-dimensionally periodic array. In fact, real crystals are not perfectly ordered but this does not seriously affect the argument. Crystals form because the state of minimal potential energy is perfectly ordered.

Thousands (millions) of possible structures can be generated by grid search or random search techniques, or by systematic generation of dimers or strings of molecules over crystal space group symmetry elements, and these (or a selection of them) can be used as starting points for energy minimization calculations.

The problem is that such calculations typically lead not to a single crystal structure that is much more stable than any of its competitors but rather to many possible crystal structures within a quite small energy range.

This kind of result is compatible with the frequent occurrence of polymorphic forms of closely similar energy, but it is obtained also for compounds for which no polymorphic forms are known, for example, benzene. Under normal laboratory conditions benzene crystallizes in the orthorhombic space group *Pbca* and retains this structure down to very low temperatures (Jeffrey, Ruble, McMullan, & Pople, 1987). At high pressure (circa 25 kbar) an alternative monoclinic structure is obtained (Piermarini, Mighell, Weir, & Block, 1969).

According to a thorough study of crystals of benzene by van Eijck et al (1998), however, there are at least 30 possible crystal structures with calculated potential energies within a 10 kJ mol^{-1} range. They observed a correlation between the calculated lattice energy versus net molecular volume (unit cell volume divided by number of molecules in unit cell) for the 30 possible crystal structures of benzene within an energy window of 10 kJ mol^{-1} (Figure 8). The problem is not so much a matter of generating stable crystal structures but rather

one of selecting one or more from many almost equi-energetic possibilities (Dunitz, 2003a).

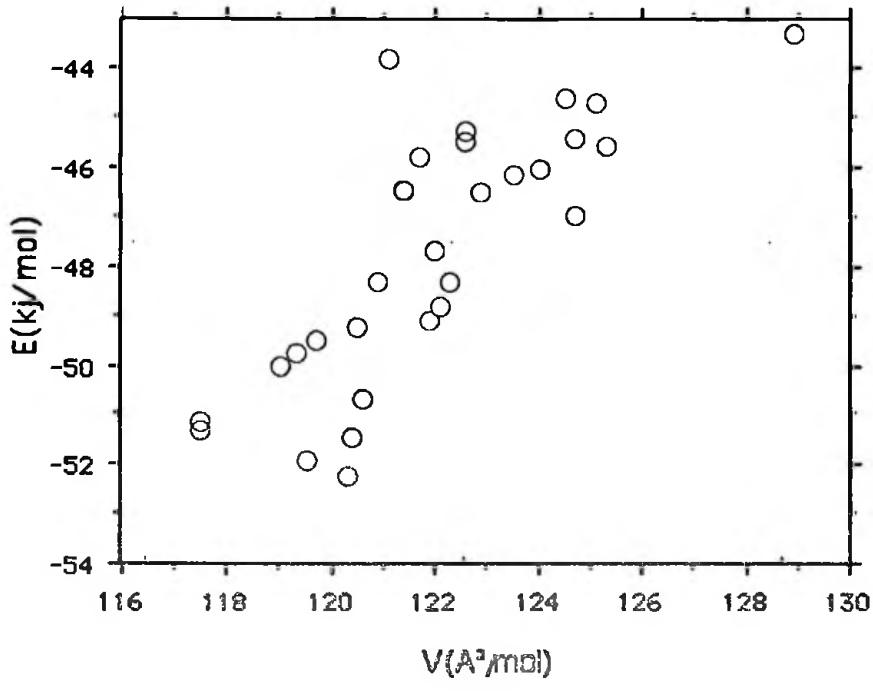

Figure 8: Scatter plot of calculated lattice energy versus net molecular volume.
Source: Dunitz, 2003a

Very little is known about how crystals form and it is much more difficult to make realistic computer calculations. Crystallization is not an equilibrium process. It requires super-cooling or supersaturation. This nucleation process is probably the rate-limiting step in crystal formation, but one may not assume that the fastest forming nuclei necessarily correspond to those of the most stable crystal structure. Computational methods for predicting crystal structures of organic compounds therefore cannot yet be regarded as reliable.

There is also the idea of structure directing 'synthons' which is based on qualitative observations that certain groupings in organic molecules exercise

attractive intermolecular interactions and so guide the molecules into distinctive patterns in their crystal structures. Almost any observed crystal structure can be described in terms of such interactions, but the physical basis of this approach is shaky and its predictive capacity is poor.

Inspired guessing may occasionally lead to a correct prediction with any approach. All this shows that interpretations of intermolecular attractions and repulsions based mainly or exclusively on r^{-6} interactions between atoms in close contact may be misleading. Although the widely used atom-atom approximation is moderately successful in calculating packing energies of crystals, it also lacks any sound physical basis.

Faster computing has enabled extensions of these methods to more complex molecules with additional degrees of conformational freedom and also to co-crystals, including hydrates and other solvates. Therefore, given a molecular formula, it is possible to obtain a list of perhaps 10–20 crystal structures within an energy window of a few $kJmol^{-1}$, among which all observable polymorphs are likely to be found.

However, the ideally periodic structures that serve as models for the energy calculations are far from the physical reality. The free energies of real crystals depend on strains associated with defects and imperfections, accidents of their growth. Besides, it is well known that crystallization experiments are sometimes not reproducible, as witnessed by the phenomenon of 'disappearing polymorphs' (Dunitz & Bernstein, 1995; Dunitz, 2003a).

Researchers have met the challenge of predicting the crystal structures of small organic molecules by computational methods without experimental

input, a goal that has been described as the Holy Grail of crystallography (ScienceX, 2007). This breakthrough was achieved in the 4th blind test of crystal structure prediction, an exercise conducted by an international group of fifteen research groups that was organised by the Cambridge Crystallographic Data Centre (CCDC) and the University of Cambridge. The results of the 2007 blind test represent a dramatic improvement over what has been achieved previously: 3 groups had one experimental structure within their three allowed predictions, 3 others had two such hits and one group predicted all four target crystal structures, each as their most likely prediction.

These very successful results were obtained by Dr Marcus Neumann of Avant-garde Materials Simulation and Drs Frank Leusen and John Kendrick of the Institute of Pharmaceutical Innovation at the University of Bradford. Dr Graeme Day, of the University of Cambridge, who co-ordinated that year's challenge said:

"The results of this year's test reflect significant development over the past few years. Things looked much less encouraging last time we held a blind test, but crystal structure prediction can now be seen as a real tool to be used alongside experimental studies, when designing new materials or developing a pharmaceutical molecule." (ScienceX, 2007).

Though the blind tests are limited to small, relatively rigid molecules, these recent results demonstrate a significant advance in the field. The method can now be viewed as applicable to a number of problems of importance in the pharmaceutical industry and more generally to improving the understanding of how molecules are held together in crystalline solids.

Dr Marcus Neumann, author of the novel computer program GRACE for crystal structure prediction, also said on that occasion that:

"Obviously, we are delighted with these results, but there is still plenty of room for improvements. Over the next few years, the range of applicability will gradually extend towards more and more complex compounds such as highly flexible molecules, solvates and salts." (ScienceX, 2007).

Dr Frank Leusen of the University of Bradford added:

"Having proven that the crystal structures of small organic compounds can be predicted reliably, the crystal structure prediction community now faces the challenge of predicting the relative stability of polymorphs as a function of crystallisation conditions to really capture the effect of temperature and solvent." (ScienceX, 2007).

Crystal structure prediction however is made more complicated by the occurrence of polymorphism and solvates/co-crystals.

Polymorphism

Solids with significantly different physical properties may be constructed from a single atom, ionic compound, or molecule. This behaviour in single-component organic crystals is called polymorphism (Stahly, 2007). Polymorphism as applied to organic compounds is that it is exhibited only in the solid state. On melting, vaporization, or dissolution, polymorphic structures are lost.

Polymorphism implies that the multidimensional potential-energy surface that describes the thermodynamics governing the molecular recognition processes that eventually leads to crystal growth is likely to contain many accessible local energy minima.

Even though molecular recognition is typically associated with molecules in solution, such interactions are also responsible for organizing molecules in the solid state. Translating principles of molecular recognition to solid-state assembly of heteromeric molecular solids is of key importance to the development of versatile and reliable strategies for practical supramolecular synthesis (Aakeröy & Salmon, 2005).

The existence of crystal polymorphs implies that the design of a desired crystal often results in more than one crystal structure solution because the minimization of the global free energy of a crystal (the free energy of the molecule convoluted with the free energy of the supramolecular crystal structure) permits different compromises between the various components (Bernstein, 2002).

This has an extremely relevant commercial impact as it carries implications for marketing and patenting of drugs formulated as crystalline solids.

Allotropes

The ability of a single chemical substance to exist in different arrangements was first recognized in inorganic materials. When exhibited by elements, this phenomenon is called allotropism.

Solid components

Single-component solids can be of various types. Both non-crystalline and crystalline forms are possible. Although it is common to refer to "amorphous" organic solids, it is generally the case that organic molecules,

being anisotropic[c] in shape, have at least short-range order in their non-crystalline forms.

Co-crystals

A co-crystal is a crystalline solid containing more than one kind of molecule. The different molecules found together in a co-crystal are distinct, separate, and separable chemical substances. Conceptually any crystal with more than one separable molecular component may be thought of as a co-crystal.

Naming multicomponent crystals

Common materials which are considered as multicomponent crystals are hydrates and solvates, which contain the "host" molecule and water or solvent as a "guest". In either case, the guest can be a structural piece of the crystal or simply fill space. The main difference between solvates and co-crystals is the physical state of the isolated pure components. If one component is a liquid at room temperature, the crystals are designated as solvates; if both components are solids at room temperature, the crystals are designated as co-crystals (Sekhon, 2009). With water as the 'guest', a nonstoichiometric (or variable) hydrate often results, wherein the amount of water in the crystal depends on the relative humidity of the surroundings.

---

[c] Different physical properties in different directions.

There is currently a controversy in the literature regarding naming conventions for these crystals In their study of sulfathiazole solvates, Bingham and co-workers (Bingham et al., 2001) called them "co-crystals" (structural guest) and "clathrates" (space-filling guest).

Co-crystals were well defined by Dunitz, who wrote:

"the word [co-crystal] provides a succinct though possibly inelegant definition of what it is intended to describe, a crystal containing two or more components together. Thus co-crystal encompasses molecular compounds, molecular complexes, hydrates, solvates, inclusion compounds, channel compounds, clathrates, and possibly other types of multi-component crystals."(Dunitz, 2003b).

The term "form" can be considered to include co-crystals if one takes the position that there is one molecule of specific interest; the Active Pharmaceutical Ingredient, API, in a pharmaceutical development program, for example.

Co-crystals have also been defined as consisting of two or more components that form a unique crystalline structure having unique properties. This definition requires clarification of the meaning of "component". If a component is defined as being an atom, ionic compound, or molecule, then a co-crystal becomes more specifically either

a) a crystal that contains two or more different atoms or molecules or
b) a crystal that contains an ionic compound plus additional atoms, ionic compounds, or molecules

Solid solution

There also exist non-stoichiometric inclusion compounds such as the clathrate hydrates and some urea inclusion compounds in which there is essentially a random distribution of one molecule within a crystal of another. These are known as *solid solutions*[d]

Organic salts

These are multicomponent species where the components are individual ions. Formation of salts of organic compounds involves proton transfer from an acid to a base.

Co-crystals and salts

Salts comprise separate anions and cations. It is impossible to separate a salt into the pure anions and pure cations. Electrostatic charge balance considerations mean that each ion must always be partnered by an oppositely charged counter-ion. Salts can also exist in non-crystalline form. A salt contains a single ionic compound, but multiple ions (Stahly, 2007).

When a pair of ionisable components crystallize, both the ΔpK_a value and the crystalline environment determine the extent of proton transfer. Hence crystalline salts and co-crystals can be considered as species that exist at either end of a continuum of multicomponent crystal structures (Kotak et al., 2015). At the salt end proton transfer is complete, and at the co-crystal end proton

---

[d] A *solid solution* is a solid mixture of one or more compounds within a 'solvent' of another solid crystalline compound. For the mixture to be considered a solid solution the crystal structure of the solvent must remain essentially unchanged upon the addition of the solute(s) and the whole mixture must remain as a single homogeneous phase.

transfer is absent as illustrated by the work of Stahly using the single-crystal structure analyses of aminophylline crystals (Figure 9) (Stahly, 2007). An anhydrous structure is on the left, and a monohydrated structure is on the right.

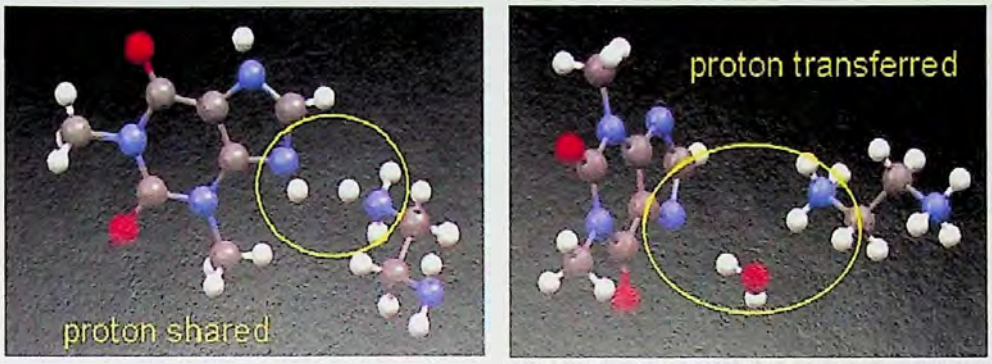

Figure 9: Single-crystal structure analyses of aminophylline crystals.

Source: Stahly, 2007

Lemmerer and Co, in a recent work on co-crystals and molecular salts of carboxylic acid/pyridine complexes, found that co-crystals were formed when the difference[e] between pKa was below 0.while salt formed when the difference is above 3; the intermediate range being favourable for both (Lemmerer, Govindraju, Johnston, Motloung, & Savig, 2015; Cruz-Cabeza, 2012).

Discovery and design of co-crystals

In many cases, co-crystals are discovered empirically. An example of this is that of a three-component co-crystal containing aspirin, *â*-cyclodextrin, and succinic acid which was determined by single-crystal X-ray analysis by

[e] ΔpKa = pKa (protonated base) − pKa (acid) less than 0 a co-crystal forms (all components in their neutral states), and for differences greater than 3, a molecular salt forms.

Nishioka and workers (Nishioka et al., 1984). The purpose of generating the co-crystal was to slow aspirin hydrolysis in aqueous media, since cyclodextrin inclusion complexes are maintained in solution. Apparently, inclusion of succinic acid in the crystalline complex was unexpected, and the relative potential utility of the three-component co-crystal was not discussed.

In contrast, co-crystal design is also possible. One of the most active researchers in the field was Dr. Margaret Etter. She viewed hydrogen bonds as design elements in organic solids, similar to the role of covalent bonds as design elements in organic molecules (Etter, 1990; Etter, 1991b).

Forming co-crystals

Since hydrogen bonds frequently form in a hierarchical fashion (best-donor to best-acceptor, second best-donor to second best-acceptor, etc.), (Etter, 1991a; Etter, 1990) the chances of producing a new binary co-crystal are greatly improved by positioning the best hydrogen-bond donor and the best hydrogen-bond acceptor on different molecular building blocks (Aakeröy, Desper, & Helfrich, 2004).

The physical validity of a best-donor/best-acceptor classification or interpretation of hydrogen-bond interactions can be rationalized in terms of a desire of the system to maximize multiple electrostatic interactions (Aakeröy & Salmon, 2005). Aakeröy and Co concluded that in order to 'convince' two different discrete chemical species to co-exist in a molecular co-crystal there needs to be some specific molecular-recognition based reason for their solid-state union. The components in a co-crystal exist in a definite stoichiometric

ratio, and assemble via non-covalent interactions such as hydrogen bonds, ionic bonds, π-π or van der Waals interactions rather than by ion pairing (Aakeröy & Salmon, 2005).

Although individual structures that defy rationalisation will appear from time to time, there is no doubt that the important 'big picture' reveals structural trends, patterns of behaviour, and reproducible motifs that, when combined, can be developed into a library of high-yielding supramolecular reactions (Aakeröy et al., 2004).

A good co-crystallizing agent (CA) should be able to form heteromeric intermolecular interactions with the target molecule that are more favourable than the homomeric interactions that may exist (Aakeröy, Beatty, Helfrich, & Nieuwenhuyzen, 2003). The CA must also have the ability to 'tolerate' the presence of a different molecular building block within the same crystalline lattice, which makes it reasonable to search for co-crystallizing agents amongst polymorphic compounds.

Selection of candidates for co-crystals

Hydrogen bonds are often the primary directors of organic crystalline structure. By evaluating the disposition of hydrogen bond donors and acceptors, and applying general rules such as those developed by Etter and Görbitz, (Görbitz, 2000; Etter, 1990; Etter, 1991b) it is sometimes possible to predict interactions that suggest the use of certain guests.

Etter's rules

Based on her work on diacetamide and acetamide (Etter, 1990) and studying hydrogen-bonding patterns in crystal structures reported in the

Cambridge Crystallographic Database, Etter came up with a set of rules with some predictive ability which became known as Etter's Rules. These rules could be used to predict hydrogen bond patterns in general. Subsequently, application of the rules and a growing understanding of crystal structures has led to an increasing number of designed co-crystals (Etter, MacDonald, & Bernstein, 1990; Etter, 1991a). These are:

a) All good proton donors and acceptors are used in hydrogen bonding [such as those found in carboxylic acids, amides, ureas, anilines, imides, phenols, etc.]

b) Six-membered-ring intramolecular hydrogen bonds form in preference to intermolecular hydrogen bonds [based on same ideas as chelate effect in inorganic chemistry and is entropically favoured. Five- and seven-membered intramolecular hydrogen-bonded rings are also common].

The best proton donors and acceptors remaining after intramolecular hydrogen bond formation form intermolecular hydrogen bonds to one another.

It is however not uncommon for weak CH donors to occupy acceptor sites on the strong chloride ion acceptor (Aakeröy, Evans, Seddon, & Pálinkó, 1999).

Graph sets

The challenge of recognizing and classifying motifs generated by multiple intermolecular interactions was also addressed by Etter et al (1990), using a system based upon graph-set notation that allow structural motifs to be described in a consistent and 'user-friendly' way.

The graph-set approach uses four principal motifs: chains (C), dimers (D), rings (R), and intramolecular hydrogen bonds (S), as descriptors of hydrogen-bonded molecular solids. Although this notation may not provide an unambiguous assignment of every structural arrangement, it is flexible enough to facilitate a systematic description of a wide range of structures.

The appealing simplicity of this approach has made it successful and descriptors such as R^2_4 (8) (an eight-membered ring with four hydrogen-bond donors and two hydrogen-bond acceptors) and R^2_2 (8) (e.g., the carboxylic head-to-head dimer), have become widely recognizable (Aakeröy & Salmon, 2005).

To develop co-crystals in industry, it is most efficient to use a combination of structural evaluation (for potential guest selection) and physical evaluation (for experimental technique selection), followed by a screening procedure similar to that used for polymorph screening (Stahly, 2007).

Techniques used for formation of co-crystals

The experimental techniques are based on those used in forming crystals in general. These experimental techniques create conditions where a co-crystal, if one can form, will crystallize instead of the individual compounds.

Mechano-synthetic Methods

Grinding

A technique that can be used that is relatively independent of the properties of the API is grinding (also known as Neat grinding or Milling). According to Stahly (2007) preparation of co-crystals in this way was reported as early as 1893 when Ling and Baker made quinhydrone derivatives by grinding solid quinones and quinols together in a mortar and pestle, with or

without solvent. Subsequent work showed that some co-crystals, which could not be prepared from solution, could be prepared by grinding. For example, in a study of co-crystal formation between imides and a variety of guest molecules, it was found that many co-crystals could be obtained both by grinding and from solution, but others, such as the 1:1 co-crystals of diacetamide with acetamide, benzamide, and 3,4- dinitrobenzoic acid, could only be prepared by grinding (Etter & Reutzel, 1991).

Solid state grinding is where the materials are mixed, pressed and crushed in a mortar and pestle. Mills can also be used for crushing. This technique provides particle size reduction (Blagden, Matas, Gavan, & York, 2007). This technique is used in this study because it is easier, simply and independent of the structural properties of the molecules.

Kneading

A variant of the standard grinding techniques is kneading (also known as solvent drop grinding). Selection of the polymorph of a caffeine/glutaric acid co-crystal was possible by inclusion of small amounts of specific solvents during grinding (Trask et al., 2004). The technique of adding small amounts of solvent during the grinding process has been shown to enhance the kinetics and facilitate co-crystal formation and has led to an increase in the use of solid-state grinding as a method for co-crystal preparation. The solvent added in this case acts as a catalyst but does not form part of the end product (Vitthalrao, Kumar, & Radheshyam, 2013). This technique is also used in this study because it is easier, simply, independent of the structural properties of the molecules and also uses little solvent.

Mixing

This method involves bringing the molecules of the two compounds together by mechanical action, for example, a spatula, without the application of force. This technique is also used in this study because it is easy and simple.

Solvent evaporation

Solvent evaporation is the most common and conventional method in case of crystallization. In this technique all the material is mixed with the common solvent serially and evaporated completely (Vitthalrao et al., 2013). To carry out solvent-based experiments (evaporation or cooling of solutions, for example) solvents or solvent mixtures must be found in which both components dissolve sufficiently. Since the co-crystals sought will typically contain a stoichiometric ratio of components, such ratios should be used, particularly in experiments where solvent is completely evaporated. For cooling or other experiments where solvents will not be completely removed, there need not be a stoichiometric ratio of the concentrations of the components.

Other more sophisticated and less common place methods found in literature (Vitthalrao et al., 2013; Blagden et al., 2007) include:-.

Slurry crystallization

This process involves the addition of crystallization solvent to the API along with its acceptable former. The suspension is stirred until the formation of co-crystal is complete. In some cases, aliquots of antisolvent may subsequently be added to the solution. Solid formed in the solution are filtered and dried. The solid is a co-crystal of the compound and conformer.

Antisolvent addition

This is one of the methods for precipitation or recrystallization of the co-crystal former and active pharmaceutical ingredient. Solvents include buffers and organic solvents.

Supercritical fluid atomization process

Co-crystallization by supercritical solvent (CSS) is a method where an API and a co-crystal former are mixed together by magnetic stirring after being pressurized by supercritical CO_2 in a high-pressure vessel. The Supercritical Anti-Solvent (SAS) technique explores the anti-solvent effect of supercritical CO_2 to precipitate particles (co-crystals) from solutions. The supercritical fluid enhanced atomization, SEA, technique explores essentially the CO_2 atomization enhancement in a spray drying process.

Hot melt extrusion

Extrusion is a useful method for synthesis of co-crystals. It involves highly efficient mixing and improved surface contacts. Co-crystals are prepared without use of solvent.

Sonocrystallization method

A sono-chemical method for preparation of organic co-crystals of very finite size has been developed. This method was primarily developed for preparation of nanocrystals. Caffeine- maleic acid co-crystal were prepared using the ultrasound method (Chaudhari & Uttekar, 2009).

Characterization of Co-crystals (Wenger & Bernstein, 2008; Allesø et al., 2008; Lu, Rodríguez-Hornedo, & Suryanarayanan, 2008; Variankaval et al., 2006; Wang & Chen, 2007; Cooke & Davey, 2008).

Wavelength of maximum peak in UV spectra

When the co-crystal solution is scanned using a UV spectrophotometer, the spectrum has a characteristic maximum peak(s) at a particular wavelength usually absorbed by the API. If the conformer is also an API, the scan will show all the peaks of at the respective wavelengths for both APIs. This study used this characterisation method.

Crystallographic methods

Crystallographic methods include both single crystal X-ray diffraction as well as powder X-ray diffraction. The single crystal X-ray diffraction study can provide unambiguous atomic positions and complete structural information, but obtaining a single crystal suitable for study can prove difficult. In such cases, powder X-ray diffraction studies using microcrystalline samples is relied upon. This study used Powder X-ray Diffraction to characterise the samples.

Differential scanning calorimetry (DSC)

DSC studies the change in heat flow between the sample and a reference. DSC can be used to obtain information about the melting point of a compound as well as any glass transitions, heats of fusion and levels of crystallinity. This was used in this study.

Thermal analysis

This is widely used in pharmaceutical industries for characterization of polymorphism, purity, solvation, degradation and drug compatibility. It includes Thermogravimetry and Differential Thermal Analysis (DTA). This was used in this study.

Vibrational spectroscopy

The study of molecular motions by use of vibrational spectroscopy is also sometimes employed in the characterization of co-crystals. This method includes infrared absorption spectroscopy and Raman spectroscopy. This study used infrared absorption spectroscopy.

Scanning electron microscopy (SEM)

Scanning Electron Microscopy (SEM) is conducted to characterize the surface morphology of the particles. This was conducted on the samples in this study.

Melting point

Melting point is an important characteristic of all solids as it gives information on the crystalline lattice energy. For co-crystals and polymorphs, the melting points are of particular importance. The melting points of the samples were determined in this study.

Solubility

Co-crystallization is a technique most frequently used when the main aim is to enhance the solubility.

Stability

Stability is an important parameter to be considered for any formulation. Hence in case of co-crystals it is also important to ensure the chemical stability, solution stability, thermal stability and relative humidity. The relative humidity of the co-crystals can be analysed by water absorption/desorption experiments.

Nuclear magnetic resonance (NMR)

Solid state NMR is also used for characterization. NMR studies give the chemical environment of the nuclei which is different in polymorphs because of magnetic non-equivalence. NMR peaks for the magnetically non-equivalent nuclei will differ in different polymorphs and can yield very useful information.

Co-crystals Produced and Studied

Nishioka et al co-crystallized β-cyclodextrin (β—CyD) with aspirin (acetylsalicylic acid) by heating a 1:1 aqueous solution of β-CyD and aspirin up to 60°C and slowly cooling the mixture to room temperature. They obtained colourless and prismatic crystals. The content of salicylic acid in the crystals was determined by dissolving them in distilled water, adding 1% of $Fe_2(SO_4)_3$ aqueous solutions and measuring the absorption at 510 nm. They went further to determine the crystal structure of the co-crystal (Nishioka et al., 1984).

Etter et al obtained co-crystals of N-Acetylbenzamide from the acid-catalysed condensation of benzamide and acetic anhydride. Recrystallization from acetone gave colourless crystal blocks while recrystallization from ethanol gave colourless plates. Melting points were determined of the co-crystals using a Fisher-Johns apparatus and infrared spectra were recorded on a Nicolet-5DXB FTIR spectrometer. ^{1}H and ^{13}C-NMR spectra were recorded on IBM-NR100AF and Varian VXR-300 spectrometers, respectively (Etter & Reutzel, 1991).

Hoogsteen produced and studied co-crystals of 9-methyladiene and 1-methythymine crystalline bases by placing stoichiometric amounts of the crystalline bases (totalling about 100 mg) in a 2.5-cm steel capsule containing a 3-mm ball bearing and grinding them using a mechanical amalgamator for 20

min. X-ray powder patterns run on the product phases were compared to the patterns of the reagents and analysed for new peaks corresponding to base pair co-crystals (Hoogsteen, 1963).

Etter et al, in another study, found that co-crystals of 9-ethylguanine (G) and 1-methylcytosine, which had been co-crystallized from solution and characterised crystallographically by O'Brien (1967), do not form in the solid state. They however remain as a G, C mixture despite intermittent grinding and heating at 50°C for more than 7 days (Etter, Reutzel, & Choo, 1993).

Huang et al prepared co-crystals from various phenol–pyridine pairs by solution and/or solid-state methods:

a) *Slow evaporation* where stoichiometric amounts of the phenols and pyridines were dissolved in a mutually miscible solvent system and allowed to recrystallize at room temperature. Whenever possible, the resulting crystals were removed from solution as soon as they were formed before the solvent had completely evaporated. Alternatively, co-crystals were obtained after all of the solvent had evaporated.

b) *Vapour Diffusion* where stoichiometric amounts of the phenols and pyridines were dissolved in a mutually miscible solvent system in a 25 mL beaker. The beaker was placed in a 200 mL jar and a second solvent was introduced into the jar as a precipitant. The jar was sealed and left to stand undisturbed. As the precipitant diffused into the solution, crystals formed in the solution.

c) *Solid-state Grinding* where stoichiometric amounts of the phenols and pyridines were ground together in a Wig-L- Bug dental amalgamator for

10 min. Conversion of the starting materials to co-crystals in the solid state often approached 100%.

Co-crystals prepared by these methods were characterized by optical microscopy, melting point measurements, IR, and ^{1}HNMR spectrometry and powder SHG[f] measurements. In all cases, where two or more methods were used for one system the same solid-state phases were obtained from the different methods (Huang, Britton, Etter, & Byrn, 1997).

Other examples are co-crystals of peptides (Görbitz & Etter, 1993), co-crystals containing the sunscreen *para*-aminobenzoic acid (Etter & Reutzel, 1991), co-crystals containing nucleotide bases (Etter et al., 1993), and co-crystals showing promise as nonlinear optical materials (Huang et al., 1997).

Pharmaceutical Co-crystals

Co-crystals are of considerable interest within the pharmaceutical industry. It is noted that compounds used in the pharmaceutical industry are quite structurally varied; there is no specific chemical attribute that renders them pharmaceutically active. On the other hand, the properties of any solid material depend not only on the identity of its constituents but also on their arrangement. Therefore, by deliberately (or otherwise) crystallising a pharmaceutical API with another molecule it is possible to modify the physical properties of the resulting crystalline solid compared to crystals of the pure API. The API co-

---

[f] Second harmonic generation (also called frequency doubling or abbreviated SHG) is a nonlinear optical process, in which photons with the same frequency interacting with a nonlinear material are effectively "combined" to generate new photons with twice the energy, and therefore twice the frequency and half the wavelength of the initial photons (Wikipedia contributors, 2016b)

crystal may therefore have improved solubility, processing stability or tableting characteristics compared to the pure compound (Stahly, 2007).

In selecting the solid form of an API for development into a drug product, for example, it should be the pharmaceutical acceptability of the components and the properties of the candidate solids that guide the selection process rather than the classification of each.

Drug development, particularly when directed to a solid oral dosage formulation, is critically dependent on the physicochemical properties of the API. Important properties include solubility, dissolution rate, bioavailability, chemical and physical stability, hygroscopicity, melting point, crystal habit, and powder handling characteristics (Huanga & Tong, 2004; Byrn, Pfeiffer, & Stowell, 1999).

For ionisable APIs with undesirable properties, salts may be generated in a search for a better solid (Stahl & Wermuth, 2002). But where salts fail, or for non-ionisable APIs, co-crystals provide expanded opportunities to alter API properties. For example, it has been demonstrated that co-crystals containing carboxylic acid guests alter the dissolution rates of itraconazole (antifungal) (Remenar et al., 2003), fluoxetine hydrochloride (antidepressant) (Childs et al., 2004), and an API investigated by the Purdue Pharma company. The latter co-crystal, containing 2-[4-(4-chloro-2-fluorophenoxy)phenyl]pyrimidine-4-

carboxamide and glutaric acid (Figure 10), afforded a 4-fold bioavailability increase in dogs (McNamara et al., 2006).

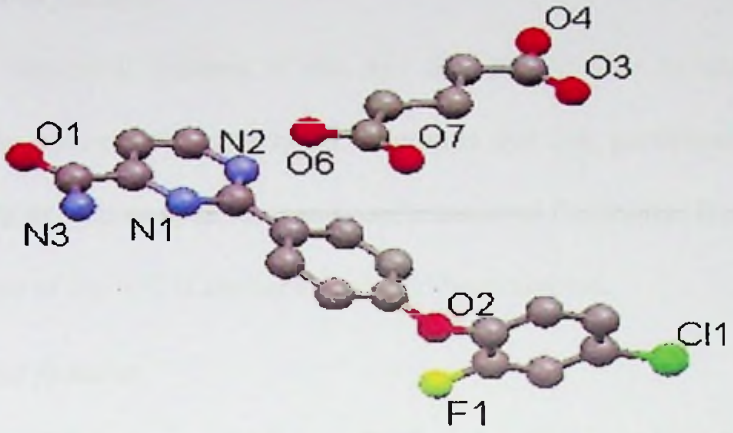

Figure 10: The structure of a co-crystal of glutaric acid.
Source: McNamara et al., 2006

Co-crystals have also been used to overcome undesirable physical properties, an example being that a co-crystal of caffeine with oxalic acid is non-hygroscopic, in contrast to crystalline caffeine, which absorbs atmospheric water to produce a hydrate (Trask, Motherwell, & Jones, 2005).

Selection of guests for a pharmaceutical co-crystal

Selection of guests for the formation of a pharmaceutical co-crystal, the host being the API, is typically based on the following criteria:

a) they have been used in commercial drug products and are thus known to be pharmaceutically acceptable (the greater the frequency of appearance the better);
b) they are nontoxic;
c) the size of the counter-ion relative to the API loading in the drug product.

Assessment of pharmaceutical co-crystals

Structural features

Structural features of the API that should also be assessed are the number, arrangement, and types of groups that can participate in hydrogen bonding as well as symmetry and conformational flexibility. If a single-crystal structure of the API is available it should be examined.

Thermal features

Another property of the API that should be evaluated is its thermal behaviour. In particular, its melting point and whether it melts without decomposition are important. For well-behaved compounds, thermomicroscopic methods provide a convenient and often-successful route to co-crystals.

Recrystallization and co-crystallization

Recrystallization is relied upon as a method of separation of a homogeneous solution containing two different molecular solutes because, unless a chemical reaction driven by the formation of covalent bonds takes place between the two solutes, one would, as a rule, expect the appearance of two separate molecular solids. This, as Dunitz said, is due to the 'inherent structural selfishness of molecules' (Dunitz, 1995) and this is relied upon every time recrystallization is employed as a method of purification.

Recrystallization processes represent essential steps during covalent synthetic procedures and are performed on a daily basis in every synthetic laboratory around the world. In the supramolecular laboratory, however, the very same process provides the supramolecular chemist with an opportunity to

move in a completely different direction—a co-crystallization is a deliberate attempt at bringing together different molecular species within one periodic crystalline lattice without making or breaking covalent bonds.

Recrystallization and co-crystallization processes are, in essence, only distinguishable by their intents. The goal of the former is a homomeric product, whereas the latter procedure strives for a heteromeric product (Figure 11); success for the former means failure for the latter.

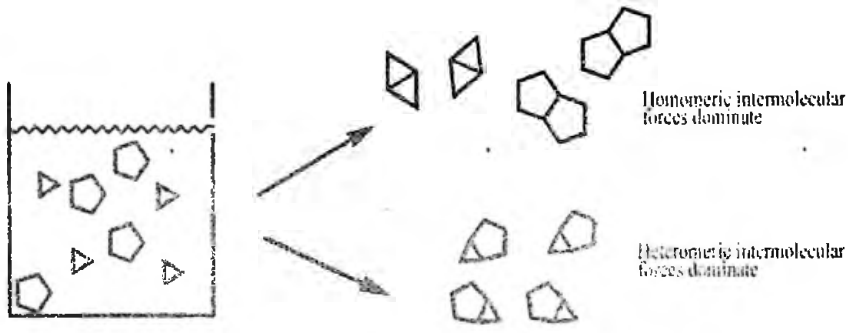

Figure 11: Recrystallization and Co-crystallization.

Source: Aakeröy & Salmon, 2005

Pharmaceutical co-crystals compared to salts

Pharmaceutical co-crystals are considered advantageous in the following situations:

a) drug molecules lacking easily ionisable functional groups (such as those containing phenol, carboxamide, weakly basic N-heterocyclic) can be intermolecular manipulated via co-crystals to tune their physicochemical properties,

b) compound having particular sensitive groups to treatment of acid and base,

c) overcoming problems in filterability through co-crystallizing a compound (Babu & Nangia, 2011; Halden, 2014).

On the other hand, use of the salt formulation approach to improve drug solubility does not work if the drug molecules lack ionisable functional groups, or have sensitive moieties that are prone to decomposition/racemization, and/or are not sufficiently acidic/basic to enable salt formation (Aakeröy, Fasulo, & Desper, 2007; Stahly, 2007; Childs, Stahly, & Park, 2007).

In their work, Babu and Nangia found that the peak dissolution for pharmaceutical co-crystals occurs in a short time (<30 min), and high solubility is maintained over a sufficiently long period (4–6 h) for the best cases. The enhanced solubility of drug co-crystals is similar to the supersaturation phenomenon characteristic of amorphous drugs.

They also noted that in contrast to the metastable nature of amorphous phases, co-crystals are stable owing to their crystalline nature. Moreover, co-crystals can exhibit dramatic solubility advantage over the stable crystalline drug form, often comparable to amorphous pharmaceuticals.

The "spring and parachute" concept for amorphous drug dissolution is adapted to explain the solubility advantage of pharmaceutical co-crystals as follows:

a) The co-crystal dissociates to amorphous or nanocrystalline drug clusters (the spring),

b) This transforms via fast dissolving metastable polymorphs to the insoluble crystalline modification following the Ostwald's Law of Stages.

c) This gives the high apparent solubility for co-crystals and optimal drug concentration (the parachute) in the aqueous medium (Babu & Nangia, 2011).

Poor dissolution rate, solubility, chemical stability and moisture uptake influence the therapeutic efficacy of many pharmaceuticals, and also significantly lower the market value of these drugs. Multi-component crystals (for example solvates, hydrates, co-crystals, salts, etc.) therefore play important roles in the design of new pharmaceuticals (Sekhon, 2009).

Physiochemical properties of pharmaceutical co-crystals

Co-crystals incorporate pharmaceutically acceptable guest molecules into a crystal lattice along with the API. Co-crystals are therefore alternate solid forms for drug development when drug molecules do not have the appropriate solid state properties. Co-crystals can also be developed if there are no ionization sites in the API (Miroshnyk, Mirza, & Sandler, 2009; Halden, 2014).

Physiochemical properties of pharmaceuticals can be improved by using co-crystallization principles and methods (Shan & Zaworotko, 2008; Trask, Motherwell, & Jones, 2006; Jones, Motherwell, & Trask, 2006) without changing their pharmacological behaviour in the process. (Schultheiss & Newman, 2009; Almarsson & Zaworotko, 2004; Zaworotko, 2008; Sun & Hou, 2008; Rodríguez-Hornedo, Nehm, & Jayasankar, 2007; Sekhon, 2009).

Pharmaceutical salts

Salts are often chosen instead of the free acid or base as these can improve crystallinity, solubility and stability of a pharmaceutical compound (Sekhon, 2009). Salt formation is an acid–base reaction between the API and an acidic or basic substance. The widespread use of salt formation is evidenced by the large number of marketed crystalline salts of APIs (Stahl & Wermuth, 2002; Serajuddin, 2007). Salt formation is a three component system having an acid (A), a base (B) and one or more solvents. A salt is formed by transfer of a proton (H+) from an acid (A) to base (B):

$$\mathbf{A\text{-}H + B \rightarrow (A^-)\ (B^+\text{-}\ H)}$$

To increase solubility, the drug could be made to undergo amorphisation to give an amorphous material (Halden, 2014).

Polymorphism and co-crystals

One proposed advantage concerning co-crystallization is their lower tendency to polymorphism than respective conformers. However, such a proposition was merely speculated based on a selected set of compounds.

Just like salts, co-crystal can also exhibit polymorphism. In some cases, it may be possible that a co-crystal may exhibit more complex polymorphism than individual coformers because of a larger number of possible spatial arrangements of multiple molecules in the crystal.

An increasing number of polymorphic co-crystals have been discovered in recent years (Childs & Hardcastle, 2007; Porter-III, Elie, & Matzger, 2008; Braga et al., 2008), some of which are trimorphic.

Whether the coformers or the co-crystal is more polymorphic depends on which one gives higher structural flexibility when crystallizing. Thus, tendency to polymorphism is linked to the total number of energy minima readily accessed by molecules but not to whether the crystal is composed of single or multiple components. In this context, it is advisable to screen, characterize and control polymorphs of a drug co-crystal similar to that for single component polymorphs (Stahly, 2007).

A key element for achieving the ultimate goal of *in silico* design of new co-crystal with desired pharmaceutical properties, is computational co-crystal screening and structure prediction (Karamertzanis et al., 2009). The direction will be the development of reliable computational methods capable of yielding accurate relative lattice energy.

Improved drugs using co-crystals

The use of co-crystals to alter the properties of pharmaceutically active compounds was reported as early as 1946, when Krantz et al (1947) found that the stoichiometric (1:1) co-crystal containing the sodium salt of theophylline and glycine increased the water solubility of the API. A clinical study using the co-crystal showed that it was tolerated in "unusually large amounts in man" and elicited the "typical theophylline response."

In the 1950s, Higuchi used solubility measurements to search for complex formation in solution between caffeine and a number of pharmaceutically active or acceptable compounds such as benzoic acid, benzoate ion, (Higuchi & Zuck, 1952; Higuchi & Zuck, 1953a) aspirin, 4-hydroxybenzoic acid, 3-hydroxybenzoic acid, salicylic acid, salicylate ion,

butyl paraben (Higuchi & Zuck, 1953b), sulfathiazole, sulfadiazine, 4-aminobenzoic acid, benzocaine, phenobarbital, and barbital (Higuchi & Lach, 1954).

Ultimately, he found and isolated co-crystals of caffeine and gentisic acid that had stoichiometries of 1:1 and 1:2 (caffeine/ gentisic acid) (Higuchi & Pitman, 1973). Those materials altered the pharmaceutically important property of dissolution rate, reducing the rate of dissolution of caffeine. Higuchi wrote:

"These complexes thus present a potentially useful way of formulating caffeine in dosage forms such as chewable tablets that are intended to linger in the mouth. Such dosage forms would only release caffeine slowly and should, consequently, have an improved taste factor over ones containing pure caffeine."(Higuchi & Pitman, 1973).

Some well-known drugs have had their properties improved using co-crystallization (Table 2).

Table 2: Known drugs and methods used to improve their properties

Drug	Category	Problem	Method to overcome problem
Aceclofenac & Paracetamol	Anti-Inflammatory, Analgesic & Antipyretic	Low Aqueous Solubility & Bioavailabilty	Solution Co-crystallization, Slurry Conversion, Liquid assisted grinding, Crystallization from Melt
Artesunate & Nicotinamide	Anti-Malarial	Low Efficacy & Bioavailability	Solvent Evaporation & Slurry Technique
Itraconazole	Antifungal	Low absorption in body	Antisolvent addition
Carbamazepne	Antiepileptic	Low water solubility & dissolution limited bioavailability	Slurry conversion
Indomethacine	NSAID	Practically insoluble in water	Solvent evaporation method
Didanosine & Aromatic drug (Benzoic acid & Salicylic acid)	Anti-HIV	Low solubility	Solvent drop grinding with methanol & acetonitrile
Ritonavir	Anti-retroviral	Low solubility	Solvent grinding method
Piracetam	Psychostimulant	Low solubility	Solution evaporation, solvent drop grinding and solvothermal
Caffeine	CNS stimulant		Solution evaporation

Source: Kotak et al., 2015

Mechanochemistry

The grinding of two solid substances generates a complex series of transformations, the mechanical energy breaking the order of the crystalline structure, producing cracks, and new surfaces. At the point of collision of the

edges the solids deform and even melt, forming hot points where the molecules can reach very high vibrational excitation leading to bond breaking. These stochastic processes occur in a period of 10^{-7} s. in which thermal equilibrium does not exist. This period, called the plasma phase, is followed by a post plasma period of 10^{-6} s. or more in which relaxation processes dissipate the energy reaching the Maxwell–Boltzmann distribution. This post plasmatic reactions are responsible for many of the products formed.

Finally, the energy accumulated in the defects of the crystalline structure can lead to slower chemical processes (Fernández-Bertran, 1999).

Mechano synthesis

It was a note by Burns and Bredig (1956) that first recorded the apparently anomalous formation of aragonite from calcite merely by grinding in a mortar. Jamieson and Goldsmith (1960) studied a number of carbonates more extensively. Among their results they found that the MgO content of natural calcites controlled the transition to aragonite, suggesting a pressure maximum in the mortar. They also found evidence of the formation of solid solutions on grinding $MgCO_3$ and $MnCO_3$ (Dachille & Roy, 1964).

Organic mechano synthesis processes are not only simpler and economical but also ecologically advantageous, eliminating the contamination of the surroundings with obnoxious chemicals.

An example of organic-mechano process, the implanting of pharmaceuticals on polymeric matrices for its transport in the organism, is also a promising pharmaceutical field (Fernández-Bertran, 1999).

The binding of small molecules to metals often imparts varied chemistry to the small molecules. Such chemistry is dependent on the coordination mode of the small molecule ligands, as the coordination mode affects the electronic distributions along the ligand atoms (Awasabisah & Richter-Addo, 2015).

Reguerra et al have also shown the non-occurrence of a linkage isomerization process in cadmium ferricyanide when this compound is heated or sonicated (Reguera, Balmaseda, Quintana, Gomez, & Fernandez-Bertran, 1998).

Toda (1993) also found that in most cases, solid state reactions proceed much faster than the solution reaction, probably because the solid state reaction is a very high concentration reaction. In the inorganic field there are experiences in the syntheses of alloys, cermets, spinels, semiconductors and superconductors, catalysts, fertilizer, ceramics construction materials, etc.

Aymard & Figlarz established that increasing the ratio of ball mass/initial powder mass decreases the time required for the formation of a crystalline alloy. At longer milling times, however, the crystalline alloy transforms into an amorphous alloy. They also established that the initial particle size the powders of the materials has an influenced the reaction kinetics and the morphology of the resulting alloys (Aymard & Figlarz, 1993).

Effect of hydrostatic pressure

Mechanical action on a solid is usually a combination of pressure and shift. Most thoroughly investigated are chemical changes that take place under hydrostatic pressure, or, three-axes loading, and the effect of pressure on chemical reactions that occurs in the system under mechanical action.

The studies of structural changes occurring under the action of pressure allowed for a series of important conclusions concerning the behaviour of hydrogen bonds in the course of phase transitions in molecular crystals. When investigating pressure-induced transformations in molecular crystals, a curious fact was discovered that different hydrogen bonds behave differently under the action of pressure on crystals. For example, in the crystals of deuterated oxalic acid under hydrostatic pressure, two hydrogen bonds are compressed, while the third one is stretched (Putkonen, Feld, Vettier, & Lehmann, 1985).

A detailed investigation of the changes in the structure of monoclinic b-hydroxyacetanilide under hydrostatic pressure was carried out (Boldyreva, Shakhtshneider, Vasilchenko, Ahsbahsc, & Uchtmannc, 1999). It was discovered that, along with the compression of O-H-O and N-H-O hydrogen bonds, the change of the torsion angle of the molecule occurs. The study also revealed an anisotropic structural distortion of the monoclinic polymorph of acetaminophen with increasing pressure. The hydrogen-bond network has been shown to play a major role in determining directions of major and minor structural compression, and also those of expansion with increasing pressure.

The combined action of pressure with shear

Along with the studies of the effect of hydrostatic pressure on physicochemical properties of solids, investigations were instituted in which mechanical action on solids involved, besides three-axial load, also a shift constituent

Dachille and Roy (1964), studied various solid phase processes in inorganic systems using the instrumentation especially constructed by them for

this purpose. They showed that the introduction of shift component along with simple loading under the mechanical action on solid, does not cause changes in the position of equilibrium point between the initial substance and the reaction product, but affects the process rate accelerating the transformation. This method was most successfully used for polymerization of solid monomers. The shift deformation caused a sharp acceleration of polymerization process.

The authors considered two possibilities to be the basis for this mechanism: Shift deformation causes the occurrence of some molecules in deformed metastable state; the reactions in which they participate require smaller activation energy. Another possible activation mechanism is explained as that the deformation energy decreases in a strained deformed molecule during the strain relaxation into vibration levels of separate bonds, thus increasing reactivity.

In covalent solids, a decrease of the forbidden zone width, under the conditions when pressure is accompanied by shift, occurs not only to bond length decrease, but because of angle changes between the bonds. The angle changes between bonds in covalent crystals lead to stronger overlapping of wave functions of valent electrons and thus simplify various processes connected with electron transfer, including oxidation–reduction reactions. Based on the observed transitions in diamond-framework semiconductors, Gilman concluded that the energy gaps in these materials vanished when compression caused the tetrahedral bond angle (109.5°) to increase to 148.2°. This is close to the average observed transformation angle of 149.2° (homopolar crystals) (Gilman, 1993).

Other examples of this combined action include metallization due to finite shear strains. For example, uniaxial compression of Si and Ge causes them to become metallic. Shear induced metallization has several important consequences, including: mechanically induced phase transformations, the hardness of semiconductors and carbides; and ultra-fast reactions at detonation fronts (Gilman, 1995).

Some chemical reactions, such as the detonation of explosives, can be initiated by mechanical forces. Unlike liquids or gases, solids can experience shear forces, and these in turn can cause bending of atomic bonds in molecules. The energy levels of these bent molecules can change in such a way as to lead to bond breaking and rearrangement (Gilman, 1996).

Phenomena occurring at stressing of particulate assemblies

The major factors inducing chemical transformations in solids under treatment are pressure and shift, as in the examples considered above, but their action on the substance is more complicated. For instance amorphisation plays a decisive role in the mechanical activation of particulate solids. This amorphisation is mainly controlled by the rate of stress and the efficiency of energy transfer in the mill (Tkáčová, Heegn, & Števulová, 1993).

A feature of all the devices used as grinding mills is pulse action (Courney, 1995), due to the mechanics of the motion of working bodies and substance under treatment in the mill. Another feature is local character of action (Urakaev & Boldyrev, 2000). Both these features form the grounds of the kinetic model of mechanical activation proposed by Boldyrev (Boldyrev & Tkáčová, 2000).

Mechanical Activation

Mechanical activation is usually a result of disordering of the crystal and generation of defects or other metastable forms that cause the decrease of activation barrier for the process. Mechanical action causes the appearance of strain field in a solid under treatment. The strain field manifests itself specifically by the shifts of atoms from the equilibrium stable positions at lattice nodes, the changes of bond lengths and angles, and, in some cases, the excitation of electron subsystem (Boldyrev & Tkáčová, 2000).

All these states are metastable, so their formation is followed by relaxation via different channels:

1. The relaxation of the energy (accumulated in strain field) into heat.
2. Plastic deformation- The accumulation of energy at this channel, in the case when there are sites in a crystal in which the strain is concentrated, can lead to the destruction of the crystal (crushing) and thus to the formation of a new surface.
3. Reduction in the size of crystals to some critical value. Further energy supply to these crystals of limiting size causes further deformation of crystals, energy accumulation in the volume or at the surface of crystals, and finally amorphisation.

In some cases, the defects are formed in order, and instead of amorphisation, transition into a metastable polymorphous state occurs. Sometimes the relaxation of strain field results in the rupture of chemical bonds (mechanochemical reaction occurs).

The four processes, namely, the accumulation of defects, amorphisation, the formation of metastable polymorphous forms, and chemical reaction, are united by the term "mechanical activation". All the three relaxation channels cause the changes of reactivity of the solid substance under treatment, which is why the resulting action is called mechanical activation. Disordering can lead not only to the accumulation of linear and point defects, but also to more exotic structural distortions.

It has been shown that not all chemical interactions occurring under mechanical action on a solid are thermally initiated processes. For instance, thermal and mechanochemical decomposition of the bromides of alkaline metals lead to different products and also the rows of mechanochemical and thermal stability of nitrates do not coincide with each other (Boldyrew, Awwakumow, Strugowa, Harenz, & Heinicke, 1972). In the studies of the composition of products formed in a top of a crack during the cleavage of potassium nitrate crystals, nitrogen oxide instead of oxygen (the product from a thermal decomposition) is evolved at the top of a crack if the crack moves sufficiently fast.

Compounding of Drugs

Compounding of drugs is the practice where a given drug is modified to have specific characteristics. It may also include changing the form of a medication from a solid pill to a liquid.

Compounding of drugs is done for reasons such as removal of a non-essential ingredient in a solid pill that a patient is allergic to, or to get the right

dose of (a) particular active pharmaceutical ingredient(s), API, for the patient. Compounding is also done to change the taste (by adding flavours) and/or the texture of a drug.

When a drug is compounded specifically for an individual, the process is known as 'traditional' compounding. This is in contrast to 'Non-traditional' compounding when a given formulation is compounded on a large scale (bulk production).

Combination Drugs and Products

Combination drugs are drug/drug combinations developed and tested and are effective, stable, easy to use and acceptable to patients for example Caduet (atorvastatin/amlodipine) or Exforge (amlodipine/valsartan) (BayviewPharmacy, 2009). A combination product on the other hand refers to products that combine different types of medical products, for example device/drug combination for use by patients (US-FDA, 2009). One advantage of a combination drug is improved medication compliance by reducing the 'pill burden' of patients. Note that 'pill burden' is not only the number of pills needing to be taken, but also the associated burdens such as keeping track of several medications, understanding their various instructions, etc. Another advantage is that such a combined drug profile can also include effects caused by interaction between the individual drugs that may be omitted in individual drug profiles. One disadvantage however is that in cases where an adverse drug reaction occurs from using a combined drug, it may be difficult to identify the active ingredient responsible for causing the reaction (Netland, 2008).

Neglected Tropical Diseases

Tropical diseases are diseases that are prevalent in or unique to tropical and subtropical regions (Farrar et al., 2013). Neglected Tropical Diseases (NTDs) are a medically diverse group of tropical infections which are especially common in low-income populations in developing regions of Africa, Asia, and the Americas. They are caused by a variety of pathogens such as viruses, bacteria, protozoa and helminths (Hotez et al., 2007; US-CDC, 2011).

The NTD caused by bacteria and protozoa are *Trachoma* (bacteria), *Buruli Ulcer* (bacteria), *Yaws* (bacteria), *Leprosy* (bacteria), *Chagas disease* (protozoa), *Human African trypanosomiasis* (sleeping sickness) (protozoa), *Leishmaniases* (protozoa), and *Mycetoma* (bacteria and/or fungi) (NTD, 2017). Patients of these diseases sometimes suffer from inflammations also.

Trachoma is a chlamydial infection transmitted through direct contact with infectious eye or nasal discharge, or through indirect contact with unsafe living conditions and hygiene practices, which when left untreated causes irreversible corneal opacities and blindness. Trachoma is a disease of the eye caused by infection with the bacterium *Chlamydia trachomatis*.

Buruli ulcer is a debilitating mycobacterial skin infection causing severe destruction of the skin, bone and soft tissue. It is caused by the *Mycobacterium ulcerans* bacterium.

Yaws is a chronic bacterial infection affecting mainly the skin and bone. Yaws forms part of a group of chronic bacterial infections commonly known as the endemic treponematoses.

Leprosy is a complex disease caused by infection mainly of the skin, peripheral nerves, mucosa of the upper respiratory tract and eyes. Leprosy is a chronic disease caused by a slow multiplying bacillus, *Mycobacterium leprae*

Chagas disease is a life-threatening illness transmitted to humans through contact with vector insects (triatomine bugs), ingestion of contaminated food, infected blood transfusions, congenital transmission, organ transplantation or laboratory accidents. Chagas disease, also known as American trypanosomiasis, is a potentially life-threatening illness caused by the protozoan parasite *Trypanosoma cruzi (T. cruzi).*

Human African trypanosomiasis (sleeping sickness) is a parasitic infection spread by the bites of tsetse flies that is almost 100% fatal without prompt diagnosis and treatment to prevent the parasites invading the central nervous system. It is caused by infection with protozoan parasites belonging to the genus *Trypanosoma.*

Leishmaniases is a disease transmitted through the bites of infected female sandflies that in its most severe (visceral) form attacks the internal organs and in its most prevalent (cutaneous) form causes face ulcers, disfiguring scars and disability. Leishmaniasis is caused by the protozoan *Leishmania* parasites.

Mycetoma is a chronic, progressively destructive inflammatory skin disease which usually affects the lower limbs. Infection is thought to be caused by the inoculation, through a thorn prick or skin damage, of fungi or bacteria into the subcutaneous tissue.

Compounds Used in Study

Three compounds were used in this study. They are Ferron, (also known as 8-Hydroxy-7-iodoquinoline-5-Sulfonic acid), Sulphamethoxazole and Carbazole.

Ferron

Other names are 8-hydroxy-7-iodoquinoline-5-sulphonic acid, 8-Hydroxy-7-iodo-5-quinolinesulfonic acid, 5-Sulfo-7-iodo-8-hydroxyquinoline; 5-Sulfo-7-iodo-8-quinolinol; 7-Iodo-5-sulfonic acid-8-hydroxyquinoline (LookChem, 2008).

Uses of Ferron

- It is used as an anti-amoebic drug.
- A mixture of Ferron and sodium bicarbonate is known as Chiniofon and is used to treat amoebic dysentery (Drugs.com, 2016).
- Ferron is a bidentate complexing agent similar to 8-hydroxyquinoline (oxine) but with greater selectivity due to the steric requirements of the 7-iodo substituent.
- It is a reagent, which has analytical applications as a selective colour reagent for the detection of iron(III) but not iron(II) (Svehla, 1979).
- It imparts water solubility to complex species, allowing its use as a colorimetric reagent for quantitative analysis (IUPAC, 1963) due to the presence of the sulfonic acid group.

The molecular structure of Ferron using IUPAC numbering is given below (Figure 12).

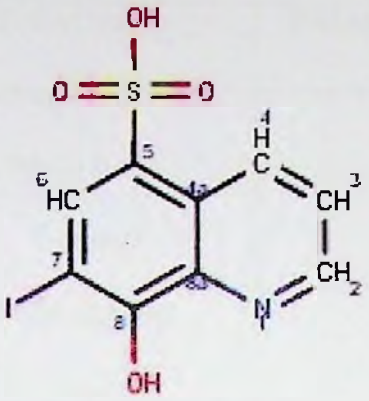

Figure 12: Molecular Structure of Ferron.

Source: Marvin Beans Suite, 2015

General Properties of Ferron

1. It is almost odourless and tasteless.
2. One gram dissolves in 500 mL cold (25°C), 170 mL boiling water; slightly soluble in alcohol, practically insoluble in ether or oils.
3. When heated to decomposition (Table 2), it emits toxic fumes of NO_x and SO_x.

Table 3: Physical and Chemical Properties of Ferron

IUPAC name	8-Hydroxy-7-iodo-5-quinolinesulfonic Acid
Molecular formula	$C_9H_6INO_4S$
Molar mass	351.12 g/mole
Density	2.193 g/cm^3
Melting point	269-270°C (decomp.)
Boiling point	N/A
Appearance	Sulphur yellow crystalline powder (Figure 13)

Figure 13: Ferron.

Crystal Structure of Ferron

Merritt Jnr and Duffin determined the crystal structure of Ferron in 1970 and report the following parameters: A monoclinic unit cell of dimensions a = 9.55, b = 13.35, c = 8.83 Å, β = 109.2°, and a $P2_1/c$ space group with cell formula units, Z, = 4 (Merritt-Jnr & Duffin, 1970).

Based on potentiometric and spectrophotometric studies they did on 8-quinolinol and its derivatives in 1952, Näsänen and Ekman proposed that Ferron was zwitterionic in acidic solutions (Näsänen & Ekman, 1952).

Balasubramanian & Muthiah later re-determined the crystal structure and confirmed it to be zwitterionic. They reported the following parameters: A monoclinic unit cell of dimensions a = 9.5704(9), b = 13.364(2), c = 8.748(2) Å, β = 108.834(10)° cell formula units, Z, = 4 and P 21/c space group (Balasubramanian & Muthiah, 1996).

Donor and Acceptor sites in Ferron

At a pH of 7, Ferron has 1 donor site, D, and 6 acceptor sites, A (Figure 14).

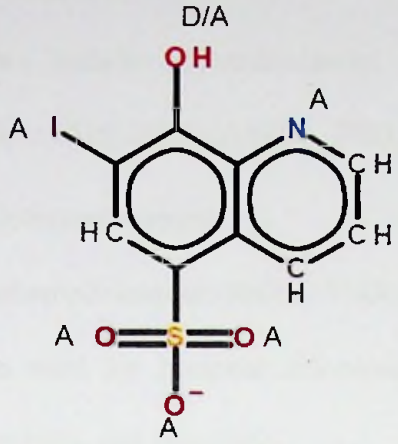

Figure 14: Donor (D) and Acceptor (A) sites on Ferron molecule.

Source: Marvin Beans Suite, 2015

Dissociation Constants of Ferron

The molecule (Figure 15) has three ionisable hydrogens but with two positive pKa, 2.82 and 7.42, and one negative pKa, -4.37 ("Marvin Beans Suite," 2015). There are various major microspecies of the molecule at different pHs.

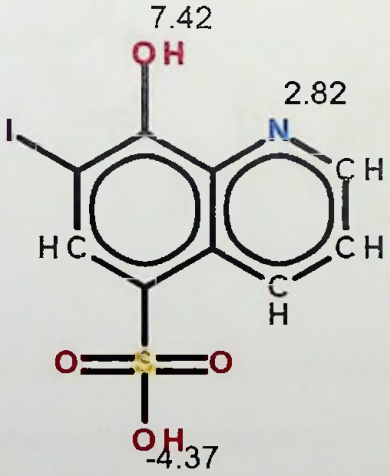

Figure 15: Ionisable hydrogens and pKas of Ferron.

Source: Marvin Beans Suite, 2015

Sulphamethoxazole

Other names include sulfamethalazole, sulfisomezole, and sulfamethazole (Merck Index, 2016; Sigma-Aldrich, 2003).

Uses of Sulphamethoxazole

- Sulphamethoxazole (SMZ or SMX), is an antibiotic and a bacteriostatic.
- It is used for bacterial infections such as urinary tract infections, bronchitis, and prostatitis.
- It is effective against both gram negative and positive bacteria such as Listeria monocytogenes and E. coli.
- It is now commonly used as part of a combination with trimethoprim (abbreviated SMX-TMP).

The IUPAC atom labelling of the Sulphamethoxazole molecule is given (Figure 16).

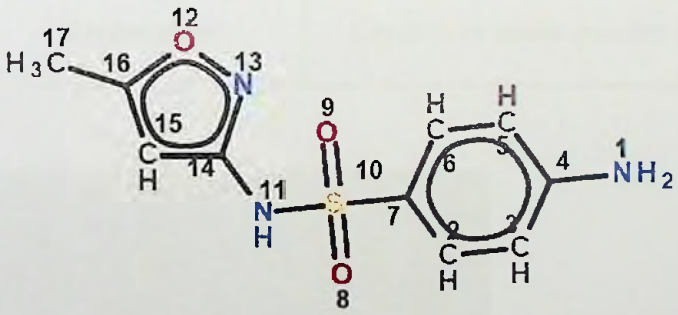

Figure 16: Molecular structure of Sulphamethoxazole.

Source: Marvin Beans Suite, 2015

General Properties of Sulphamethoxazole

1. Sulphamethoxazole is practically insoluble in water, ether, chloroform and sparingly soluble in alcohol.

2. Sulphamethoxazole is soluble 1 in 50 of alcohol and 1 in 3 of acetone, in alkali hydroxides.
3. It forms bitter crystals from dilute ethanol.

The physical and chemical properties of Sulphamethoxazole are given below (Table 4).

Table 4: Physical and Chemical Properties of Sulphamethoxazole

IUPAC name	4-Amino-*N*-(5-methylisoxazol-3-yl)-benzenesulfonamide
Molecular formula	$C_{10}H_{11}N_3O_3S$
Molar mass	253.27 g/mole
Density	1.462 g/cm3
Melting point	166°C
Boiling point	482.1°C
Appearance	Crystals or white powder (Figure 17)

Figure 17: Sulphamethoxazole.

Crystal Structure of Sulphamethoxazole

The crystal structures of two polymorphs of Sulphamethoxazole have been published by Price et al. (2005). The parameters are given below (Table 5).

Table 5: Crystal Lattice Parameters of Sulphamethoxazole

Common name	Sulphamethoxazole	
Formula	$C_{10}H_{11}N_3O_3S$	$C_{10}H_{11}N_3O_3S$
Calculated formula	$C_{10}H_{11}N_3O_3S$	$C_{10}H_{11}N_3O_3S$
a	11.64 ± 0.003 Å	5.4895 ± 0.0009 Å
b	6.8189 ± 0.0019 Å	16.761 ± 0.003 Å
c	15.419 ± 0.004 Å	12.422 ± 0.002 Å
α	90°	90°
β	107.106 ± 0.005°	97.08 ± 0.002°
γ	90°	90°
Cell volume	1169.7 ± 0.6 $Å^3$	1134.2 ± 0.3 $Å^3$
Cell temperature	153 ± 2 K	153 ± 2 K
Ambient diffraction temperature	153 ± 2 K	153 ± 2 K
Number of distinct elements	5	5
Space group	P 1 21/c 1	P 1 21/n 1

Donor and Acceptor sites in Sulphamethoxazole

At a pH of 7, there are 2 donor sites, D, and 8 acceptor sites, A, on the molecule. The sites on the major microspecies at a pH of 7 are given (Figure 18) ("Marvin Beans Suite," 2015).

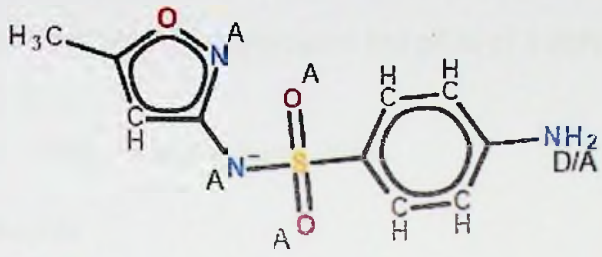

Figure 18: Donor (D) and Acceptor (A) sites on Sulphamethoxazole molecule.

Source: Marvin Beans Suite, 2015

Dissociation Constants of Sulphamethoxazole

The hydrogens on the various nitrogen atoms in the molecule are ionisable but to different extents from 0.25 to 6.16 ("Marvin Beans Suite," 2015) as shown (Figure 19). At various pHs, different microspecies of the molecule are prevalent.

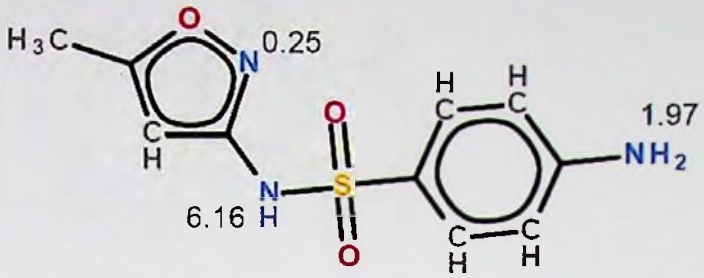

Figure 19: Ionisable hydrogens and pKas of Sulphamethoxazole.

Source: Marvin Beans Suite, 2015

Carbazole

Other names include 9-azafluorene, 9H-Carbazol , 9H-Carbazole, 9H-Carbazole, carbazol and dibenzopyrrole.

Uses of Carbazole

- It is an important dye intermediate used in making of photographic plate.
- Due to extended π-electron bond, Carbazole is used in luminescence chemistry as a photo-sensitising and additional charge transport material.
- 4, 4'-Bis (carbazol-9-yl) biphenyl is used as an OLED hole transport material.
- Carbazole is used as a reagent in analysis of carbohydrates, lignin and formaldehydes

The IUPAC numbering of the atoms in Carbazole is as follows (Figure 20).

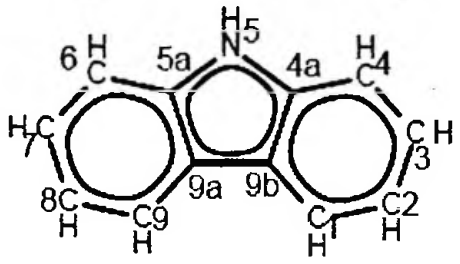

Figure 20: Molecular Structure of Carbazole.

Source: Marvin Beans Suite, 2015

General Properties of Carbazole

1. Carbazole is an extremely weak base.
2. It dissolves in quinolone, acetic acid, petroleum ether, benzene, absolute alcohol and concentrated sulphuric acid.
3. With potassium hydroxide (KOH), carbazole yields *N*-potassium salt.
4. Poly (9-vinylcarbazole) is an organic semiconductor.
5. It exhibits strong fluorescence and long phosphorescence on exposure to ultra violet light.

The physical and chemical properties of Carbazole are given in Table 6.

Table 6: Physical and Chemical Properties of Carbazole

IUPAC name	9*H*-carbazole
Molecular formula	$C_{12}H_9N$
Molar mass	167.206 g/mole
Density	1.301 g/cm3
Melting point	246.3°C
Boiling point	354.69°C
Appearance	Off-white crystalline powder (Figure 21)

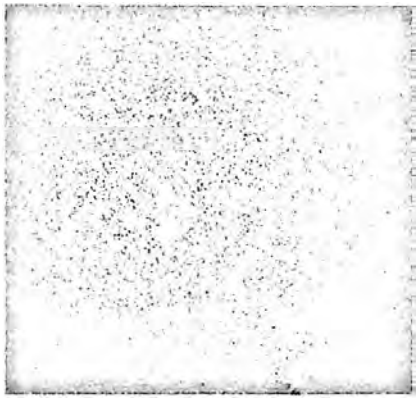

Figure 21: Carbazole.

Crystal Structure of Carbazole

A partial determination of the structure of Carbazole was undertaken in 1968 by Robinson and Scott (1969). They reported that the symmetry is orthorhombic, space group *Pnam*, and the lattice parameters are a=7.779 Å, b=5.722 Å, c=19.15 Å. The structure has four molecules in the unit cell arranged in two close packed layers parallel to the (001) plane.

In a redetermination of the crystal structure of Carbazole, Gajda et al reported a space group *of Pnma* and an orthorhombic crystal system (Gajda, Zarychta, Kopka, Daszkiewicz, & Ejsmont, 2014). The lattice parameters (unit cell dimensions) were $a = 7.6371$ (2) Å, $b = 19.0042$ (6) Å, $c = 5.67758(14)$ Å. They confirmed that the structure had 4 molecules in the unit cell ($Z = 4$).

Donor and Acceptor sites in Carbazole molecule

There is only one donor site, D, in the Carbazole molecule at the nitrogen atom at a pH of 7 (Figure 22).

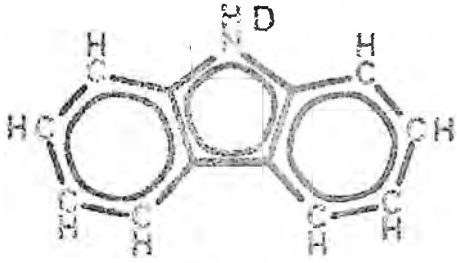

Figure 22: Donor (D) site in Carbazole molecule.

Source: Marvin Beans Suite, 2015

Dissociation Constant of Carbazole

This dissociation constant is a quantitative measure of the strength of an acid in solution. An acid dissociation constant, K_a, (also known as acidity constant, or acid-ionization constant) is a quantitative measure of the strength of an acid in solution. pK_a is a logarithmic measure of the acid dissociation constant, $-\log_{10}K_a$. The larger the value of pK_a, the smaller the extent of dissociation at any given pH that is, the weaker the acid. A weak acid has a pK_a

value in the approximate range −2 to 12 in water (Wikipedia contributors, 2016a).

The pKa of Carbazole is 14.97 ("Marvin Beans Suite," 2015). The ionisable hydrogen is that on the nitrogen (Figure 23).

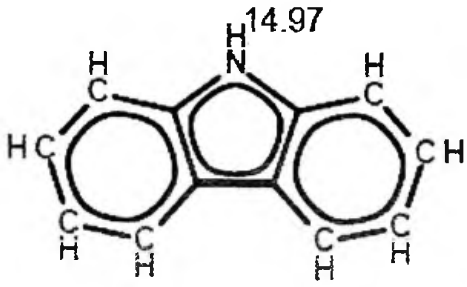

Figure 23: Ionisable hydrogen and pKa of Carbazole.
Source: Marvin Beans Suite, 2015

Chapter Summary

The chapter looked at co-crystallization, the methods and techniques used in preparing co-crystals and characteristics of molecules which form co-crystals under mechanochemical regimes. The candidate compounds used in the study have these characteristics and the methods and techniques used for co-crystal preparation in this study conform to those suggested in literature.

The co-crystals to be formed are Ferron with Sulphamethoxazole and Ferron with Carbazole. The techniques for characterization of co-crystals have also been established and most of them are used in this study.

CHAPTER THREE

MATERIAL AND METHODS

This chapter presents the materials and equipment used in preparing the co-crystals of Ferron with Sulphamethoxazole and Ferron with Carbazole, and the instruments used in the analysis of the starting materials and co-crystals formed. The chapter also covers the methods used in the preparation and analysis of the products including the quantities of material used in each experiment and the names of the various samples used for analysis.

Material

The starting compounds, Ferron (8-Hydroxy-7-Iodoquinoline-5-Sulfonic Acid) (Spot-Test reagent grade) and Carbazole (98% purity Analar grade) were acquired from BDH Chemicals, Poole, England and Sulphamethoxazole (98% purity Analar grade) acquired from Central Drug House (CDH), New Delhi, India.

The Ethanol was purchased from Pharmacos Banbury, United Kingdom. The purity was 99.7 – 100%, Analar Grade. The distilled water used was prepared at the Institute of Industrial Research using an Accumax (India) stainless steel water distillation unit. All chemicals were used without further purification.

Solvent system

A solvent system comprising ethanol and water in the volume ratio of 1:1 was used in this study. The solvents were selected based on the solubility of the compounds, Ferron, Sulphamethoxazole and Carbazole, as reported in literature.

Equipment

The following equipment were used in the study.

1. The *Panalytical Empyrean Powder X-ray Diffractometer* (Plate 1). Manufactured by PANalytical B.V., The Netherlands. The anode material is Cu with the K-Alpha1 wavelength 1.5406 Å, K-Alpha2 as 1.54443 Å and K-Beta 1.39225 Å.

Plate 1: PANalytical Empyrean Powder X-Ray Diffractometer.

2. The *FRITSCH Pulverisette 2 Laboratory Mortar Grinder* (Plate 2). Manufactured by Fritsch GmbH, Idar-Oberstein, Germany. It can be used for universal dry and wet milling to a fineness level suitable for analysis. It crushes mineral and organic samples for analysis, quality checks or material testing, for example, drugs, tablets, pastes, synthetic organic plant materials, etc. The material in the laboratory mortar grinder is crushed with the use of pressure and friction.

3. *PerkinElmer UATR Two InfraRed Spectrometer* (Plate 3). Manufactured by PerkinElmer, Inc. Waltham, U.S.A. This equipment can be used to analyse solid samples in powder form. It uses a fixed mirror-pair digitized interferometer design incorporating a simple, non-critical bearing.

4. *Spectroquant UV/VIS Spectrophotometer Pharo 300* (Plate 4). Manufactured by Merck KGaA, Darmstadt, Germany. It has a wavelength spectrum from 190 to 1100 nm, a xenon flashlamp and a grating monochromator with step motor. The accuracy is ± 1 nm and resolution is 1 nm.

Plate 2: FRITSCH Pulverisette 2 Laboratory Mortar Grinder.

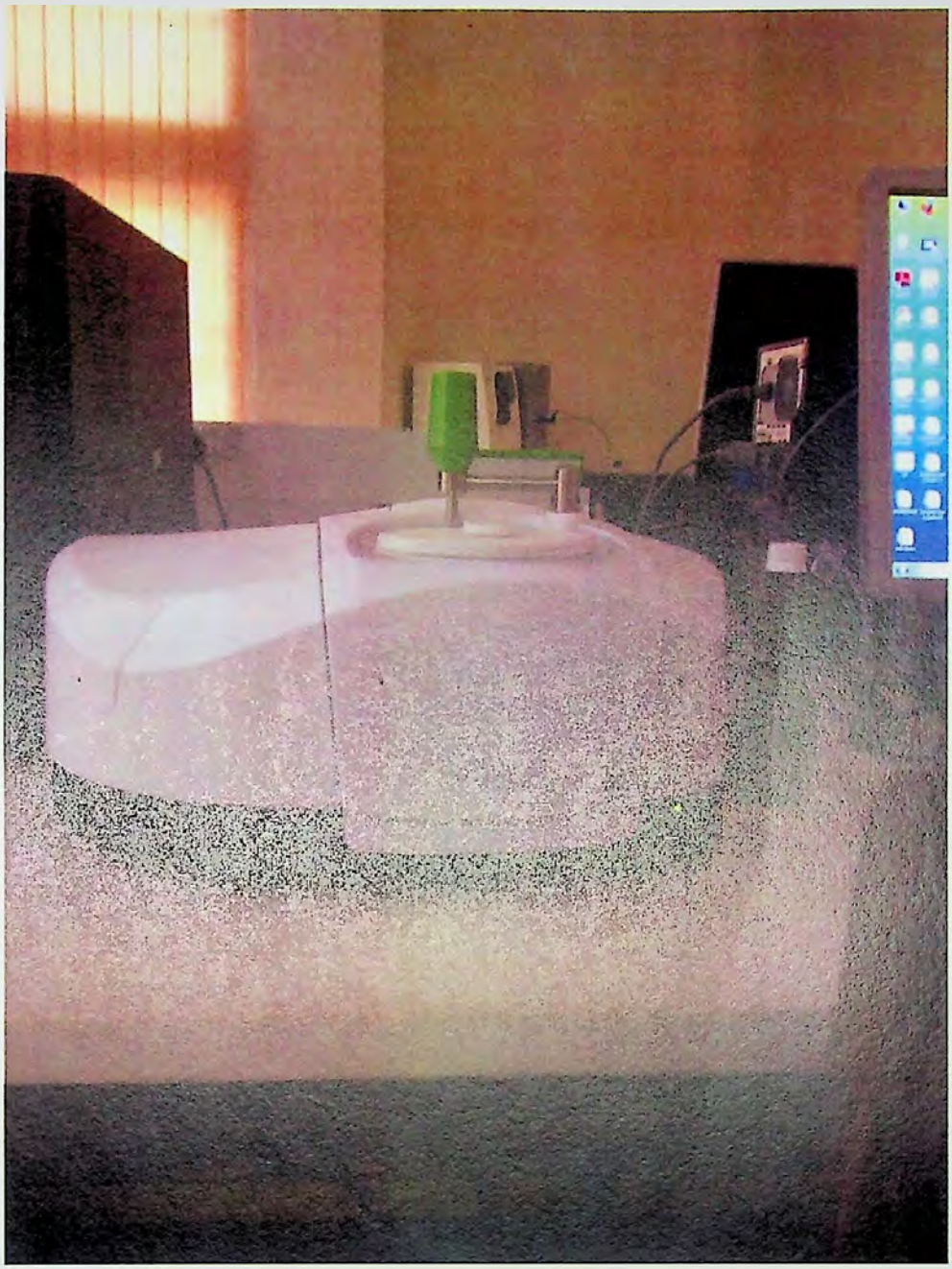

Plate 3: PerkinElmer UATR Two InfraRed Spectrometer.

Plate 4: Spectroquant UV/VIS Spectrophotometer Pharo 300.

5. *TA INSTRUMENTS SDT-Q600 Simultaneous Differential Thermal Analyzer V20.9 Build 20* (for Thermogravimetric analysis - TGA) (Plate 5). Manufactured by TA Instruments, New Castle, DE, U. S. A. The SDT-Q600 provides an accurate simultaneous measurement of weight change.

6. *Mettler Toledo DSC 822e* (for Differential Scanning Calorimetry) (Plate 6). Manufactured by Mettler-Toledo GmbH, Analytical, Schwerzenbach, Switzerland. A highly sensitive ceramic sensor is used to measure the difference between the heat flows to the sample and reference crucibles based on the Boersma principle.

7. *JEOL JSM-6390LV Scanning Electron Microscope (SEM)* (Plate 7). Manufactured by JEOL USA, Inc, Peabody, Massachusetts, U. S. A. This is a powerful magnification tool that utilizes focused beams of electrons to obtain information. The high-resolution, three-dimensional images produced by SEMs provide topographical, morphological and compositional information. SEMs handle solid, inorganic samples that can handle moderate vacuum pressure. The tungsten-filament SEM utilizes a tilting and rotating mechanical stage. It incorporates low vacuum back-scattered electron imaging for acquisition of high-resolution images of non-conductive, unprocessed samples.

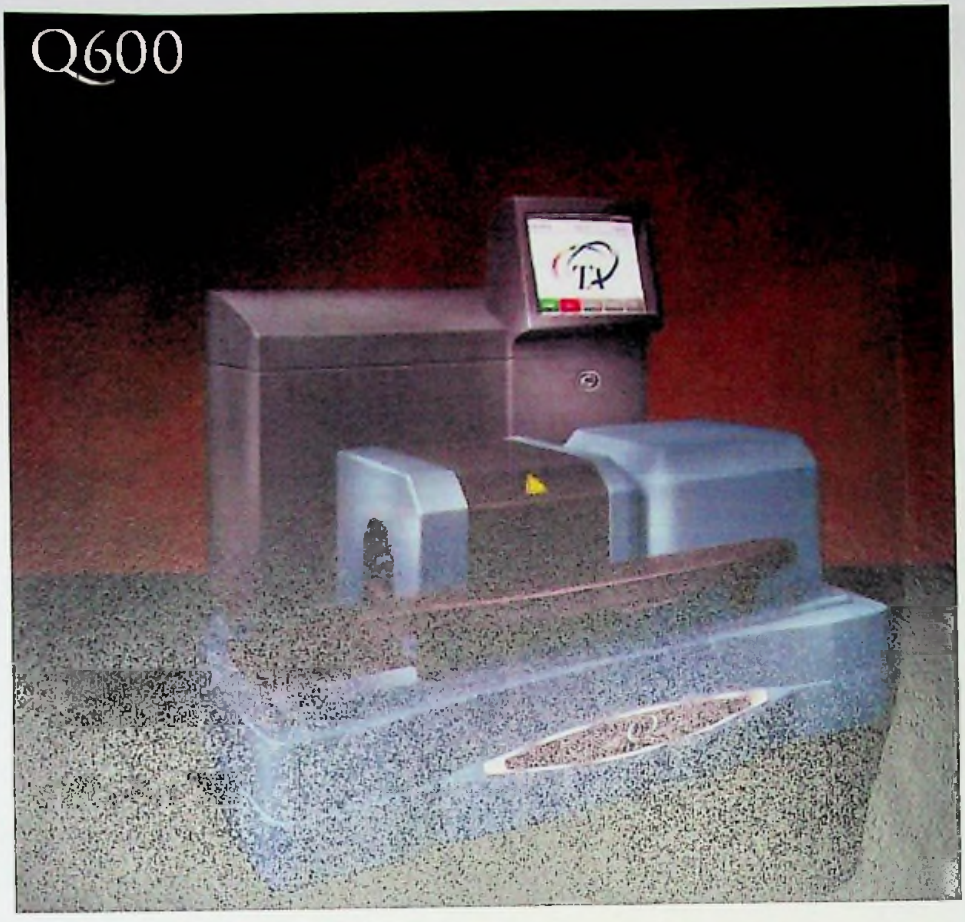

Plate 5: TA Instruments Q600-SDT V20.9 Build 20.

Plate 6: Mettler Toledo DSC 822e.

Plate 7: JEOL JSM-6390LV Scanning Electron Microscope.

8. *Stuart Melting Point Apparatus SMP 10* (Plate 8). Manufactured by Bibby Scientific Ltd., Staffordshire, United Kingdom. This equipment has been designed for maximum safety and ease of use. The temperature can be selected, measured and displayed digitally ensuring accuracy and avoiding the use of a glass thermometer.

9. *Cyberscan 2100 pH meter* (Plate 9). Manufactured by Eutech Instruments, Singapore. This equipment is used for water quality testing, soil/fertilizer testing, food processing (for HACCP compliance), R&D and QC applications in the food and pharmaceutical industries, paper/pulp processing, chemical industries and related fields. It features direct ion concentration measurement with use of many Ion Selective Electrodes. This pH meter is available at the Chemistry Laboratory of the Institute of Industrial Research (I. I. R.) of the Council for Scientific and Industrial Research (C. S. I. R.), Ghana.

Plate 8: Stuart Melting Point Apparatus.

Plate 9: Cyberscan 2100 pH meter.

Combination of Materials in Different Ratios

Materials were combined in the ratios of 1:1, 1:2, 1:3, 1:4, 2:1, 3:1, 4:1 [Ferron:Sulphamethoxazole or Ferron:Carbazole]. An analysis of the products from these combinations showed that only the 1:1 ratio of starting materials gave co-crystals.

Mechano-Synthesis of Ferron and Sulphamethoxazole

Equimolar quantities of Ferron with Sulphamethoxazole were measured into a mortar bowl of a Fritsch 'Pulverisette 2' Mortar Grinder and mechano-synthesized. This equipment is located at the Ghana Atomic Energy Commission, Reactor Centre Laboratory.

The sample names/codes for the various products are given (Figure 24). The resulting combined products were characterised. Details of the sample preparations for each characterisation are given below.

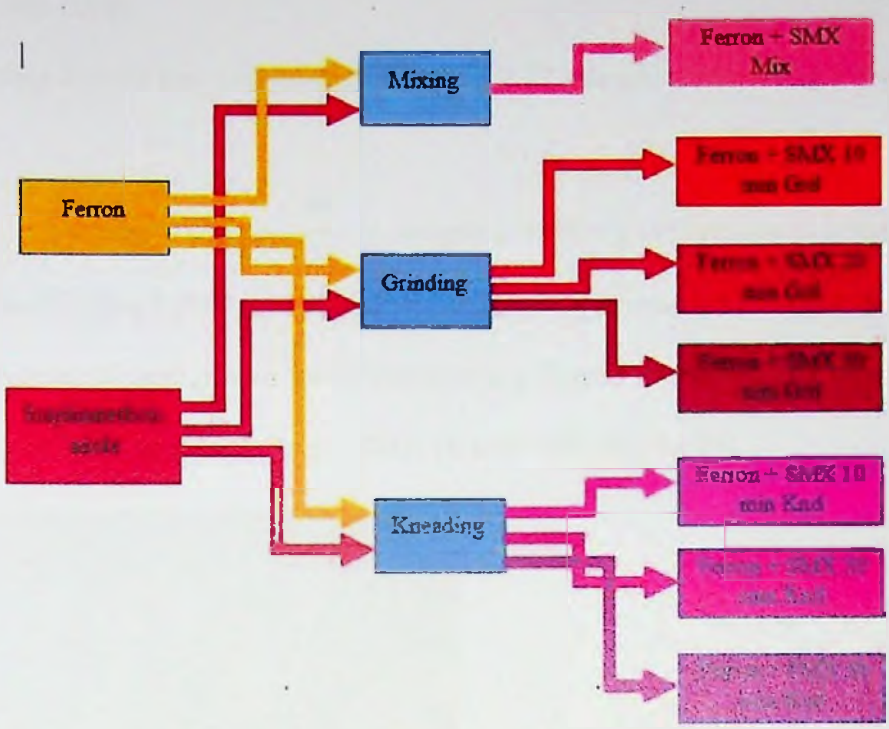

Figure 24: Scheme of Mechano-synthesis of combinations of Ferron and Sulphamethoxazole.

Ferron combined with Sulphamethoxazole

Measured quantities of Ferron (Figure 13) and Sulfamethoxzole (SMX) (Figure 17) were combined together mechano-chemically as indicated as follows:

Grinding (Grd)

Grinding Ferron and Sulphamethoxazole for 10 min (Ferron + SMX 10 min Grd)

This sample was prepared by weighing 0.6965 g of Ferron into a mortar bowl and adding 0.5005 g of Sulphamethoxazole representing a 1:1 mole ratio. The mixture is then ground for 10 minutes in a Fritsch 'Pulverisette 2' Mortar Grinder to give sample 'Ferron + SMX 10 min Grd' (Figure 25).

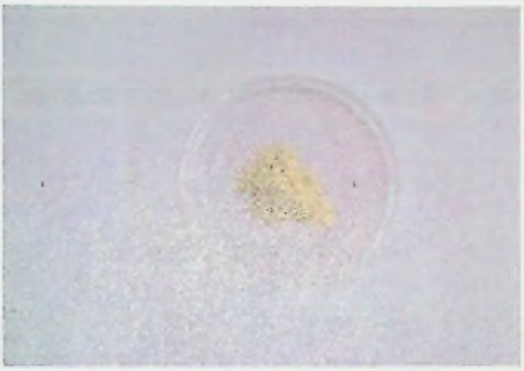

Figure 25: Ferron + SMX 10 min Grd.

Grinding Ferron and Sulphamethoxazole for 20 min (Ferron + SMX 20 min Grd)

This sample was prepared by weighing 0.6941 g of Ferron into a mortar bowl and adding 0.4995 g of Sulphamethoxazole, representing a 1:1 mole ratio. The mixture is then ground for 20 minutes in a Fritsch 'Pulverisette 2' Mortar Grinder to give sample 'Ferron + SMX 20 min Grd' (Figure 26).

Figure 26: Ferron + SMX 20 min Grd.

Grinding Ferron and Sulphamethoxazole for 30 min (Ferron + SMX 30 min Grd)

This sample was prepared by weighing 0.6966 g of Ferron into a mortar bowl and adding 0.4972 g of Sulphamethoxazole, representing a 1:1 mole ratio. The mixture is then ground for 30 minutes in a Fritsch 'Pulverisette 2' Mortar Grinder to give sample 'Ferron + SMX 30 min Grd' (Figure 27).

Figure 27: Ferron + SMX 30 min Grd.

Kneading (Knd)

Kneading Ferron and Sulphamethoxazole for 10 min (Ferron + SMX 10 min Knd)

This sample was prepared by weighing 0.6917 g of Ferron into a mortar bowl and adding 0.5004 g of Sulphamethoxazole, representing a 1:1 mole ratio. Five drops of the solvent system of Ethanol:Water (1:1 vol) was added to the mixture. The mixture is then kneaded for 10 minutes in a Fritsch 'Pulverisette 2' Mortar Grinder to give sample 'Ferron + SMX 10 min Knd' (Figure 28).

Figure 28: Ferron + SMX 10 min Knd.

Kneading Ferron and Sulphamethoxazole for 20 min (Ferron + SMX 20 min Knd)

This sample was prepared by weighing 0.6978 g of Ferron into a mortar bowl and adding 0.5020 g of Sulphamethoxazole, representing a 1:1 mole ratio. Five drops of the solvent system of Ethanol:Water (1:1 vol) was added to the mixture. The mixture is then kneaded for 20 minutes in a Fritsch 'Pulverisette 2' Mortar Grinder to give sample 'Ferron + SMX 20 min Knd' (Figure 29).

Figure 29: Ferron + SMX 20 min Knd.

Kneading Ferron and Sulphamethoxazole for 30 min (Ferron + SMX 30 min Knd)

This sample was prepared by weighing 0.6898 g of Ferron into a mortar bowl and adding 0.4992 g of Sulphamethoxazole, representing a 1:1 mole ratio. Five drops of the solvent system of Ethanol:Water (1:1 vol) was added to the mixture. The mixture is then kneaded for 30 minutes in a Fritsch 'Pulverisette 2' Mortar Grinder to give sample 'Ferron + SMX 30 min Knd' (Figure 30).

Figure 30: Ferron + SMX 30 min Knd.

Mixing (Mix)

Mixing Ferron and Sulphamethoxazole (Ferron + SMX Mix)

This sample was prepared by weighing 0.6925 g of Ferron into a mortar bowl and adding 0.5017 g of Sulphamethoxazole, representing a 1:1 mole ratio. The mixture is then carefully mixed using a spatula for 5 minutes to give sample 'Ferron + SMX Mix' (Figure 31).

Figure 31: Ferron + SMX Mix.

Mechano-Synthesis of Ferron and Carbazole

Equimolar quantities of Ferron with Carbazole were measured into a mortar bowl of a Fritsch 'Pulverisette 2' Mortar Grinder and mechano-

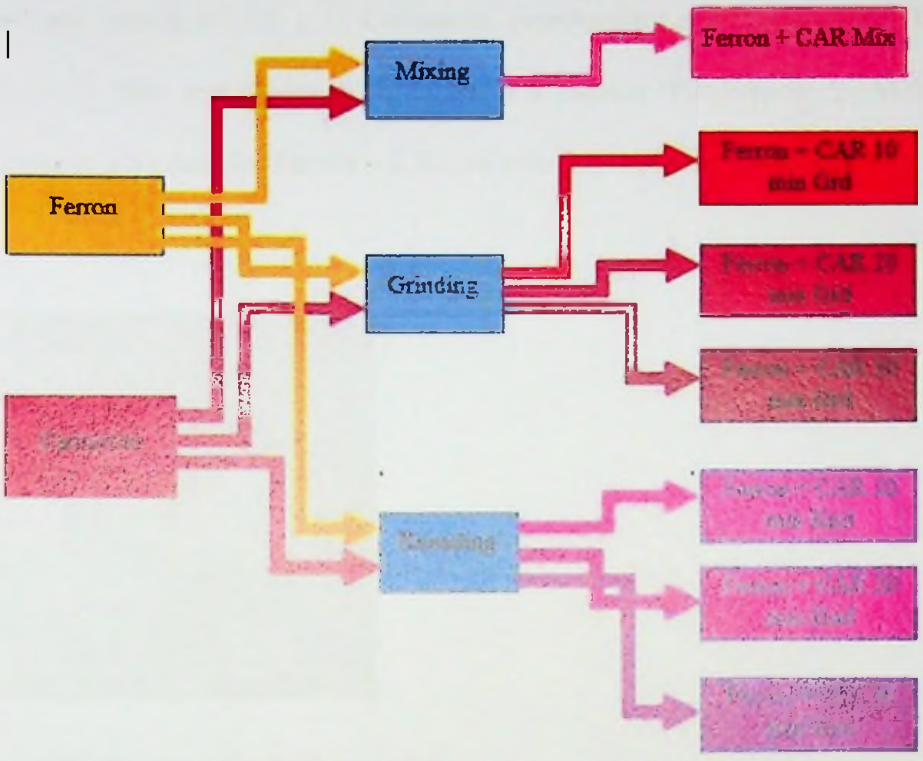

Figure 32: Scheme of Mechano-synthesis of combinations of Ferron and Carbazole.

synthesized. The sample names/codes for the various products are given (Figure 32). The resulting combined products were characterised. Details of the sample preparations for each characterisation are given below.

Ferron combined with Carbazole

Measured quantities of Ferron (Figure 13) and Carbazole (Figure 21) were combined together mechano-chemically as follows:

Grinding (Grd)

Grinding Ferron and Carbazole for 10 min (Ferron + CAR 10 min Grd)

This sample was prepared by weighing 0.6943 g of Ferron into a mortar bowl and adding 0.3301 g of Carbazole, representing a 1:1 mole ratio. The mixture is then ground for 10 minutes in a Fritsch 'Pulverisette 2' Mortar Grinder to give sample 'Ferron + CAR 10 min Grd' (Figure 33).

Figure 33: Ferron + CAR 10 min Grd.

Grinding Ferron and Carbazole for 20 min (Ferron + CAR 20 min Grd)

This sample was prepared by weighing 0.6936 g of Ferron into a mortar bowl and adding 0.3361 g of Carbazole, representing a 1:1 mole ratio. The mixture is then ground for 20 minutes in a Fritsch 'Pulverisette 2' Mortar Grinder to give sample 'Ferron + CAR 20 min Grd' (Figure 34).

Figure 34: Ferron + CAR 20 min Grd.

Grinding Ferron and Carbazole for 30 min (Ferron + CAR 30 min Grd)

This sample was prepared by weighing 0.6861 g of Ferron into a mortar bowl and adding 0.3319 g of Carbazole, representing a 1:1 mole ratio. The mixture is then ground for 30 minutes in a Fritsch 'Pulverisette 2' Mortar Grinder to give sample 'Ferron + CAR 30 min Grd' (Figure 35).

Figure 35: Ferron + CAR 30 min Grd.

Kneading (Knd)

Kneading Ferron and Carbazole for 10 min (Ferron + CAR 10 min Knd)

This sample was prepared by weighing 0.6891 g of Ferron into a mortar bowl and adding 0.3404 g of Carbazole, representing a 1:1 mole ratio. Five

drops of the solvent system of Ethanol:Water (1:1 vol) was added to the mixture. The mixture is then kneaded for 10 minutes in a Fritsch 'Pulverisette 2' Mortar Grinder to give sample 'Ferron + CAR 10 min Knd' (Figure 36).

Figure 36: Ferron + CAR 10 min Knd.

Kneading Ferron and Carbazole for 20 min (Ferron + CAR 20 min Knd)

This sample was prepared by weighing 0.6938 g of Ferron into a mortar bowl and adding 0.3416 g of Carbazole, representing a 1:1 mole ratio. Five drops of the solvent system of Ethanol:Water (1:1 vol) was added to the mixture. The mixture is then kneaded for 20 minutes in a Fritsch 'Pulverisette 2' Mortar Grinder to give sample 'Ferron + CAR 20 min Knd' (Figure 37).

Figure 37: Ferron + CAR 20 min Knd.

Kneading Ferron and Carbazole for 30 min (Ferron + CAR 30 min Knd)

This sample was prepared by weighing 0.6863 g of Ferron into a mortar bowl and adding 0.3344 g of Carbazole, representing a 1:1 mole ratio. Five drops of the solvent system of Ethanol:Water (1:1 vol) was added to the mixture. The mixture is then kneaded for 30 minutes in a Fritsch 'Pulverisette 2' Mortar Grinder to give sample 'Ferron + CAR 20 min Knd' (Figure 38).

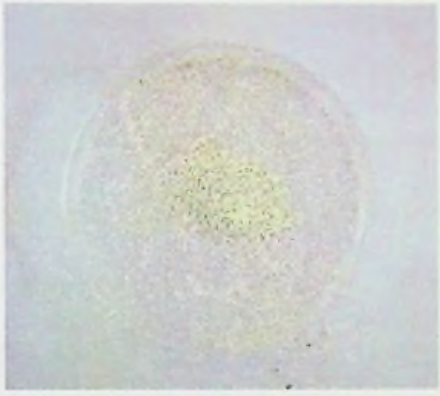

Figure 38: Ferron + CAR 30 min Knd.

Mixing (Mix)

Mixing Ferron and Carbazole (Ferron + CAR Mix)

This sample was prepared by weighing 0.6922 g of Ferron into a mortar bowl and adding 0.3390 g of Carbazole, representing a 1:1 mole ratio. The mixture is then carefully mixed using a spatula for 5 minutes to give sample 'Ferron + CAR Mix' (Figure 39).

Figure 39: Ferron + CAR Mix.

Sample Preparation and Characterisation

Preparation of samples for Ultraviolet/Visible Spectrometry (UV-Vis)

Successive dilution was used to gradually lower the concentration of the samples dissolved in the solvent system to facilitate their Ultraviolet spectrophotometric analysis. This UV-Vis Spectrophotometer is at the Chemistry Laboratory of the Institute of Industrial Research, C. S. I. R., Accra, Ghana.

Preparation of Ferron sample for Ultraviolet/Visible Spectrometry (UV-Vis)

Ferron sample was prepared for UV Spectrophotometry by dissolving 0.0060 g of Ferron in 5 mL of the solvent system (Ethanol:Water 1:1 vol%) (called solution A) at room temperature. The solution was diluted by adding 0.5 mL of the solvent system to 4.5 mL of solution A. This new solution, solution B, was further diluted by taking 3.0 mL of solution B and adding 2.0 mL of the solvent system. The resulting solution, solution C, was further diluted by taking 2.0 mL of solution C and adding 3.0 mL of solvent system to give solution D.

The concentration of solution D was therefore 1.296 x 10^{-3} g Ferron in 5 mL solvent system (equivalent to 7.38 x 10^{-7} M Ferron solution). The UV spectrum for solution D was then determined using a Spectroquant Pharo 300 UV-VIS Spectrophotometer.

Preparation of Sulphamethoxazole sample for Ultraviolet/Visible Spectrometry (UV-Vis)

Sulphamethoxazole (SMX) sample was prepared for UV Spectrophotometry by dissolving 0.0080 g of Sulphamethoxazole in 5 mL of the solvent system (Ethanol:Water 1:1 vol%) (called solution A) at room temperature. The solution was diluted by adding 0.5 mL of the solvent system to 4.5 mL of solution A. This new solution, solution B, was further diluted by taking 3.0 mL of solution B and adding 2.0 mL of the solvent system. The resulting solution, solution C, was further diluted by taking 2.0 mL of solution C and adding 3.0 mL of solvent system to give solution D. The concentration of solution D was therefore 1.728 x 10^{-3} g SMX in 5 mL solvent system (equivalent to 1.365 x 10^{-6} M SMX solution). The UV spectrum for solution D was then determined using a Spectroquant Pharo 300 UV-VIS Spectrophotometer.

Preparation of Carbazole (CAR) sample for Ultraviolet/Visible Spectrometry (UV-Vis)

Carbazole (CAR) sample was prepared for UV spectrophotometry by dissolving 0.0037 g of carbazole in 5 mL of the solvent system (Ethanol:Water 1:1 vol%) (called solution A) at room temperature. The solution was diluted by adding 0.5 mL of the solvent system to 4.5 mL of solution A. This new solution,

solution B, was further diluted by taking 3.0 mL of solution B and adding 2.0 mL of the solvent system. The resulting solution, solution C, was further diluted by taking 2.0 mL of solution C and adding 3.0 mL of solvent system to give solution D. The concentration of solution D was therefore 7.992×10^{-4} g CAR in 5 mL solvent system (equivalent to 9.56×10^{-7} M CAR solution). The UV spectrum for solution D was then determined using a Spectroquant Pharo 300 UV-VIS Spectrophotometer.

Preparation of Ferron + SMX 10 min Grd sample for Ultraviolet/Visible Spectrometry (UV-Vis)

Ferron + SMX 10 min Grd sample was prepared for UV Spectrophotometry by dissolving 0.0115 g of the mixture in 5 mL of the solvent system (Ethanol:Water 1:1 vol%) (called solution A) at room temperature. The solution was diluted by adding 0.5 mL of the solvent system to 4.5 mL of solution A. This new solution, solution B, was further diluted by taking 3.0 mL of solution B and adding 2.0 mL of the solvent system. The resulting solution, solution C, was further diluted by taking 2.0 mL of solution C and adding 3.0 mL of solvent system to give solution D. The concentration of solution D was therefore 2.484×10^{-3} g Ferron + SMX 10 min Grd in 5 mL solvent system. The UV spectrum for solution D was then determined using a Spectroquant Pharo 300 UV-VIS Spectrophotometer.

Preparation of Ferron + SMX 20 min Grd sample for Ultraviolet/Visible Spectrometry (UV-Vis)

Ferron + SMX 20 min Grd sample was prepared for UV Spectrophotometry by dissolving 0.0105 g of the mixture in 5 mL of the solvent system (Ethanol:Water 1:1 vol%) (called solution A) at room temperature. The solution was diluted by adding 0.5 mL of the solvent system to 4.5 mL of solution A. This new solution, solution B, was further diluted by taking 3.0 mL of solution B and adding 2.0 mL of the solvent system. The resulting solution, solution C, was further diluted by taking 2.0 mL of solution C and adding 3.0. mL of solvent system to give solution D. The concentration of solution D was therefore 2.268×10^{-3} g Ferron + SMX 20 min Grd in 5 mL solvent system. The UV spectrum for solution D was then determined using a Spectroquant Pharo 300 UV-VIS Spectrophotometer.

Preparation of Ferron + SMX 30 min Grd sample for Ultraviolet/Visible Spectrometry (UV-Vis)

Ferron + SMX 30 min Grd sample was prepared for UV Spectrophotometry by dissolving 0.0096 g of the mixture in 5 mL of the solvent system (Ethanol:Water 1:1 vol%) (called solution A) at room temperature. The solution was diluted by adding 0.5 mL of the solvent system to 4.5 mL of solution A. This new solution, solution B, was further diluted by taking 3.0 mL of solution B and adding 2.0 mL of the solvent system. The resulting solution, solution C, was further diluted by taking 2.0 mL of solution C and adding 3.0 mL of solvent system to give solution D. The concentration of solution D was therefore 2.074×10^{-3} g Ferron + SMX 30 min Grd in 5 mL solvent system. The

UV spectrum for solution D was then determined using a Spectroquant Pharo 300 UV-VIS Spectrophotometer.

Preparation of Ferron + SMX 10 min Knd sample for Ultraviolet/Visible Spectrometry (UV-Vis)

Ferron + SMX 10 min Knd sample was prepared for UV Spectrophotometry by dissolving 0.0104 g of the mixture in 5 mL of the solvent system (Ethanol:Water 1:1 vol%) (called solution A) at room temperature. The solution was diluted by adding 0.5 mL of the solvent system to 4.5 mL of solution A. This new solution, solution B, was further diluted by taking 3.0 mL of solution B and adding 2.0 mL of the solvent system. The resulting solution, solution C, was further diluted by taking 2.0 mL of solution C and adding 3.0 mL of solvent system to give solution D. The concentration of solution D was therefore 2.246×10^{-3} g Ferron + SMX 10 min Knd in 5 mL solvent system. The UV spectrum for solution D was then determined using a Spectroquant Pharo 300 UV-VIS Spectrophotometer.

Preparation of Ferron + SMX 20 min Knd sample for Ultraviolet/Visible Spectrometry (UV-Vis)

Ferron + SMX 20 min Knd sample was prepared for UV Spectrophotometry by dissolving 0.0118 g of the mixture in 5 mL of the solvent system (Ethanol:Water 1:1 vol%) (called solution A) at room temperature. The solution was diluted by adding 0.5 mL of the solvent system to 4.5 mL of solution A. This new solution, solution B, was further diluted by taking 3.0 mL of solution B and adding 2.0 mL of the solvent system. The resulting solution, solution C, was further diluted by taking 2.0 mL of solution C and adding 3.0

mL of solvent system to give solution D. The concentration of solution D was therefore 2.549 x 10^{-3} g Ferron + SMX 20 min Knd in 5 mL solvent system. The UV spectrum for solution D was then determined using a Spectroquant Pharo 300 UV-VIS Spectrophotometer.

Preparation of Ferron + SMX 30 min Knd sample for Ultraviolet/Visible Spectrometry (UV-Vis)

Ferron + SMX 30 min Knd sample was prepared for UV Spectrophotometry by dissolving 0.0176 g of Ferron in 5 mL of the solvent system (Ethanol:Water 1:1 vol%) (called solution A) at room temperature. The solution was diluted by adding 0.5 mL of the solvent system to 4.5 mL of solution A. This new solution, solution B, was further diluted by taking 3.0 mL of solution B and adding 2.0 mL of the solvent system. The resulting solution, solution C, was further diluted by taking 2.0 mL of solution C and adding 3.0 mL of solvent system to give solution D. The concentration of solution D was therefore 3.802 x 10^{-3} g Ferron + SMX 30 min Knd in 5 mL solvent system. The UV spectrum for solution D was then determined using a Spectroquant Pharo 300 UV-VIS Spectrophotometer.

Preparation of Ferron + SMX Mix sample for Ultraviolet/Visible Spectrometry (UV-Vis)

Ferron + SMX Mix sample was prepared for UV Spectrophotometry by dissolving 0.0162 g of the mixture in 5 mL of the solvent system (Ethanol:Water 1:1 vol%) (called solution A) at room temperature. The solution was diluted by adding 0.5 mL of the solvent system to 4.5 mL of solution A. This new solution, solution B, was further diluted by taking 3.0 mL of solution B and adding 2.0

mL of the solvent system. The resulting solution, solution C, was further diluted by taking 2.0 mL of solution C and adding 3.0 mL of solvent system to give solution D. The concentration of solution D was therefore 3.499×10^{-3} g Ferron + SMX Mix in 5 mL solvent system. The UV spectrum for solution D was then determined using a Spectroquant Pharo 300 UV-VIS Spectrophotometer.

Preparation of Ferron + CAR 10 min Grd sample for Ultraviolet/Visible Spectrometry (UV-Vis)

Ferron + CAR 10 min Grd sample was prepared for UV Spectrophotometry by dissolving 0.0145 g of the mixture in 5 mL of the solvent system (Ethanol:Water 1:1 vol%) (called solution A) at room temperature. The solution was diluted by adding 0.5 mL of the solvent system to 4.5 mL of solution A. This new solution, solution B, was further diluted by taking 3.0 mL of solution B and adding 2.0 mL of the solvent system. The resulting solution, solution C, was further diluted by taking 2.0 mL of solution C and adding 3.0 mL of solvent system to give solution D. The concentration of solution D was therefore 3.132×10^{-3} g Ferron + CAR 10 min Grd in 5 mL solvent system (equivalent to 7.38×10^{-7} M Ferron solution). The UV spectrum for solution D was then determined using a Spectroquant Pharo 300 UV-VIS Spectrophotometer.

Preparation of Ferron + CAR 20 min Grd sample for Ultraviolet/Visible Spectrometry (UV-Vis)

Ferron + CAR 20 min Grd sample was prepared for UV Spectrophotometry by dissolving 0.0129 g of Ferron in 5 mL of the solvent system (Ethanol:Water 1:1 vol%) (called solution A) at room temperature. The

solution was diluted by adding 0.5 mL of the solvent system to 4.5 mL of solution A. This new solution, solution B, was further diluted by taking 3.0 mL of solution B and adding 2.0 mL of the solvent system. The resulting solution, solution C, was further diluted by taking 2.0 mL of solution C and adding 3.0 mL of solvent system to give solution D. The concentration of solution D was therefore 2.786 x 10^{-3} g Ferron + CAR 20 min Grd in 5 mL solvent system.The UV spectrum for solution D was then determined using a Spectroquant Pharo 300 UV-VIS Spectrophotometer.

Preparation of Ferron + CAR 30 min Grd sample for Ultraviolet/Visible Spectrometry (UV-Vis)

Ferron + CAR 30 min Grd sample was prepared for UV Spectrophotometry by dissolving 0.0183 g of the mixture in 5 mL of the solvent system (Ethanol:Water 1:1 vol%) (called solution A) at room temperature. The solution was diluted by adding 0.5 mL of the solvent system to 4.5 mL of solution A. This new solution, solution B, was further diluted by taking 3.0 mL of solution B and adding 2.0 mL of the solvent system. The resulting solution, solution C, was further diluted by taking 2.0 mL of solution C and adding 3.0 mL of solvent system to give solution D. The concentration of solution D was therefore 3.953 x 10^{-3} g Ferron + CAR 30 min Grd in 5 mL solvent system.The UV spectrum for solution D was then determined using a Spectroquant Pharo 300 UV-VIS Spectrophotometer.

Preparation of Ferron + CAR 10 min Knd sample for Ultraviolet/Visible Spectrometry (UV-Vis)

Ferron + CAR 10 min Knd sample was prepared for UV Spectrophotometry by dissolving 0.0184 g of the mixture in 5 mL of the solvent system (Ethanol:Water 1:1 vol%) (called solution A) at room temperature. The solution was diluted by adding 0.5 mL of the solvent system to 4.5 mL of solution A. This new solution, solution B, was further diluted by taking 3.0 mL of solution B and adding 2.0 mL of the solvent system. The resulting solution, solution C, was further diluted by taking 2.0 mL of solution C and adding 3.0 mL of solvent system to give solution D. The concentration of solution D was therefore 3.974×10^{-3} g Ferron + CAR 10 min Knd in 5 mL solvent system. The UV spectrum for solution D was then determined using a Spectroquant Pharo 300 UV-VIS Spectrophotometer.

Preparation of Ferron + CAR 20 min Knd sample for Ultraviolet/Visible Spectrometry (UV-Vis)

Ferron + CAR 20 min Knd sample was prepared for UV Spectrophotometry by dissolving 0.0195 g of Ferron in 5 mL of the solvent system (Ethanol:Water 1:1 vol%) (called solution A) at room temperature. The solution was diluted by adding 0.5 mL of the solvent system to 4.5 mL of solution A. This new solution, solution B, was further diluted by taking 3.0 mL of solution B and adding 2.0 mL of the solvent system. The resulting solution, solution C, was further diluted by taking 2.0 mL of solution C and adding 3.0 mL of solvent system to give solution D. The concentration of solution D was therefore 4.212×10^{-3} g Ferron + CAR 20 min Knd in 5 mL solvent system. The

UV spectrum for solution D was then determined using a Spectroquant Pharo 300 UV-VIS Spectrophotometer.

Preparation of Ferron + CAR 30 min Knd sample for Ultraviolet/Visible Spectrometry (UV-Vis)

Ferron + CAR 30 min Knd sample was prepared for UV Spectrophotometry by dissolving 0.0184 g of Ferron in 5 mL of the solvent system (Ethanol:Water 1:1 vol%) (called solution A) at room temperature. The solution was diluted by adding 0.5 mL of the solvent system to 4.5 mL of solution A. This new solution, solution B, was further diluted by taking 3.0 mL of solution B and adding 2.0 mL of the solvent system. The resulting solution, solution C, was further diluted by taking 2.0 mL of solution C and adding 3.0 mL of solvent system to give solution D. The concentration of solution D was therefore 3.974×10^{-3} g Ferron + CAR 30 min Knd in 5 mL solvent system. The UV spectrum for solution D was then determined using a Spectroquant Pharo 300 UV-VIS Spectrophotometer .

Preparation of Ferron + CAR Mix sample for Ultraviolet/Visible Spectrometry (UV-Vis)

Ferron + CAR Mix sample was prepared for UV Spectrophotometry by dissolving 0.0144 g of Ferron in 5 mL of the solvent system (Ethanol:Water 1:1 vol%) (called solution A) at room temperature. The solution was diluted by adding 0.5 mL of the solvent system to 4.5 mL of solution A. This new solution,

solution B, was further diluted by taking 3.0 mL of solution B and adding 2.0 mL of the solvent system. The resulting solution, solution C, was further diluted by taking 2.0 mL of solution C and adding 3.0 mL of solvent system to give solution D. The concentration of solution D was therefore 3.110×10^{-3} g Ferron + CAR Mix in 5 mL solvent system. The UV spectrum for solution D was then determined using a Spectroquant Pharo 300 UV-VIS Spectrophotometer.

Preparation of samples for Infrared Spectrometry (IR)

Samples of the starting materials (Ferron, Sulphamethoxazole and Carbazole) and the various products of mechano-synthesis were analysed using a Perkin Elmer Spectrum 2 FT-IR Spectrometer. This equipment is situated at the KNUST Central Laboratories, Kumasi. The quantity of each sample was 50 mg.

Preparation of samples for Powder X-Ray Diffraction (PXRD)

For Powder X-Ray Diffraction analyses, 1 g of each powdered sample was used. The powder samples were completely mixed using a spatula. A flat surface was used to press down on the powder, packing it into the well. This ensured that the particles were densely packed and randomly oriented. The flat plate sample therefore had a smooth flat surface. The samples were continuously scanned from 5.0400 to 80.0000 in step sizes of 0.0800. The measurement temperature was 25°C. Analyses were done using a PANalytical Empyrean Powder X-ray Diffractometer located at the Physics Department, University of Ghana, Legon.

The *General Structure Analysis System* (GSAS 1 & 2) set of programs, *Materials Analysis Using Diffraction, (MAUD)*, and *CMPR* were used to process and analyse the powder x-ray diffraction data obtained and also to refine the structural parameters for phases in the samples.

Melting Point Determination

The melting points of the starting compounds were determined using a .Stuart SMP10 capillary melting point apparatus. This equipment is in the Chemistry Department of the CBAS, U.G. These melting points and those of products from mechano-synthesis were also determined using the Differential Scanning Calorimeter (Plate 6).

Thermal Analysis

Thermogravimetric analysis (TGA)

The quantities of each sample used in the Thermogravimetric Analyses, TGA, are given (Table 7). This equipment is located at the Chemistry Department of the University of Johannesburg, South Africa.

Table 7: Masses of Samples used in TGA

No.	Sample	Mass (mg)
1	Ferron	11.899
2	Sulphamethoxazole (SMX)	6.107
3	Carbazole (CAR)	3.209
4	Ferron + SMX 10 min Grd	7.585
5	Ferron + SMX 20 min Grd	5.224
6	Ferron + SMX 30 min Grd	5.296
7	Ferron SMX 10 min Knd	8.701
8	Ferron + SMX 20 min Knd	8.324
9	Ferron + SMX 30 min Knd	7.246
10	Ferron + SMX Mix	8.001
11	Ferron + CAR 10 min Grd	4.929
12	Ferron + CAR 20 min Grd	4.475
13	Ferron + CAR 30 min Grd	5.812
14	Ferron + CAR 10 min Knd	5.407
15	Ferron + CAR 20 min Knd	6.990
16	Ferron + CAR 30 min Knd	6.327
17	Ferron + CAR Mix	6.036

Thermogravimetric analyses were carried out on a TA INSTRUMENTS SDT-Q600 Simultaneous Differential Thermal Analyzer. The analyses were carried out within the temperature scanning range of 25°C to 800°C at 10 °C/min using N_2 as a purge gas. Samples were not analysed under an inert atmosphere since the investigation required the determination of decomposition

characteristics that may not have been achieved if analysis was done in an inert atmosphere.

Differential Scanning Calorimetry (DSC)

The quantities of each sample used in the Differential Scanning Calorimetry, DSC, analyses are given (Table 8). This equipment is located at the Chemistry Department of the University of Johannesburg, South Africa.

Table 8: Masses of Samples used in DSC Analyses

No.	Sample	Mass (mg)
1	Ferron	6.1300
2	Sulphamethoxazole (SMX)	3.4800
3	Carbazole (CAR)	2.2700
4	Ferron + SMX 10 min Grd	3.0000
5	Ferron + SMX 20 min Grd	6.0000
6	Ferron + SMX 30 min Grd	5.1600
7	Ferron SMX 10 min Knd	6.9400
8	Ferron + SMX 20 min Knd	5.5800
9	Ferron + SMX 30 min Knd	4.7900
10	Ferron + SMX Mix	5.0300
11	Ferron + CAR 10 min Grd	3.9900
12	Ferron + CAR 20 min Grd	4.5100
13	Ferron + CAR 30 min Grd	4.4100
14	Ferron + CAR 10 min Knd	4.6400
15	Ferron + CAR 20 min Knd	6.6500
16	Ferron + CAR 30 min Knd	6.6200
17	Ferron + CAR Mix	3.6200

DSC analyses were carried out on a METTLER Toledo 822e Differential Scanning Calorimeter. In this study, the DSC analysis was carried out within the temperature scanning range of 25°C to 400°C at 5 °C/min using N_2 as a purge gas. Samples were not analysed under an inert atmosphere since

the investigation required the determination of decomposition characteristics that may not have been achieved if analysis was done in an inert atmosphere.

Scanning Electron Microscopy (SEM)

The morphology of samples of the starting materials (Ferron, Sulphamethoxazole and Carbazole) and the various products of mechano-synthesis were studied using images generated by JEOL JSM-6390LV Scanning Electron Microscope (SEM). This equipment is situated at the College of Basic and Applied Sciences (CBAS), University of Ghana, Legon, Accra. A single layer of each sample was mounted on a stub using double-sided adhesive carbon sheets. The samples of the mechano-synthesised products were not stable and therefore only those ground and kneaded for 30 minutes were recorded. The images were taken at magnifications between was 800 and 950.

***In-Silico* Calculations**

In silico experiments were performed on the compounds to determine some theoretical structural properties.

Using the Gaussian 09 program package (M. J. Frisch, Trucks, Schlegel, et al., 2009; M. J. Frisch, Trucks, Cheeseman, et al., 2009), using the GaussView 05 visualization program (Æ. Frisch et al., 2009), the molecules of the starting compounds and the combined pairs were modelled. The geometrical structures (rotational spectra), rovibrational energy levels (infrared spectra) were theoretically determined.

The method used for all elements was the Time Dependent Density Functional Theory, TD-DFT, at the CAM-B3LYP (Yanai, Tew, & Handy, 2004) level of theory.

The basis set assigned for Hydrogen, Nitrogen and Oxygen was 6-31G (2df,p) (Curtiss, Raghavachari, Redfern, Rassolov, & Pople, 1998) (with polarization functions). For Carbon, the assigned basis set was 6-311++G(2d,2p) (Krishnan, Binkley, Seeger, & Pople, 1980; Michael J. Frisch, Pople, & Binkley, 1984; Timothy, Chandrasekhar, Spitznagel, & Schleyer, 1983) (with polarization and diffuse functions).

A polarization-consistent (pc), Pople-type basis set, aug-pc-3 (Jensen & Helgaker, 2004) was assigned for Sulphur atoms. Pseudopotentials or effective core potentials (ECP), ECP28MDF, (Rappoport & Furche, 2010; Peterson, Figgen, Goll, Stoll, & Dolg, 2003) were used for Iodine atoms, (Kim, Yoon, Won, & Kim, 2006; Zipse, 2016).

All basis sets were sourced from the EMSL Basis Set Library, using the Basis Set Exchange (BSE) software (Feller, 1996; Schuchardt et al., 2007). Self-Consistent Field, SCF, calculations and Full Geometry Optimization, FGO, was carried out for each molecule.

The VEDA 4 (Jamróz, 2015) programme was used to analyse Infrared spectra. Potential Energy Distribution (PED) analysis of all theoretical vibrational spectra was done with the aid of the VEDA 4 program (Jamróz, 2015).

Chapter Summary

The mechanochemical method was used in the preparation of the co-crystals and the different equipment and instruments needed to characterise the products formed are used in the study.

CHAPTER FOUR

RESULTS AND DISCUSSIONS

In this chapter, the results from the various analysis and characterisation experiments have been discussed. The format used is the results and discussion from each equipment and/or instrument are given separately under the heading of the technique. In all, six techniques were used including UltraViolet Spectroscopy (UV/Vis), Powder X-Ray Diffractometry (PXRD), Differential Scanning Calorimetry (DSC), Thermogravimetry (TGA), Infra-Red Spectroscopy, (IR) and Scanning Electron Microscopy (SEM). Results from *in-silico* analysis of the data on the starting materials is also discussed at the end of this chapter.

Ultraviolet/Visible Spectral (UV-Vis) Analyses

Ultraviolet/Visible Spectral (UV-Vis) Analyses of both starting materials and products were taken in solution on the understanding that though there was a breakdown of the crystal structure of the materials, a few non-covalent bonds initially in the material are likely to remain and produce unique spectra. This view was confirmed by the observation of colour changes which manifested when the compounds were combined. The work therefore was designed to compare the spectra of the starting materials with the products to observe changes in the spectra due to the formation of the products.

The relevance of this approach is premised on the fact that though the co-crystal drugs are solid, they will be dissolved in body fluids to increase their bioavailability to the patient. So their UV/Vis characteristics in solution will be a relevant characteristic to be noted.

UV/Vis spectra analyses of Ferron

The Ultraviolet – Visible (UV-Vis) spectrum of Ferron has a major absorption peak at wavelength 294.5 nm in the ultraviolet radiation range. In the visible radiation range, the major peak of absorption is at a wavelength of

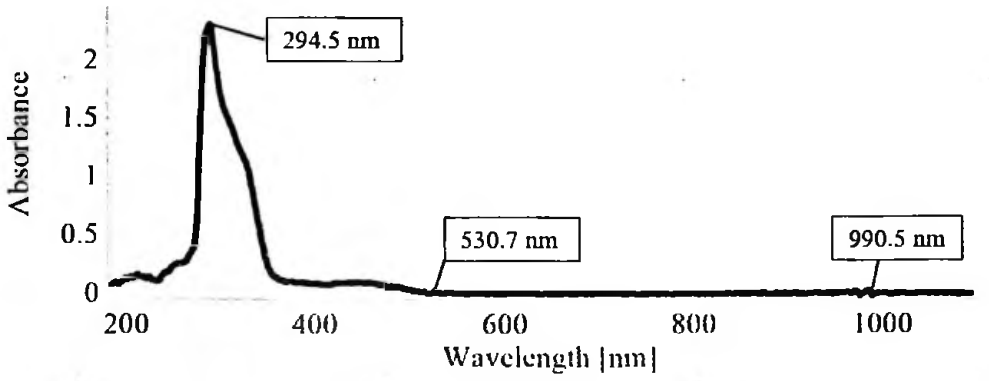

Figure 40: Ultraviolet and Visible Spectrum of Ferron in Ethanol-Water (1:1) Solvent.

530.7 nm. There is an absorption in the near infrared region with a major peak at 990.5 nm (Figure 40). There is also a shoulder at 320 nm and 342 nm (Figure 40). There are other minor peaks in both ultraviolet and visible range .

This spectrum agrees with the findings of Näsänen and Ekman (1952) for the compound in mildly acidic medium. According to Näsänen and Ekman, the shoulder between 320 nm and 342 nm is due to the iodo- substituent on the molecule.

The major peak at 294.5 nm is due to transitions of *pi* electrons, π, to anti-bonding *pi* orbitals, π^*, ($\pi \rightarrow \pi^*$) transitions by the delocalized π-electrons of the aromatic rings in the molecule. The other absorptions at longer wavelengths are due to transitions of non-bonding orbital electrons, *n*, of the lone pairs of

electrons on the oxygen atoms to anti-bonding *pi* orbitals, π^* ($n \rightarrow \pi^*$). Absorptions at the shorter wavelengths are due to $\sigma \rightarrow \pi^*$ transitions.

UV/Vis spectra analyses of Sulphamethoxazole

The Ultraviolet – Visible (UV-Vis) spectrum of Sulphamethoxazole has a major peak at wavelength 299.7 nm in the ultraviolet radiation range (Figure 41). There is an absorption in the near infrared region with a major peak at 977.4 nm (Figure 41).

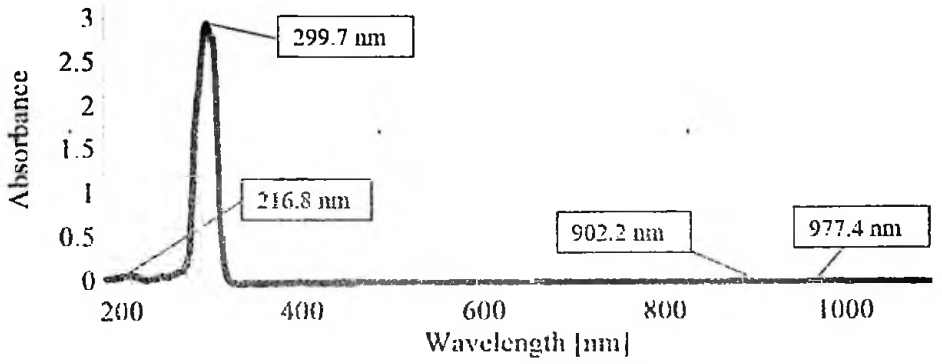

Figure 41: Ultraviolet and Visible Spectrum of Sulphamethoxazole in Ethanol-Water (1:1) Solvent.

The major peak at 299.7 nm is due to transitions of electrons, *pi* bonding, π, to anti-bonding *pi* orbitals, π^*, ($\pi \rightarrow \pi^*$) transitions by the delocalized π-electrons of the aromatic rings in the molecule. The other absorptions at longer wavelengths are due to transitions of non-bonding orbital electrons, *n*, of the lone pairs of electrons on the oxygen atoms to anti-bonding *pi* orbitals, π^* ($n \rightarrow \pi^*$) . Absorptions at the shorter wavelengths are due to $\sigma \rightarrow \pi^*$ transitions.

UV/Vis spectra analyses of Carbazole

The Ultraviolet – Visible (UV-Vis) spectrum of Carbazole has a major peak at wavelength 291.4 nm in the ultraviolet radiation range (Figure 42). In the visible radiation range, the major peak of absorption is at a wavelength of 407.2 nm. There is an absorption in the near infrared region with a major peak at 990.5 nm (Figure 42).

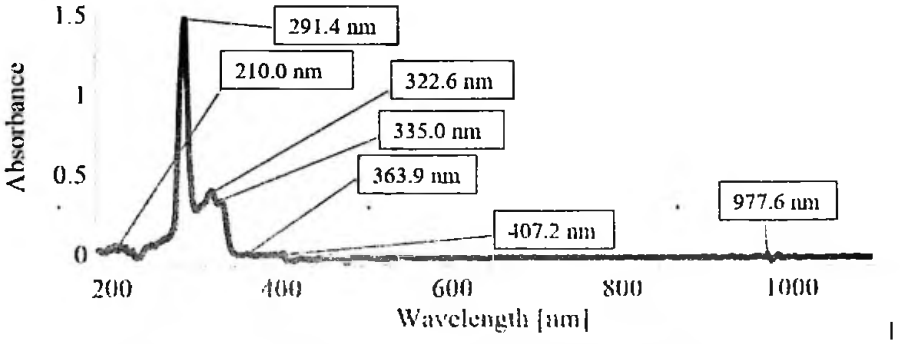

Figure 42: Ultraviolet and Visible Spectrum of Carbazole in Ethanol-Water (1:1) Solvent.

The highest peak at 291.4 nm is attributed to the *pi* bonding orbital electrons, π, to anti-bonding *pi* orbitals, π^* ($\pi \rightarrow \pi^*$) transitions by the delocalized π-electrons of the aromatic rings in the molecule. The other absorptions at longer wavelengths are due to transitions of non-bonding orbital electrons, *n*, of the lone pairs of electrons on the nitrogen atoms to anti-bonding *pi* orbitals, π^* ($n \rightarrow \pi^*$). Absorptions at the shorter wavelengths are due to $\sigma \rightarrow \pi^*$ transitions.

There is a weak peak at 407.2 nm, which is close to the visible range. With such a relatively low absorbance, the sample does not absorb enough of the electromagnetic radiation in the visible region. This confirms that the colour of the sample is white.

UV/Vis spectra analyses of Ground of Ferron and Sulphamethoxazole

The UV-Vis spectra of the samples of Ferron ground with Sulphamethoxazole have peaks at slightly different wavelengths from those of the starting materials (Figure 43).

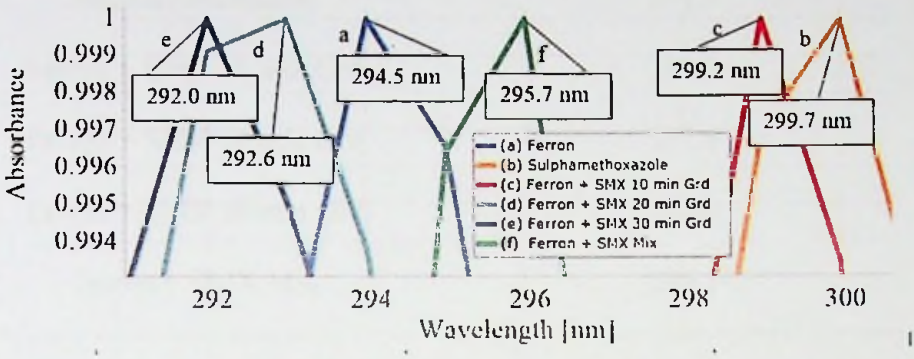

Figure 43: Maximum peaks in UV-Vis Spectra of Ferron ground with Sulphamethoxazole in Ethanol-Water (1:1) Solvent.

The maximum peak of Ferron (at wavelength 294.5 nm) shifted to a longer wavelength (a bathochromic shift) of 299.2 nm when the compounds were ground for 10 minutes (Ferron + SMX 10 min Grd) (Table 9).

Table 9: Maximum peaks in UV-Vis Spectra of Grinding Ferron with Sulphamethoxazole

Sample	Major Peak Wavelength (nm)
Ferron	294.5
Sulphamethoxazole	299.7
Ferron + SMX 10 min Grd	299.2
Ferron + SMX 20 min Grd	292.6
Ferron + SMX 30 min Grd	292.0
Ferron + SMX Mix	295.7

On the other hand when the two compounds are ground for 20 and 30 minutes, the wavelength for the maximum peak becomes shorter (a hypsochromic shift) to 292.6 nm and 292.0 nm respectively (Table 9).

The shoulder due to Ferron is however maintained in all sample which were ground (Figure 44) at between 320 nm and 342 nm.

When the two compounds are mixed, the maximum peak of Ferron is shifted from 294.5 nm to 295.7 nm (Figure 43). Here also, the shoulder is maintained at between 320 nm and 342 nm (Figure 44)

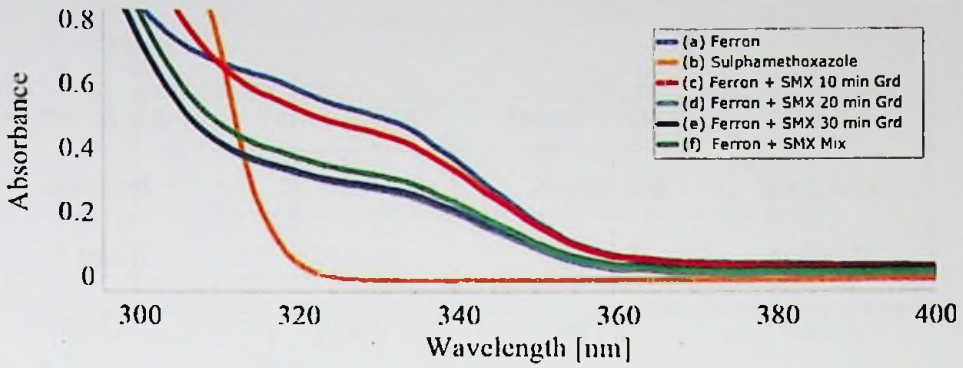

Figure 44: Shoulder in UV Spectra of Grinding Ferron with Sulphamethoxazole in Ethanol-Water (1:1) Solvent.

In the visible range, all the ground samples have absorptions between 400 nm and 480 nm wavelengths (Table 10). The expected colours are yellow and orange. Though the ratios are the same in all cases, the results indicate that the products are not always the same; the interaction between the components in forming the co-crystals are to different degrees. This will have an effect on the UV-Vis spectra because the spectra measures the degree to which the energy levels are changed in a non-covalent interaction.

Table 10: Peaks of Ground Ferron with Sulphamethoxazole in Visible range

Ferron + SMX 10 min Grd (λ [nm])	Ferron + SMX 20 min Grd (λ [nm])	Ferron + SMX 30 min Grd (λ [nm])	Ferron + SMX Mix (λ [nm])
407.3	428.3	407.2	482.1
428.7	450.4	428.6	526.0
450.5	463.4	450.5	539.9
463.3	494.3	463.3	695.9
530.9	531.0	494.3	761.9
544.7	544.8	531.0	
	599.8	544.8	
	613.4	599.7	
	630.1	613.2	
		629.9	

λ:- Wavelength

UV/Vis spectra analyses of Kneaded of Ferron and Sulphamethoxazole

The UV-Vis spectra of the samples of Ferron kneaded with Sulphamethoxazole have peaks at slightly different wavelengths from those of the starting materials (Figure 45).

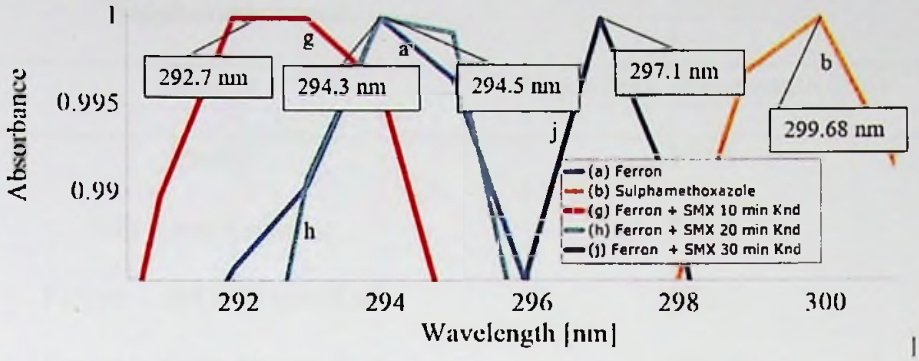

Figure 45: Maximum peaks in UV-Vis Spectra of Ferron kneaded with Sulphamethoxazole in Ethanol-Water (1:1) Solvent.

The wavelength at which Ferron has its maximum peak (294.5 nm) is shifted to a shorter one, 292.7 nm when the compounds are kneaded together for 10 minutes, Ferron + SMX 10 min Knd. When the duration for kneading is increased to 20 minutes (Ferron + SMX 20 min Knd), the maximum peak remains almost at the same wavelength, 294.3 nm. When the kneading is done for 30 minutes (Ferron + SMX 30 min Knd), the peak shifts to a longer wavelength, 297.1 nm (Table 11).

Table 11: Maximum peaks in UV-Vis Spectra of Kneading Ferron with Sulphamethoxazole

Sample	Major Peak Wavelength (nm)
Ferron	294.5
Sulphamethoxazole	299.7
Ferron + SMX 10 min Knd	292.7
Ferron + SMX 20 min Knd	294.3
Ferron + SMX 30 min Knd	297.1
Ferron + SMX Mix	295.7

The shoulder due to Ferron is however maintained in all samples which were kneaded at between 320 nm and 342 nm (Figure 46).

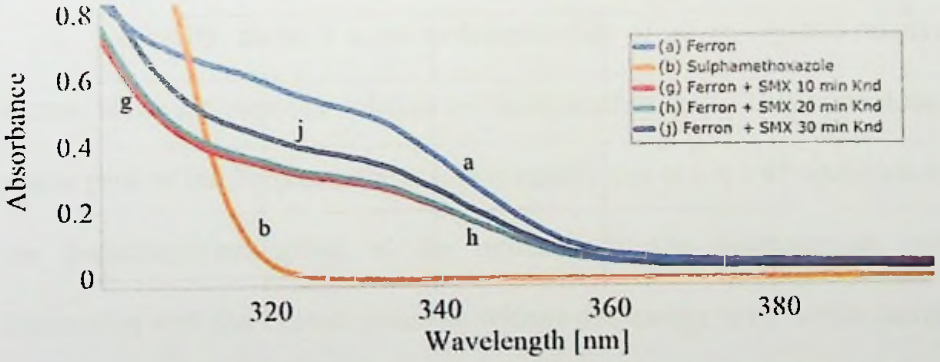

Figure 46: Shoulder in UV Spectra of Kneading Ferron with Sulphamethoxazole in Ethanol-Water (1:1) Solvent.

The colours of the kneaded samples are different shades of yellow and orange (Figures 28 to 30) and these are confirmed by the absorption of the

kneaded samples within the 400 nm to 480 nm wavelength region according to the colour wheel.

Table 12: Peaks of Kneaded Ferron with Sulphamethoxazole in Visible range

Ferron + SMX 10 min Knd (λ [nm])	Ferron + SMX 20 min Knd (λ [nm])	Ferron + SMX 30 min Knd (λ [nm])
407.2	407.0	481.9
481.7	482.0	525.9
526.1	526.1	762.1
	762.2	

λ:- Wavelength

Generally, there is a bathochromic shift of all co-crystals relative to Ferron while the opposite relative to Sulphamethoxazole. This is because the major peak of the Sulphamethoxazole is mainly due to a $\pi - \pi^*$ transition from the p-aminophenyl group of the molecule to the sulphonamide group. Interaction with the Ferron molecule widens this energy level which therefore requires a higher energy (shorter wavelength) for the transition to take place. This is a hypsochromic shift. In the same vein, the $\pi - \pi^*$ transition which takes place between the sulphonamide group on the Ferron to the hydroquinoline part is shortened requiring a lower energy (longer wavelength) for the same transition. This is a bathochromic shift (Kumar, 2006). This indicates that there is a form of interaction between the two molecules resulting in a new product.

UV/Vis spectra analyses of Ground of Ferron and Carbazole

The UV-Vis spectra of the samples of Ferron ground with Carbazole have peaks at slightly different wavelengths from those of the starting materials (Figure 47).

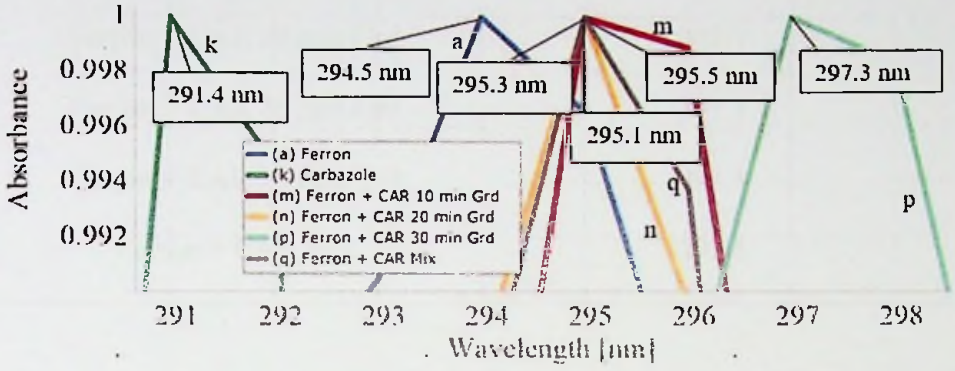

Figure 47: Wavelengths of maximum peaks in UV-Vis Spectra of grinding Ferron with Carbazole in Ethanol-Water (1:1) Solvent.

The wavelength at which Ferron has its maximum, 294.5 nm, has shifted slightly to a longer wavelength when Ferron was ground with Carbazole for 10 minutes (Ferron + CAR 10 min Grd) to 295.5 nm (Table 13). The same effect is seen when the two compounds are ground for 20 minutes (Ferron + CAR 20 min Grd) and 30 minutes (Ferron + CAR 30 min Grd); it shifted to 295.1 nm for the 20-minute ground sample and 297.3 nm for the 30 minute ground sample (Table 13).

Table 13: Maximum peaks in UV-Vis Spectra of grinding Ferron with Carbazole

Sample	Major Peak Wavelength (nm)
Ferron	294.5
Carbazole	291.4
Ferron + CAR 10 min Grd	295.5
Ferron + CAR 20 min Grd	295.1
Ferron + CAR 30 min Grd	297.3
Ferron + CAR Mix	295.3

The minor peaks at the wavelengths of 322.6 nm and 335.0 nm of Carbazole are transformed into shoulders when Carbazole is ground with Ferron. They combine and enhance the shoulder of the Ferron spectrum (Figure 48).

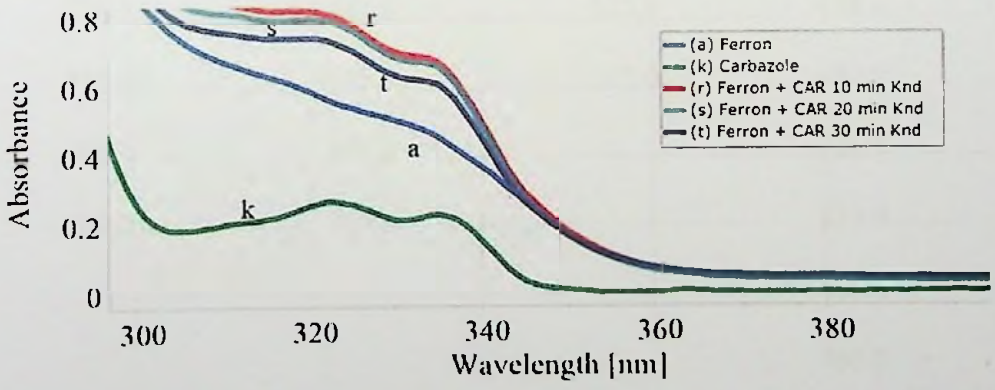

Figure 48: Minor peaks in UV-Vis Spectra of grinding Ferron with Carbazole in Ethanol-Water (1:1) Solvent.

When Ferron is mixed with Carbazole, the major peak of Ferron is shifted to 295.3 nm (Table 13) while the minor peaks of Carbazole at 322.6 nm and 335.0 nm are converted to shoulders and merged with the shoulders of Ferron (Figure 48).

In the visible range, both 10-minute and 30-minute ground samples have an absorption peak at 482.0 nm and 481.8 nm respectively (Table 14). The expected perceived colour of these samples are orange. The 20-minute ground sample has two absorption peaks at 407.1 nm and 481.8 nm (Table 14). This means its perceived colour is yellowish orange. These were observed by visually inspecting the respective samples (Figures 33, 34 and 35).

Table 14: Absorbance of Ground Ferron with Carbazole in Visible range

Ferron + CAR 10 min Grd λ [nm]	Ferron + CAR 20 min Grd λ [nm]	Ferron + CAR 30 min Grd λ [nm]	Ferron + CAR Mix λ [nm]
482.0	407.1	481.8	407.1
526.1	481.8	525.8	458.0
539.8	525.9	762.0	482.0
695.9	695.8		526.1
762.0	762.0		539.9
			696.0
			761.9

λ:- Wavelength

UV/Vis spectra analyses of Kneaded of Ferron and Carbazole

The UV-Vis spectra of the samples of Ferron kneaded with Carbazole have peaks at slightly different wavelengths from those of the starting materials (Figure 49).

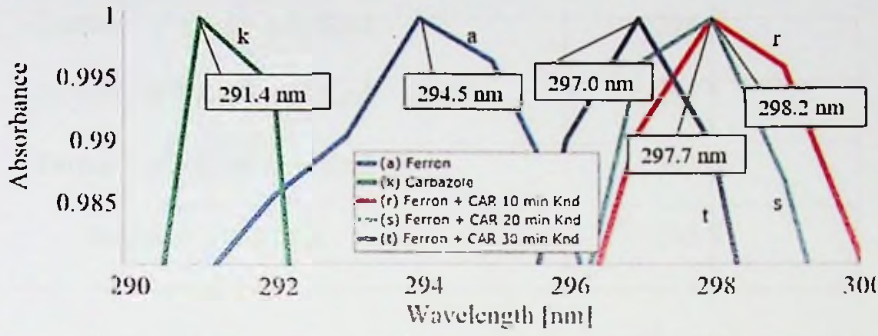

Figure 49: Maximum peaks in UV-Vis Spectra of kneading Ferron with Carbazole in Ethanol-Water (1:1) Solvent.

The wavelength at which Ferron has its maximum, 294.5 nm, has shifted slightly to a longer wavelength when Ferron was kneaded with Carbazole for 10 minutes (Ferron + CAR 10 min Knd) to 298.2 nm (Table 15). The same effect is seen when the two compounds are kneaded for 20 minutes (Ferron + CAR 20 min Knd) and 30 minutes (Ferron + CAR 30 min Knd); it shifted to 297.7 nm for the 20-minute kneaded sample and 297.0 nm for the 30-minute kneaded sample (Table 15).

Table 15: Maximum peaks in UV-Vis Spectra of Kneading Ferron with Carbazole

Sample	Major Peak Wavelength (nm)
Ferron	294.5
Carbazole	291.4
Ferron + CAR 10 min Knd	298.2
Ferron + CAR 20 min Knd	297.7
Ferron + CAR 30 min Knd	297.0
Ferron + CAR Mix	295.7

The minor peaks at the wavelengths of 322.6 nm and 335.0 nm of Carbazole are transformed into shoulders when Carbazole is kneaded with Ferron. They combine and enhance the shoulder of the Ferron spectrum (Figure 50).

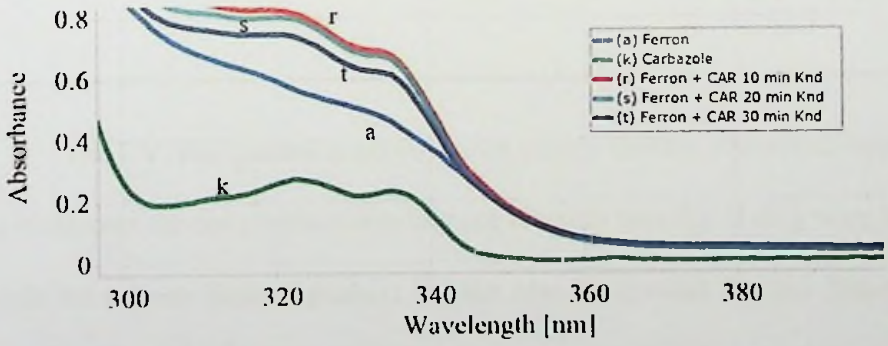

Figure 50: Wavelengths of minor peaks in UV-Vis Spectra of kneading Ferron with Carbazole in Ethanol-Water (1:1) Solvent.

In the visible range, both 10-minute and 30-minute kneaded samples have two absorption peaks at 407.3 nm and 481.8 nm respectively (Table 16). The expected perceived colour of these samples are yellowish-orange. The 20-minute ground sample has one absorption peaks at 481.8 nm (Table 16). This means its perceived colour is orange. These were observed by visually inspecting the respective samples (Figures 39, 40 and 41).

Table 16: Absorbance of Kneaded Ferron with Carbazole in Visible range

Ferron + CAR 10 min Knd (λ [nm])	Ferron + CAR 20 min Knd (λ [nm])	Ferron + CAR 30 min Knd (λ [nm])
407.3	481.8	407.1
481.8	526.0	481.8
539.8	762.0	526.1
695.8		539.9
761.9		695.9
		762.1

The UV-Vis spectral analysis shows clearly that the interaction between the molecules are not covalent bonding nor electron transfer. If they were, there would have been distinct peak(s) for the new compound formed. Since the wavelengths for absorption, though not constant, were close to those of the starting compounds, this study shows that the bonds formed were non-covalent bonds as expected in co-crystal formation (Khristi, Soni, & Suhagia, 2015).

Powder X-Ray Diffraction (PXRD) Analyses

The x-ray diffraction patterns were used to determine the cell parameters of the phases in the products. These cell parameters are unique to the phase and were found to be different from the cell parameters of the starting materials. This is proof enough that new phases, in this case, co-crystals were formed. The properties of the components which were charged were mainly the crystal structure (crystal packing, bond lengths and angles between the various atoms, etc.) which determines other physical and chemical properties such as melting point, colour, degradation point, stability, bioavailability and solubility.

Powder X-Ray Diffraction analyses of Ferron

The diffraction pattern of Ferron has sharp peaks (Figure 51) which shows that the sample is made up mainly of crystalline material. There are however, peaks with broad bases at diffraction angles at 19.20°, 29.52° and 40.32° indicating that some amorphous material is also present.

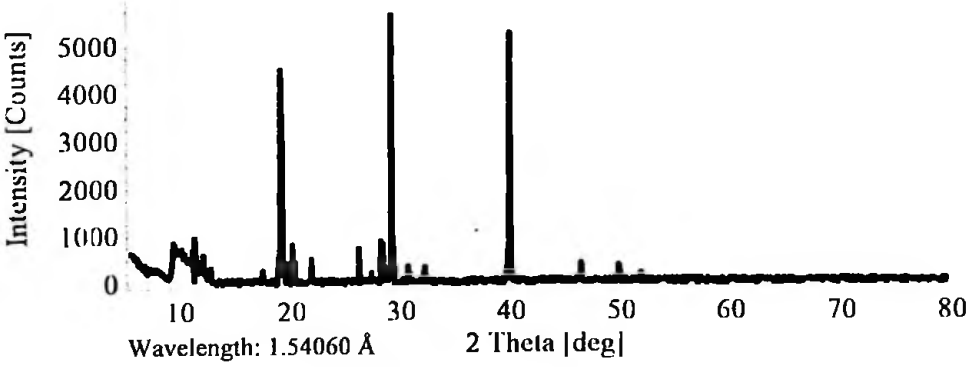

Figure 51: Diffraction pattern of Ferron.

The powder diffraction pattern of Ferron gives the highest peak at a diffraction angle, 2 theta, of 29.52° (Table 17).

Table 17: Diffraction Peaks and Intensities for Ferron

Diffraction Angle, 2 Theta [deg]	Intensity [Counts]
29.52	5,682
40.32	5,286
19.52	4,514
11.76	975
28.56	893
9.84	869

Peaks at these wavelengths are also found in the diffraction pattern as simulated from single crystal diffraction data of Ferron determined by Balasubramanian and Muthiah (1996). The Mercury software (Macrae et al., 2008) was used to simulate the powder diffraction pattern from the single crystal data and compared to the experimental pattern (Figure 52).

For the simulated diffraction pattern, the highest peak is at a diffraction angle of 12.56° (Table 18). The intensities of the experimental peaks are low because the experimental measurements had a low signal to noise ratio and the strong preferred orientation effect due to the crystal shapes.

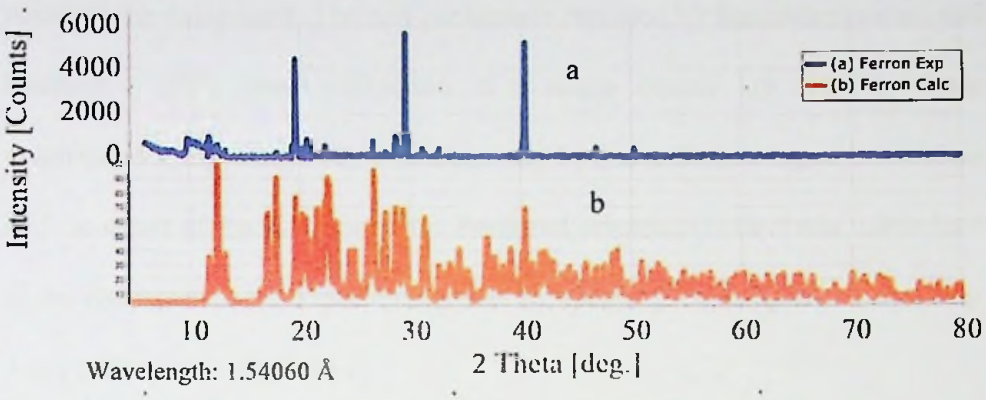

Figure 52: Comparison of Experimental (Exp) and Simulated (Calc) Diffraction Patterns of Ferron.

Table 18: Simulated Diffraction Peaks and Intensities for Ferron

2 Theta [deg]	Intensity [Counts]
12.56	10,000.00
12.58	9,434.91
26.66	9,066.90
22.46	8,187.96
17.84	8,130.34
17.86	8,092.44

Reduction of Ferron PXRD data

Indexing of the diffraction peaks was performed to calculate the lattice parameters (Table 19) of the unit cell using CMPR (Toby, 2006) and GSAS 2 (Larson & Von Dreele, 2004). The major peaks were used as characteristic peaks of the compound. The cell parameters reported by Balasubramanian and Muthiah (1996), using diffraction of a single crystal are close to those determined in this study. The variations may be due to the low signal/noise ratio and the effect of the $K_{\alpha 1+2}$ radiation. Preferred orientation effect was minimized in the collection of the experimental data by spinning the sample in the powder x-ray diffractometer (Plate 1).

Table 19: Experimental and Literature Cell Parameters of Ferron

Cell Parameter	Value	
	Experimental	Literature
a (Å)	9.5691	9.5704 ± 0.0009
b (Å)	13.3739	13.364 ± 0.002
c(Å)	8.7489	8.748 ± 0.002
α (°)	90	90
β (°)	108.77	108.83 ± 0.01
γ (°)	90	90
Cell volume ($Å^3$)	1060.06	1059 ± 0.3

Powder X-Ray Diffraction analyses of Sulphamethoxazole

The diffraction pattern of Sulphamethoxazole has sharp peaks (Figure 53) which shows that the sample is made up mainly of crystalline material. There are however, peaks with broad bases at diffraction angles 21° and 24° indicating that some amorphous material is also present.

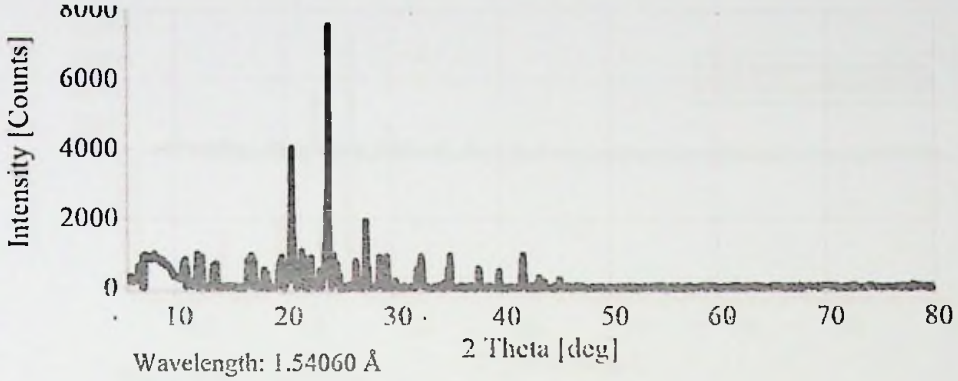

Figure 53: Diffraction pattern of Sulphamethoxazole.

The experimental powder diffraction pattern of Sulphamethoxazole gives the highest peak at a diffraction angle, 2 theta, of 24.08° (Table 20).

Table 20: Experimental Diffraction Peaks and Intensities for Sulphamethoxazole

2 Theta [deg]	Intensity [Counts]
24.08	7608
20.72	4049
27.52	1961
12.16	998
8.24	995
42.00	983

Peaks at these wavelengths are also found in the diffraction pattern simulated from single crystal diffraction data of Sulphamethoxazole determined by Perlovich et al (2013). The Mercury software (Macrae et al., 2008) was used to simulate the powder diffraction pattern from the single crystal data and compared to the experimental pattern (Figure 54).

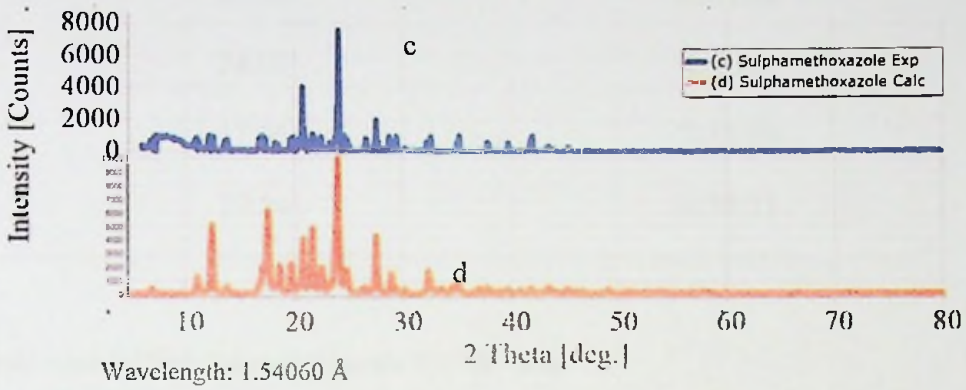

Figure 54: Experimental (Exp) and Simulated (Calc) Diffraction Patterns of Sulphamethoxazole.

For the simulated diffraction pattern, the highest peak is at a diffraction angle of 23.98° (Table 21). The intensities of the experimental peaks are low because the experimental measurements had a low signal to noise ratio and the strong preferred orientation effect due to the crystal shapes.

Table 21: Simulated Diffraction Peaks and Intensities for Sulphamethoxazole

2 Theta [deg]	Intensity [Counts]
23.98	10000.00
24.00	9969.66
23.96	8203.59
24.02	8021.2
17.56	7285.08
17.54	6758.71

Reduction of Sulphamethoxazole PXRD data

Indexing of the diffraction peaks was performed to calculate the lattice parameters (Table 22) of the unit cell using CMPR (Toby, 2006) and GSAS 2 (Larson & Von Dreele, 2004). The major peaks were used as characteristic peaks for the compound. The cell parameters reported by Perlovich et al (2013) using diffraction of a single crystal are close to those determined in this study. The variations may be due to the low signal/noise ratio and the effect of the $K_{\alpha 1+2}$ radiation. Preferred orientation effect was minimized in the collection of the experimental data by spinning the sample in the powder x-ray diffractometer (Plate 1).

Table 22: Experimental and Literature Cell Parameters of Sulphamethoxazole

Cell Parameter	Value	
	Experimental	Literature
a (Å)	16.0610	16.079 ± 0.006
b (Å)	5.4788	5.4807 ± 0.0019
c(Å)	25.7645	25.763 ± 0.009
α (°)	90	90
β (°)	96.13157	96.116 ± 0.006
γ (°)	90	90
Cell volume ($Å^3$)	2253.90	2257.4 ± 1.4

Powder X-ray Diffraction analyses of Carbazole

The experimental diffraction pattern of Carbazole has sharp peaks (Figure 55) which shows that the sample is made up mainly of crystalline material.

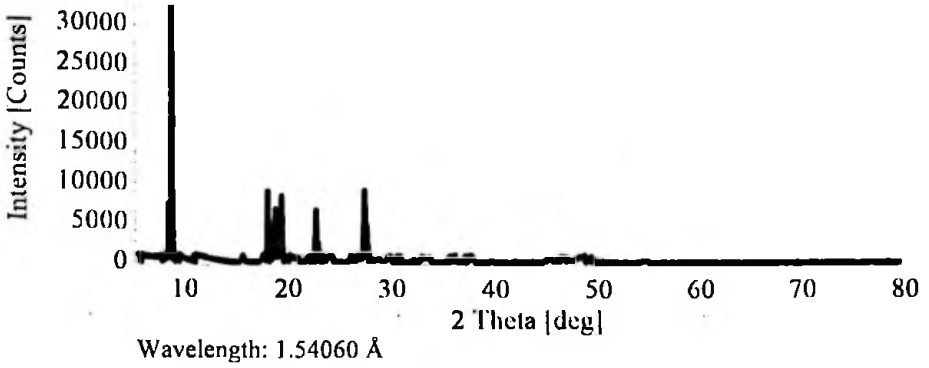

Figure 55: Experimental diffraction pattern of Carbazole.

There are however, peaks with broad bases at diffraction angles 9°, 19° and 27° indicating that some amorphous material is also present.

The experimental powder diffraction pattern of Ferron gives the highest peaks at a diffraction angle, 2 theta, of 9.2° (Table 23).

Table 23: Experimental Diffraction Peaks and Intensities for Carbazole

2 Theta [deg]	Intensity [Counts]
9.20	32340
27.84	9146
18.48	8977
19.84	8373
23.12	6562
6.32	994

The Mercury software (Macrae et al., 2008) was used to simulate the powder diffraction pattern from the single crystal diffraction data of Carbazole determined by Gajda et al (2014) and compared to the experimental pattern (Figure 56). Some of the peaks in the simulated diffraction pattern are at higher wavelengths than wavelengths of the corresponding peaks in the experimental diffraction pattern. This may be due to slight variations in the lattice parameters or the d-spacing of the unit cells.

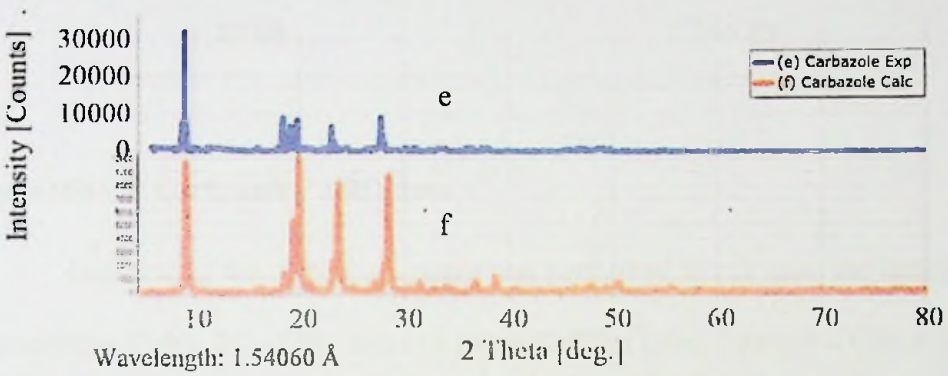

Figure 56: Experimental (Exp) and Simulated (Calc) Diffraction Patterns of Carbazole.

For the simulated diffraction pattern, the highest peak is at a diffraction angle of 20.02° (Table 24). The intensities of the experimental peaks are low because the experimental measurements had a low signal to noise ratio and the strong preferred orientation effect due to the crystal shapes.

Table 24: Simulated Diffraction Peaks and Intensities for Carbazole

2 Theta [deg]	Intensity [Counts]
20.02	10,000
9.30	9,639.47
20.04	9,031.53
28.54	8,736.77
9.28	8,424.07
20.00	8,365.89

Reduction of Carbazole PXRD data

Indexing of the diffraction peaks was performed to calculate the lattice parameters (Table 24) of the unit cell using CMPR (Toby, 2006) and GSAS 2 (Larson & Von Dreele, 2004). The major peaks were used as characteristic peaks for the compound. The cell parameters reported by Gajda et al (2014) using diffraction of a single crystal are different from those determined in this study. This may be due to the Bravais lattice and space group used in the calculated model. Preferred orientation effect was minimized in the collection of the experimental data by spinning the sample in the powder x-ray diffractometer.

Table 25: Experimental and Calculated Cell Parameters of Carbazole

Cell Parameter	Value	
	Experimental	Calculated
a (Å)	5.37120	7.6371 ± 0.0002
b (Å)	10.2175	19.0042 ± 0.0006
c(Å)	19.2597	5.67758 ± 0.00014
α (°)	90	90
β (°)	90	90
γ (°)	90	90
Cell volume ($Å^3$)	1057.130	824.03 ± 0.04

Powder X-ray Diffraction analyses of Ferron Mixed with Sulphamethoxazole

The diffraction peaks of the sample of mixing Ferron with Sulphamethoxazole have intensities far lower than that of the starting materials (Figure 57). The major peaks of the starting materials however can be seen in the diffraction pattern of the starting materials. The peaks of the mixed sample however are broad at the base indicating a quantity of amorphous material present.

The intensities of diffraction pattern of the mixed sample are not a simple arithmetic summation of those of the diffraction patterns of the starting materials (Table 26).

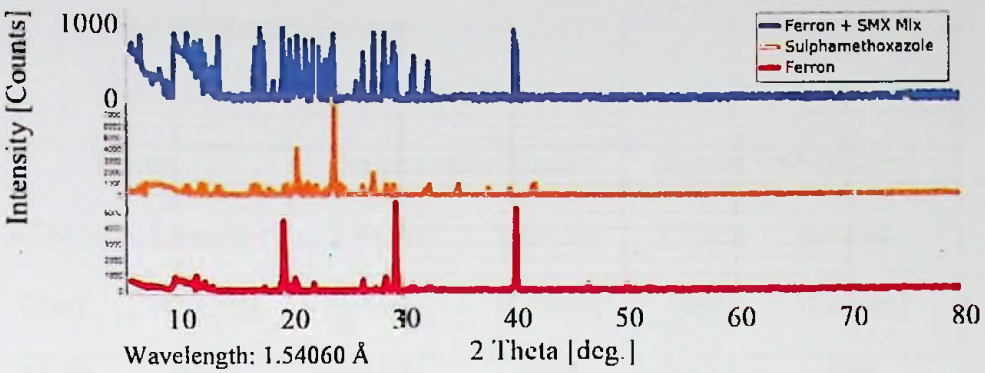

Figure 57: Experimental (Exp) Diffraction patterns of Ferron,

Sulphamethoxazole and Ferron + SMX Mix.

Table 26: Diffraction angles of major peaks of Mixed sample of Ferron and Sulphamethoxazole

Ferron		Sulphamethoxazole		Ferron + SMX Mix	
2 Theta [deg]	Intensity [Counts]	2 Theta [deg]	Intensity [Counts]	2 Theta [deg]	Intensity [Counts]
29.52	5682	24.08	7608	17.52	992
40.32	5286	20.72	4049	19.52	992
19.52	4514	27.52	1961	40.24	950
11.76	975	12.16	998	27.6	938
28.56	893	8.24	995	28.56	921
9.84	869	42	983	11.04	906
20.56	825	7.36	979	24	906
26.56	751	35.2	968	9.92	900
6.08	661	17.04	955	20.8	877
22.24	517	29.36	935	6.88	861
46.8	432	32.56	929	13.76	860
50.24	387	19.84	914	12.24	807
31.04	360	11.04	841	29.44	785
32.56	355	26.56	805	26.64	658
17.84	268	13.84	740	31.2	602
52.24	214	37.84	593	32.48	530
73.36	117	18.24	553	8.56	421

Powder X-ray Diffraction analyses of Ferron Ground with Sulphamethoxazole

The experimental diffraction pattern of samples of Ferron ground with Sulphamethoxazole generally have lower intensities than those of the starting compounds (Figures 58, 59 and 60). However, these intensities increase as the duration of grinding is increased from 10 minutes to 30 minutes. The peaks become increasingly broader as the duration for grinding increases.

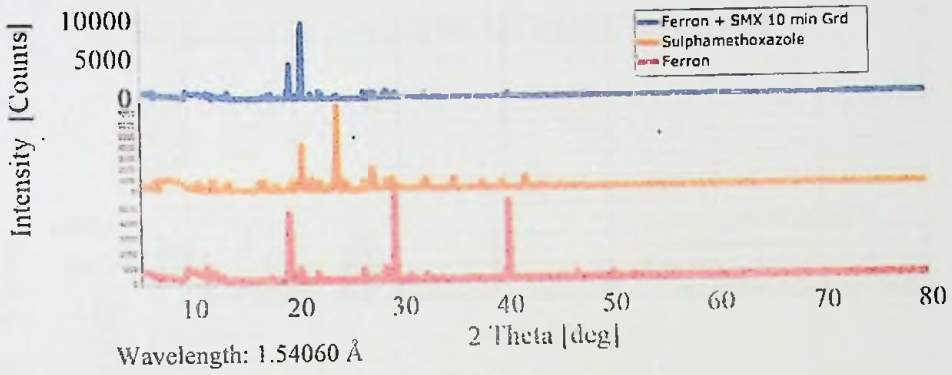

Figure 58: Experimental (Exp) Diffraction patterns of Ferron, Sulphamethoxazole and Ferron + SMX 10 min Grd.

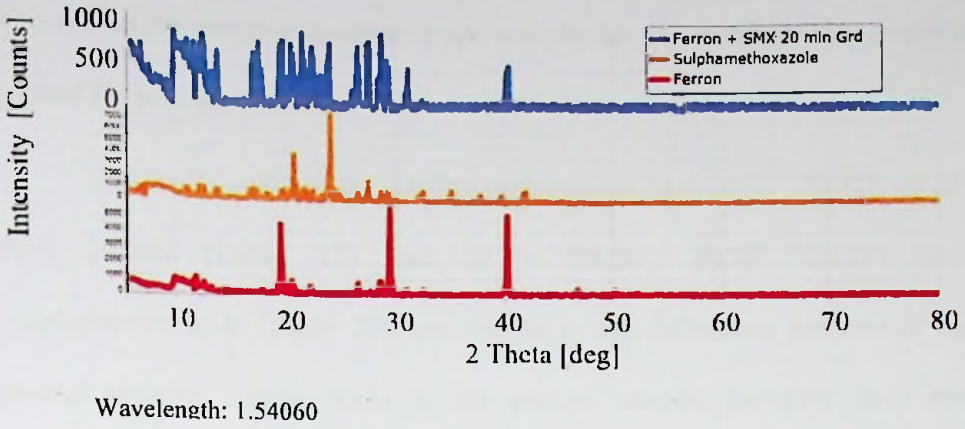

Figure 59: Experimental (Exp) Diffraction patterns of Ferron,

Sulphamethoxazole and Ferron + SMX 20 min Grd.

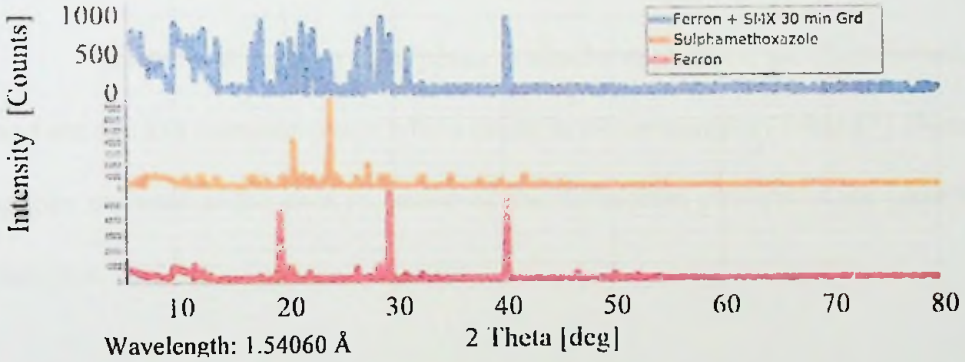

Figure 60: Experimental (Exp) Diffraction patterns of Ferron,

Sulphamethoxazole and Ferron + SMX 30 min Grd.

This means the amorphous phase in the samples are increasing as the sample is ground for a longer period of time.

The major peaks of the starting materials, at $2\theta = 19.52°, 29.52°, 40.32°$ from Ferron (Table 17) and $2\theta = 24.08°, 20.72°, 20.72°$ from Sulphamethoxazole (Table 20), are visible in the diffraction patterns of the ground samples. These peaks in the ground samples however have low intensities except the peak around $2\theta = 20°$ in the diffraction pattern of the 10-minute ground sample, Ferron + SMX 10 min Grd. This is because around this angle, both starting compounds have peaks, which reinforce each other. The peak due to Ferron at $2\theta = 40.32°$ has its intensity increasing as the duration for grinding is increased.

The ground samples have peaks at similar angles that are characteristic and are due to a common phase which exists in all the samples (Table 27).These angles are used in the data reduction of the diffraction patterns of the ground samples.

Table 27: Diffraction angles of major peaks of Ground samples of Ferron and Sulphamethoxazole

Ferron + SMX 10 min Grd		Ferron + SMX 20 min Grd		Ferron + SMX 30 min Grd	
2 Theta [deg]	Intensity [Counts]	2 Theta [deg]	Intensity [Counts]	2 Theta [deg]	Intensity [Counts]
20.8	9,681	*28.8*	*966*	*28.8*	*995*
*19.6**	*4,453*	21.52	954	40.24	986
28.72	*998*	*9.84*	*922*	*17.76*	*944*
9.84	*972*	12.4	891	*9.92*	*925*
22.4	*958*	*27.6*	*872*	21.52	911
26.64	*891*	*19.68*	*853*	*27.6*	*851*
11.04	*841*	24	831	12.56	840
13.76	*804*	*17.52*	*817*	*22.56*	*832*
6.8	*795*	*11.04*	*812*	*6.16*	*811*
17.84	*740*	*26.56*	*793*	*26.72*	*730*
27.6	*716*	*22.4*	*776*	20.48	705
32.48	662	*6.88*	*740*	*13.76*	*701*

*Diffraction angles common to all samples are in italics

Powder X-ray Diffraction analyses of Ferron Kneaded with Sulphamethoxazole.

The experimental diffraction pattern of samples of Ferron kneaded with Sulphamethoxazole generally have lower intensities than those of the starting compounds (Figures 61, 62 and 63).

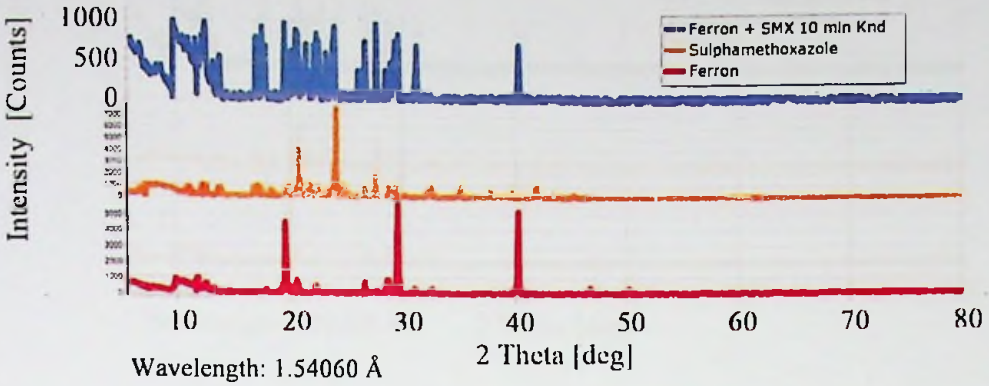

Figure 61: Experimental (Exp) Diffraction patterns of Ferron,

Sulphamethoxazole and Ferron + SMX 10 min Knd.

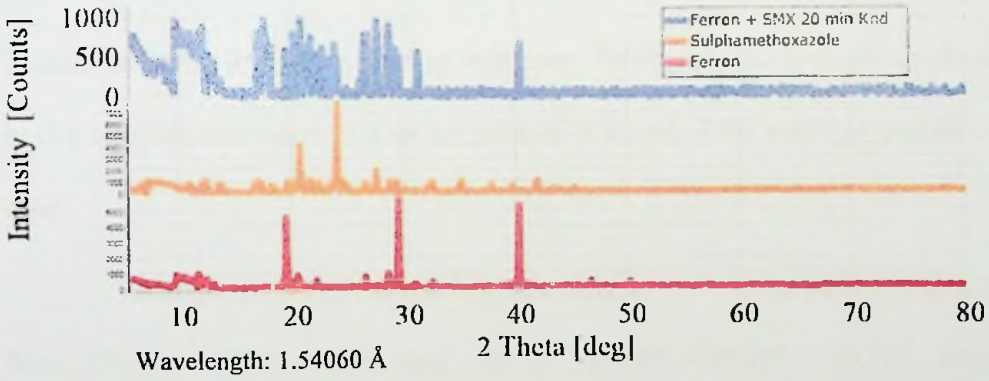

Figure 62: Experimental (Exp) Diffraction patterns of Ferron,

Sulphamethoxazole and Ferron + SMX 20 min Knd.

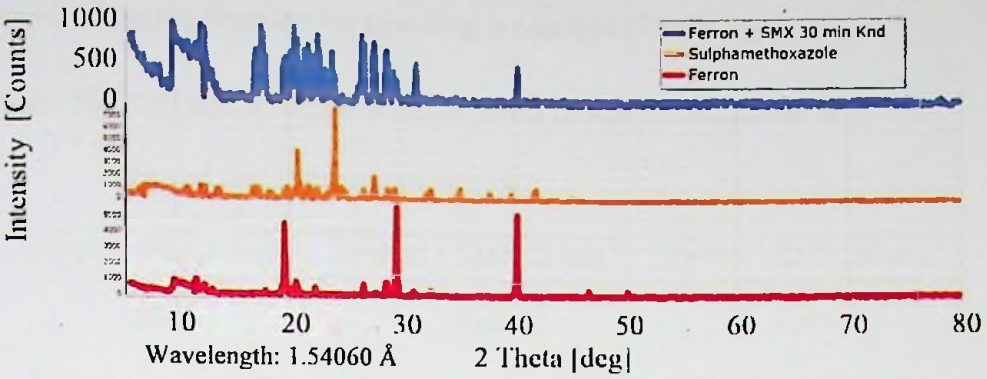

Figure 63: Experimental (Exp) Diffraction patterns of Ferron, Sulphamethoxazole and Ferron + SMX 30 min Knd.

However, these intensities decrease slightly as the duration of kneading is increased from 10 minutes to 30 minutes. The peaks become increasingly broader as the duration for kneading increases. This means the amorphous phase in the samples are increasing as the sample is kneaded for a longer period of time.

The major peaks of the starting materials, at $2\theta = 19.52°, 29.52°, 40.32°$ from Ferron (Table 17) and $2\theta = 24.08°, 20.72°, 20.72°$ from Sulphamethoxazole (Table 20), are visible in the diffraction patterns of the kneaded samples. These peaks in the kneaded samples however have low intensities similar to all the other peaks. This implies that kneading the starting compounds together quickly brings the kneaded sample to an increased amorphous state and drastically reduces the crystalline nature of the samples.

The kneaded samples have peaks at similar angles between $2\theta = 13°$ and $33°$. This range is used in indexing the diffraction patterns in this study.

However, there are no similarities nor trend in the intensities for each diffraction angle, 2θ, as the duration for kneading is changed (Table 28).

Table 28: Diffraction angles of major peaks of Kneaded samples of Ferron and Sulphamethoxazole

Ferron + SMX 10 min Knd		Ferron + SMX 20 min Knd		Ferron + SMX 30 min Knd	
2 Theta [deg]	Intensity [Counts]	2 Theta [deg]	Intensity [Counts]	2 Theta [deg]	Intensity [Counts]
*9.76**	*991*	*20.8*	*990*	*9.76*	*981*
27.6	*984*	*17.52*	*982*	*20.48*	*973*
19.52	977	*27.52*	*972*	*12.24*	*955*
12.48	*973*	9.76	969	*17.52*	*941*
23.92	*939*	28.64	918	26.48	863
17.52	*928*	*12.24*	*896*	*22.56*	*857*
20.56	*887*	21.68	769	6.24	845
29.6	852	*40.32*	*688*	*27.52*	*772*
22.32	*846*	*23.84*	*679*	21.68	714
26.64	766	*22.72*	*632*	28.64	670
40.32	*730*	*31.2*	*576*	*23.84*	*644*
31.2	*718*	8.4	469	*31.28*	*518*
13.76	547	36.88	119	*40.32*	*491*
8.64	434	35.68	99	14.8	99
32.48	105	49.04	99	15.92	99
36.08	99	60.72	99	34.72	99
44.08	99	66.24	99	48.96	99

* Diffraction angles common to all samples are in italics

Reduction of Ferron + SMX 30 min Knd PXRD data

The x-ray diffraction patterns were used to determine the cell parameters of the phases in this sample.

Indexing of the diffraction peaks of the 30-minute kneaded sample, Ferron + SMX 30 min Knd, was performed to determine the lattice parameters (Table 28) of the unit cell using CMPR (Toby, 2006) and GSAS 2 (Larson & Von Dreele, 2004). The major peaks were used as characteristic peaks for the phase. The cell is monoclinic with a space group of C2/m (Table 29).

Table 29: Determined Cell Parameters of Ferron + SMX 30 min Knd

Cell Parameter	Values
a (Å)	21.00356
b (Å)	10.43984
c(Å)	28.16611
α (°)	90
β (°)	133.584
γ (°)	90
Cell volume (Å^3)	4473.721

These cell parameters are unique to the phase and were found to be different from the cell parameters of the starting materials. This is proof enough that new phases, in this case, co-crystals were formed. The properties of the components which were changed were mainly the crystal structure (crystal packing, bond lengths and angles between the various atoms, etc.) which

determines other physical and chemical properties such as melting point, colour, degradation point, stability, bioavailability and solubility.

Powder X-ray Diffraction analyses of Ferron Mixed with Carbazole

The diffraction peaks of the sample of mixing Ferron with Carbazole have intensities far lower than that of the starting materials (Figure 64). The major peaks of the starting materials however can be seen in the diffraction pattern of the starting materials. The peak at 19.52° in the diffraction pattern of Ferron with an intensity of 4,518 counts corresponds to the highest peak in the pattern of the mixed sample at 19.76° with approximately twice the same intensity, 8,822 counts (Table 29). This could possibly be an overlap effect from the peak of the Carbazole at 19.84°. The peaks of the mixed sample are relatively sharp indicating the crystalline structure is maintained when the starting compounds are mixed together (Figure 64).

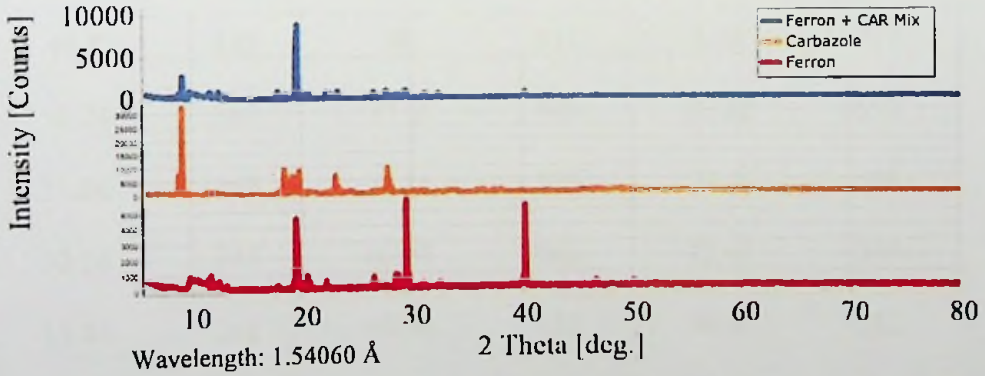

Figure 64: Experimental (Exp) Diffraction patterns of Ferron, Carbazole and Ferron + CAR Mix.

Table 30: Diffraction angles of major peaks of Mixed sample of Ferron and Carbazole

Ferron		Carbazole		Ferron + CAR Mix	
2 Theta [deg]	Intensity [Counts]	2 Theta [deg]	Intensity [Counts]	2 Theta [deg]	Intensity [Counts]
29.52	5,682	9.2	32,340	19.6	8,822
40.32	5,286	27.84	9,146	9.2	2,835
19.52	4,514	18.48	8,977	29.44	970
11.76	975	19.84	8,373	12.48	969
28.56	893	23.12	6,562	17.84	967
9.84	869	6.32	994	27.68	961
20.56	825	11.52	986	23.28	871
26.56	751	36.56	978	22.24	848
6.08	661	24.64	959	26.56	762
22.24	517	49.12	933	20.72	759
46.8	432	38	911	6.08	719
50.24	387	31.2	908	40.32	650
31.04	360	30.24	898	31.2	596
32.56	355	16.08	866	32.48	590
17.84	268	46.96	830	46.8	252
52.24	214	33.36	773	36.88	99
73.36	117	54.96	333	42.72	99

Powder X-ray Diffraction analyses of Ferron Ground with Carbazole

The experimental diffraction pattern of samples of Ferron ground with Carbazole have similar intensities to those of Ferron (same order of magnitude) especially for samples ground for 10 and 20 minutes (Figures 65 and 66). For the sample of Ferron and Carbazole ground for 30 minutes, (Figure 67) the intensities are relatively low and almost equal, implying that the material had become more amorphous (less crystalline) than those of the starting compounds.

The peak due to Carbazole at the diffraction angle of 9.20° has a higher intensity in the 10-minute ground sample (5,715 counts) (Table 31) than 20-minute ground sample (1,126 counts) (Table 31). The only peak due to Ferron which maintains its intensity when the samples are ground for either 10 or 20 minutes is the peak at 19.52°; the corresponding peaks are both at 19.6° (the intensities are 6,434 counts and 7,319 counts respectively) (Table 31). The other major peaks of Ferron at 29.52° and 40.32° have low intensities when Ferron is ground with Carbazole for either10, 20 or 30 minutes (Figures 65, 66 and 67). The peaks remain relatively sharp whether the samples are ground for 10 or 20 minutes but become broad when the sample is ground for 30 minutes indicating the loss of crystallinity.

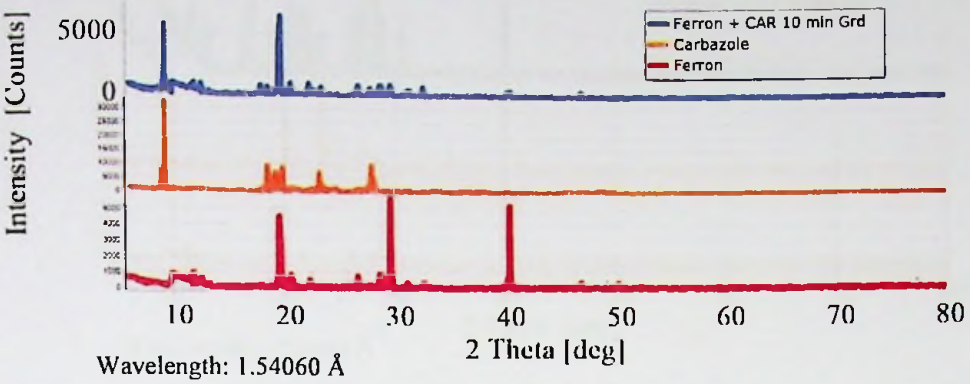

Figure 65: Experimental (Exp) Diffraction patterns of Ferron,

Carbazole and Ferron + CAR 10 min Grd.

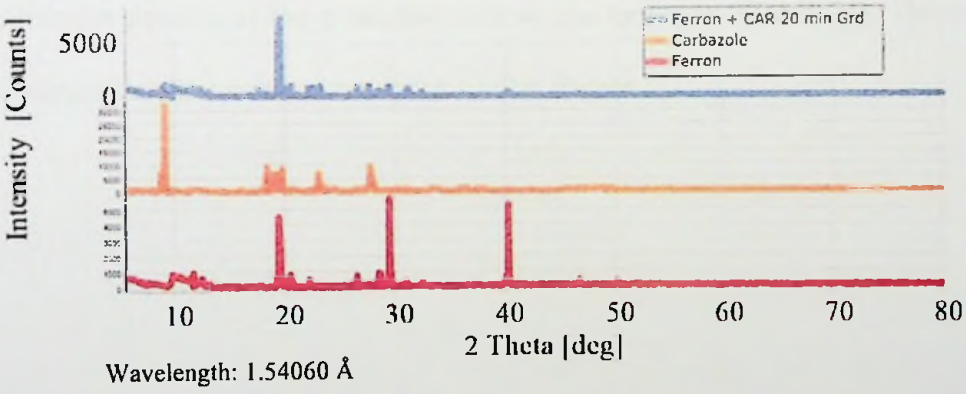

Figure 66: Experimental (Exp) Diffraction patterns of Ferron,

Carbazole and Ferron + CAR 20 min Grd.

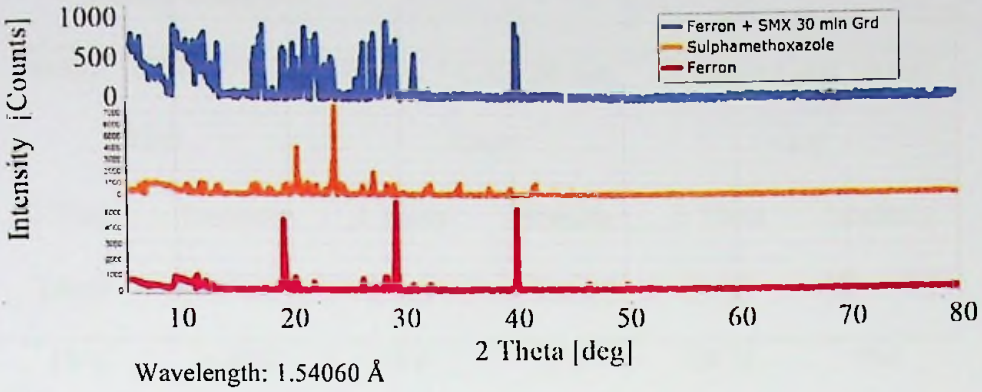

Figure 67: Experimental (Exp) Diffraction patterns of Ferron, Carbazole and Ferron + CAR 30 min Grd.

When Ferron is ground with Carbazole, the major peaks of the diffraction patterns of the products occur at similar angles (Table 31). This is indicative that the products comprise similar phases.

Table 31: Diffraction angles of major peaks of Ground samples of Ferron and Carbazole

Ferron + CAR 10 min Grd		Ferron + CAR 20 min Grd		Ferron + CAR 30 min Grd	
2 Theta [deg]	Intensity [Counts]	2 Theta [deg]	Intensity [Counts]	2 Theta [deg]	Intensity [Counts]
19.6	6,434	19.6	7,319	28.72	944
9.2	*5,715*	*9.2*	*1,126*	*9.84*	*925*
22.16	*945*	*20.64*	*995*	*31.2*	*857*
20.56	*938*	29.52	957	8.96	838
11.84	931	*27.68*	*954*	*23.2*	*831*
29.52	899	*26.64*	*926*	12.56	816
26.64	*813*	*23.28*	*916*	*17.84*	*739*
17.84	*761*	*22.24*	*874*	*20.64*	*731*
32.48	*719*	11.68	820	*22.16*	*703*
23.28	*638*	*17.76*	*804*	*26.56*	*650*
27.68	*595*	*31.2*	*753*	*40.48*	*575*
31.2	*498*	6.16	734	*27.6*	*514*
40.4	*456*	28.64	570	16.96	407
46.8	404	*40.32*	*444*	*32.48*	*147*
50.32	202	*32.48*	*436*	45.12	99
51.76	99	46.8	172	47.76	99
58.24	99	50.16	99	63.52	99

* Diffraction angles common to all samples are in italics

Powder X-ray Diffraction analyses of Ferron Kneaded with Carbazole

The experimental diffraction pattern of samples of Ferron kneaded with Carbazole (Figures 68, 69 and 70) generally have lower intensities (less than 1000 counts) than those of the starting compounds. The Carbazole diffraction peak at 9.2° decreases in intensity from 32,340 counts to a low 826 counts for the 10-minute kneaded sample (at 8.96°), 992 counts for the 20-minute kneaded sample (at 9.60°) and 751 counts for the 30 –minute kneaded sample (at 8.96°) (Table 32). This indicates that the kneading process makes the samples more amorphous even after a kneading duration of just 10 minutes, the shortest duration in this study.

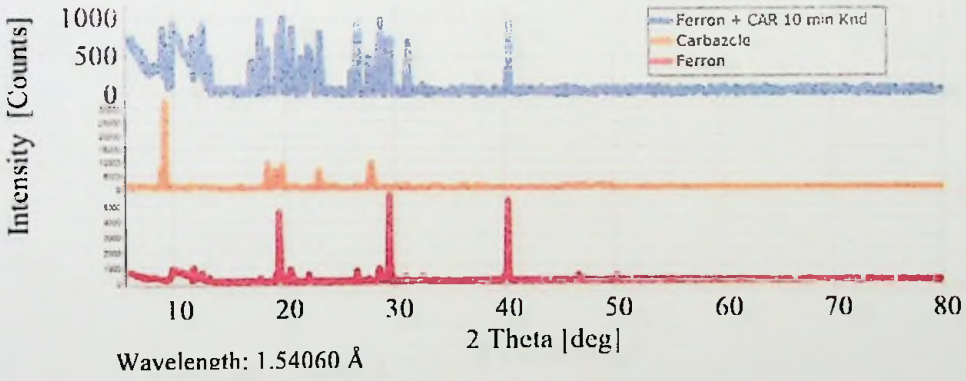

Figure 68: Experimental (Exp) Diffraction patterns of Ferron, Carbazole and Ferron + CAR 10 min Knd.

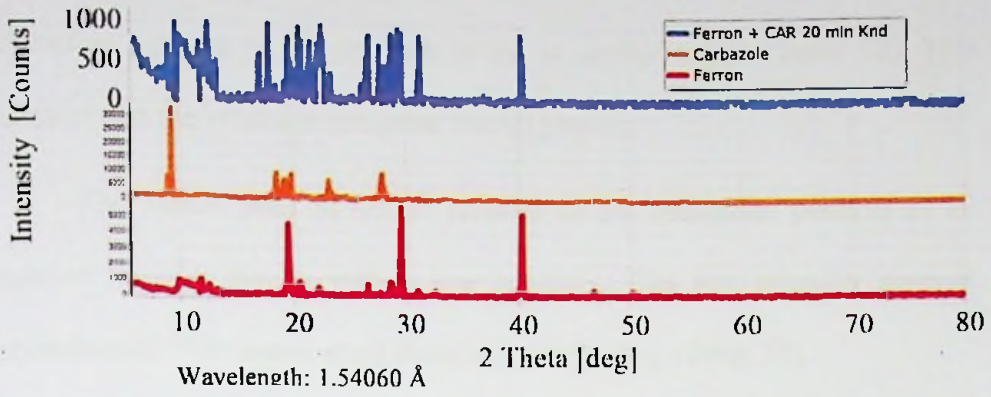

Figure 69: Experimental (Exp) Diffraction patterns of Ferron, Carbazole and Ferron + CAR 20 min Knd.

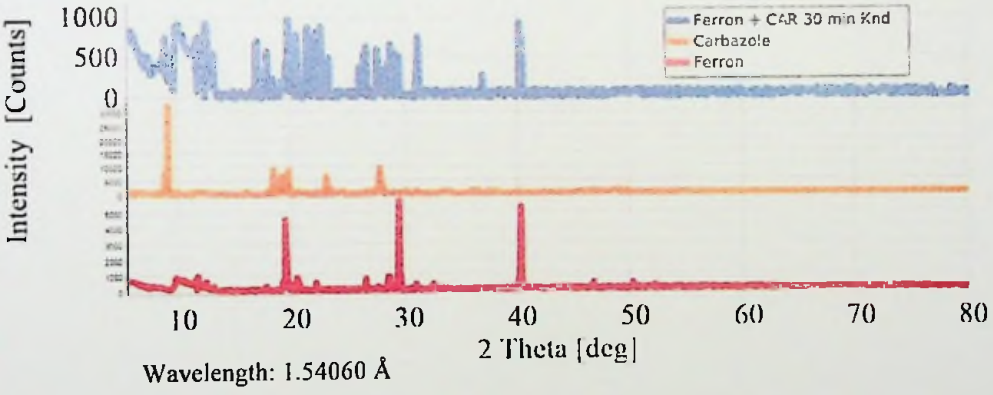

Figure 70: Experimental (Exp) Diffraction patterns of Ferron, Carbazole and Ferron + CAR 30 min Knd.

When Ferron is kneaded with Carbazole, the major peaks of the diffraction patterns of the products occur at similar angles (Table 32). This indicates that the products comprise similar phases.

The Ferron peak at 40.32° remains in the diffraction patterns of all kneaded samples though with a low intensity. This low intensity remains approximately 900 counts at all durations of kneading (Table 32).

Table 32: Diffraction angles of major peaks of Kneaded samples of Ferron and Carbazole

Ferron + CAR 10 min Knd		Ferron + CAR 20 min Knd		Ferron + CAR 30 min Knd	
2 Theta [deg]	Intensity [Counts]	2 Theta [deg]	Intensity [Counts]	2 Theta [deg]	Intensity [Counts]
19.76	*999*	*12.4*	*998*	*19.76*	*971*
28.72	987	9.6	992	*40.24*	*939*
17.76	*975*	*17.84*	*987*	*12.48*	*926*
40.4	*959*	*22.48*	*980*	10.16	914
26.56	*930*	29.28	955	*22.64*	*885*
12.56	927	20.48	949	21.52	869
9.84	912	*40.24*	*907*	*31.2*	*755*
20.64	868	*26.72*	*871*	8.96	751
8.96	862	*31.2*	*870*	17.04	715
23.2	813	*19.6*	*818*	28.8	663
29.6	751	6.08	780	*26.64*	636
6.24	743	*27.6*	*742*	*27.6*	*602*
31.2	*707*	36.96	131	*17.92*	*580*
22.16	*633*	44.64	99	36.96	278
27.6	*506*	66.32	99	32.96	99
32.48	141	67.28	99	38.56	99
36.16	99	69.52	99	51.04	99

* Diffraction angles common to all samples are in italics

The x-ray diffraction patterns could not be used to determine the cell parameters of the phases in the products. This is proof enough that no new phases, in this case, co-crystals were formed.

Differential Scanning Calorimetry (DSC)

In Differential Scanning Calorimetry, DSC, the heat absorbed or liberated during heating or cooling of a sample is measured. A change in phase involves structural changes in the material that are accompanied by evolution or absorption of heat. The transformation (melting, crystallization, decomposition, etc.) temperatures are measured as the peaks in the resulting curve. The transformation enthalpy (heat capacity, etc.) are proportional to the areas under the curve.

DSC curves of Ferron, Sulphamethoxazole and Carbazole

The DSC curves for the Ferron, Sulphamethoxazole and Carbazole were measured to determine their melting points, decomposition temperatures and the latent heats of these thermal events.

Analyses of DSC curve of Ferron

The melting point is taken as the temperature at which the curve has the highest first order derivative, which is 269.25°C (Figure 71). This is within the melting point range of 269-270°C for Ferron reported in literature. The laboratory determined melting point of Ferron in this study was 267-270°C using the capillary tube method. The melting process merges with the decomposition of Ferron which starts at 286.07°C and peaks at a temperature of 291.30°C.

The area under the curve, A, was determined to be 2,304.09 mJ. Given the mass of sample as 6.13 mg, the latent heat of melting/decomposition was calculated as -375.87 J/g.

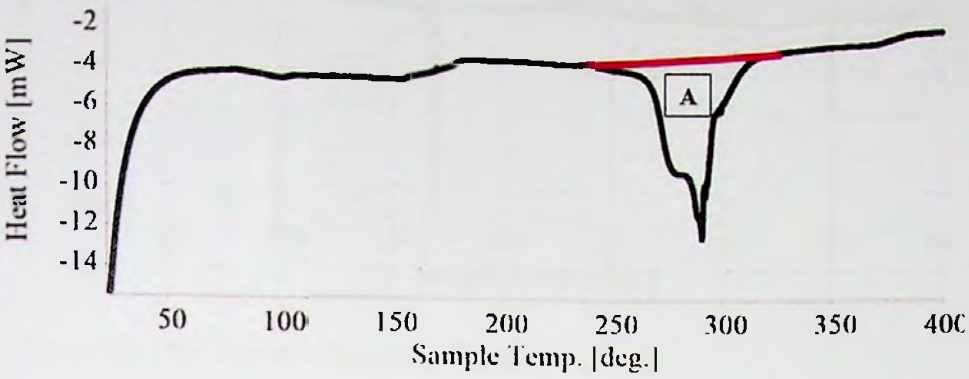

Figure 71: DSC curve of Ferron.

Analyses of DSC curve of Sulphamethoxazole

The melting point peak is sharp indicating the sample is pure; the melting point is therefore taken as the onset temperature which is 168.30°C (Figure 72). This falls within the range of the literature value of 166-171.5°C and agrees with that determined in the laboratory, which was 170°C. Sulphamethoxazole decomposes exothermically at 250.07°C, with a peak temperature of 264.42°C (Figure 72).

The area under the curve for the melting point, B, was found to be -390.93 mJ. Given the sample size of 3.48 mg, the latent heat of melting was calculated as -112.34 J/g. The area under the curve for the decomposition process, C, is 1,641.35 mJ, giving a latent heat of decomposition of 471.65 J/g.

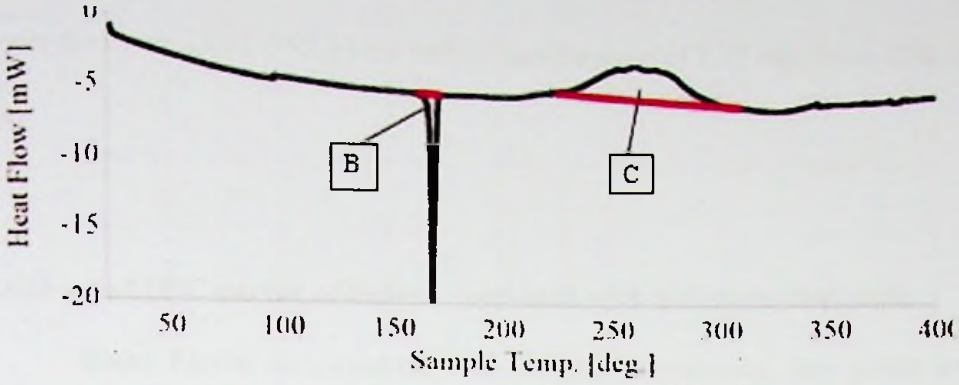

Figure 72: DSC curve of Sulphamethoxazole.

Analyses of DSC curve of Carbazole

The melting point peak is sharp indicating a pure sample; the melting point is 244.09°C (Figure 73). Literature gives the melting point of Carbazole as 243-246°C while laboratory determination in this study put the melting point of Carbazole as 244 – 245°C. Carbazole undergoes an almost instantaneous endothermic decomposition at about 286°C (Figure 73).

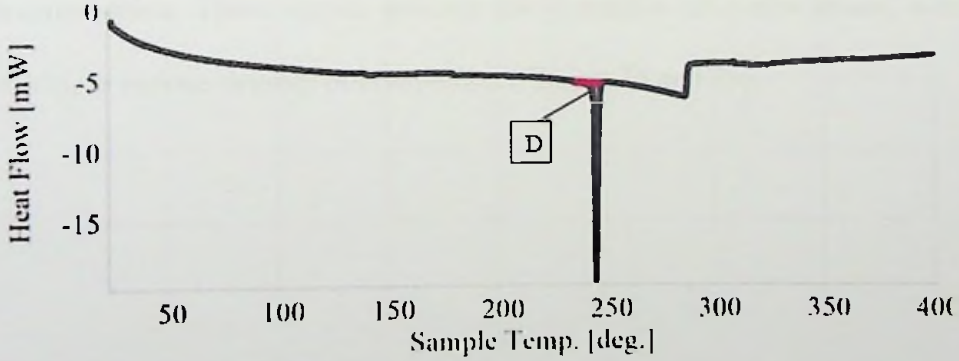

Figure 73: DSC curve of Carbazole.

The latent heat of melting of Carbazole was calculated (using the area under the curve, D, as -295.33 mJ and the sample mass of 2.27 mg) to be -130.10 J/g.

Analyses of DSC curves of Ferron combined with Sulphamethoxazole

When Ferron is combined with Sulphamethoxazole, two peaks are observed; an endothermic peak which is the melting event and an exothermic peak from a decomposition event (Figures 74 and 75). The area under the former peak is latent heat of melting of the sample while the area under the later peak is the enthalpy of this decomposition event. The peaks of the exothermic decomposition event are relatively sharp (Figures 74 and 75) indicating that they are due to a new phase formed by these components.

The DSC of the product-samples showed sharp and distinct peaks meaning a unique product was formed. This new product melts at a different temperature from the starting materials and undergoes an exothermic decomposition. These curves indicate the formation of a new phase, a co-crystal, to various degrees of completion (Figures 74 and 75).

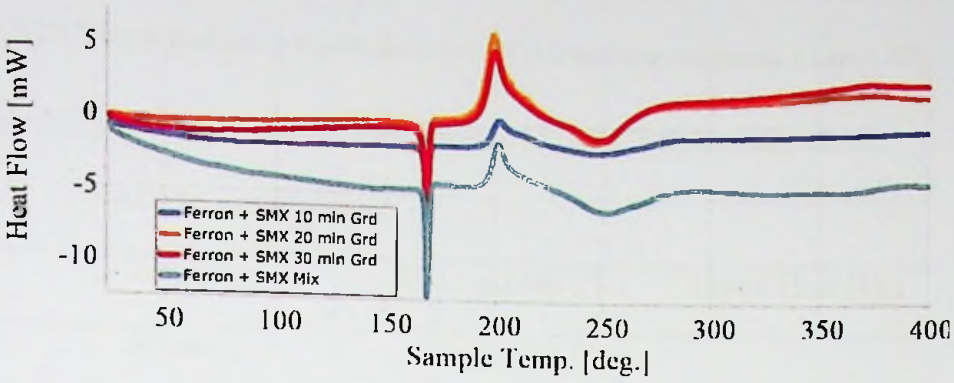

Figure 74: DSC curves of Ground Ferron and Sulphamethoxazole.

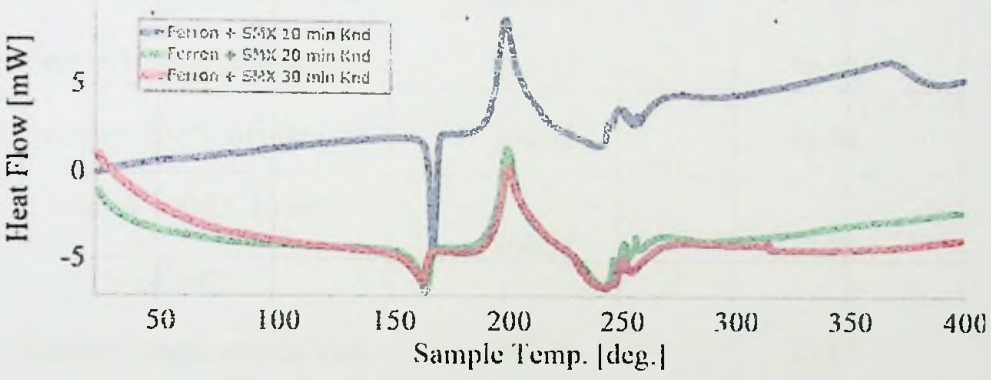

Figure 75: DSC curves of Kneaded Ferron and Sulphamethoxazole.

Melting Points of Combinations of Ferron and Sulphamethoxazole

The melting points of all the samples prepared were lower than that of the starting compounds, Ferron and Sulphamethoxazole (Table 33); they were however closer to the melting point of Sulphamethoxazole (168.30°C). The melting points of samples from grinding were 167±1°C. On the other hand, apart from the 10-minute kneaded sample, Ferron + SMX 10 min Knd whose melting

point was 166.52°C, the melting points of samples from kneading, Ferron + SMX 20 min Knd (m.p. 160.21°C) and Ferron + SMX 30 min Knd (m.p. 156.92°C) were distinctly lower than that of the starting materials (Table 33).

Table 33: Melting points and Latent Heats of Ferron, Sulphamethoxazole and their Combinations

Sample	Melting point (°C)	Latent Heat (J/g)
Ferron	269.25	
SMX	168.30	-112.34
Ferron + SMX Mix	167.50	-38.85
Ferron + SMX 10 min Grd*	167.00	-39.54
Ferron + SMX 20 min Grd	166.14	-38.52
Ferron + SMX 30 min Grd	166.32	-38.96
Ferron + SMX 10 min Knd**	166.52	-38.84
Ferron + SMX 20 min Knd	160.21	-37.86
Ferron + SMX 30 min Knd	156.92	-40.25

* Ground; ** Kneaded

The 'melting' peaks of the ground samples are sharp indicating a distinct new phase (Figure 74). The latent heats involved in these processes are also approximately the same,-39.0±0.5 J/g and are the same as when the samples were mixed (-38.85 J/g). Mixing or grinding Ferron and Sulphamethoxazole together therefore gives products with similar thermal properties. This implies that the products are combinations of the starting materials and the minor

differences in the thermal properties may be due to the arbitrary variations in the quantities of each material in the products.

In the case of kneading, the melting point decreased with the duration of kneading from 166.52°C (for 10 minutes) to 156.92°C (for 30 minutes).The 'melting' peaks are sharp (Figure 75), especially for the 20 and 30 minute samples, indicating a new phase. The latent heat of melting for the kneaded samples are quite different from each other (the latent heat of melting for the 30-minute kneaded sample is -40.25 J/g while that of the 20-minute kneaded sample is -37.86 J/g). The latent heat of melting of the 10-minute kneaded sample is however similar to that of the mixed or ground samples. The thermal properties of the 20-minute and 30-minute kneaded products (Ferron + SMX 20 min Knd and Ferron + SMX 30 min Knd) are different from those of either starting materials. This indicates the presence of a new phase or material in these products (Table 33).

Decomposition of Combinations of Ferron and Sulphamethoxazole

All the products decompose exothermically (Table 34). The trend observed with the melting of the samples are also observed when the products decompose. The temperature at which decomposition starts for all the combined samples are far lower than that of either Ferron or Sulphamethoxazole, the lowest being 192.55°C (Ferron ground with Sulphamethoxazole for 20 minutes) and the highest being 195.81°C for mixing Ferron with Sulphamethoxazole (Table 34). However, these temperatures are all statistically the same, i.e.,,

194±2°C. Likewise, the maximum temperature attained during decomposition are also statistically the same, that is, 200.00 ±2°C (Table 34).

Table 34: Decomposition temperatures of Ferron, Sulphamethoxazole and their combinations

Sample	Onset Decomposition Point (°C)	Peak Decomposition Point (°C)	Latent Heat of Decomposition (J/g)
Ferron	283.07	291.30	-375.87
SMX	250.07	264.42	471.65
Ferron + SMX Mixed	195.81	201.61	159.01
Ferron + SMX 10 min Grd	195.63	202.10	149.29
Ferron + SMX 20 min Grd	192.55	199.32	241.33
Ferron + SMX 30 min Grd	193.16	199.84	230.91
Ferron + SMX 10 min Knd	193.41	200.03	185.78
Ferron + SMX 20 min Knd	194.10	201.24	278.13
Ferron + SMX 30 min Knd	194.66	201.69	298.60

The decomposition peaks are all relatively sharper than that of Sulphamethoxazole indicating that the phases which are decomposing at this temperature in the samples are relatively pure (Table 34). The highest enthalpy recorded is from the sample formed from kneading Ferron with Sulphamethoxazole for 30 minutes (298.60 J/g) (Table 34). This means that this sample is likely to have the highest quantity of the unknown new phase as compared to the other samples.

Mixing the compounds or grinding for 10 minutes gave the lowest enthalpies, 159.01 J/ g and 149.29 J/g respectively (Table 34) as expected since the conditions of mechano-synthesis of these samples were least severe. For the most 'severe' form of mechano-synthesis used in this study, kneading, increasing the duration increased the enthalpy of the resulting sample, the lowest being 185.78 J/g and the highest being 298.60 J/g (Table 34).

Analyses of DSC curve of Ferron combined with Carbazole

The DSC curves of samples from the combination of Ferron with Carbazole generally show two peaks, both endothermic; the melting process and

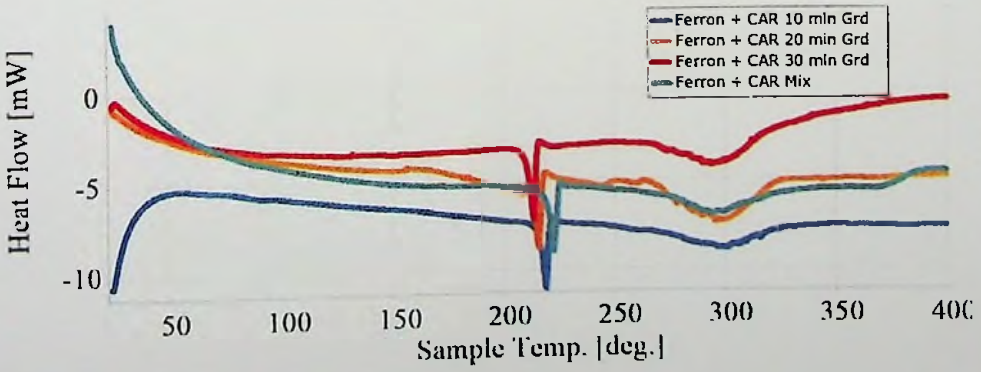

Figure 76: DSC curves of Ground Ferron and Carbazole.

the decomposition process. The melting process gives a sharp peak in all cases (Figures 76 and 77) indicating that the phases have similar structures and are relatively pure.

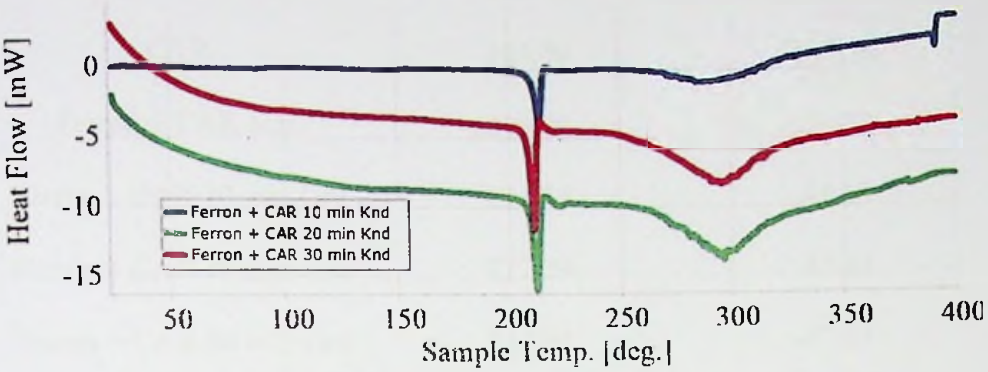

Figure 77: DSC curves of Kneaded Ferron and Carbazole.

Melting Points of Combinations of Ferron and Carbazole

The melting point of the samples where the compounds are ground together decrease as the duration for grinding increases from 215.24°C for the sample ground for 10 minutes to 210.01°C for the sample ground for 30 minutes (Table 35).

Table 35: Melting points and Latent Heats of Ferron, Carbazole and their Combinations

Sample	Melting point (°C)	Latent Heat (J/g)
Ferron	269.25	-
CAR	244.09	-130.10
Ferron + CAR Mix	218.79	-59.20
Ferron + CAR 10 min Grd	215.24	-42.13
Ferron + CAR 20 min Grd	212.29	-33.30
Ferron + CAR 30 min Grd	210.01	-42.27
Ferron + CAR 10 min Knd	210.26	-45.85
Ferron + CAR 20 min Knd	209.03	-44.61
Ferron + CAR 30 min Knd	208.74	-44.98

These temperatures however are lower than that of the starting compounds Ferron (269.25°C) and Carbazole (244.09°C). The melting point for the mixed sample is 218.79°C which is close to that of the ground samples (Table 35). This indicates a similarity in the phase structure of combining the compounds together by either mixing or grinding. A look at the latent heat of melting of the samples (Table 35) indicate that no new phases were formed when the compounds were combined together because the heats are dissimilar and do not correlate to the mechano-synthesis conditions applied to prepare the samples. The disarray is indicative of a mixture of phases.

Similarly, the melting point of samples of kneaded compounds also have melting points lower than the starting compounds and even lower than the

ground samples. The melting points decrease as the duration of the mechano-synthesis is increased from 10 minutes (m. p. 210.26°C) to 30 minutes (m. p. 208.74°C). Here also the latent heat of melting do not correlate to the duration used to prepare the samples; the highest latent heat is -44.61 J/g for sample kneaded for 20 minutes, followed by -44.98 J/g for the 30-minute kneaded sample and the lowest latent heat is for the 10-minute kneaded sample (-45.85 J/g) (Table 35). This confirms the deduction that the combination of Ferron and Carbazole gives a mixture whose thermal properties do not correlate with the method/process used in combining them and therefore cannot be predicted.

Decomposition of Combinations of Ferron and Carbazole

The apparently uncorrelated thermal behaviour of the combination of Ferron and Carbazole is confirmed by looking at the decomposition process of the samples. The temperature at which the samples start to decompose do not follow or correlate with the mode of preparation; the highest temperature is that of mixing the compounds together (290.20°C) and the lowest is that of kneading them together for 30 minutes (226.07°C). In between these extremes are the decomposition temperatures of the other samples including that of the starting compounds, Ferron (283.07°C) and Carbazole (286.00°C) (Table 36).

Table 36: Decomposition of Ferron, Carbazole and their Combinations

Sample	Onset Decomposition Point (°C)	Peak Decomposition Point (°C)	Latent Heat of Decomposition (J/g)
Ferron	283.07	291.30	-375.87
CAR	286 00	286.00	
Ferron + CAR Mix	290.20	293.10	-164.60
Ferron + CAR 10 min Grd	240.77	300.49	-173.68
Ferron + CAR 20 min Grd	287.23	295.57	-206.69
Ferron + CAR 30 min Grd	266.76	294.09	-221.00
Ferron + CAR 10 min Knd	244.14	291.45	-167.96
Ferron + CAR 20 min Knd	287.82	296.20	-352.28
Ferron + CAR 30 min Knd	226.07	295.44	-289.12

The peak temperatures of decomposition however all lie within a narrow range, 293.00±3°C, excluding that for the mixed sample which is 300.49°C. In all cases, they are higher than that of Carbazole (286.00°C) but close to that of

Ferron (291.30°C) (Table 36). This confirms that no new phase were formed when the compounds were combined together in this study. This notion is supported also by the array of latent heats for the decomposition of the samples which vary from -164.60 J/g for the 30-minute kneaded sample to -352.28 J/g for the 20-minute kneaded sample but with no particular correlation with how the samples were prepared (Table 36).

Thermogravimetric Analyses (TGA)

The thermal curve (the plot from the Thermogravimetrc Analysis, TGA) of a sample indicates the temperatures at which it loses weight sharply, known as thermal events. This curve also gives the thermal profile of a sample. The Derivative Thermogravimetry (DTG) is the first derivative of the thermal curve, and gives more details on the thermal events

Analysis of Thermal curve of Ferron

The first thermal event of Ferron starts at 256.36°C and ends at 286.13°C and a second thermal event starts at 286.13°C and ends at 371.27°C (Figure 78).

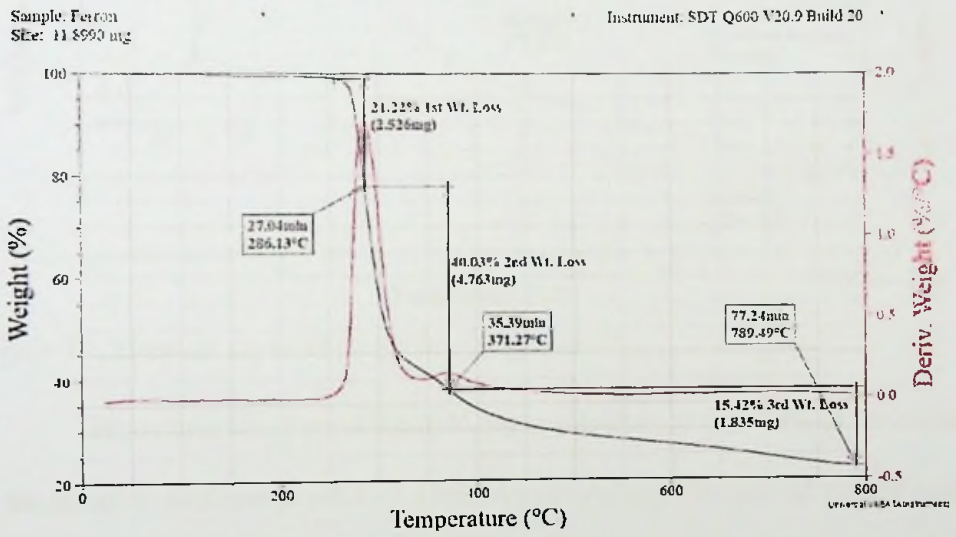

Figure 78: Thermal curve of Ferron.

The first weight loss of 21.22%, equivalent to 2.526 mg of the sample, occurs within the first 27 minutes of the analysis (Figure 78). This weight loss is probably due to the loss of hydrogen iodide (Scientific Inc, 2015), (Lewis, 2004). There is a much larger weight loss of 40.03% (equivalent to 4.763 mg of sample) which occurs between 286.13°C and 371.27°C. This is believed to be due to the loss of the carbon oxides and the nitrogen oxides. This process ends

after 35.39 minutes. The sulphur oxides are the final products from the thermal decomposition and account for about 15.42% of the sample weight.

Analysis of Thermal curve of Sulphamethoxazole

The thermal curve of Sulphamethoxazole seems smooth but the DTG plot shows three events are taking place between 25°C and 300°C. The first starts at 160.86°C and ends at 169.20°C (Figure 79).

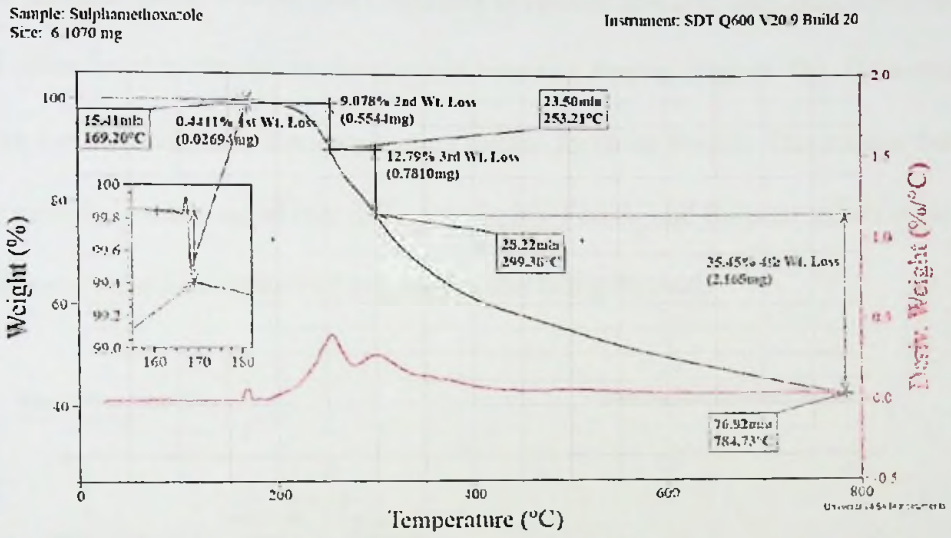

Figure 79: Thermal curve of Sulphamethoxazole.

The weight loss here is 0.02694 mg (equivalent to 0.4410% of the mass of the sample), and occurs after 15.4 minutes of heating. The second weight loss is much larger, 0.5544 mg (i.e., 9.078% of sample mass), starts at 169.20°C at and ends at 253.21°C. This occurs within 23.5 minutes of heating.

This is due to the nitrogen oxides (Toxnet, 2016b) being given off. Other products of the thermal decomposition are sulphur oxides which are also given off subsequently by the time the temperature gets to 299.38°C (Figure 79). This thermal event occurs after 28.22 minutes and the weight loss involved is 12.79%.

Analysis of Thermal curve of Ferron Mixed with Sulphamethoxazole

When Ferron is mixed with Sulphamethoxazole, sample Ferron + SMX Mix, the thermal event within 18.24 minutes, between 164.91°C and 198.87°C, (Figure 80) is similar to the first thermal event in Sulphamethoxazole (Figure 79). The thermal event within 23.76 minutes (between 239.31°C and 254.21°C) is also similar to the second thermal event of Sulphamethoxazole (Figure 79). The thermal event within 24.61 minutes (between 254.2°C and 262.72°C) on the other hand is similar to the thermal event of Ferron (Figure 78). However there are differences in the temperature ranges for these events. This means that the sample is made up of two different phases, Ferron and Sulphamethoxazole, with very minimal amount of any new phase being formed.

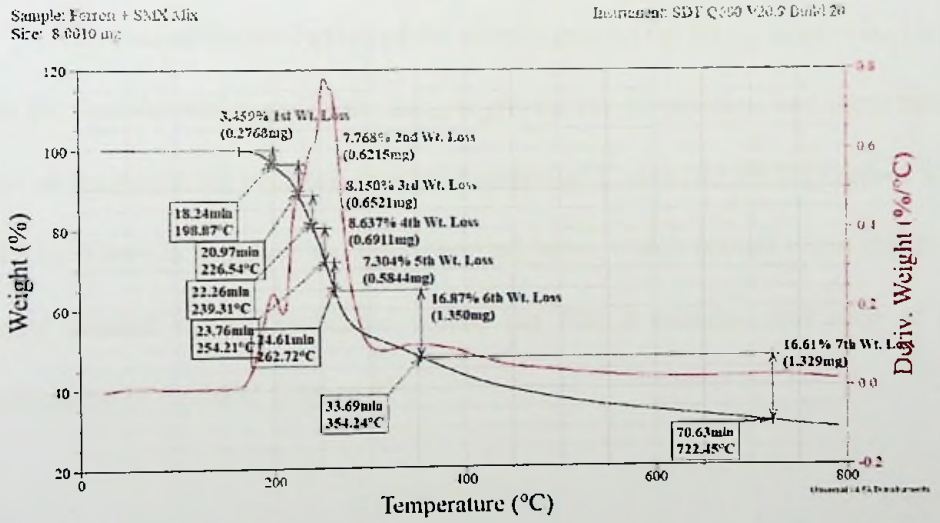

Figure 80: Thermal curve for Ferron + SMX Mix.

Analyses of Thermal curves of Ferron Ground with Sulphamethoxazole

The thermal curves of heating the various samples of Ferron ground with Sulphamethoxazole show the first thermal event as taking place at temperatures

between 160.10°C and 196.24°C for the sample ground for 10 minutes (Figure 81).

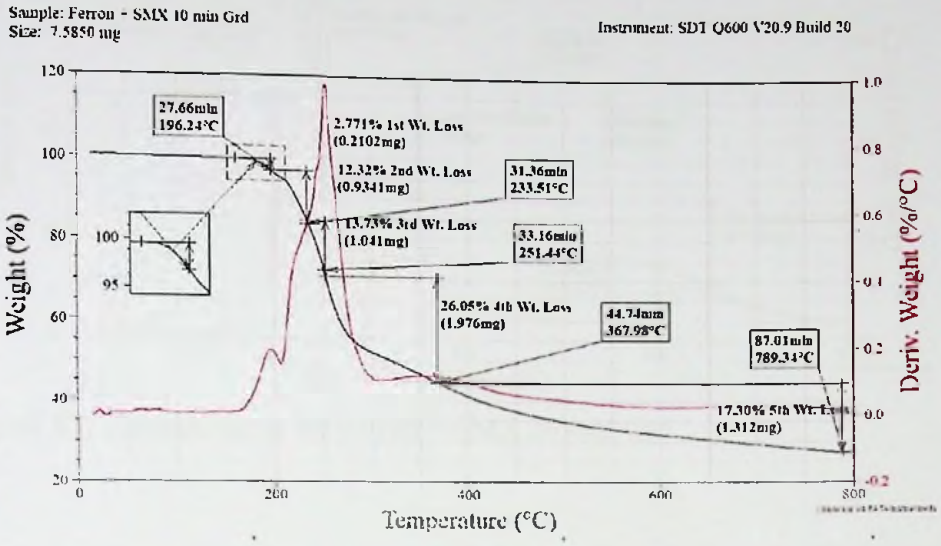

Figure 81: Thermal curve for Ferron + SMX 10 min Grd.

The second thermal event of the sample ground for 20 minutes coincides with the first thermal event of the sample ground for 30 minutes, and these take place at temperatures between approximately 160°C and 195.09°C (Figures 82 and 83). There is however an initial thermal event which occurs when the 20-minute ground sample is heated within the first 6 minutes and ends at a temperature of 77.26°C (Figure 82).

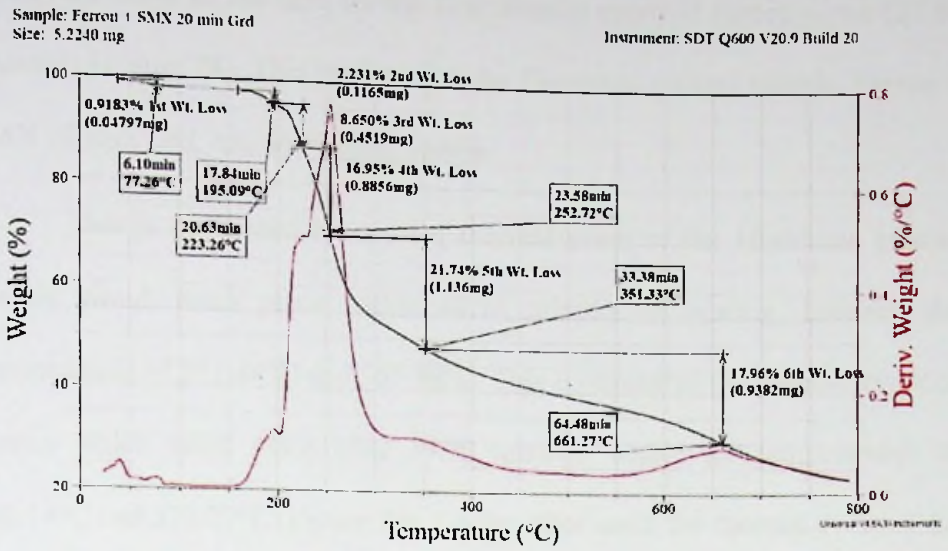

Figure 82: Thermal curve for Ferron + SMX 20 min Grd.

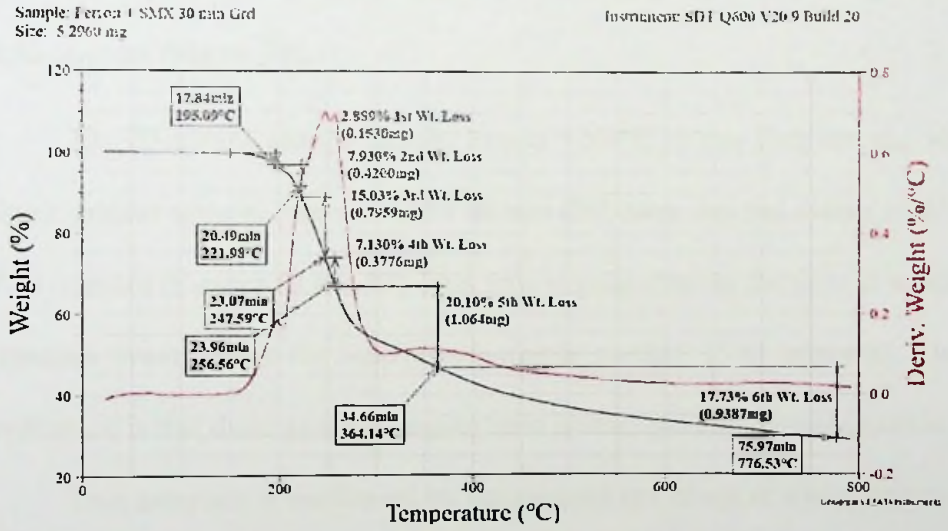

Figure 83: Thermal curve for Ferron + SMX 30 min Grd.

The first thermal event of the 10-minute ground sample, Ferron + SMX 10 min Grd, takes place within 27.66 minutes. Although the temperature at the end of this first thermal event of this sample (196.24°C) is different from those of the starting compounds (286.13°C for Ferron and 169.20°C for Sulphamethoxazole), the time at which it occurs (27.66 minutes) (Figure 81) is

almost the same as the time for the first thermal event of Ferron alone (27.06 minutes) (Figure 78). This implies that the 10-minute ground sample, Ferron + SMX 10 min Grd, has unchanged Ferron.

This is confirmed by another thermal event of the 10-minute ground sample which takes place within 44.74 minutes of heating, between the temperatures of 251.44°C and 367.98°C. This is similar to the thermal event of Ferron which takes place after 35.39 minutes within the temperatures of 286.14°C and 371.27°C (Figure 78). On the other hand, the thermal event of the sample between 233.51°C and 251.44°C (after 33.16 minutes) shows that the sample has unchanged Sulphamethoxazole as a component since a similar thermal event occurs for Sulphamethoxazole at 253.21°C after heating it for 23.50 minutes (Figure 79).

The 20-minute ground sample, Ferron + SMX 20 min Grd, and the 30-minute ground sample, Ferron + SMX 30 min Grd, have thermal events within 17.84 minutes (Figures 82 and 83). This time is quite close to the time in which a thermal event occurs for Sulphamethoxazole (within 15.41 minutes). The implication is that these ground samples have unchanged Sulphamethoxazole.

This assertion is confirmed by the temperature range at which another thermal event for the ground samples, Ferron + SMX 20 min Grd and Ferron + SMX 30 min Grd, takes place, between 223.26°C and 252.72°C (within 23.58 minutes) and between 247.59°C and 256.56°C (within 23.96 minutes) respectively (Figures 82 and 83). This event corresponds to the thermal event of Sulphamethoxazole which occurs between 169.20°C and 253.21°C and by the 23rd minute.

The samples also show the presence of Ferron since the thermal events taking place between 252.72°C and 351.33°C (after 33.38 minutes) and between 256.56°C and 364.14°C (after 34.66 minutes) in the 20-minute ground sample and 30-minute ground sample respectively (Figures 82 and 83) correspond to the thermal event of Ferron between 286.14°C and 371.27°C (after 35.39 minutes) (Figure 78). These samples therefore have both Ferron and Sulphamethoxazole in their original form.

Analyses of Thermal curves of Ferron Kneaded with Sulphamethoxazole

The initial thermal event when the compounds are kneaded together takes place within 17 minutes; that is, 17.48 minutes for the 10-minute kneaded sample (Figure 84), 17.05 minutes for the 20-minute kneaded sample (Figure 85) and 17.43 minutes for the 30-minute kneaded sample (Figure 86).

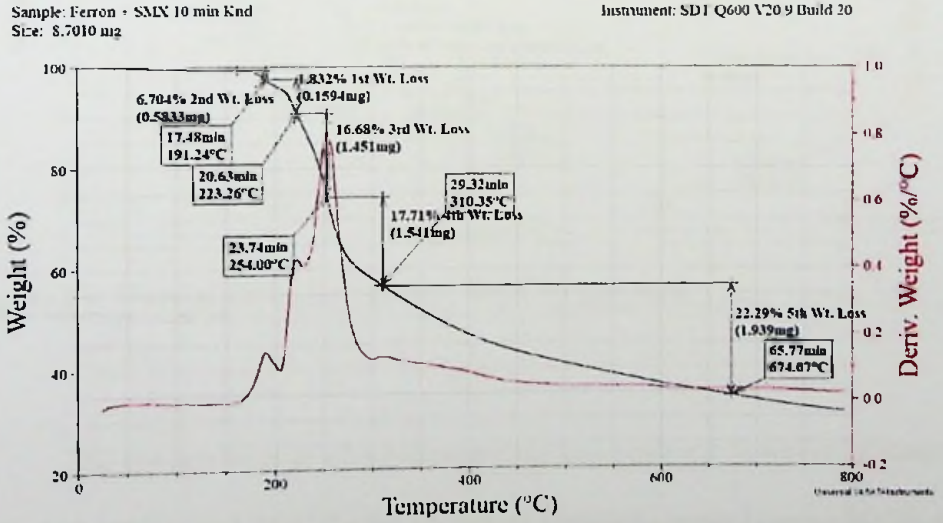

Figure 84: Thermal curve for Ferron + SMX 10 min Knd.

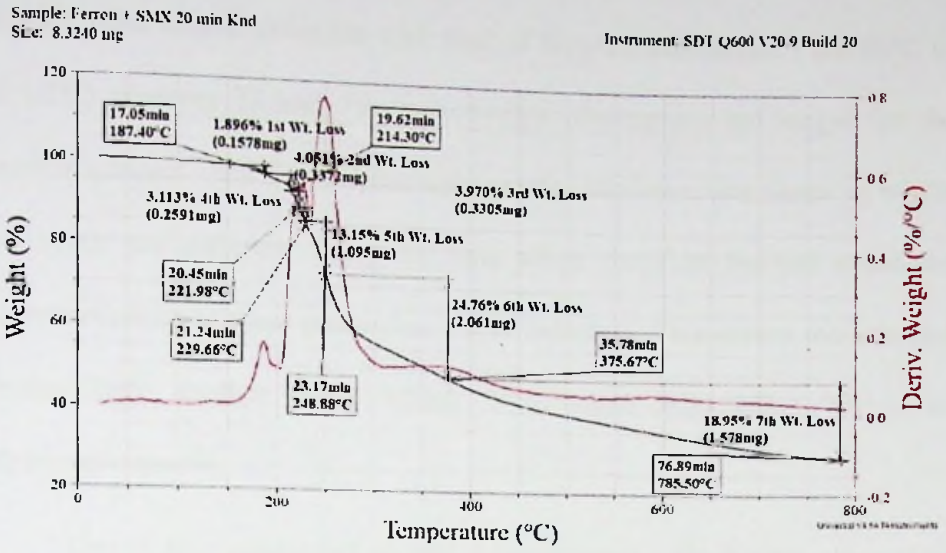

Figure 85: Thermal curve for Ferron + SMX 20 min Knd.

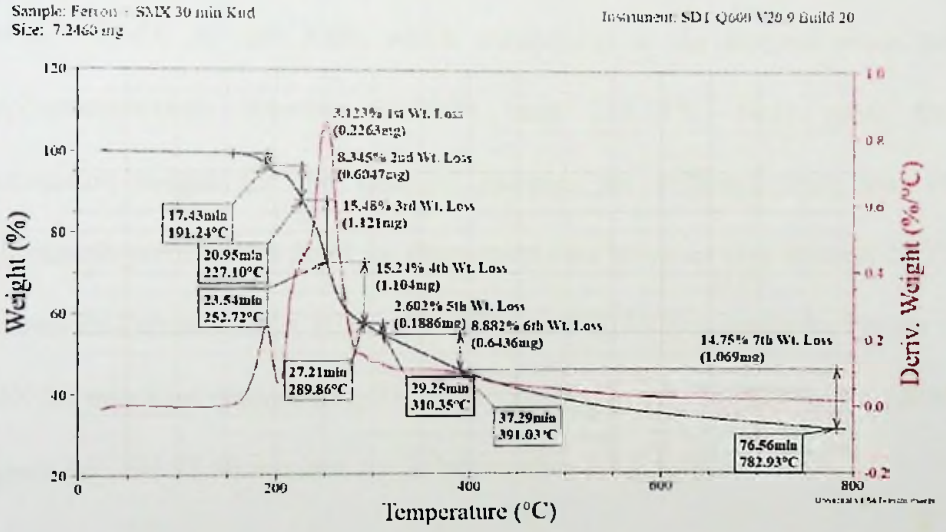

Figure 86: Thermal curve for Ferron + SMX 30 min Knd.

The temperatures at which these events take place are however different; from 160.10°C to 191.24°C for the 10-minute kneaded sample (Figure 84), from 159.01°C to 187.40°C for the 20-minute kneaded sample (Figure 85) and from 160.03°C to 191.24°C for the 30-minute kneaded sample (Figure 86).

These temperature ranges are different from that of Ferron (256.36°C to 286.13°C) but almost coincide with that of Sulphamethoxazole (160.86°C to 169.20°C) (Figures 78 and 79 respectively). The ranges are longer for the kneaded samples than for Sulphamethoxazole. Moreover the times at which they occur are different from the time when the first thermal event for Sulphamethoxazole takes place (i.e., 15.41 minutes). This means the kneaded samples have another phase which is different from either Ferron or Sulphamethoxazole.

This is also confirmed by the thermal events which take place from 223.26°C to 254.00°C (for Ferron + SMX 10 min Knd), from 229.66°C to 248.88°C (for Ferron + SMX 20 min Knd) and from 227.10°C to 252.72°C (for Ferron + SMX 30 min Knd) which correspond to the thermal event for Sulphamethoxazole between 169.20°C and 253.21°C. Here again the temperature ranges for the kneaded samples are different from that of Sulphamethoxazole. The times for these events are however very similar; 23.74 minutes for Ferron + SMX 10 min Knd (Figure 84), 23.17 minutes for Ferron + SMX 20 min Knd (Figure 85), 23.54 minutes for Ferron + SMX 30 min Knd (Figure 86) and 23.50 minutes for Sulphamethoxazole (Figure 79).

A closer look at the thermal curves for both ground and kneaded combinations of Ferron and Sulphamethoxazole shows a thermal event taking place between 221.98°C and 227.10°C (Table 37) except for Ferron + SMX 10 min Grd. The times for these events are similar. This implies the presence of a new phase when these compounds are brought together. This new phase or substance is a co-crystal of Ferron and Sulphamethoxazole.

Although the time at which the first thermal event occurs for the products of combining Ferron with Sulphamethoxazole, about 17 minutes, is close to that of Sulphamethoxazole (15 minutes), the next thermal event in the products does not correspond to a thermal event in either Sulphamethoxazole or Ferron. The third event after 23 minutes and approximately 253°C that occurs in the products however, correspond to a thermal that occurs at the same time and temperature in Sulphamethoxazole (Table 37). The thermal events due to Ferron do not influence the thermal events of the products in the first 23 minutes of heating. This indicates that a co-crystal is formed when Ferron is combined with Sulphamethoxazole.

Table 37: Thermal Events and Temperatures for Ferron, Sulphamethoxazole and their Combinations

Sample	Thermal event 1		Thermal event 2		Thermal event 3	
	Temp. (°C)	Time (min)	Temp. (°C)	Time (min)	Temp. (°C)	Time (min)
Ferron	286.13	27.04	371.27	35.39		
Sulphamethox-azole	169.20	15.41			253.21	23.50
Ferron + SMX Mix	198.87	18.24	226.54	20.97	254.21	23.76
Ferron + SMX 10 min Grd	196.24	27.66	233.51	31.36	251.44	33.16
Ferron + SMX 20 min Grd	195.09	17.84	223.26	20.63	252.72	23.58
Ferron + SMX 30 min Grd	195.09	17.84	221.98	20.49	256.56	23.96
Ferron + SMX 10 min Knd	191.24	17.48	223.26	20.63	254.00	23.74
Ferron + SMX 20 min Knd	187.40	17.05	221.98	20.45	248.88	23.17
Ferron + SMX 30 min Knd	191.24	17.43	227.10	20.93	252.72	23.54

Analysis of Thermal curve of Carbazole

The thermal curve of Carbazole shows only one weight loss event, which is confirmed by the DTG. This weight loss starts at 134.91°C and ends at 232.23°C and the weight loss involved is 2.346 mg (equivalent to 73.09% of the sample mass (Figure 87). The products of this thermal event are fumes of nitroxides (NO_x) (Lewis, 2004) (Toxnet, 2016a).

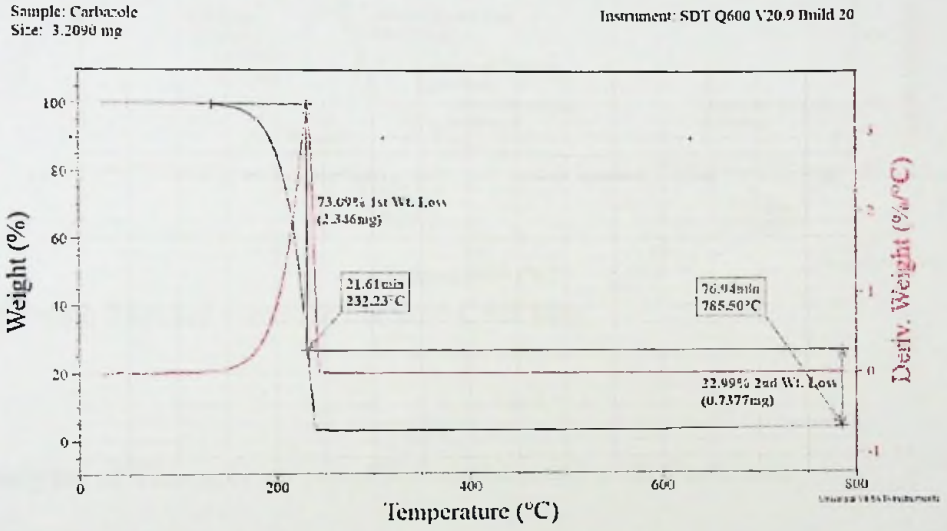

Figure 87: Thermal curve of Carbazole.

The weight of the residue remains constant after this one major thermal event which occurs after 21.61 minutes of heating.

Analysis of Thermal curve of Ferron Mixed with Carbazole

Two thermal events in the mixed sample of Ferron and Carbazole, Ferron + CAR Mix, one by 219.09°C (within 20.26 minutes) and the other by 285.07°C (within 26.81 minutes) (Figure 88) are similar to that of the individual

compounds, Carbazole by 232.28°C (within 21.61 minutes) and Ferron by 286.13°C (within 27.04 minutes). The differences are attributed to the 'impurity' effect of one compound on the other in the product.

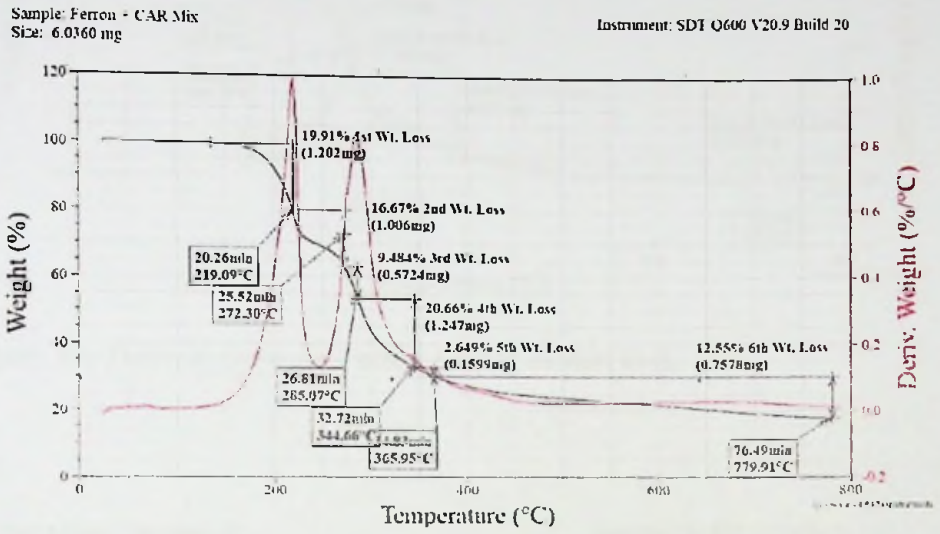

Figure 88: Thermal curve for Ferron + CAR Mix.

Analyses of Thermal curves of Ferron Ground with Carbazole

The thermal curves of the ground samples of Ferron and Carbazole show that the first thermal event occurs within the temperature range of 142.18°C to 215.58°C for the 10-minute ground sample, Ferron + CAR 10 min Grd, within 19.93 minutes (Figure 89). For both 20-minute ground sample (Ferron + CAR 20 min Grd) and 30-minute ground sample (Ferron + CAR 30 min Grd), the first thermal events occurs from 142.78°C to 211.73°C and from 143.62°C to 211.64°C respectively (Figures 90 and 91).

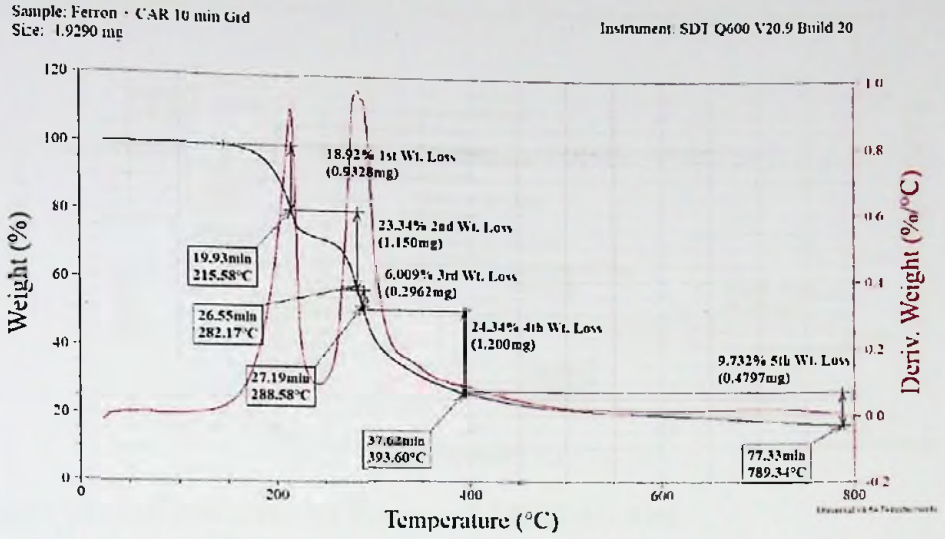

Figure 89: Thermal curve for Ferron + CAR 10 min Grd.

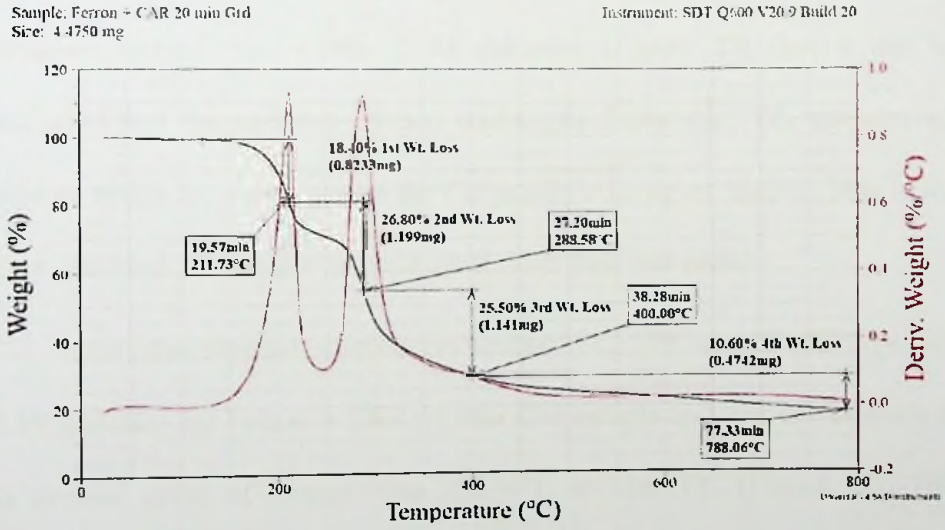

Figure 90: Thermal curve for Ferron + CAR 20 min Grd.

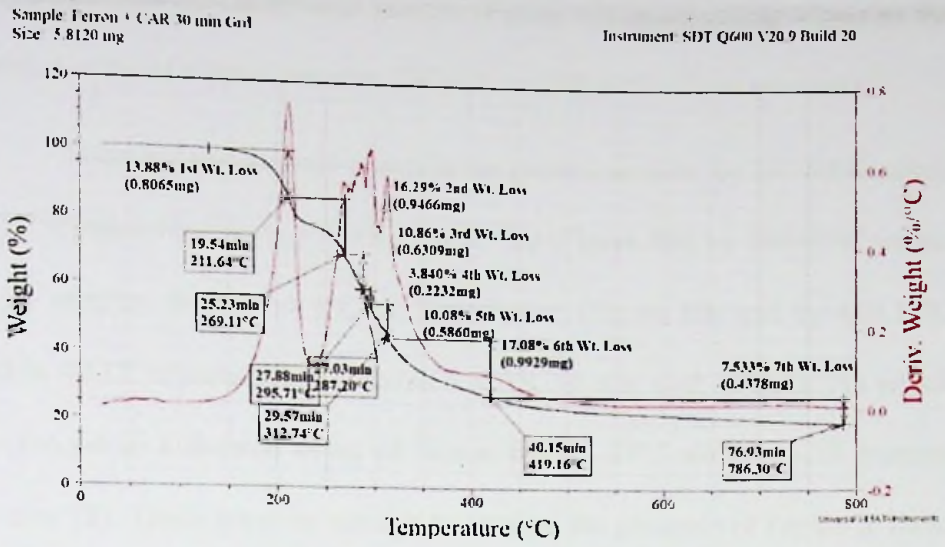

Figure 91: Thermal curve for Ferron + CAR 30 min Grd.

The times for these events are also similar; within 19.57 minutes (Ferron + CAR 20 min Grd) and 19.54 minutes (Ferron + CAR 30 min Grd). These first thermal events occur sufficiently close to the time that the thermal event of Carbazole occurs, i.e., within 21.61 minutes, (Figure 87) that it can be concluded that the samples contain unchanged Carbazole. The temperature range at which the event occurs for Carbazole is however higher. This is the effect observed if a sample is made up of more than one phase.

One other thermal event occurs between 282.17°C and 288.50°C (within 27.19 minutes) for Ferron + CAR 10 min Grd sample and this corresponds to the thermal event of Ferron from 256.36°C to 286.13°C (Figure 78). This implies the presence of Ferron in the sample.

The presence of Ferron is inferred from the analysis of the other ground samples, Ferron + CAR 20 min Grd and Ferron + CAR 30 min Grd; the thermal events from 211.73°C to 288.58°C, within 27.20 minutes, for the 20-minute ground sample and from 211.64°C to 287.20°C, within 27.03 minutes (Figure

90), for the 30-minute ground sample (Figure 91) have similar times as the thermal event of Ferron between 256.36°C to 286.14°C (27.04 minutes).

There are also thermal events in the ground samples, by 393.60°C within 37.62 minutes for Ferron + CAR 10 min Grd (Figure 89), by 400.00°C within 38.28 minutes for Ferron + CAR 20 min Grd (Figure 90) and by 419.16°C within 40.15 minutes for the Ferron + CAR 30 min Grd, (Figure 91) which correspond to a thermal event of Ferron by 371.27°C within 35.39 minutes (Figure 78). These are close enough to confirm the presence of Ferron in these samples.

Analyses of Thermal curves of Ferron Kneaded with Carbazole

When Ferron is kneaded with Carbazole, the thermal event for the 10-minute kneaded sample within 19.65 minutes in a temperature range from 141.09°C to 212.70°C (Figure 92) corresponds to a thermal event of Carbazole which occurs within 21.61 minutes in the temperature range from 134.91°C to 232.28°C (Figure 87).

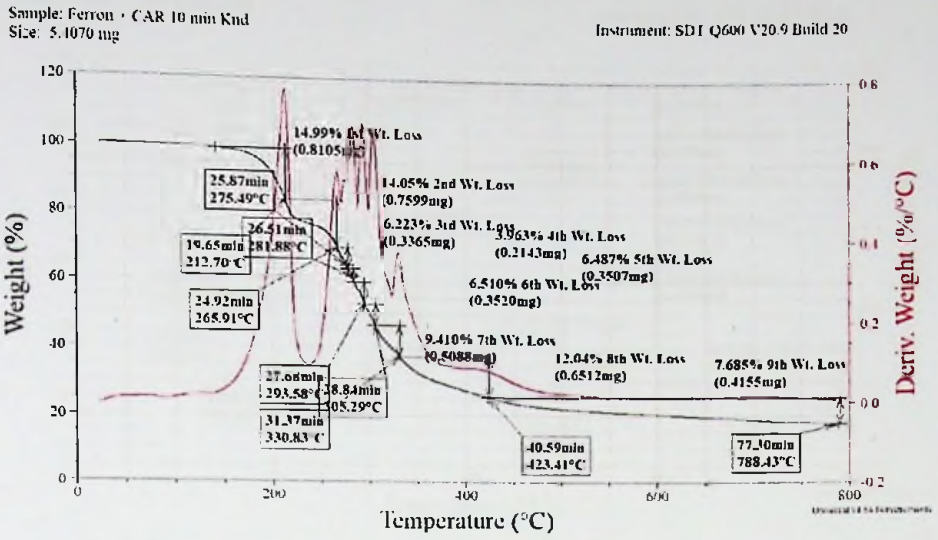

Figure 92: Thermal curve for Ferron + CAR 10 min Knd.

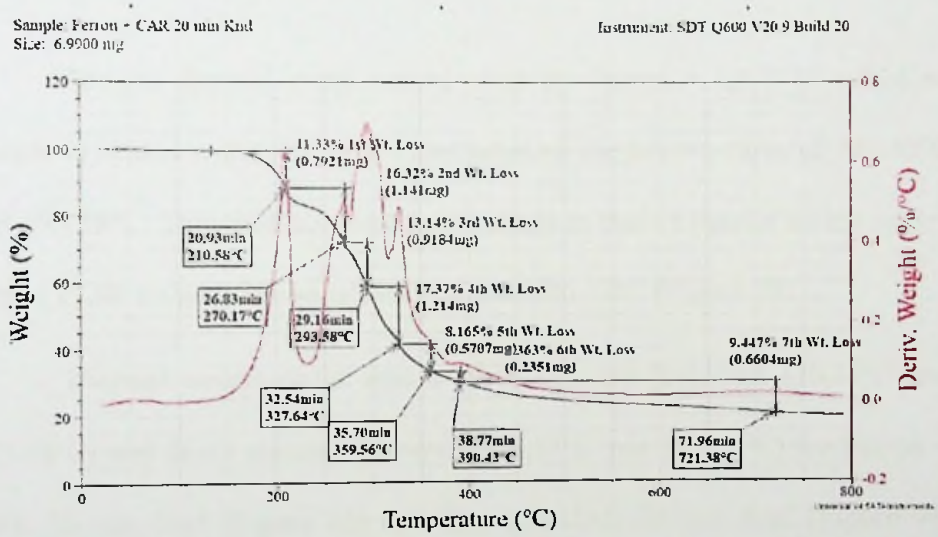

Figure 93: Thermal curve for Ferron + CAR 20 min Knd.

Similar thermal events occur for the 20-minute kneaded sample, Ferron + CAR 20 min Knd, within 20.93 minutes from 141.09°C to 210.58°C (Figure 93) and the 30-minute kneaded sample, Ferron + CAR 30 min Knd, within 19.43 minutes from 140.25°C to 210.58°C (Figure 94). The temperature ranges here are also different from that of Carbazole.

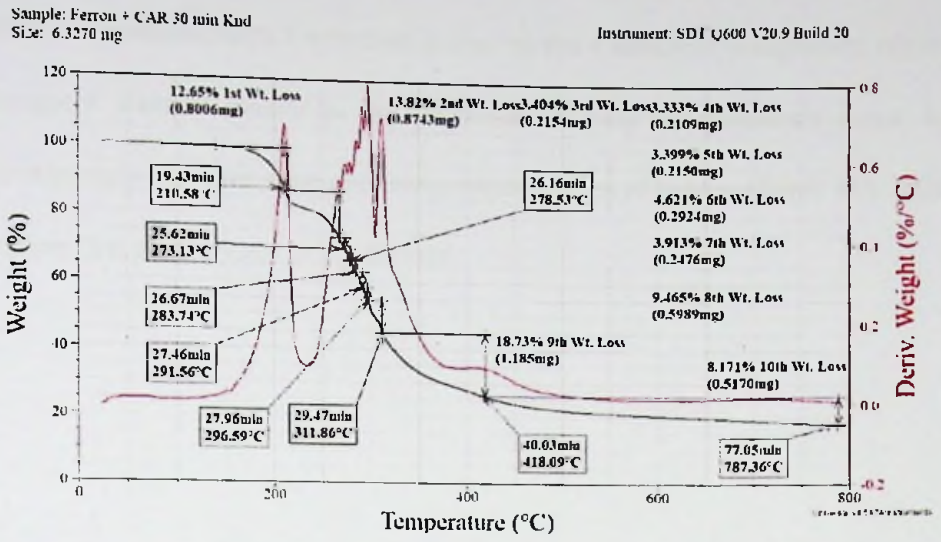

Figure 94: Thermal curve for Ferron + CAR 30 min Knd.

Another thermal event occurs when the Ferron + CAR 10 min Knd sample is heated within 27.68 minutes between the temperatures of 281.88°C and 293.58°C. This thermal event corresponds to that of Ferron which occurs within 27.04 minutes between 256.36°C and 286.13°C (Figure 78).

Thermal events occur within 29.16 minutes (between 270.17°C and 293.58°C) and 26.67 minutes (between 278.53°C and 283.74°C) for Ferron + CAR 20 min Knd (Figure 93) and Ferron + CAR 30 min Knd (Figure 94) respectively. These also correspond to a thermal event for Ferron.

A thorough look at the thermal events when Ferron is combined with Carbazole does not reveal any consistent temperature ranges or times of heating apart from those that could be attributed to the starting compounds. This indicates that probably no new phase or crystal was formed from these combinations under these conditions.

The temperature at which the initial thermal event takes place when Ferron is combined with Carbazole is due to the Carbazole component while subsequent thermal events in the products of these combinations occur at approximately the same time and temperature as that of Ferron (Table 38). This confirms that a co-crystal is not formed.

Table 38: Thermal Events and Temperatures of Ferron, Carbazole and their Combinations

Sample	Thermal event 1		Thermal event 2		Thermal event 3	
	Temp. (°C)	Time (min)	Temp. (°C)	Time (min)	Temp. (°C)	Time (min)
Ferron			286.13	27.04	371.27	35.39
Carbazole	232.28	21.61				
Ferron + CAR Mix	219.09	20.26	285.07	26.81	365.95	34.83
Ferron + CAR 10 min Grd	215.58	19.93	288.50	27.19	393.60	37:62
Ferron + CAR 20 min Grd	211.73	19.57	288.58	27.20	400.00	38.28
Ferron + CAR 30 min Grd	211.64	19.54	287.20	27.03	419.16	40.15
Ferron + CAR 10 min Knd	212.70	19.65	293.58	27.68	423.41	40.59
Ferron + CAR 20 min Knd	210.58	20.93	293.58	29.16	390.42	38.77
Ferron + CAR 30 min Knd	210.58	19.43	296.59	27.96	418.09	40.03

The products of combining Ferron and Sulphamethoxazole are co-crystals as compared to the products from combining Ferron with Carbazole

which were not. The evidence is that in the case of Ferron combined with Sulphamethoxazole, the thermal profile of the product, though a combination of that of the starting materials, also includes that of a new phase or product. On the other hand, the thermal profile of the combination of Ferron and Carbazole was just the combination of the starting materials.

Infra-Red Spectral Analyses

Infrared spectroscopy can be used to detect the functional groups present in a sample, and information can sometimes be obtained about the proximity of one group to another. In this study of co-crystals, it is expected that the infra-red spectra of both starting materials and products should be almost identical especially in the 'group' region. The formation of co-crystals is expected to manifest in small changes in the 'fingerprint' region of the spectra.

Analysis of Infra-Red spectrum of Ferron

The Infra-red spectrum of Ferron shows a broad band between the wavenumbers 3000 cm^{-1} and 2200 cm^{-1} with its peak at 2740 cm^{-1} (Figure 95). This band is due to the –OH bonds in water molecules adsorbed onto the surface of the Ferron crystals. The weak peak at 3088 cm^{-1} wavenumber is due to the =C-H bond stretch. The peak at 1621 cm^{-1} wavenumber is due to the stretching of the C-C in the aromatic rings in the molecule.

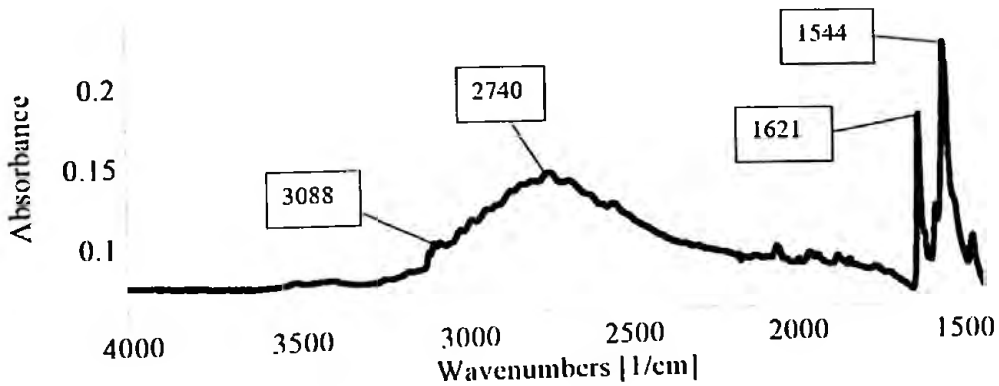

Figure 95: Group frequency region of IR spectrum of Ferron.

The strong peak at 1544 cm^{-1} is due to N-H hydrogen bond found in the molecule.

The fingerprint region has its strongest sharp peak at 598 cm^{-1} (Figure 96) which is attributed to the C-I bond stretch.

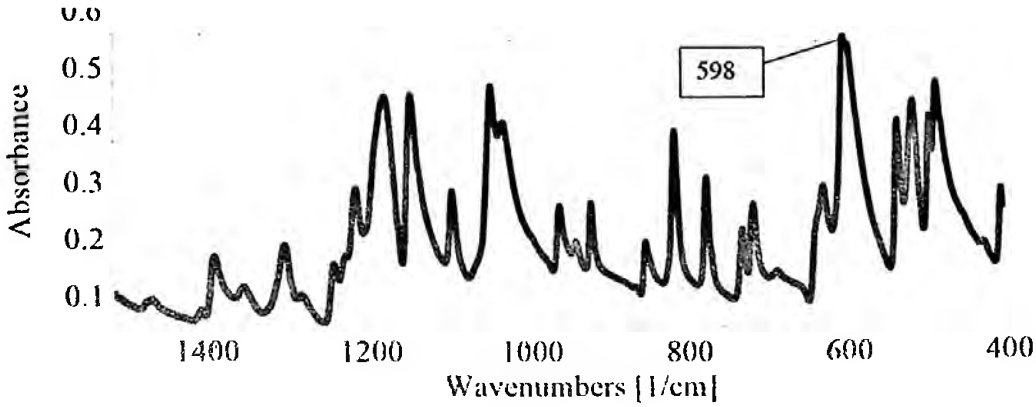

Figure 96: 'Fingerprint' region of IR spectrum of Ferron.

Analysis of Infra-Red spectrum of Sulphamethoxazole

The peaks at the wavenumbers 3467 cm^{-1}, 3377 cm^{-1}, and 3298 cm^{-1} (Figure 97) are due the stretching of the C-H bond of the methyl group on the

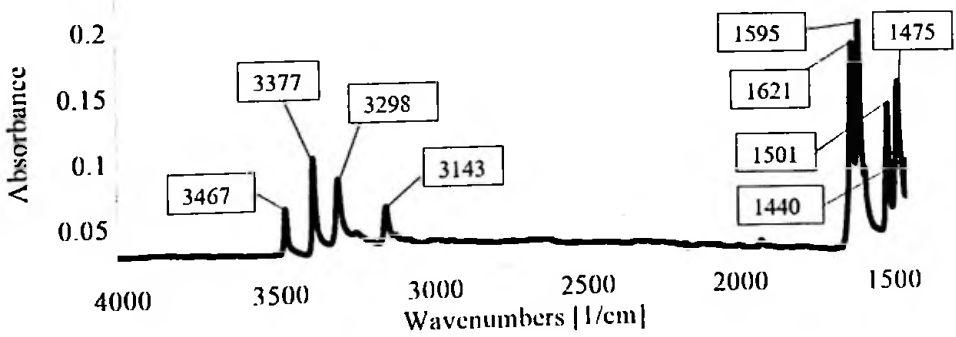

Figure 97: Group frequency region of IR spectrum of Sulphamethoxazole.

Sulphamethoxazole molecule. The peak at 3143 cm^{-1} are due to intermolecular O-H dimers formed in the structure of Sulphamethoxazole.

The peak at 1621 cm^{-1} is due to the C-H bonds in the aromatic rings while the C-C bonds stretching in the rings absorb at 1595 cm^{-1} and 1475 cm^{-1}.The N-O bonds stretching absorb at 1501 cm^{-1} and the S=O bonds absorb at 1440 cm^{-1}.

The 'fingerprint' region of the spectrum (1400 cm^{-1} to 400 cm^{-1}) has peaks at 1363 cm^{-1}, 1303 cm^{-1}, 1188 cm^{-1} and 827 cm^{-1} which are due to the S=O bond group (Figure 98). The aromatic ring-nitrogen, Ar-N, bond stretch absorbs at 1266 cm^{-1}. Likewise, the N-H bonds absorb at 1142 cm^{-1}, 1090 cm^{-1} and 681 cm^{-1} wavenumbers (Figure 98).

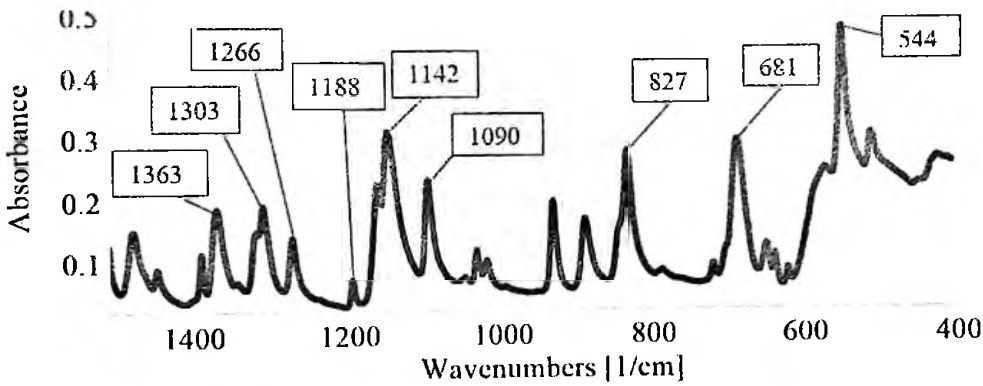

Figure 98: 'Fingerprint' region of IR spectrum of Sulphamethoxazole.

Analysis of Infra-Red spectrum of Carbazole

The peaks at wavenumbers of 3417 cm^{-1} and 3049 cm^{-1} are due to the stretching of the C-H bonds and the aromatic ring-hydrogen, Ar-H, bonds respectively (Figure 99).

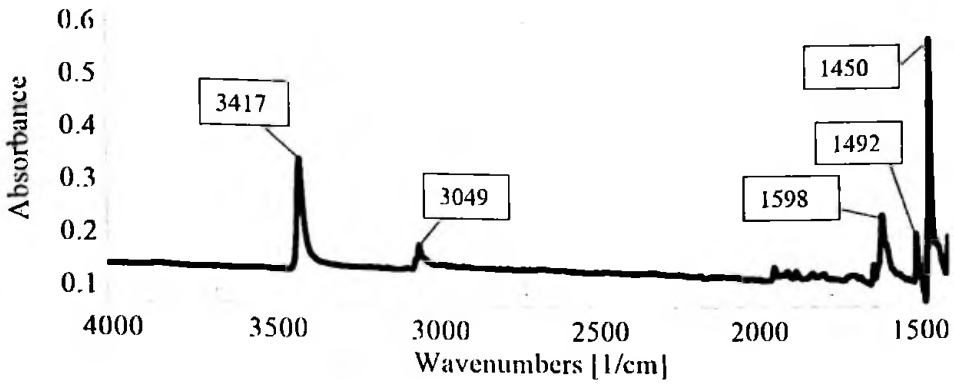

Figure 99: Group frequency region of IR spectrum of Carbazole.

The peaks at 1598 cm^{-1}, 1492 cm^{-1} and 1450 cm^{-1} are due to the stretching of the C-C bonds in the aromatic rings.

In the 'fingerprint' region of the spectrum, the peak at 1324 cm^{-1} is the absorbance when the aromatic ring – nitrogen, Ar-N, bond stretches (Figure 100).

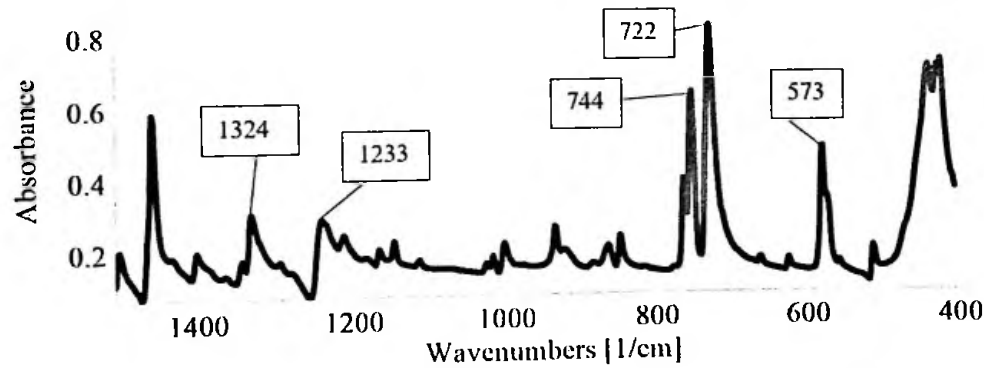

Figure 100: 'Fingerprint' region of IR spectrum of Carbazole.

The peaks at 1233 cm^{-1},744 cm^{-1}, 722 cm^{-1} and 573 cm^{-1} are due to the wagging of the C-H bonds in the molecule.

Analyses of Infra-Red spectra of Ferron Ground with Sulphamethoxazole

The infra-red spectra of the products of grinding Ferron with Sulphamethoxazole, Ferron + SMX 10 min Grd, Ferron + SMX 20 min Grd and Ferron + SMX 30 min Grd have peaks at the same frequencies, especially in the group frequency region, as those of the starting compounds, Ferron and Sulphamethoxazole (Figure 101).

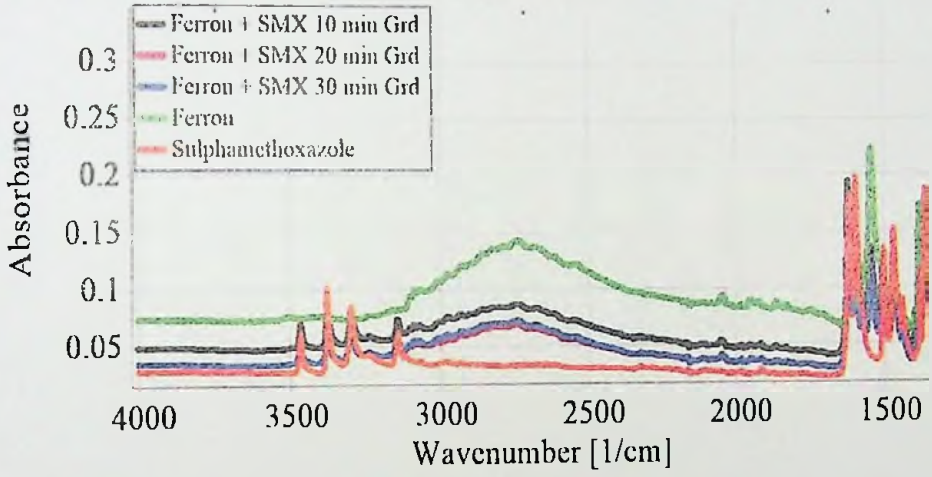

Figure 101: Spectra in Group frequency region of Ground Ferron and Sulphamethoxazole.

The absorbance at 3467 cm^{-1}, 3377 cm^{-1}, and 3298 cm^{-1} found in the spectra of the ground sample are attributed to the presence of Sulphamethoxazole. The absorbance at 2740 cm^{-1} and 1544 cm^{-1} found in the spectra of the ground samples are from the Ferron component in them. The

absorbance at approximately 1620 cm^{-1} however is from both starting compounds.

The absorbance, however, are not an algebraic summation of those of the starting materials. For example, the absorbance of Ferron at approximately 1620 cm^{-1} is 0.1765 while that of Sulphamethoxazole is 0.1836 (Table 39). The absorbance at approximately 1620 cm^{-1} however of the Ferron + SMX 10 min Grd is 0.1946, that of Ferron + SMX 20 min Grd is 0.1599 while that of Ferron + SMX 30 min Grd is 0.1689 (Table 39). This implies an interaction between the two starting compounds at the bonds absorbing at this frequency (the C-C and C-H bonds found in the aromatic rings) (Table 39).

Table 39: Absorbance of Ferron, Sulphamethoxazole and their Ground products

Wavenumber [1/cm]	Absorbance of Samples				
	Ferron	Ferron + SMX 10 min Grd	Ferron + SMX 20 min Grd	Ferron + SMX 30 min Grd	Sulphamethox-azole
3497		0.0712	0.0530	0.0544	0.0629
3377		0.1013	0.0751	0.0789	0.1013
3298		0.0832	0.0632	0.0655	0.0851
3143		0.0744	0.0565	0.0585	0.0627
1619	0.1765	0.1946	0.1599	0.1689	0.1836
1595		0.1574	0.1335	0.1363	0.1991
1544	0.2226	0.1355	0.1182	0.1242	
1501		0.1277	0.1021	0.1066	0.1345
1363		0.1555	0.1600	0.1311	0.1870

Analyses of Infra-Red spectra of Ferron Kneaded with Sulphamethoxazole

The infra-red spectra of the samples from kneading Ferron with Sulphamethoxazole (i.e., Ferron + SMX 10 min Knd, Ferron + SMX 20 min Knd and Ferron + SMX 30 min Knd) have absorbance at the same frequencies, especially in the group frequency region, as the starting compounds (Figure 102).

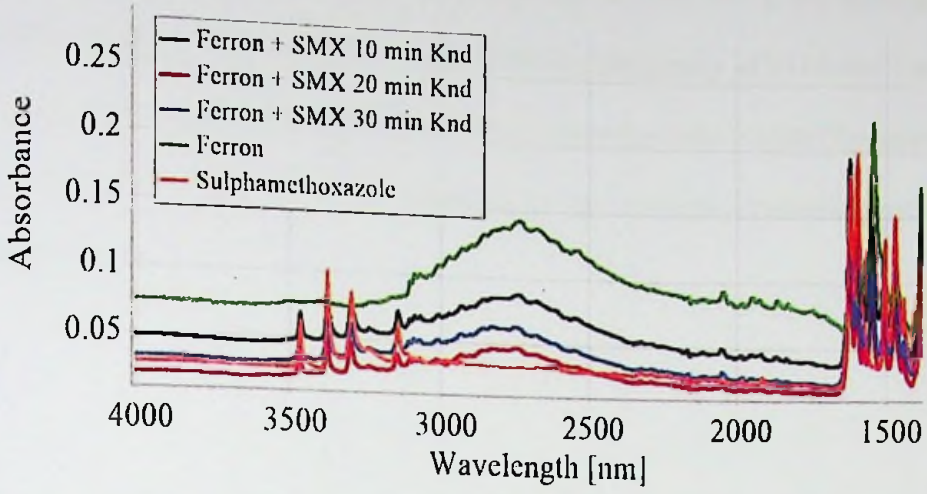

Figure 102: Spectra in Group frequency region of Kneaded Ferron and Sulphamethoxazole.

The absorbance of Ferron + SMX 20 min Knd are generally the lowest among the samples.

At frequencies where the absorbance are due to a particular starting compound, the absorbance for the pure compounds are generally highest, for example at 3378 cm^{-1} and 3298 cm^{-1} the Sulphamethoxazole spectrum has the highest absorbance, 0.1013 and 0.0851 respectively (Table 40). Likewise, the absorbance at 3089 cm^{-1} and 2740 cm^{-1} are highest for Ferron, 0.101 and 0.1451 respectively (Table 40). When the frequency is common to both the starting materials (e.g.,, 1620 cm^{-1}) however, the 10-minute kneaded sample, Ferron + SMX 10 min Knd, has the highest absorbance, 0.1953 (Table 40).

The kneading of Ferron and Sulphamethoxazole together therefore generally reduces the absorbance of the products except at certain particular frequencies such as 3467 cm^{-1}, 3144 $cm^{-1}$and 1544 cm^{-1} where it appears the

absorbance is enhanced. These absorbance are due to the adducts methyl group on the Sulphamethoxazole molecule (frequency of 3467 cm^{-1}), the hydrogen bond between the Sulphamethoxazole molecules (frequency of 3144 cm^{-1}) and the N-H hydrogen bond formed between the molecules of the Ferron (frequency of 1544 cm^{-1}). These bonds are changed by the mechano-synthesis process being applied.

Table 40: Absorbance of Ferron, Sulphamethoxazole and their Kneaded products

Wavenumber [1/cm]	Absorbance of Samples				
	Ferron	Ferron + SMX 10 min Grd	Ferron + SMX 20 min Grd	Ferron + SMX 30 min Grd	Sulphamethox-azole
3467		0.0691	0.0369	0.0501	0.0629
3378		0.0949	0.0603	0.0795	0.1013
3298		0.0805	0.0469	0.0615	0.0851
3144		0.0726	0.0398	0.0541	0.0627
3089	0.1010	0.0694	0.0383	0.0537	
2740	0.1451	0.0892	0.0484	0.0643	
1620	0.1765	0.1953	0.1355	0.1661	0.1825
1617					0.1825
1597		0.1251	0.1605	0.1609	0.1991
1544	0.0226	0.1435	0.0987	0.1258	
1502		0.1243	0.0808	0.1009	0.1345
1469		0.1284	0.0881	0.1096	0.1521
1459	0.0991				
1365		0.1516	0.1069	0.1310	0.1870
1302		0.1930	0.1302	0.1561	0.1920

The IR absorption bands of the co-crystals show slight differences especially in the fingerprint region which can be assigned to the formation of

weak van der Waal forces or hydrogen bonds. The absorption spectra were also similar to that of the starting materials because no covalent bonds are expected to be formed.

Analyses of Infra-Red spectra of Ferron Ground with Carbazole

The infra-red spectra of the samples from grinding Ferron with Carbazole have major peaks at the same frequencies, especially in the group frequency region, as those of the starting materials Ferron and Sulphamethoxazole (Figure 103).

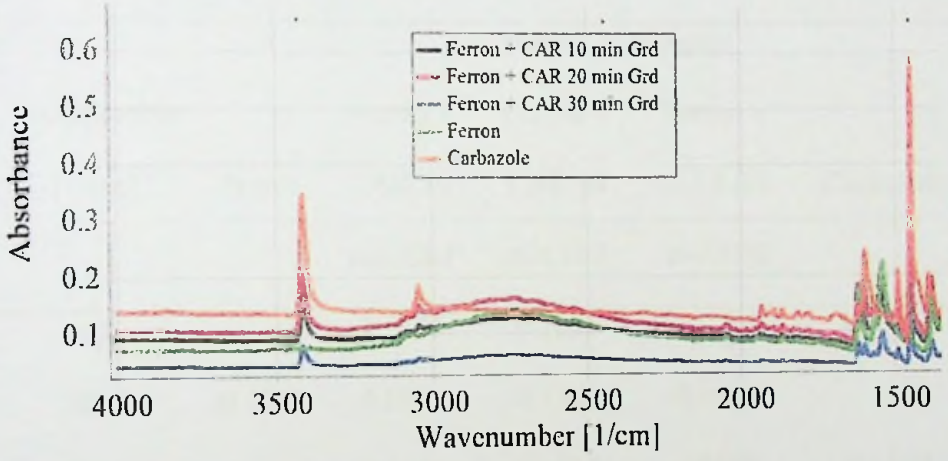

Figure 103: Spectra in Group frequency region of Ground Ferron and Carbazole.

The absorption at the frequencies of 3417 cm^{-1}, 3049 cm^{-1}, and 1492 cm^{-1} are examples of the absorbance in the ground samples attributed to the Carbazole component in the sample. The absorbance at 3008 cm^{-1} and 1621 cm^{-1} are attributed to the Ferron component in the samples. The broad peak with its

maximum at 2740 cm^{-1} is attributed to water molecules adsorbed onto the surface of the Ferron component.

It is interesting to note that the 20-minute ground sample has a higher absorbance in this group frequency region than the Ferron. This may be because the absorbance base line due to the Carbazole component is high in this region.

Generally, the absorbance of pure Carbazole is higher than the absorbance of the ground samples (Table 41)

Table 41: Absorbance of Ferron, Carbazole and their Ground products

	Absorbance of Samples				
Wavenumber [1/cm]	Ferron	Ferron + CAR 10 min Grd	Ferron + CAR 20 min Grd	Ferron + CAR 30 min Grd	Carbazole
3417		0.1490	0.2051	0.0798	0.3480
3088	0.1003	0.1063	0.1340	0.0576	
3049		0.1177	0.1518	0.0578	0.1859
2740	0.1434	0.1301	0.1648	0.0649	
1621	0.1765	0.1438	0.1834	0.0785	
1598		0.1340	0.1786	0.0751	0.2466
1543	0.2226	0.1749	0.2257	0.0995	
1492		0.1216	0.1549	0.0672	0.2093
1450		0.2154	0.2914	0.1339	0.5935
1324		0.1517	0.2052	0.0953	0.3086

The absorbance of the 10- and 20-minute ground samples are between those of Ferron and Carbazole. The exception here is the absorbance of the 30-minute ground sample which is the lowest at all wavenumbers (Table 41).

The absorbance of the ground samples at any particular frequency is attributable to only one of the components, either Ferron or Carbazole (Table 41). The effect is as if one molecule is masking the other molecule at the absorption frequency. This shows that there may not be any chemical interaction between the molecules of Ferron and Carbazole under the conditions in this study.

Analyses of Infra-Red spectra of Ferron Kneaded with Carbazole

The frequencies at which the kneaded samples absorb the infra-red radiation is the same for the starting compounds especially in the group frequency region (Figure 104). The major peaks are at 3417 cm^{-1}, 3049 cm^{-1}, 1598 cm^{-1} and 1450 cm^{-1} all attributed to the Carbazole component in the samples and 1622 cm^{-1}, 2740 cm^{-1},1544 cm^{-1} and 1385 cm^{-1} attributed to the Ferron component (Table 42).

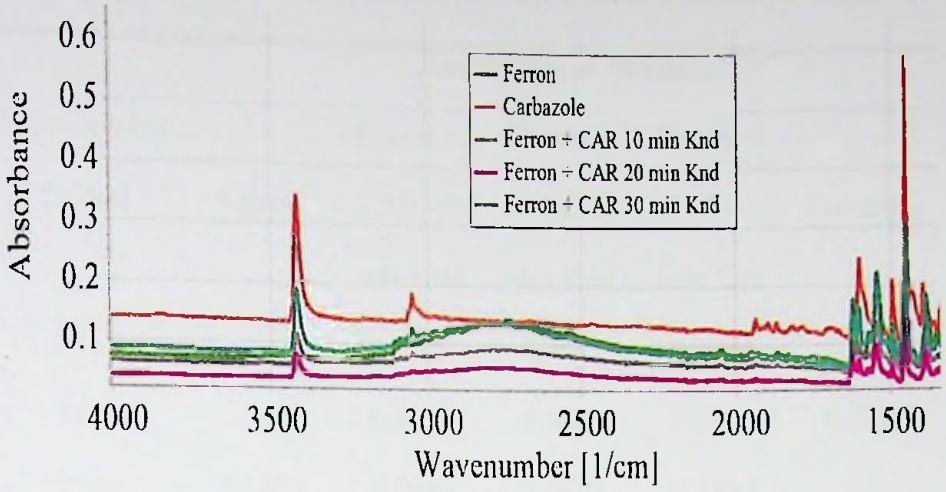

Figure 104: Spectra in Group frequency region of Kneaded Ferron and Carbazole.

The absorbance of the kneaded samples at any particular frequency are attributable to only one of the components, either Ferron or Carbazole (Table 42). This means there may not be any chemical bonds formed when Ferron is kneaded with Carbazole under the conditions of this study.

Table 42: Absorbance of Ferron, Carbazole and their Kneaded products

Wavenumber [1/cm]	Absorbance of Samples				
	Ferron	Ferron + CAR 10 min Knd	Ferron + CAR 20 min Knd	Ferron + CAR 30 min Knd	Carbazole
3417		0.1179	0.0841	0.1934	0.3478
3049		0.0873	0.0600	0.1291	0.1859
2740	0.1453	0.0940	0.0633	0.1382	
1622	0.1765	0.1126	0.0815	0.1754	
1544	0.2226	0.1374	0.0992	0.2192	
1493		0.0935	0.0628	0.1333	0.2093
1450		0.1898	0.1374	0.3040	0.0991
1385	0.1731	0.1178	0.0845	0.1831	

The IR absorption bands of the products showed practically no differences to those of the starting materials. The absorption spectra are virtually a summation of that of the starting materials.

Scanning Electron Microscopy (SEM) Images

The SEM images are to show how the crystals actually look like under very high magnification. The differences between the co-crystals and the starting materials are expected to be manifested in the appearance and morphology of their crystals or crystallites.

Morphology of Ferron crystals

The crystals of Ferron are blocky (Figure 105). The average length is 40 μm. The particles are translucent.

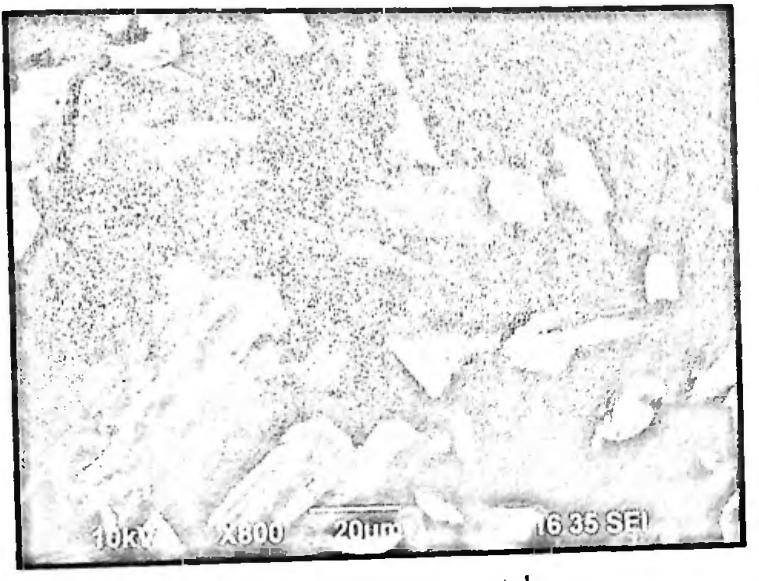

Figure 105: SEM image of Ferron crystals.

Morphology of Sulphamethoxazole crystals

The crystals of Sulphamethoxazole are tabular (Figure 106). The sizes however are not uniform.

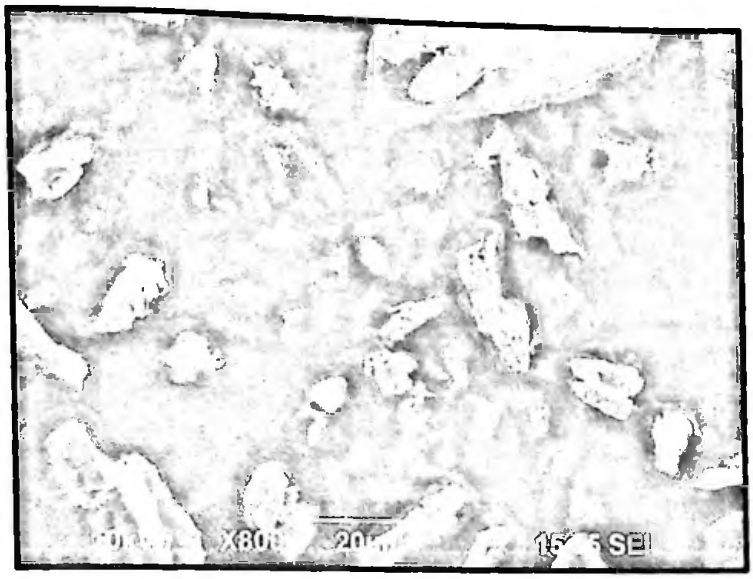

Figure 106: SEM image of Sulphamethoxazole crystals.

Morphology of Carbazole crystals

The crystals of Carbazole are stubby and distinct (Figure 107). They are small and uniform, about 20 μm in length. The particles are opaque.

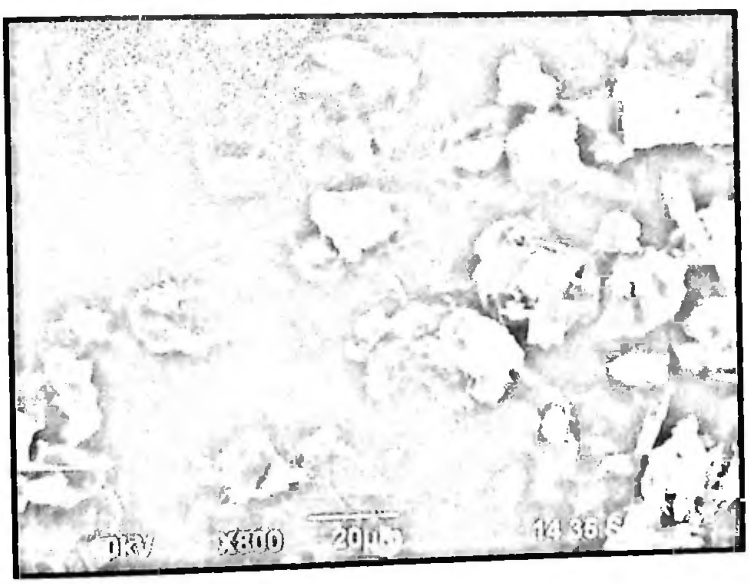

Figure 107: SEM image of Carbazole crystals.

Morphology of crystals of Ferron Mixed with Sulphamethoxazole

Mixing Ferron with Sulphamethoxazole, Ferron + SMX Mix, gives a sample made up of distinct crystals which are opaque with the Sulphamethoxazole crystals on the surface of the Ferron crystals (Figure 108)

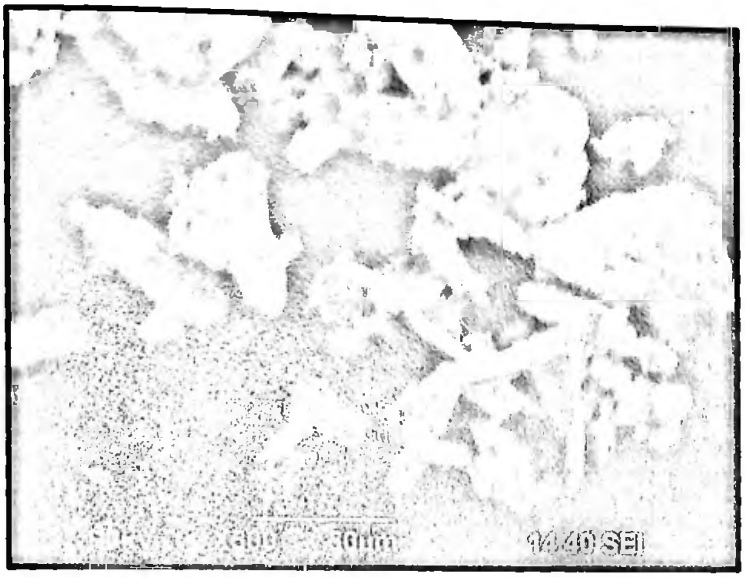

Figure 108: SEM image of Ferron + SMX Mix.

Morphology of crystals of Ferron Ground with Sulphamethoxazole

The crystals of Ferron ground with Sulphamethoxazole for 30 minutes, Ferron + SMX 30 min Grd, are blocky and brittle-looking (Figure 109). However their edges are not sharp. The crystals of Ferron are 'coated' with the Sulphamethoxazole crystals. The particles are semi-translucent.

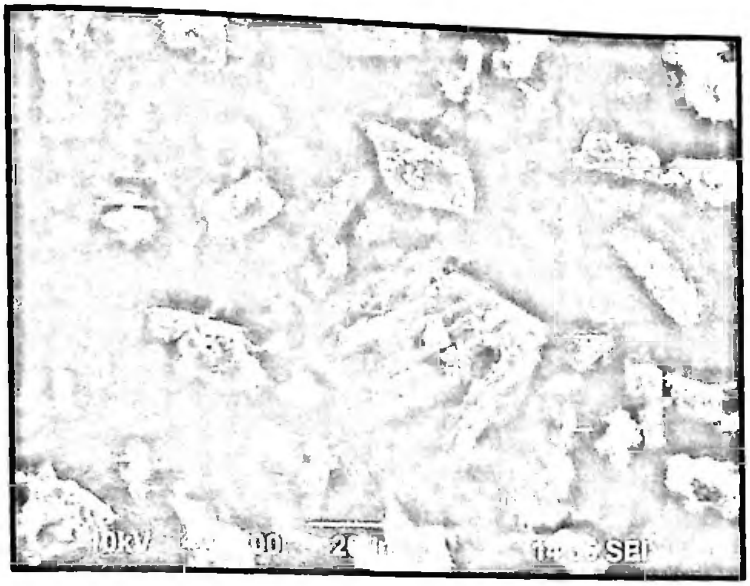

Figure 109: SEM image of Ferron + SMX 30 min Grd.

Morphology of crystals of Ferron Kneaded with Sulphamethoxazole

When Ferron is kneaded with Sulphamethoxazole for 30 minutes, the crystals sizes are reduced and massive (indiscernible masses of crystals too fine to see). The crystals are opaque and fibrous (Figure 110)

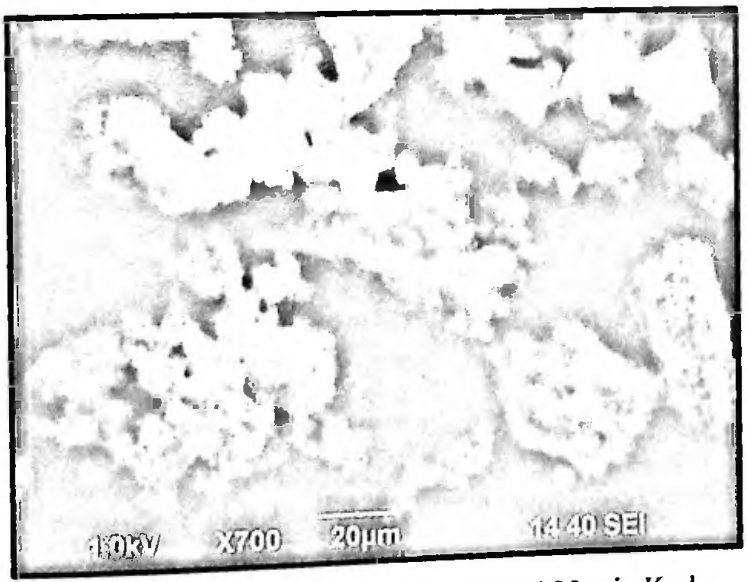

Figure 110: SEM image of Ferron + SMX 30 min Knd.

Morphology of crystals of Ferron Mixed with Carbazole

Mixing Ferron with Carbazole, Ferron + CAR Mix, gives a sample made up of distinct particles which are opaque (Figure 111). The image is blurred due to crystal movement while scanning.

Figure 111: SEM image of Ferron + CAR Mix.

Morphology of crystals of Ferron Ground with Carbazole

The crystals of Ferron ground with Carbazole for 30 minutes, Ferron + CAR 30 min Grd, are prismatic and encrusting (Figure 112). Some of the crystals are translucent and the others are opaque. There are a few amorphous particles.

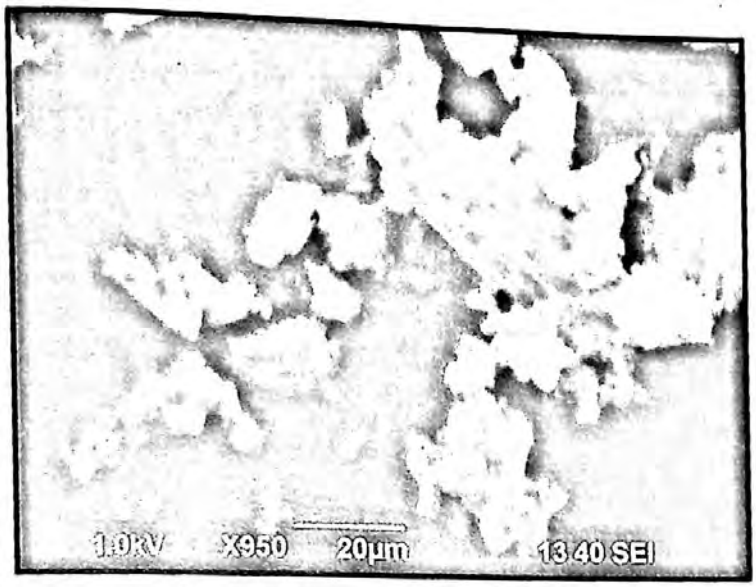

Figure 112: SEM image of Ferron + CAR 30 min Grd.

Morphology of crystals of Ferron Kneaded with Carbazole

When Ferron is kneaded with Carbazole for 30 minutes, Ferron + CAR 30 min Knd, the crystals sizes are not uniform (Figure 113). The crystals are encrusting. There is an amorphous material visible.

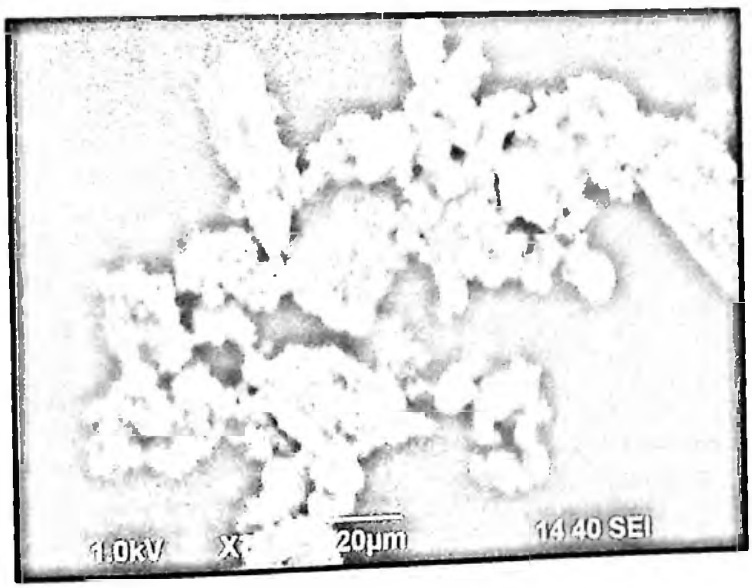

Figure 113: SEM image of Ferron + CAR 30 min Knd.

Analyses of *In-Silico* Infra-Red Spectra

There are techniques requiring computational support which are used to elucidate experimental and theoretical infrared spectra. This is because numerous 'finger-print' bands are not easily assignable based solely on experimental knowledge. In this study, the theoretical infrared spectra of the starting materials were elucidated to help identify the possible formation of weak forces between molecules when the co-crystals are formed.

Analysis of In–Silico Infra-Red spectrum of Ferron

An *in Silico* analysis of Ferron was undertaken in this study. The theoretical peaks for Ferron were calculated using Gaussian 09 software package, GaussView 5 software. The VEDA 4 software package was then used for the theoretical interpretation of the infra-red spectrum. To facilitate the discussion of the geometrical structures (rotational spectra) and rovibrational energy levels (infrared spectra), the atoms in the molecule were labelled (Figure 114).

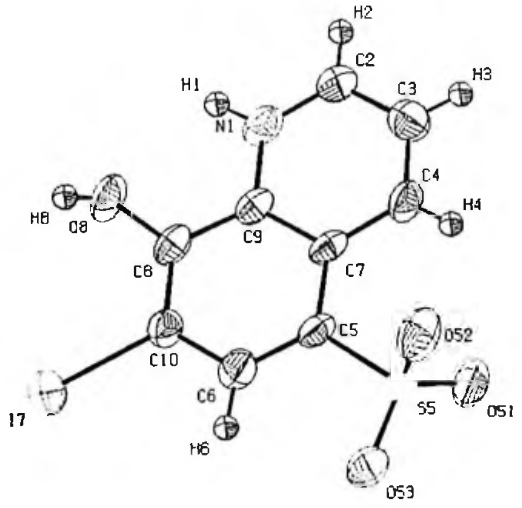

Figure 114: Labelled atoms in Ferron molecule.

Source: Balasubramanian & Muthiah, 1996

The highest peak from the experimental data is at 598 cm^{-1} (Figure 96) and this is shown in the calculated data at 600.82 cm^{-1}. This is assigned to stretching of the bond between C6 and H6. There is also a contribution from the torsion involving H2, C2, C3 and C4.

A C - C pure mode was determined at 1401 cm^{-1} to be due to stretching between C4 and C7. This is shown experimentally at 1383 cm^{-1} (Table 43). Most of the C–C bonds gave peaks theoretically varying from 850 cm^{-1} to 1500 cm^{-1} but these were mixed with other modes.

A C – H bond (C4-H4) has a pure stretching mode at a calculated wavelength of 1037.18 cm^{-1}; experimentally it is shown at 1042 cm^{-1}. At a wavelength of 707.52 cm^{-1} (experimentally at 726 cm^{-1}), the stretching of the bonds C3-H3 and N1-H1 are mixed though the N-H contributes more to the absorbance.

The stretching of the O8-H8 bond was assigned the wavelengths 3254, 1710, 237 and 209 cm^{-1} but these were not shown clearly experimentally. This may be due to the location of the lone pair of electrons in the antibonding orbital of H8.

The stretching of the S5 –O51 bond (Figure 114) gives a pure mode at 397.3 cm^{-1} (experimentally at 403 cm^{-1}). This is the moiety whose hydrogen was moved in the formation of the zwitterion.

The calculated infrared spectrum has no vibrational modes between the wavenumbers of 3000 cm^{-1} and 1700 cm^{-1} (Figure 115). Comparing the calculated infrared spectrum of Ferron with the experimental spectrum from this study (Figure 95), it is observed that the broad peak at 2740 cm^{-1}in the

experimental spectrum is absent in the calculated spectrum. This implies that the sample of Ferron used for the infrared analysis may have been moist.

The weak peak at 3088 cm^{-1} wavenumber in the experimental spectrum is due to the =C-H bond stretch and this has a corresponding peak at 3022.2 cm^{-1} in the calculated spectrum of Ferron (Table 43). The peaks in the group region is similar in both experimental and calculated spectra.

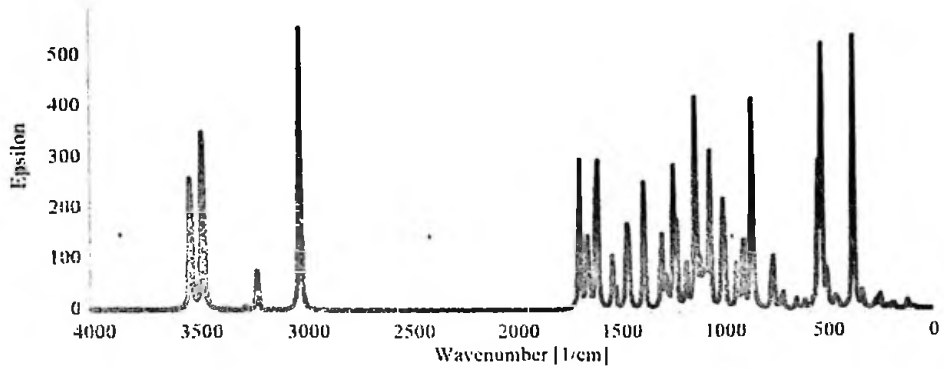

Figure 115: Calculated Infrared Spectrum of Ferron.

Table 43: Peaks common to both Experimental and Calculated Spectra of Ferron

Experimental Peaks		Calculated Peaks	
wavenumber [1/cm]	absorbance	wavenumber [1/cm]	Epsilon
3088.3	0.10022	3022.2	474.73
1620.8	0.17602	1605.7	256.14
1383.3	0.17305	1374.5	222.68
1237.6	0.16116	1229.5	234.33
1141.6	0.46199	1124.5	340.09

Analysis of In–Silico Infra-Red spectrum of Sulphamethoxazole

An *in Silico* analysis of Sulphamethoxazole was undertaken in this study. The theoretical peaks for Sulphamethoxazole were calculated using Gaussian 09 software package, GaussView 5 software. The VEDA 4 software package was then used for the theoretical interpretation of the infra-red spectrum. To facilitate the discussion of the geometrical structures (rotational spectra) and rovibrational energy levels (infrared spectra), the atoms in the molecule were labelled (Figure 116).

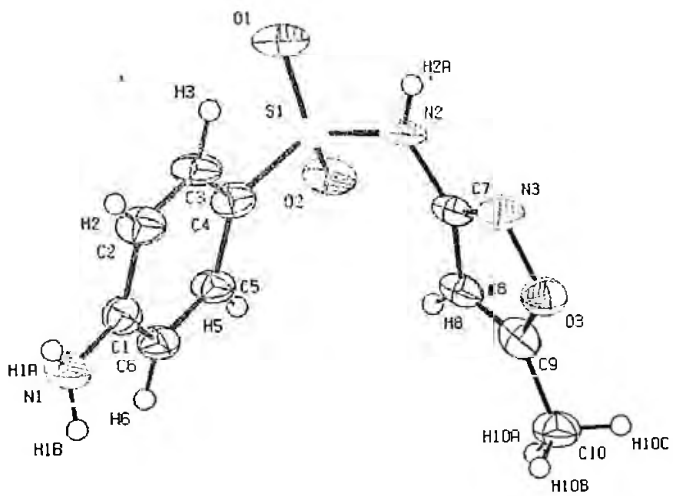

Figure 116: Labelled atoms in Sulphamethoxazole molecule.

Source: Perlovich et al., 2013

The highest peak in the calculated spectrum of Sulphamethoxazole is at a frequency of 507.75 cm^{-1} corresponds to the peak at 561.84 cm^{-1} in the experimental spectrum from this study (Figure 98). This is attributed to the torsion of the planes which pass through H2-C2-C3-C4 and H3-C3-C4-S1 (Figure 115). The peaks around the 3000 cm^{-1} are due mainly to torsion of some

planes in the molecule. For example, the peaks at 3377 cm^{-1} and 3298 cm^{-1} (Figure 97),calculated to be at 3354.13 cm^{-1} and 3262.24 cm^{-1} respectively, are due in part to torsion in the plane through H1B-N1-C1-C2 (Figure 116). However, the peaks at calculated frequencies of 3171.04 cm^{-1} and 3088.09 cm^{-1} are due to pure bending modes between O3-N3-C7 and H2A-N2-O2 respectively.

The peak at 1509.14 cm^{-1} in the calculated spectrum, corresponding to the peak at 1501 cm^{-1} in the experimental spectrum, is also due to a pure mode of torsion in the plane C1-C6-C5-C8 (Figure 116). The stretching modes between atoms in the group frequency region are mainly mixed with other modes except for the calculated modes at 1053.32 $cm^{-1}$and 1038.59 cm^{-1} which are single modes attributed to the stretching of the C3-H3 bond and the O2-N2 (Figure 116) bonds respectively. These bonds are seen around the 1000 cm^{-1} in the experimental spectrum (Figure 98).

The pure bending mode between atoms H10A-C10-C9 (Figure 116) gives a peak at a calculated frequency of 1300.24 cm^{-1} which corresponds the peak at 1303 cm^{-1} determined experimentally (Figure 98). The is a pure bending modes between the atoms H6-C6-C1 and N1-C1-C6 give peaks at calculated frequencies of 1361.9 cm^{-1} and 1358.44 cm^{-1} respectively. These peaks correspond to the peak at the frequency of 1363 cm^{-1} determined experimentally (Figure 98) in this study.

Comparing the calculated infrared spectrum of Sulphamethoxazole (Figure 117) with the experimental spectrum from this study (Figure 98), the

peaks are at similar frequencies especially in the group frequency region (Table 44).

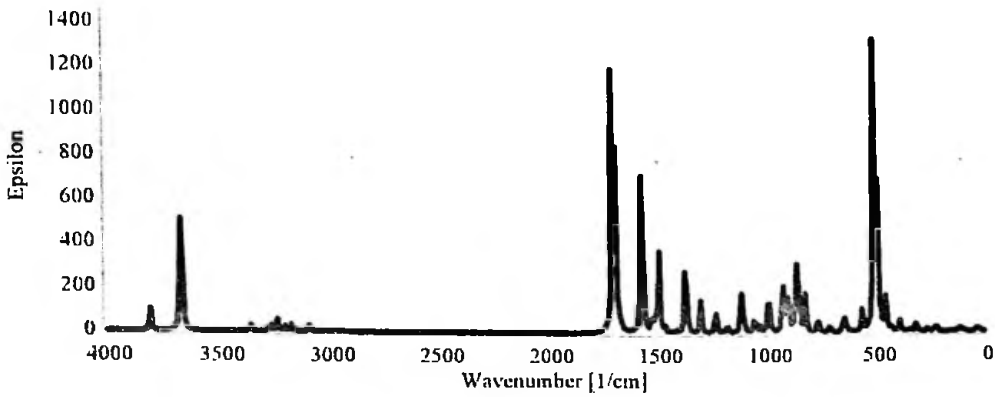

Figure 117: Calculated Infrared Spectrum of Sulphamethoxazole.

The peaks at the wavenumbers 3377 cm^{-1} and 3298 cm^{-1} (Table 44) are due the stretching of the C-H bond of the methyl group on the Sulphamethoxazole molecule. These have corresponding peaks at 3341.1 cm^{-1} and 3232 cm^{-1} in the calculated spectrum of Sulphamethoxazole (Table 44).

Table 44: Peaks common to both Experimental and Calculated Spectra of Sulphamethoxazole

Experimental Peaks		Calculated Peaks	
Wavenumber [1/cm]	Absorbance	Wavenumber [1/cm]	Epsilon
3376.7	0.10101	3344.1	7.5206
3297.7	0.085016	3232	41.515
1617.4	0.18221	1695.8	537.02
1595.3	0.19885	1565.5	574.48
1381.9	0.11466	1366.3	214.6
1141.8	0.31496	1114.3	151.76

Analysis of In–Silico Infra-Red spectrum of Carbazole

An *in Silico* analysis of Carbazole was undertaken in this study. The theoretical peaks for Carbazole were calculated using Gaussian 09 software package, GaussView 5 software. The VEDA 4 software package was then used for the theoretical interpretation of the infra-red spectrum. To facilitate the discussion of the geometrical structures (rotational spectra) and rovibrational energy levels (infrared spectra), the atoms in the molecule were labelled (Figure 118).

The C-H and C-C stretching vibrations of Carbazole are predicted at 1516.17 cm^{-1} (C2a-H2a) (Figure 121), 1367.21 cm^{-1} (C3-H3), 1257.58 cm^{-1} (C1-H1), and 771.17 cm^{-1} (C3a-H3a) for the C-H bonds and 1014.64 cm^{-1} (C2-C1) for the C-C bond. These were observed experimentally at 1492 cm^{-1} (Figure 99), 1357.63 cm^{-1} (Table 45), 1233 cm^{-1} (Figure 100), 756.69 cm^{-1} and 1010 cm^{-1}

$^{-1}$ (Table 45) respectively. These stretching vibrations are predicted to be pure nodes. The N-C stretching vibration is also predicted to be a pure node at 1250.38 cm^{-1}(N9-C9A) and this was observed at 1233 cm^{-1} (Figure 100).

Bending pure modes are predicted at 1058.03 cm^{-1} (H2-C2-C3), 892.65 cm^{-1} (C2-C1-C9A), 609.81 cm^{-1} (H9-N9-C9Aa), 580.53 cm^{-1}(H4-C4-C4A) and 463.15 cm^{-1} (C4Aa-C4a-C3a). These were observed at 1019.42 cm^{-1}, 857.44 cm^{-1}, 573.41 $cm^{-1}$and 551.26 cm^{-1}respectively.

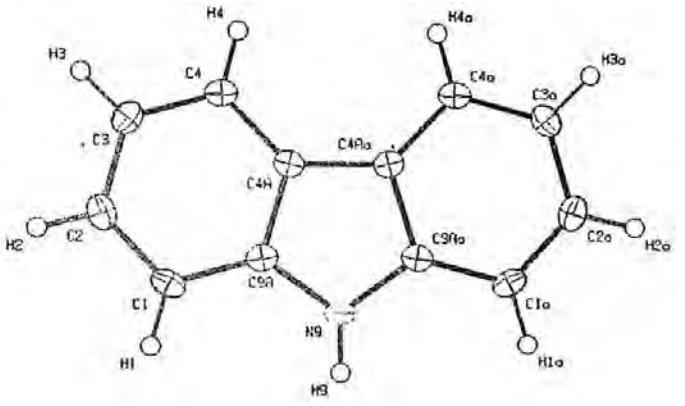

Figure 118: Labelled atoms in Carbazole molecule.

Source: Gajda et al., 2014

The PED analysis showed that the C-C and N-C stretching, bending and torsion vibrations are mixed with other vibrations and with themselves. An example is the prediction of a mode at 1610.62 $cm^{-1}$for the stretching of C4a-C4Aa mixed with the stretching of C4-C4A which was observed at 1598 cm^{-1} (Figure 99). Another example is the mode predicted at 1377.01 cm^{-1} for the stretching of N9-C9A and the bending of N9-C9A-C1 which was observed at 1357.6 cm^{-1} (Table 45).

Comparing the calculated infrared spectrum of Carbazole (Figure 119) with the experimental spectrum from this study (Figure 99), the peaks are at similar frequencies especially in the group frequency region (Table 45).

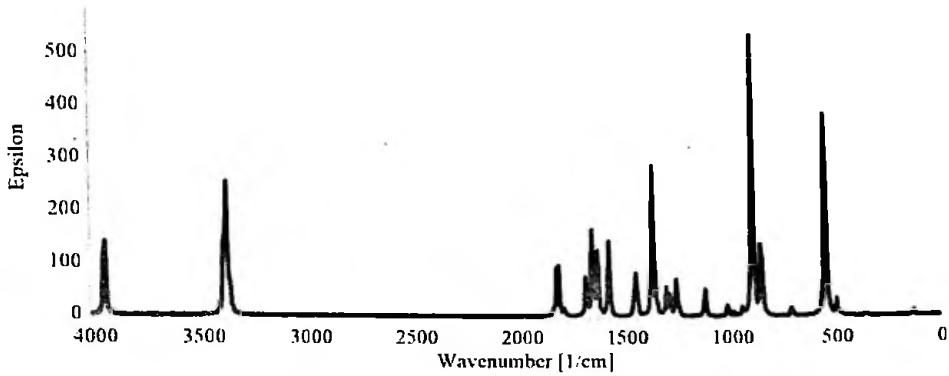

Figure 119: Calculated Infrared Spectrum of Carbazole.

The peak at wavenumber of 3417.1 cm^{-1} found in the experimental spectrum is due to the stretching of the C-H bonds. This peak corresponds to the peak at 3381.6 cm^{-1} found in the calculated spectrum (Table 45).

Table 45: Peaks common to both Experimental and Calculated Spectra of Carbazole

Experimental Peaks		Calculated Peaks	
Wavenumber [1/cm]	Absorbance	Wavenumber [1/cm]	Epsilon
3417.1	0.34783	3381.6	189.08
1814.9	0.13409	1814.2	94.806
1666.4	0.12628	1645.7	138.11
1357.6	0.13652	1357.3	236.42
1233.1	0.29128	1246.9	64.867
1107.2	0.17338	1109.5	41.999
1010	0.18176	1003.3	15.791

Chapter Summary

From the discussion of the results from Powder X-Ray Diffractometry (PXRD), Differential Scanning Calorimetry (DSC) and Thermogravimetry (TGA), in this study, the combination of Ferron with Sulphamethoxazole forms a co-crystal while the combination of Ferron with Carbazole does not form a co-crystal. The results from the UltraViolet Spectroscopy (UV/Vis)and the Infra-Red Spectroscopy, (IR), though indicating the possible formation of new materials, are not conclusive enough to indicate the presence of a co-crystal or not. The Scanning Electron Microscopy (SEM) show that the morphology of the products are different from the starting materials and indicate that though the Ferron particles are coated with the Carbazole particles, the product of

Ferron combined with Sulphamethoxazole shows some slight modification in the morphology of the starting materials.

CHAPTER FIVE

SUMMARY, CONCLUSIONS AND RECOMMENDATIONS

Summary

This study aimed at investigating the possibility of forming pharmaceutical co-crystals from existing active pharmaceutical ingredients using grinding, an environmentally friendly method from mehanochemistry. The study showed that though all three starting compounds were likely candidates for the formation of co-crystals, the combination of Ferron with Sulphamethoxazole yielded a co-crystal while combining Ferron with Carbazole did not yield a co-crystal. The physico-chemical properties of the co-crystal of Ferron with Sulphamethoxazole showed an improvement over those of only Ferron or Sulphamethoxazole as given by the lowering of the melting point and decomposition temperatures. This implies that, for example, the temperature at which drugs based on the co-crystal of Ferron with Sulphamethoxazole should be produced or stored should be lower than that for producing and storing drugs based on only Ferron and/or Sulphamethoxazole.

Conclusions

Though Ferron, Sulphamethoxazole and Carbazole, satisfy the supramolecular chemistry conditions for compounds most likely to form co-crystals, i.e., the candidate compounds have donor and acceptor sites and also have ionisable hydrogens, this study shows the combination of Ferron with Sulphamethoxazole formed a co-crystal while the combination of Ferron with Carbazole did not form a co-crystal.

A co-crystal of Ferron with Sulphamethoxazole was produced using kneading, a mechano-synthesis method based on green chemistry principles. However, a co-crystal was not produced when Ferron was combined with Carbazole using the same mechano-synthesis method under the same conditions.

Thermal profiles and diffraction patterns of the products of mechano-synthesis confirmed the presence of co-crystals of Ferron and Sulphamethoxazole.

The crystal lattice parameters derived from the powder x-ray diffraction data indicates that the unit cell has a monoclinic Bravais Lattice and belongs to the space group C2/m. The cell parameters are a = 21.00356 Å, b = 10.43984 Å, c = 28.16611 Å and β = 133.584°.The cell volume is 4,473.721 Å^3.

The melting point of the co-crystal is obtained to be 156.92°C which is lower than that of Ferron (269.25°C) or Sulphamethoxazole (168.30°C). The latent heat of the sample is obtained to be -40.25 J/g.

The thermal stability of the co-crystal of Ferron and Sulphamethoxazole (decomposes at 194.66°C) is lower than that Ferron (decomposes at 283.07°C) and Sulphamethoxazole (decomposes at 250.07°C).

The melting point of the combinations of Ferron with Carbazole were between 208°C and 219°C which are lower than the melting point of Ferron (269.25°C) and Carbazole (244.09°C).

The decomposition temperature range of the products formed from combining Ferron with Carbazole is 226°C to 290°C.

When Ferron is mixed or ground with Sulphamethoxazole, the crystals of Sulphamethoxazole are found on the surface of the Ferron crystals. When they are kneaded together, however, there is a clear change in the morphology; the product was opaque and massive, i.e., an indiscernible mass of crystals too fine to see.

On the other hand, when Ferron was mixed, ground or kneaded with Carbazole, the crystals of Carbazole generally remained on the surface of the Ferron crystals.

Recommendations

Single crystals of the co-crystals of Ferron and Sulphamethoxazole should be prepared by the 'Hot-melt' method. In this method, Ferron is melted together with Sulphamethoxazole and the melt allowed to slowly crystallize. This method may be successful in yielding a single crystal since the melting point of the co-crystal is lower than that of Ferron or Sulphamethoxazole as shown by the DSC in this study.

The theoretical structure of the co-crystal of Ferron and Sulphamethoxazole should be further refined and its physicochemical properties examined. This can then be compared to the experimentally determined properties.

The dissolution rate and bioavailability of the co-crystal of Ferron and Sulphamethoxazole should be established to find out how they compare to those of the individual starting APIs.

REFERENCES

Aakeröy, C. B. (2011). From molecules, via supramolecular assembly, to tunable physical properties. *Acta Crystallographica Section A*, *A67*, C66–C67. http://journals.iucr.org/a/issues/2011/a1/00/a46760/a46760.pdf

Aakeröy, C. B., Beatty, A. M., & Helfrich, B. A. (2002). A High-Yielding Supramolecular Reaction. *J. Am. Chem. Soc*, *124*(48), 14425–14432. https://doi.org/10.1021/ja027845q

Aakeröy, C. B., Beatty, A. M., Helfrich, B. A., & Nieuwenhuyzen, M. (2003). Do Polymorphic Compounds Make Good Cocrystallizing Agents? A Structural Case Study that Demonstrates the Importance of Synthon Flexibility. *Crystal Growth & Design*, *3*(2), 169–165. https://doi.org/10.1021/cg025593z

Aakeröy, C. B., Desper, J., Fasulo, M., Hussain, I., Levin, B., & Schultheiss, N. (2008). Ten years of co-crystal synthesis; the good, the bad, and the ugly. *CrystEngComm*, *10*, 1816–1821. https://doi.org/10.1039/b811809d

Aakeröy, C. B., Desper, J., & Helfrich, B. A. (2004). Heteromeric intermolecular interactions as synthetic tools for the formation of binary co-crystals. *CrystEngComm*, *6*, 19–24. https://doi.org/10.1039/B315181F

Aakeröy, C. B., Desper, J., Helfrich, B. A., Metrangolo, P., Pilati, T., Resnati, G., & Stevenazzi, A. (2007). Combining halogen bonds and hydrogen bonds in the modular assembly of heteromeric infinite 1-D chains. *Chem. Commun*, (41), 4236–4238. https://doi.org/10.1039/B707458A

Aakeröy, C. B., Desper, J., & Smith, M. M. (2007). Constructing, deconstructing, and reconstructing ternary supermolecules. *Chem. Commun.*, 3936–3938. https://doi.org/10.1039/B707518A

Aakeröy, C. B., Evans, T. A., Seddon, K. R., & Pálinkó, I. (1999). The C–H···Cl hydrogen bond: does it exist? *New J. Chem.*, *23*(2), 145–152. https://doi.org/10.1039/A809309A

Aakeröy, C. B., Fasulo, M. E., & Desper, J. (2007). Cocrystal or Salt: Does It Really Matter? *Mol. Pharmaceutics*, *4*(3), 317–322. https://doi.org/10.1021/mp060126o

Aakeröy, C. B., Forbes, S., & Desper, J. (2009). Using Cocrystals To Systematically Modulate Aqueous Solubility and Melting Behavior of an Anticancer Drug. *J. Am. Chem. Soc.*, *131*(47), 17048–17049. https://doi.org/10.1021/ja907674c

Aakeröy, C. B., & Salmon, D. J. (2005). Building co-crystals with molecular sense and supramolecular sensibility. *CrystEngComm*, *7*(72), 439–448. https://doi.org/10.1039/b505883j

Agyemang-Mensah, K. (2014, September). Ghana's pharmaceutical industry to be transformed. Retrieved November 12, 2016, from http://www.ghanaweb.com/GhanaHomePage/health/Ghana-s-pharmaceutical-industry-to-be-transformed-325105

Allesø, M., Velaga, S., Alhalaweh, A., Cornett, C., Rasmussen, M. A., Berg, F. van den, … Rantanen, J. (2008). Near-Infrared Spectroscopy for Cocrystal Screening. A Comparative Study with Raman Spectroscopy. *Anal. Chem*, *80*(20), 7755–7764. https://doi.org/10.1021/ac8011329

Almarsson, Ö., & Zaworotko, M. J. (2004). Crystal engineering of the composition of pharmaceutical phases. Do pharmaceutical co-crystals represent a new path to improved medicines? *Chemical Communications*, (17), 1889–1896. https://doi.org/10.1039/B402150A, Feature Article

Anslyn, E. V., & Dougherty, D. A. (2006). *Modern Physical Organic Chemistry* (1st ed.). Sausalito: University Science Books, Sausalito, CA, USA.

Anslyn, E. V., & Dougherty, D. A. (2009). Nature of Supramolecular Interactions. In J. W. Steed & J. L. Atwood (Eds.), *Supramolecular Chemistry* (2nd ed., pp. 27–37). Chichester, West Sussex, U.K.: John Wiley & Sons Ltd.

Awasabisah, D., & Richter-Addo, G. B. (2015). Chapter One – NOx Linkage Isomerization in Metal Complexes. *Advances in Inorganic Chemistry*, *67*, 1–86. https://doi.org/10.1016/bs.adioch.2014.11.003

Aymard, L., & Figlarz, M. (1993). Production of Ag-Pd alloys by mechanical alloying. *Solid State Ionics*, *63–65*, 143–147. https://doi.org/10.1016/0167-2738(93)90097-M

Babu, N. J., & Nangia, A. (2011). Solubility Advantage of Amorphous Drugs and Pharmaceutical Cocrystals. *Cryst. Growth Des.*, *11*(7), 2662–2679. https://doi.org/10.1021/cg200492w

Bailey, R. D., Drake, G. W., Grabarczyk, M., Hanks, T. W., Hooka, L. L., & Pennington, W. T. (1997). Synthesis, structure and thermal decomposition of nitrogen–iodine charge-transfer complexes. *J. Chem. Soc., Perkin Trans. 2*, (12), 2773–2780. https://doi.org/10.1039/A700203C

Balasubramanian, T., & Muthiah, P. T. (1996). Hydrogen-Bonding Patterns in Substituted Oxines. Redetermination of 8-Hy-droxy-7-iodo-quinoline-5-sulfonic Acid. *Acta Crystallographica Section C STRUCTURAL CHEMISTRY*, *C52*(Part 8), 2072–2073. https://doi.org/10.1107/S0108270195010286

BayviewPharmacy. (2009). 5-in-1 PolyPill Treatment May Prevent Heart Disease. Retrieved from http://www.bayviewrx.com/bayview-

blog/bid/18766/5-in-1-PolyPill-Treatment-May-Prevent-Heart-Disease

Bernstein, J. (2002). *Polymorphism in Molecular Crystals*. Oxford, NewYork: Oxford University Press Inc.

Berryman, O. B., Bryantsev, V. S., Stay, D. P., Johnson, D. W., & Hay, B. P. (2007). Structural criteria for the design of anion receptors: The interaction of halides with electron-deficient arenes. *J. Am. Chem. Soc.*, *129*(1), 48–58. https://doi.org/10.1021/ja063460m

Bingham, A. L., Hughes, D. S., Hursthouse, M. B., Lancaster, R. W., Tavener, S., & Threlfall, T. L. (2001). Over one hundred solvates of sulfathiazole. *Chem. Commun*, (7), 603–604. https://doi.org/10.1039/B009540K

Blagden, N., Matas, M. de, Gavan, P. T., & York, P. (2007). Crystal engineering of active pharmaceutical ingredients to improve solubility and dissolution rates. *Advanced Drug Delivery Reviews*, *59*(7), 617–630. https://doi.org/10.1016/j.addr.2007.05.011

Blessy, M., Patel, R. D., Prajapati, P. N., & Agrawal, Y. K. (2014). Development of forced degradation and stability indicating studies of drugs - A review. *Journal of Pharmaceutical Analysis*. https://doi.org/10.1016/j.jpha.2013.09.003

Boldyreva, E. V., Shakhtshneider, T. P., Vasilchenko, M. A., Ahsbahsc, H., & Uchtmannc, H. (1999). Anisotropic crystal structure distortion of the monoclinic polymorph of acetaminophen at high hydrostatic pressures. *Acta Crystallographica Section B*, *B56*, 299–309. https://doi.org/10.1107/S0108768199013634

Boldyrev, V. V., & Tkáčová, K. (2000). Mechanochemistry of Solids: Past, Present, and Prospects. *Journal of Materials Synthesis and Processing*, *8*(3/4), 121–132. https://doi.org/1064-7562/ 00/ 0700-0121

Boldyrew, W. W., Awwakumow, E. G., Strugowa, L. I., Harenz, H., & Heinicke, G. (1972). Zur Tribochemischen Zersetzung von Alkali-Bromaten und -Nitraten To tribochemical decomposition of alkaline bromates and nitrates. *Zeitschrift Für Anorganische Und Allgemeine Chemie*, *393*(2), 152–158. https://doi.org/10.1002/zaac.19723930209

Braga, D., Brammer, L., & Champness, N. R. (2005). New trends in crystal engineering. *Cryst. Eng. Comm*, *7*(1), 1–19. https://doi.org/10.1039/B417413E

Braga, D., Giaffreda, S. L., Grepioni, F., & Polito, M. (2004). Mechanochemical and solution preparation of the coordination polymers Ag[N(CH2CH2)3N]2[CH3COO]?5H2O and Zn[N(CH2CH2)3N]Cl2. *CrystEngComm*, *6*(75), 458–462. https://doi.org/10.1039/b406375a

Braga, D., Grepioni, F., & Desiraju, G. R. (1998). Crystal Engineering and

Organometallic Architecture. *Chemical Reviews*, *98*(4), 1375–1406. https://doi.org/10.1021/cr960091b

Braga, D., Grepioni, F., Maini, L., Capucci, D., Nanna, S., Wouters, J., … Quéré, L. (2012). Combining piracetam and lithium salts: ionic co-crystals and codrugs? *Chemical Communications*, (48), 8219–8221. https://doi.org/10.1039/C2CC33855F

Braga, D., Palladino, G., Polito, M., Rubini, K., Grepioni, F., Chierotti, M. R., & Gobetto, R. (2008). Three Polymorphic Forms of the Co-Crystal 4,4′-Bipyridine/Pimelic Acid and their Structural, Thermal, and Spectroscopic Characterization. *Chemistry A European Journal*, *14*(32), 10149–10159. https://doi.org/10.1002/chem.200801051

Breiten, B., Lockett, M. R., Sherman, W., Fujita, S., Al-Sayah, M., Lange, H., … Whitesides, G. M. (2013). Water Networks Contribute to Enthalpy/Entropy Compensation in Protein–Ligand Binding. *Journal of American Chemical Society*, *135*(41), 15579–15584. https://doi.org/10.1021/ja4075776

Brooker, S., Akhwale, W., Pullan, R., Estambale, B., Clarke, S. E., Snow, R. W., & Hotez, P. J. (2007). Epidemiology of Plasmodium-Helminth Co-Infection in Africa: Populations at Risk, Potential Impact on Anemia, and Prospects for Combining Control. *Am J Trop Med Hyg*, *77*(6_Suppl), 88–98. Retrieved from http://www.ajtmh.org/cgi/content/long/77/6_Suppl/88

Brooker, S., Clements, A. C. A., Hotez, P. J., Hay, S. I., Tatem, A. J., Bundy, D. A. P., & Snow, R. W. (2006). The co-distribution of Plasmodium falciparum and hookworm among African schoolchildren. *Malaria Journal*, *5*(99). https://doi.org/10.1186/1475-2875-5-99

Burns, J. H., & Bredig, M. A. (1956). Transformation of Calcite to Aragonite by Grinding. *The Journal of Chemical Physics*, *25*(6), 1281. https://doi.org/http://dx.doi.org/10.1063/1.1743198

Byrn, S. R., Pfeiffer, R. R., & Stowell, J. G. (1999). *Solid-state chemistry of drugs* (2nd ed.). West Lafayette, IN: SSCI, Inc., 1999. http://www.openisbn.com/isbn/0967067103/

Cannon, A. S., & Warner, J. C. (2002). Noncovalent Derivatization: Green Chemistry Applications of Crystal Engineering. *Crystal Growth & Design*, *2*(4), 255–257. https://doi.org/10.1021/cg0255218

Chaudhari, P. D., & Uttekar, P. S. (2009). Melt-Sonocrystallization: A Novel Particle Engineering Technique for Solubility Enhancement. *International Journal of PharmTech Research*, *1*(1), 111–120. http://sphinxsai.com/pdf/pt/PT PRINT -12.pdf

Childs, S. L., Chyall, L. J., Dunlap, J. T., Smolenskaya, V. N., Stahly, B. C., & Stahly, G. P. (2004). Crystal Engineering Approach To Forming

Cocrystals of Amine Hydrochlorides with Organic Acids. Molecular Complexes of Fluoxetine Hydrochloride with Benzoic, Succinic, and Fumaric Acids. *J. Am. Chem. Soc.*, *126*(41), 13335–13342. https://doi.org/10.1021/ja048114o

Childs, S. L., & Hardcastle, K. I. (2007). Cocrystals of Piroxicam with Carboxylic Acids. *Crystal Growth & Design*, *7*(7), 1291–1304. https://doi.org/10.1021/cg060742p

Childs, S. L., Stahly, G. P., & Park, A. (2007). The Salt-Cocrystal Continuum: The Influence of Crystal Structure on Ionization State. *Molecular Pharmaceutics*, *4*(3), 323–338. https://doi.org/10.1021/mp0601345

Collier, R. (2012). Reducing the "pill burden." *Canadian Medical Association Journal, CMAJ*, *184*(2), E117–E118. https://doi.org/DOI:10.1503/cmaj.109-4076

Cooke, C. L., & Davey, R. J. (2008). On the Solubility of Saccharinate Salts and Cocrystals. *Cryst. Growth Des*, *8*(10), 3483–3485. https://doi.org/10.1021/cg800621q

Cooper, P. J. (2004). Intestinal worms and human allergy. *Parasite Immunology*, *26*, 455–467. http://onlinelibrary.wiley.com/doi/10.1111/j.0141-9838.2004.00728.x/epdf

Corey, E. J. (1988). Robert Robinson Lecture. Retrosynthetic thinking—essentials and examples. *Chemical Society Reviews*, *17*(0), 111–113. https://doi.org/10.1039/CS9881700111

Cosic, I. (1994). Macromolecular bioactivity: is it resonant interaction between macromolecules?-theory and applications. *IEEE Transactions on Biomedical Engineering*, *41*(12), 1101–1114. https://doi.org/10.1109/10.335859

Courney, T. H. (1995). Process Modelling of Mechanical Alloying (Overview). *Materials Transactions, JIM*, *36*(2), 110–122. https://www.jstage.jst.go.jp/article/matertrans1989/36/2/36_2_110/_pdf

Cruz-Cabeza, A. J. (2012). Acid–base crystalline complexes and the pKa rule. *CrystEngComm, 14*(20), 6362–6365. https://doi.org/10.1039/C2CE26055G, Communication

Curtiss, L. A., Raghavachari, K., Redfern, P. C., Rassolov, V., & Pople, J. A. (1998). Gaussian-3 (G3) theory for molecules containing first and second-row atoms. *The Journal of Chemical Physics*, *109*(18), 7764–7776. https://doi.org/10.1063/1.477422

Dachille, F., & Roy, R. (1964). Effectiveness of Shearing Stresses in Accelerating Solid Phase Reactions at Low Temperatures and High

Pressures. *The Journal of Geology*, *72*(2), 243–247. https://doi.org/10.1086/626979

Desiraju, G. R. (1995). Supramolecular Synthons in Crystal Engineering—A New Organic Synthesis. *Angewandte Chemie International Edition in English*, *34*(21), 2311–2327. https://doi.org/10.1002/anie.199523111

Drugs.com. (2016). Chiniofon. Retrieved April 11, 2016, from http://www.drugs.com/dict/chiniofon.html

Dunitz, J. D. (1995). Thoughts on Crystals as Supermolecules. In Gautam R. Desiraju (Ed.) (2nd ed., pp. 1–30). Chichester . New York . Brisbane . Toronto . Singapore: John Wiley & Sons.

Dunitz, J. D. (2003a). Are crystal structures predictable? *Chemical Communications*, (5), 545–548. https://doi.org/10.1039/b211531j

Dunitz, J. D. (2003b). Crystal and co-crystal: a second opinion. *CrystEngComm*, (91), 506–506. https://doi.org/10.1039/B315687G

Dunitz, J. D., & Bernstein, J. (1995). Disappearing Polymorphs. *Acc. Chem. Res*, *28*(4), 193–200. https://doi.org/10.1021/ar00052a005

Eicher, T., & Hauptmann, S. (2003). Preface. In *The Chemistry of Heterocycles* (2nd ed., pp. ix–ix). Weinheim: Wiley-VCH Verlag GmbH & Co. KGaA.

Erk, P., Hengelsberg, H., Haddow, M. F., & van Gelder, R. (2004). The innovative momentum of crystal engineering. *CrystEngComm*, *6*(78), 475–483. https://doi.org/10.1039/B409282A

Etter, M. C. (1990). Encoding and decoding hydrogen-bond patterns of organic compounds. *Accounts of Chemical Research*, *23*(4), 120–126. https://doi.org/10.1021/ar00172a005

Etter, M. C. (1991a). Hydrogen bonds as design elements in organic chemistry. *J. Phys. Chem.*, *95*(12), 4601–4610. https://doi.org/10.1021/j100165a007

Etter, M. C. (1991b). Hydrogen bonds as design elements in organoc chemistry. *J. Phys. Chem*, *95*(12), 4601–4610. https://doi.org/10.1021/j100165a007

Etter, M. C., MacDonald, J. C., & Bernstein, J. (1990). Graph-set analysis of hydrogen-bond patterns in organic crystals. *Acta Crystallographica Section B STRUCTURAL SCIENCE, CRYSTAL ENGINEERING AND MATERIALS*, *B46*(2), 256–262. https://doi.org/10.1107/S0108768189012929

Etter, M. C., & Reutzel, S. M. (1991). Hydrogen bond directed

cocrystallization and molecular recognition properties of acyclic imides. *J. Am. Chem. Soc*, *113*(7), 2586–2598. https://doi.org/10.1021/ja00007a037

Etter, M. C., Reutzel, S. M., & Choo, C. G. (1993). Self-organization of adenine and thymine in the solid state. *J. Am. Chem. Soc*, *115*(10), 4411–4412. https://doi.org/10.1021/ja00063a089

Falagas, M. E., Grammatikos, A. P., & Michalopoulos, A. (2008). Potential of old-generation antibiotics to address current need for new antibiotics. *Expert Review of Anti-Infective Therapy*, *6*(5), 593–600. https://doi.org/10.1586/14787210.6.5.593.

Falagas, M. E., & Kasiakou, S. K. (2005). Colistin: the revival of polymyxins for the management of multidrug-resistant gram-negative bacterial infections. *Clinical Infectious Diseases*, *40*(9), 1333–1341. http://www.ncbi.nlm.nih.gov/pubmed/15825037

Farrar, J., Hotez, P. J., Junghanss, T., Kang, G., Lalloo, D., & White, N. (2013). *Manson's tropical diseases* (New Editio). Philadelphia: Saunders.

Farrugia, L. J. (2012). WinGX and ORTEP for Windows: an update. *Journal of Applied Crystallography*, *45*, 849–854. https://doi.org/10.1107/S0021889812029111

Feller, D. (1996). The Role of Databases in Support of Computational Chemistry Calculations. *Journal of Computational Chemistry*, *17*(13), 1571–1586. https://doi.org/10.1002/(SICI)1096-987X(199610)17:13<1571::AID-JCC9>3.0.CO;2-P

Fernández-Bertran, J. F. (1999). Mechanochemistry: an overview. *Pure Appl. Chem*, *71*(4), 581–586. http://pac.iupac.org/publications/pac/pdf/1999/pdf/7104x0581.pdf

Ferrari, M., Lutterotti, L., Matthies, S., Polonioli, H., & Wenk, H.-R. (1996). New Opportunities in the texture and stress field by the whole pattern analysis. *Material Science Forum*, *228–231*(83–88).

Foxman, B. M., Guarrera, D. J., Taylor, L. D., VanEngen, D., & Warner, J. C. (1998). Environmentally Benign Synthesis Using Crystal Engineering: Steric Accommodation in Non-Covalent Derivatives of Hydroquinones. *Crystal Engineering*, *1*(1), 109–118. https://doi.org/http://dx.doi.org/10.1016/S0025-5408(98)00039-7

Frisch, Æ., Hratchian, H. P., Dennington II, R. D., Keith, T. A., Millam, J., Nielsen, A. B., … Hiscocks, J. (2009). GaussView 5.0. Wallingford,: Gaussian, Inc. 340 Quinnipiac Street, Building 40 Wallingford, CT 06492 USA. www.gaussian.com

Frisch, M. J., Pople, J. A., & Binkley, J. S. (1984). Self-consistent molecular

orbital methods 25. Supplementary functions for Gaussian basis sets. *The Journal of Chemical Physics*, *80*(7), 3265–3269. https://doi.org/10.1063/1.447079

Frisch, M. J., Trucks, G. W., Cheeseman, J. R., Scalmani, G., Caricato, M., Hratchian, H. P., … Nakai, H. (2009). Gaussian 09 Advances. Wallingford CT: Gaussian, Inc.

Frisch, M. J., Trucks, G. W., Schlegel, H. B., Scuseria, G. E., Robb, M. A., Cheeseman, J. R., … Fox, D. J. (2009). Gaussian 09. Wallingford CT: Gaussian, Inc.,.

Fujii, K., Young, M. T., & Harris, K. D. M. (2011). Exploiting powder X-ray diffraction for direct structure determination in structural biology: The P2X4 receptor trafficking motif YEQGL. *Journal of Structural Biology*, *174*, 461–467. https://doi.org/10.1016/j.jsb.2011.03.001

Gajda, K., Zarychta, B., Kopka, K., Daszkiewicz, Z., & Ejsmont, K. (2014). Substituent effects in nitro derivatives of carbazoles investigated by comparison of low-temperature crystallographic studies with density functional theory (DFT) calculations. *Acta Crystallographica Section C Crystal Structure Chemistry*, *70*(10), 987–991. https://doi.org/10.1107/S2053229614020634

Gavezzotti, A. (1994). Are Crystal Structures Predictable? *Acc. Chem. Res*, *27*(10), 309–314. https://doi.org/10.1021/ar00046a004

Giamarellou, H., & Poulakou, G. (2009). Multidrug-resistant Gram-negative infections: what are the treatment options? *Drugs*, *69*(14), 1879–1901. https://doi.org/10.2165/11315690-000000000-00000

Gilman, J. J. (1993). Shear-induced metallization. *Philosophical Magazine Part B*, *67*(2), 207–214. https://doi.org/10.1080/13642819308207868

Gilman, J. J. (1995). Mechanism of Shear-Induced Metallization. *Czechoslovak Journal of Physics*, *45*(11), 913–919. http://link.springer.com/journal/10582/45/11/page/1#page-2

Gilman, J. J. (1996). Mechanochemistry. *Science*, *274*(5284), 65. https://doi.org/10.1126/science.274.5284.65

Görbitz, C. H. (2000). A new "hydrogen-bond rule" applied to the structure of L-seryl-L-alanine and pairs of dipeptide retroanalogues. *Acta Crystallographica Section C STRUCTURAL CHEMISTRY*, *56*(4), 500–502. https://doi.org/10.1107/S0108270100001463

Görbitz, C. H., & Etter, M. C. (1993). Structure of a 1:1 complex between L-Asp-L-Phe and L-His-Gly. *Acta Crystallographica Section C STRUCTURAL CHEMISTRY*, *C49*, 1673–1679. https://doi.org/10.1107/S010827019300246X

Halden, B. (2014, July). Solubility Advantage of Amorphous Drugs and Pharmaceutical Cocrystals. Retrieved March 23, 2016, from https://developingtheprocess.wordpress.com/2014/07/09/solubility-advantage-of-amorphous-drugs-and-pharmaceutical-cocrystals/

Harrison, J. J. E. K., Tabuchi, Y., Ishida, H., & Kingsford-Adaboh, R. (2009). Crystal structure of three solvated Alpinumisoflavones. *Structural Chemistry*, *20*(2), 203–211. https://doi.org/10.1007/s11224-008-9399-3

Higuchi, T., & Lach, J. L. (1954). Investigation of some complexes formed in solution by caffeine. IV. Interactions between caffeine and sulfathiazole, sulfadiazine, p-aminobenzoic acid, benzocaine, phenobarbital, and barbital. *J Am Pharm Assoc Am Pharm Assoc*, *43*(6 1), 349–354. http://www.ncbi.nlm.nih.gov/pubmed/13174434

Higuchi, T., & Pitman, I. H. (1973). Caffeine complexes with low water solubility: synthesis and dissolution rates of 1:1 and 1:2 caffeine-gentisic acid complexes. *J Pharm Sci.*, *62*(1), 55–58. http://www.ncbi.nlm.nih.gov/pubmed/?term=Higuchi+T%3B+Ptman+I.+H.+1973

Higuchi, T., & Zuck, D. A. (1952). Solubilizing action of caffeine on benzoic acid. *J Am Pharm Assoc Am Pharm Assoc.*, *41*(1), 10–13. http://www.ncbi.nlm.nih.gov/pubmed/?term=Solubilizing+action+of+caffeine+on+benzoic+acid

Higuchi, T., & Zuck, D. A. (1953a). Investigation of some complexes formed in solution by caffeine. II. Benzoic acid and benzoate ion. *J Am Pharm Assoc Am Pharm Assoc.*, *42*(3), 132–138. http://www.ncbi.nlm.nih.gov/pubmed/13034651

Higuchi, T., & Zuck, D. A. (1953b). Investigation of some complexes formed in solution by caffeine. III. Interactions between caffeine and aspirin, p-hydroxybenzoic acid, m-hydroxybenzoic acid, salicylic acid, salicylate ion, and butyl paraben. *J Am Pharm Assoc Am Pharm Assoc.*, *42*(3), 138–145. http://www.ncbi.nlm.nih.gov/pubmed/13034652

Hoogsteen, K. (1963). The crystal and molecular structure of a hydrogen-bonded complex between 1-methylthymine and 9-methyladenine. *Acta Cryst.*, *16*, 907–916. https://doi.org/10.1107/S0365110X63002437

Hosseini, M. W. (2003). Molecular tectonics: from molecular recognition of anions to molecular networks. *Coordination Chemistry Reviews*, *240*(1), 157–166. https://doi.org/10.1016/S0010-8545(03)00021-3

Hotez, P. J., Molyneux, D. H., Fenwick, A., Kumaresan, J., Sachs, S. E., Sachs, J. D., & Savioli, L. (2007). Control of Neglected Tropical Diseases. *The New England Journal of Medicine*, *357*(10), 1018–1027. https://doi.org/10.1056/NEJMra064142

Huang, K.-S., Britton, D., Etter, M. C., & Byrn, S. R. (1997). A novel class of phenol–pyridine co-crystals for secondharmonic generation. *J. Mater. Chem*, *7*(5), 713–720. https://doi.org/10.1039/A604311J

Huanga, L.-F., & Tong, W.-Q. (Tony). (2004). Impact of solid state properties on developability assessment of drug candidates. *Advanced Drug Delivery Reviews*, *56*(3), 321–334.

Hunter, C. A., Lawson, K. R., Perkins, J., & Urch, C. J. (2001). Aromatic interactions. *J. Chem. Soc., Perkin Trans. 2*, 651–669.

IUPAC. (1963). *Spectrophotometric Data for Colorimetric Analysis*. London: Butterworths, London. http://www.abebooks.co.uk/book-search/title/spectrophotometric-data-for-colorimetric-analysis/author/international-union-of-pure-and-applied-chemistry/

Jamieson, J. C., & Goldsmith, J. R. (1960). Some Reactions produced in Carbonates by Grinding. *The American Mineralogist*, *45*(7–8), 818–827. http://www.minsocam.org/ammin/AM45/AM45_818.pdf

Jamróz, M. H. (2013). Vibrational energy distribution analysis (VEDA): scopes and limitations. *Spectrochimica Acta. Part A, Molecular and Biomolecular Spectroscopy*, *114*, 220–30. https://doi.org/10.1016/j.saa.2013.05.096

Jamróz, M. H. (2015). Vibrational Energy Distribution Analysis (VEDA) 4. Warsaw, Poland: The Spectroscopy and Molecular Modeling Group.

Jeffrey, G. A. (1997). *An Introduction to Hydrogen Bonding*. Oxford University Press. http://www.oupcanada.com/catalog/9780195095494.html

Jeffrey, G. A., Ruble, J. R., McMullan, R. K., & Pople, J. A. (1987). The Crystal Structure of Deuterated Benzene. *Proceedings of the Royal Society A: Mathematical, Physical and Engineering Science*, *414*(1846), 47–57. https://doi.org/10.1098/rspa.1987.0132

Jensen, F., & Helgaker, T. (2004). Polarization consistent basis sets. V. The elements Si–Cl. *Journal of Chemical Physics*, *121*(8), 3463–3470. https://doi.org/10.1063/1.1756866

Jones, W., Motherwell, W. D. S., & Trask, A. V. (2006). Pharmaceutical Cocrystals: An Emerging Approach to Physical Property Enhancement. *MRS Bulletin Formerly Materials Research Society Newsletter*, *31*(11), 875–879. https://doi.org/http://dx.doi.org/10.1557/mrs2006.206

Karamertzanis, P. G., Kazantsev, A. V., Issa, N., Welch, G. W. A., Adjiman, C. S., Pantelides, C. C., & Price, S. L. (2009). Can the Formation of Pharmaceutical Cocrystals Be Computationally Predicted? 2. Crystal Structure Prediction. *Journal of Chemical Theory and Computation*, *5*(5),

1432–1448. https://doi.org/10.1021/ct8004326

Khristi, A. P., Soni, T., & Suhagia, B. N. (2015). Development, Characterisation and Evaluation of Sildenafil Aspirin Co-crystals. *Indo American Journal of Pharmaceutical Research*, *5*(7), 2700–2708. https://www.google.com.gh/url?sa=t&rct=j&q=&esrc=s&source=web&cd=2&cad=rja&uact=8&ved=0ahUKEwiNwejJyoTVAhUCa1AKHS8KBTQQFgguMAE&url=http%3A%2F%2Fwww.ejmanager.com%2Fmnstemps%2F36%2F36-1439201917.pdf&usg=AFQjCNEXTq1inTEa2xfcy7eAxnSdIDBkeQ

Kim, C. K., Yoon, S. H., Won, J., & Kim, C. K. (2006). Examination of Gaussian-Type Basis Sets on Alkali Metal Iodides. *Bulletin of Korean Chemical Society*, *27*(8), 1219–1221. journal.kcsnet.or.kr/main/j_search/j_download.htm?code=B060824

Kitaigorodskii, A. I. (1961). *Organic Chemical Crystallography*. New York: Consultants Bureau, Press of the Academy of Sciences of the USSR, Moscow.

Kitaigorodsky, A. I. (1973). Structure of Crystals. In A. I. Kitaigorodsky (Ed.), *Molecular Crystals and Molecules* (pp. 1–133). New York & London: ACADEMIC PRESS.

Kotak, U., Prajapati, V., Solanki, H., Jani, G., & Jha, P. (2015). Co-crystallization Technique - Its rationale and recent progress. *World Journal of Pharmacy and Pharmaceutical Sciences*, *4*(4), 1484–1508. Retrieved from www.wjpps.com/download/article/1427970181.pdf

Krantz, J. C., & Holbert, J. M. (1947). Sodium theophylline glycinate. *Journal of the American Pharmaceutical Association. American Pharmaceutical Association*, *36*(8), 248–50. http://www.ncbi.nlm.nih.gov/pubmed/20256465

Krishnan, R., Binkley, J. S., Seeger, R., & Pople, J. A. (1980). Self-consistent molecular orbital methods. XX. A basis set for correlated wave functions. *The Journal of Chemical Physics*, *72*(1), 650–654. https://doi.org/10.1063/1.438955

Krumkamp, R., Sarpong, N., Schwarz, N. G., Adelkofer, J., Loag, W., Eibach, D., … May, J. (2015). Gastrointestinal Infections and Diarrheal Disease in Ghanaian Infants and Children: An Outpatient Case-Control Study. *PLOS Neglected Tropical Diseases*, *9*(3). https://doi.org/10.1371/journal.pntd.0003568

Kumar, S. (2006). Spectroscopy of Organic Compounds. Amritsar: Guru Nanak Dev University. Retrieved from http://www.uobabylon.edu.iq/eprints/publication_11_8282_250.pdf

Larson, A. C., & Von Dreele, R. B. (2004). *GSAS- General Structure Analysis*

System. Los Alamos National Laboratory Report LAUR. https://subversion.xor.aps.anl.gov/EXPGUI/gsas/all/GSAS Manual.pdf

Lehn, J.-M. (1995). *Supramolecular Chemistry: Concepts and Perspectives*. (U. Anton & H. J. Maier, Eds.). Weinheim: VCH Verlagsgesellschaft mbH, VCH Publishers, Inc. https://doi.org/10.1002/3527607439

Lemmerer, A., Govindraju, S., Johnston, M., Motloung, X., & Savig, K. L. (2015). Co-crystals and molecular salts of carboxylic acid/ pyridine complexes: can calculated pKa's predict proton transfer? A case study of nine complexes. *CrystEngComm*, *17*(19), 3591–3595. https://doi.org/10.1039/C5CE00102A

Lewis, R. J. (2004). *Sax's Dangerous Properties of Industrial Materials* (11th ed.). Hoboken, New Jersey: John Wiley & Sons, Inc.

Lockett, M. R., Lange, H., Breiten, B., Heroux, A., Sherman, W., Rappoport, D., … Whitesides, G. M. (2013). The Binding of Benzoarylsulfonamide Ligands to Human Carbonic Anhydrase is Insensitive to Formal Fluorination of the Ligand. *Angew. Chem. Int. Ed*, *52*(30), 7714–7717. https://doi.org/10.1002/anie.201301813

LookChem. (2008). 8-Hydroxy-7-iodo-5-quinolinesulfonic acid. Retrieved April 11, 2016, from http://www.lookchem.com/8-Hydroxy-7-iodo-5-quinolinesulfonic-acid/

Lu, E., Rodríguez-Hornedo, N., & Suryanarayanan, R. (2008). A rapid thermal method for cocrystal screening. *CrystEngComm*, *10*(6), 665–668. https://doi.org/10.1039/B801713C

Lu, J. (2012). Crystallization and transformation of pharmaceutical solid forms. *African Journal of Pharmacy and Pharmacology*, *6*(9), 581–591. https://doi.org/10.5897/AJPP12.044

Lutterotti, L., Bortolotti, M., Ischia, G., Lonardelli, I., & Wenk, H.-R. (2007). Rietveld texture analysis from diffraction images. *Z. Kristallogr., Suppl.*, *26*, 125–130. https://doi.org/10.1524/zksu.2007.2007.suppl_26.125

Ma, J. C., & Dougherty, D. (1997). The cation-π interaction. *Chem. Rev.*, *97*, 1303–1324.

Macrae, C. F., Bruno, I. J., Chisholm, J. A., Edgington, P. R., McCabe, P., Pidcock, E., … Wood, P. A. (2008). Mercury CSD 2.0 - new features for the visualization and investigation of crystal structures. *Journal of Applied Crystallography*, *41*, 466–470. https://doi.org/10.1107/S0021889807067908

Maddox, J. (1988). Crystals from first principles. *Nature*, *335*(6187), 201–201. https://doi.org/10.1038/335201a0

Marvin Beans Suite. (2015). ChemAxon Ltd. http://www.chemaxon.com

Matthies, S., Lutterotti, L., & Wenk, H.-R. (1997). Advances in Texture Analysis from Diffraction Spectra. *Journal of Applied Crystallography*, *30*, 31–42.

McNamara, D. P., Childs, S. L., Giordano, J., Iarriccio, A., Cassidy, J., Shet, M. S., … Park, A. (2006). Use of a Glutaric Acid Cocrystal to Improve Oral Bioavailability of a Low Solubility API. *Pharmaceutical Research*, *23*(8), 1888–1897. https://doi.org/10.1007/s11095-006-9032-3

Menges, F. (2015). Spekwin32 - optical spectroscopy software. http://www.effemm2.de/spekwin/

Merck Index. (2016). *Sulfamethoxazole*. New Jersey, U.S.A. Retrieved from https://www.rsc.org/Merck-Index/monograph/m10320?q=authorize

Merritt-Jnr, L. L., & Duffin, B. (1970). The crystal structures of two derivatives of 8-hydroxyquinoline-5-sulfonic acid, 2-methyl-8-hydroxyquinoline-5-sulfonic acid monohydrate, and 7-iodo-8-hydroxyquinoline-5-sulfonic acid. *Acta Crystallographica Section B STRUCTURAL SCIENCE, CRYSTAL ENGINEERING AND MATERIALS*, *B26*(6), 734–744. https://doi.org/10.1107/S0567740870003060

Miroshnyk, I., Mirza, S., & Sandler, N. (2009). Pharmaceutical co-crystals–an opportunity for drug product enhancement. *Expert Opinion on Drug Delivery*, *6*(4), 333–341. https://doi.org/10.1517/17425240902828304

Moulton, B., & Zaworotko, M. J. (2001). From Molecules to Crystal Engineering: Supramolecular Isomerism and Polymorphism in Network Solids. *Chemical Reviews*, *101*(6), 1629–1658. https://doi.org/10.1021/cr9900432

Muller, P. (2009). Practical suggestions for better crystal structures. *Crystallography Reviews*, *15*(1), 57–83. https://doi.org/10.1080/08893110802547240

Munnings, C., Badwal, S. P. S., & Fini, D. (2014). Spontaneous stress-induced oxidation of Ce ions in Gd-doped ceria at room temperature. *Ionics*, *20*(8), 1117–1126. https://doi.org/10.1007/s11581-014- 1079-2

Nangia, A., & Desiraju, G. R. (1998). Supramolecular Structures - Reason and Imagination. *Acta Crystallographica Section A FOUNDATIONS AND ADVANCES*, *A54*(6), 934–944. https://doi.org/10.1107/S0108767398008551

Netland, P. A. (Ed.). (2008). *GLAUCOMA MEDICAL THERAPY Principles and Management* (2nd ed.). New York: Oxford University Press In cooperation with The American Academy of Ophthalmology.

http://www.oculist.net/downaton502/prof/ebook/glaucoma/GlaucomaMedicalTherapy.pdf#page=162

Nicolaou, K. C., & Sorensen, E. J. (1996). *Classics in Total synthesis; Targets, Strategies, Methods*. (R. Schmidt-Radde, Ed.). Weinheim (Federal Rep. og Germany); NewYork (USA): VCH Verlagsgesellschaft mbH, VCH Publishers, Inc.

Nishioka, F., Nakanishi, I., Fujiwara, T., & Tomita, K. (1984). The crystal and molecular structure of the β-cyclodextrin inclusion complex with aspirin and salicylic acid. *Journal of Inclusion Phenomena*, *2*(3), 701–714. https://doi.org/0167-7861/84.15

NTD, W. (2017). *Neglected tropical diseases – Summary*. http://www.who.int/neglected_diseases/diseases/summary/en/

Näsänen, R., & Ekman, A. (1952). Potentiometric and Spectrophotomtric Studies on 8-Quinolinol and its derivatives. V. Ionization of 8-Quinolinol-5-Sulfonic acid and 7-iodo-8-Quinolinol-5-Sulfonic acid in Aqueous Solution. *Acta Chemica Scandinavica*, *6*, 1384–1390. https://doi.org/10.3891/acta.chem.scand.06-1384

O'Brien, E. J. (1967). Crystal structures of two complexes containing guanine and cytosine derivatives. *Acta Cryst.*, *23*, 92–106. https://doi.org/10.1107/S0365110X67002191

Perlovich, G. L., Ryzhakov, A. M., Tkachev, V. V., Hansen, L. K., & Raevsky, O. A. (2013). Sulfonamide Molecular Crystals: Structure, Sublimation Thermodynamic Characteristics, Molecular Packing, Hydrogen Bonds Networks. *Crystal Growth & Design*, *13*(9), 4002.

Peterson, K. A., Figgen, D., Goll, E., Stoll, H., & Dolg, M. (2003). Systematically convergent basis sets with relativistic pseudopotentials. II. Small-core pseudopotentials and correlation consistent basis sets for the post-d group 16–18 elements. *The Journal of Chemical Physics*, *119*(21), 11113–11123. https://doi.org/10.1063/1.1622924

Piermarini, G. J., Mighell, A. D., Weir, C. E., & Block, S. (1969). Crystal Structure of Benzene II at 25 Kilobars. *Science*, *165*(3899), 1250–1255. https://doi.org/10.1126/science.165.3899.1250

Porter-III, W. W., Elie, S. C., & Matzger, A. J. (2008). Polymorphism in Carbamazepine Cocrystals. *Cryst. Growth Des*, *8*(1), 14–16. https://doi.org/10.1021/cg701022e

Price, C. P., Grzesiak, A. L., & Matzger, A. J. (2005). Crystalline Polymorph Selection and Discovery with Polymer Heteronuclei. *Journal of the American Chemical Society*, *127*(15), 5512–5517. https://doi.org/10.1021/ja042561m

Putkonen, M.-L., Feld, R., Vettier, C., & Lehmann, M. S. (1985). Powder neutron diffraction analysis of the hydrogen bonding in deutero-oxalic acid dihydrate at high pressures. *Acta Crystallographica Section B*, *B41*, 77–79. https://doi.org/10.1107/S0108768185001598

Pyykkö, P. (1997). Strong closed-shell interactions in inorganic chemistry. *Chem. Rev.*, *97*, 597–636.

Rappoport, D., & Furche, F. (2010). Property-optimized Gaussian basis sets for molecular response calculations. *The Journal of Chemical Physics*, *133*(13), 134105–(1–11). https://doi.org/10.1063/1.3484283

Reguera, E., Balmaseda, J., Quintana, G., Gomez, A., & Fernandez-Bertran, J. (1998). Transformation of cadmium ferricyanide by heating, milling and sonication. *Polyhedron*, *17*(13–14), 2353–2361. https://doi.org/10.1016/S0277-5387(97)00518-4

Remenar, J. F., Morissette, S. L., Peterson, M. L., Moulton, B., MacPhee, J. M., Guzmán, H. R., & Almarsson, Ö. (2003). Crystal Engineering of Novel Cocrystals of a Triazole Drug with 1,4-Dicarboxylic Acids. *J. Am. Chem. Soc*, *125*(28), 8456–8457. https://doi.org/10.1021/ja035776p

Robinson, P. M., & Scott, H. G. (1969). The Crystal Structure of Carbazole: a Partial Determination. *Molecular Crystals and Liquid Crystals*, *5*, 405–411. http://www.tandfonline.com/na101/home/literatum/publisher/tandf/journals/content/gmcl15/1969/gmcl15.v005.i04/15421406908082948/production/15421406908082948.fp.png_v03

Rodríguez-Hornedo, N., Nehm, S. J., & Jayasankar, A. (2007). Cocrystals: Design, Properties and Formation Mechanisms. In J. Swarbrick (Ed.), *Encyclopaedia of Pharmaceutical Technology* (3rd ed., pp. 615–635). Informa Healthcare USA, Inc.

Saha, B. K., Nangia, A., & Jaskólski, M. (2005). Crystal engineering with hydrogen bonds and halogen bonds. *CrystEngComm*, *7*(58), 355–358. https://doi.org/10.1039/B501693B

Schmidt, G. M. J. (1971). Photodimerization in the solid state. *Pure and Applied Chemistry*, *27*(4), 647–678. https://doi.org/10.1351/pac197127040647

Schuchardt, K. L., Didier, B. T., Elsethagen, T., Sun, L., Gurumoorthi, V., Chase, J., … Windus, T. L. (2007). Basis Set Exchange: A Community Database for Computational Sciences. *Journal of Chemical Information and Modelling*, *47*(3), 1045–1052. https://doi.org/10.1021/ci600510j

Schultheiss, N., & Newman, A. (2009). Pharmaceutical Cocrystals and Their Physicochemical Properties. *Crystal Growth and Design*, *9*(6), 2950–2967. https://doi.org/10.1021/cg900129f

ScienceX. (2007, November 26). Major advances made in predicting crystal structures. *PhysOrg*. https://www.google.com.gh/url?sa=t&rct=j&q=&esrc=s&source=web&cd=1&cad=rja&uact=8&ved=0ahUKEwjG16GctOjLAhUFWhoKHTV9CC8QFggbMAA&url=http%3A%2F%2Fphys.org%2Fpdf115310423.pdf&usg=AFQjCNF4yNjSQaf8uNO5WDGFMe9gtiXooQ

Scientific Inc, A. K. (2015). 7-Iodo-8-hydroxyquinoline-5-sulfonic acid. AK Scientific, Inc. https://aksci.com/sds/Q047_SDS.pdf

Sekhon, B. S. (2009). Pharmaceutical co-crystals - A review. *Ars Pharmaceutica*, *50*(3), 99–117. https://doi.org/10.1088/0034-4885/68/4/R03

Serajuddin, A. T. M. (2007). Salt formation to improve drug solubility. *Advanced Drug Delivery Reviews*, *59*(7), 603–616. https://doi.org/10.1016/j.addr.2007.05.010

Shan, N., Toda, F., & Jones, W. (2002). Mechanochemistry and co-crystal formation: effect of solvent on reaction kinetics. *Chem. Commun.*, 2372–2373. https://doi.org/10.1039/B207369M

Shan, N., & Zaworotko, M. J. (2008). The role of cocrystals in pharmaceutical Science. *Drug Discovery Today*, *13*(9–10), 440–446. https://doi.org/10.1016/j.drudis.2008.03.004

Sigma-Aldrich. (2003). Sulfamethoxazole Prduct Information. Sigma-Aldrich, Inc.

Smithrud, D. B., Sanford, E. M., Chao, I., & Al, E. (1990). Solvent effects in molecular recognition. *Pure Appl. Chem*, *62*, 2227–2236.

Southall, N. T., Dill, K. A., & Haymet, A. D. J. (2002). A view of the hydrophobic effect. *J. Phys. Chem. B*, *106*, 521–533.

Stahl, P. H., & Wermuth, C. G. (Eds.). (2002). *Handbook of Pharmaceutical Salts; Properties, Selection and Use*. Zurich, Weinheim: Wiley-Verlag Chimica Helvetica (VCH).

Stahly, G. P. (2007). Diversity in Single- and Multiple-Component Crystals. The Search for and Prevalence of Polymorphs and Cocrystals. *Crystal Growth & Design*, *7*(6), 1007–1026. https://doi.org/10.1021/cg060838j

Steed, J. W., & Atwood, J. L. (2009a). Crystal Engineering- Concepts-Introduction. In *Supramolecular Chemistry* (2nd ed., p. 998). John Wiley & Sons, Ltd.

Steed, J. W., & Atwood, J. L. (2009b). *Supramolecular Chemistry* (2nd ed.). Chichester, West Sussex, United Kingdom: John Wiley & Sons, Ltd.

Stephens, P. W., & Huq, A. (2002). PSSP: An open source Powder Structure Solution Program for direct space simulated annealing. *Transactions of the American Crystallographic Association*, *37*, 1–18. Retrieved from http://www.ccp14.ac.uk/ccp/web-mirrors/pssp/pdf/pssp_aca.pdf

Strachan, D. P. (1989). Hay fever, hygiene, and household size. *British Medical Journal, BMJ*, *299*(6710), 1259–1260.

Su, D., Wang, X., Simard, M., & Wuest, J. D. (1995). Molecular tectonics. *Supramolecular Chemistry*, *6*(1–2), 171–178. https://doi.org/10.1080/10610279508032533

Sun, C. C., & Hou, H. (2008). Improving Mechanical Properties of Caffeine and Methyl Gallate Crystals by Cocrystallization. *Crystal Growth & Design*, *8*(5), 1575–1579. https://doi.org/10.1021/cg700843s

Svehla, G. (1979). IRON, Fe (Ar: 55·85)- IRON(III). In *VOGEL'S TEXTBOOK OF MACRO AND SEMIMICRO QUALITATIVE INORGANIC ANALYSIS* (5th ed., pp. 245–248). New York: Longman Group Limited London.

Syssa-Magalé, J.-L., Boubekeur, K., Palvadeau, P., Meerschaut, A., & Schöllhorn, B. (2005). The tailoring of crystal structures via the self-assembly of organic coordination compounds by N···I non-covalent halogen bonds: co-crystals of sterically hindered N-heterocycles and 1,4-diiodo-tetrafluorobenzene. *CrystEngComm*, *7*(50), 302–308. https://doi.org/10.1039/B500009B

Thompson, M. (2005). Argus Lab. Planaria Softare LLC. Retrieved from http://www.arguslab.com/arguslab.com/ArgusLab.html

Timothy, C., Chandrasekhar, J., Spitznagel, G. W., & Schleyer, P. V. R. (1983). Efficient diffuse function-augmented basis sets for anion calculations. III.† The 3-21+G basis set for first-row elements, Li–F. *Journal of Computational Chemistry*, *4*(3), 294–301. https://doi.org/10.1002/jcc.540040303

Tkáčová, K., Heegn, H., & Števulová, N. (1993). Energy transfer and conversion during comminution and mechanical activation. *International Journal of Mineral Processing*, *40*(1–2), 17–31. https://doi.org/10.1016/0301-7516(93)90037-B

Toby, B. (2006). CMPR. https://www.ncnr.nist.gov/Xtal/software/cmpr/cmprdoc.html

Toda, F. (1993). Solid State Organic Reactions. *Synlett*, *1993*(5), 303–312. https://doi.org/10.1055/s-1993-22441

Toxnet. (2016a). Carbazole. Bethesda. https://toxnet.nlm.nih.gov/cgi-bin/sis/search2/r?dbs+hsdb:@term+@rn+@rel+86-74-8

Toxnet. (2016b). Sulfamethoxazole. Bethesda: National Library of Medicine's TOXNET system. https://toxnet.nlm.nih.gov/cgi-bin/sis/search2/f?./temp/~BIcMYk:1

Trask, A. V., Motherwell, W. D. S., & Jones, W. (2004). Solvent-drop grinding: green polymorph control of cocrystallisation. *Chem. Commun.*, (7), 890–891. https://doi.org/10.1039/B400978A

Trask, A. V., Motherwell, W. D. S., & Jones, W. (2005). Pharmaceutical Cocrystallization: Engineering a Remedy for Caffeine Hydration. *Crystal Growth & Design*, *5*(3), 1013–1021. https://doi.org/10.1021/cg0496540

Trask, A. V., Motherwell, W. D. S., & Jones, W. (2006). Physical stability enhancement of theophylline via cocrystallization. *International Journal of Pharmaceutics*, *320*(1–2), 114–123. https://doi.org/10.1016/j.ijpharm.2006.04.018

Urakaev, F. K., & Boldyrev, V. V. (2000). Mechanism and kinetics of mechanochemical processes in comminuting devices. *Powder Technology*, *107*(3), 197–206. https://doi.org/10.1016/S0032-5910(99)00200-4

US-CDC. (2011). Which diseases are considered Neglected Tropical Diseases? Retrieved March 28, 2016, from http://www.cdc.gov/globalhealth/ntd/diseases/index.html

US-FDA. (2009). Combination Products Definition. U.S. Food and Drug Administration. http://www.fda.gov/CombinationProducts/AboutCombinationProducts/default.htm

van Eijck, B. P., Spek, A. L., Mooij, W. T. M., & Kroon, J. (1998). Hypothetical Crystal Structures of Benzene at 0 and 30 kbar. *Acta Crystallographica Section B STRUCTURAL SCIENCE, CRYSTAL ENGINEERING AND MATERIALS*, *B54*(3), 291–299. https://doi.org/10.1107/S0108768197013384

Variankaval, N., Wenslow, R., Murry, J., Hartman, R., Helmy, R., Kwong, E., … Santos, I. (2006). Preparation and Solid-State Characterization of Nonstoichiometric Cocrystals of a Phosphodiesterase-IV Inhibitor and l-Tartaric Acid. *Crystal Growth & Design*, *6*(3), 690–700. https://doi.org/10.1021/cg050462u

Vishweshwar, P., McMahon, J. A., & Zaworotko, M. J. (2006). Crystal engineering of Pharmaceutical Cocrystals. In E. R. T. Tiekink & J. J. Vittal (Eds.), *Frontiers in Crystal Engineering* (pp. 24–49). John Wiley & Sons Ltd.

Vitthalrao, M. A., Kumar, F. N., & Radheshyam, B. K. (2013). Co-crystallization: An Alternative Approach for Solid Modification. *Journal*

of Drug Delivery and Therapeutics, *3*(4), 166–172. http://jddtonline.info/index.php/jddt/article/view/555/340

Wang, S., & Chen, J. (2007). Gossypol co-crystals and the use thereof. http://www.google.com/patents/US7432300

Warner, J. C., Cannon, A. S., & Dye, K. M. (2004). Green chemistry. *Environmental Impact Assessment Review*, *24*, 775–799. https://doi.org/10.1016/j.eiar.2004.06.006

Wenger, M., & Bernstein, J. (2008). An Alternate Crystal Form of Gabapentin: A Cocrystal with Oxalic Acid. *Cryst. Growth Des*, *8*(5), 1595–1598. https://doi.org/10.1021/cg7008732

Westrip, S. P. (2010). publCIF: software for editing, validating and formatting crystallographic information files. *Journal of Applied Crystallography*, *43*, 920–925. https://doi.org/10.1107/S0021889810022120

Wikipedia contributors. (2016a). Acid dissociation constant. In *Wikipedia*. Wikipedia, The Free Encyclopedia. https://en.wikipedia.org/wiki/Acid_dissociation_constant

Wikipedia contributors. (2016b). Second-harmonic generation. In *Wikipedia*. Wikipedia, The Free Encyclopedia. https://en.wikipedia.org/wiki/Second-harmonic_generation

Yanai, T., Tew, D. P., & Handy, N. C. (2004). A new hybrid exchange-correlation functional using the Coulomb-attenuating method (CAM-B3LYP). *Chemical Physics Letters*, *393*(1–3), 51–57. https://doi.org/10.1016/j.cplett.2004.06.011

Zaworotko, M. (2008). Crystal engineering of co-crystals and their relevance to pharmaceuticals and solid-state chemistry. *Acta Crystallographica Section A FOUNDATIONS AND ADVANCES*, *A64*(a1), C11–C12. https://doi.org/10.1107/S0108767308099637

Zipse, H. (2016). Effective Core Potentials (ECP). Munich: Faculty for Chemisty and Pharmacy, The Ludwig-Maximilians-University Munich. http://www.cup.uni-muenchen.de/oc/zipse/teaching/computational-chemistry-2/topics/effective-core-potentials-ecp/